AN INVESTIGATION INTO A NEW APPROACH TO UHS PROTECTION OF EHV TRANSMISSION LINES BASED ON DETECTION OF FAULT GENERATED NOISE

by

PRAMOD AGRAWAL

B.E.(India), M.E.(India), A.I.E.E.(U K)

Thesis submitted to the City University
for the degree of Doctor of Philosophy,
May, 1989

Power System Protection Laboratory

Department   of   Electrical,   Electronic

and   Information Engineering

City University

LONDON (U K)

This thesis is dedicated to

CHITRA,

ANKUR, SANYAM,

and

AKANSHI

CONTENTS

CHAPTER 1

CHAPTER 4

INVESTIGATIONS BASED ON STACK-TUNER-OUTPUT-RESPONSES OF THE FAULTED PHASE ONLY

CHAPTER 5

NATURAL MODES OF PROPAGATION. DIGITAL SIMULATION AND SIMULATED TEST RESULTS

CHAPTER 6

APPLICATION OF THE PRINCIPLE CONSIDERING

BUS BAR CAPACITANCE

CHAPTER 7

DIGITAL SIMULATION OF ELECTRIC ARC MODEL AND

SUPERIMPOSED ARC VOLTAGES

CHAPTER 8

INVESTIGATION OF THE SCHEME BASED ON THE

SUPERIMPOSED ARC VOLTAGES

ACKNOWLEDGEMENT

The author wishes to thank his supervisor Prof.
A.T.Johns D.Sc., Ph.D., C.Eng., F.I.E.E.,
S.M.I.E.E.E., F.R.S.A., Head of the Department of
Electrical, Electronic and Information Engineering
and Professor of Electrical and Electronic
Engineering with profound sense of gratitude for
his valuable guidance, financial assistance and
encouragement at all times since the inception of
the project.

Thanks are due to Mr. Steve Lewis for the whole-
hearted help in developing programs for simulation
studies to enable the completion of the project in
the earliest possible time. Thanks are also due
to Mr. M Gasparro for preparing the figures. The
author also thanks his colleagues for useful
discussions related to this thesis.

DECLARATION

COPYRIGHT DECLARATION

I grant powers of discretion to the University Librarian to
allow this thesis (AN INVESTIGATION INTO A NEW APPROACH TO
UHS PROTECTION OF THE EHV TRANSMISSION LINES BASED ON
DETECTION OF FAULT GENERATED NOISE) to be copied in whole
or in part without further reference to me. This covers
only single copies made for study purposes, subject to
normal conditions of acknowledgement.

PRAMOD AGRAWAL

LONDON 1989

SUMMARY

This thesis describes a new approach to UHS protection
of HV transmission line using high frequency
components of fault generated noise. The approach is
based on a scheme of the non-unit type which has
features of unit type of protection. Advantages of
unit-type protection are very well known for
providing discrimination between internal and external
faults. Such a scheme makes use of a stack-tuner
circuit of the HV system which has a conventional
coupling capacitor of the voltage transformer. The
stack-tuner is tuned to a certain frequency bandwidth
which does not interfere with the frequency of carrier
communication if used, and the output is processed for
comparison with a threshold voltage and the resulting
signal being fed to a decision logic. A high speed
directional detector has been used for discrimination
against external faults. A signal from this
directional detector can also be fed to the decision
logic. The final operation of tripping depends on the
output signal of the decision logic. For testing the
scheme, a 100 km long 400 kV transmission line has
been digitally simulated with sources of 5 GVA and 20
GVA for high frequency applications, typically 300
kHz. In order to cancel out the effect of noise due
to other sources like communication etc., the tuner
output of each phase has been summed in Aerial mode-2
form (1, -2, 1) and tests have been carried out for
cases with and without bus bar capacitance.
Further effects of an electric arc on the newly
developed scheme have been discussed as most faults
involve arcing or some other kind of discharge. In the
present scheme, a significant high frequency component
of the arc voltage has been noticed which can affect
the performance of the scheme. When carrying out
simulation tests, a remarkable feature of the arc
repeating every half cycle has been noticed. Another
revolutionary feature of the arc model has been
noticed; a significant response which repeats every
half cycle, even for zero voltage fault inception. It
has thereby been found that the scheme can operate at
least in principle, for zero-voltage point-on-wave
faults. This represents a significant improvement over
schemes based on travelling wave phenomena which have
been considered a failure for faults at zero degree
fault inception angle. This has been a difficult task
to simulate the system due to limited memory of the
computer Gould 9095 available at the City University,
London. For this purpose, program has been optimised
for two power cycles of observation time for tuner
frequency of 100 kHz.

LIST OF SYMBOLS

C_C = coupling capacitor

CVT = capacitor voltage transformer

NC = short circuit or normally close mode

NO = open circuit or normally open mode

S_S, S_R = stack tuner as switch at sending end and receiving end

S = a switch of the stack tuner operated by high speed direction detector

SE = sending end

RE = receiving end

DD or dd = high speed directional detector

F_2 = in-zone or internal fault

F_1 = out of zone or reverse fault

V_F = stack tuner output voltage signal after summation (if used)

V_A = auto-correlator output voltage signal

V_T = threshold voltage

V_D = logic output 1 or 0 of the level detector

T_F or TF = forward direction logic signal of DD 0 or 1

T_R or TR = reverse direction logic signal of DD 0 or 1

V_o or V_{OUT} = stack tuner output voltage

V_1 or V_{IN} = stack tuner input voltage or line voltage

14

C_{BB} = bus bar capacitance

V_{oa}, V_{ob}, V_{oc} = stack tuner output voltages for three phases a, b, c

$T_{F,R}$ = forward or reverse signal logic of DD 0 or 1

ST = stack tuner

TRIP or T_S = tripping signal logic 0 or 1

L, L_1, L_2, L_3 = inductive components of power line carrier system used in Britain

$C_S, C, C_1,$ = capacitive components of power line carrier
C_2, C_3, C_4 system used in Britain

R_o = line characteristic impedance for plc system

$w_o = 2\pi f_o$ = angular power frequency (angular resonant or mid band frequency in plc applications)

Z_T = line trap or bus bar impedance

R_T, X_T = resistance, reactance of line trap

E = transmitter voltage

V_1, V_2 = high frequency voltage on line without and with R_T

f = bandwidth in plc applications

f_1, f_2 = lower and upper cut-off frequency

CS, CL = coupling capacitance and series tuning coil inductance for designed stack tuner

Q_c = quality factor of coil for designed stack tuner

RS = resistance of series tuning coil

RSP = output impedance of stack tuner for short mode

CP, CLP = capacitance, inductance of parallel tuned circuit

RP	=	resistance of parallel tuned circuit
RS1	=	matching resistance for output of stack tuner
$\bar{V}, \bar{I}$	=	voltage and current transform
x	=	distance to fault
Z, Y	=	series-impedance and shunt-admittance matrices per unit length
Q	=	voltage eigenvector matrix
Γ	=	propagation constant matrix
$\bar{V}_i, \bar{V}_r$	=	incident and reflected voltage transform
A_1, B_1, C_1, D_1	=	matrices defining line section up to point of fault
A_f, B_f, C_f, D_f	=	matrices defining fault discontinuity
A_2, B_2, C_2, D_2	=	matrices defining line section beyond point of fault
L	=	line length
$f(t)$	=	time varying function
$f(w)$	=	Fourier transform of $f(t)$
w	=	angular frequency
α	=	frequency shift constant
Ω	=	truncation frequency
$f(w-j\alpha)$	=	modified fourier transform
σ	=	sigma factor
Φ	$= Q \Gamma Q^{-1}$	
$\bar{E}_{fS}, \bar{E}_{fR}$	=	transform of voltage at fault point
$\bar{I}_{fS}, \bar{E}_{fR}$	=	transform of current at fault point
$v_f(t)$	=	voltage at fault point (time domain)

$v_{fs}(t)$ = pre-fault voltage at fault point (time domain)

t = instantaneous time

$\hat{V}_{fs}$ = peak value of voltage $v_{fs}(t)$

Θ_{fs} = phase angle of voltage $v_{fs}(t)$

$v_{ff}(t)$ = superimposed voltage at fault point in time domain

$\bar{V}_{ff}(jw)$ = transform of superimposed voltage ($v_{ff}(t) = 0$, $t < 0$)

$\bar{V}_{fs}$ = transform of prefault voltage at point of fault

$\bar{V}_{ff}, \bar{E}_{ff}$ = transform of superimposed voltages at fault point

$\bar{V}_{Ss}, \bar{I}_{Ss}$ = transform of prefault voltages and currents at sending end of line

$\bar{V}_{Rs}, \bar{I}_{Rs}$ = transform of prefault voltages and currents at receiving end of line

$\bar{V}_{S}, \bar{V}_{R}$ = sending and receiving end voltage transforms

$\bar{I}_{S}, \bar{I}_{R}$ = sending and receiving end current transforms

$h(t)$ = unit step function

$\bar{V}_{Sf}, \bar{I}_{Sf}$ = transform of superimposed voltage and current at sending end of line

$\bar{I}_{fSf}, \bar{I}_{fRf}$ = transform of superimposed currents at fault point

$\bar{V}_{Rf}, \bar{I}_{Rf}$ = transform of superimposed voltage and current at receiving end of line

Z_{SS}, Z_{SR} = sending and receiving end source impedance matrices

R_f = fault resistance matrix

$\bar{E}_{Sa}, \bar{E}_{Sb}, \bar{E}_{Sc}$ = phase a, b, c source voltage transform

$\bar{I}_{Sa}, \bar{I}_{Sb}, \bar{I}_{Sc}$ = phase a, b, c source current transform

a,b,c = phases a,b,c

U = unit matrix

Z_{S0}, Z_{S1} = zero and positive phase-sequence source impedances

Z_{Sn} = neutral impedance of source

SCL = short-circuit level

$|V_L|$ = magnitude of line voltage

I_{sc} = short circuit current

R_{S1}, L_{S1}, X_{S1} = source resistance, inductance, reactance

Y_{ST} = admittance matrix of stack tuner

Y_{S1}, Y_{Sn} = positive sequence, neutral admittance of source

Y_{Sn1} = series combination of Y_{S1}, Y_{Sn} admittances

Y_{TT} = total source admittance

Y_{CB} = bus bar capacitive admittance matrix

$\bar{V}_{fsnew}$ = transform of stack tuner output pre-fault voltages at fault point

$\bar{V}_{Sfnewc}$ = transform of close mode stack tuner output superimposed voltages at sending end

$\bar{V}_{Rfnewc}$ = transform of close mode stack tuner output superimposed voltages at receiving end

$\bar{V}_{Sfnewo}$ = transform of open mode stack tuner output superimposed voltages at sending end

$\bar{V}_{Rfnewo}$ = transform of open mode stack tuner output superimposed voltages at receiving end

$\bar{V}_{ffMAX(w)}$ = maximum superimposed voltage at fault point

$\bar{V}_{ffMIN(w)}$ = minimum superimposed voltage at fault point

T_{DD} = operating time delay of DD

Z_L = load impedance used for refraction coefficient

R_r = refraction coefficient

$'x',y$ = signals of signal processing scheme

$P_{xy}(T)$ = auto-correlated function

$x(k\delta t)$ = window of N samples where k=1---N and δt is sampling time

A_{y1},B_{y1} = coefficients of two-port admittance matrix

z,y = impedance, admittance per unit length of line

V = Voltage vector of a semi-infinite line

V_i = incident voltage vector of semi-infinite line

v,v_i = variables related to modal analysis

$\Gamma1,\Gamma3$ = mode 1, mode 3 propagation constants

a_s = symmetrical component operator

V_0,V_1,V_2 = modal voltages

V_a,V_b,V_c = three phase voltages

T_T = operating time of the scheme/relay

R_1 = reflection coefficient

V_X,V_Y,V_Z = signals of signal processing scheme

WS = moving window for auto-correlation

WC = fixed window for auto-correlation

n,N_s = number of samples of signal

I_p = peak value of steady state arc current

V_p = maximum arc voltage per cm length of arc

$I_l = 0.15I_p$ = current at point where arc voltage is constant for increasing current

$I_h = 0.38I_p$ = current at point where arc voltage follows a slope for decreasing current

o,a,b,c,b,o = positive cycle arc cyclogram

o,a',b',
c',b',o = negative cycle arc cyclogram

$V_r(t)$ = reignition voltage kV/cm

T_e = arc extinguishing time

$K(T_e)$ = rate of increase of reignition voltage

$\bar{V}_{arc}, \bar{I}_{arc}$ = transform of arc voltage, current at fault point

$\bar{E}_T$ = total voltage transform at fault point

$\bar{Z}_T$ = thevnin equivalent source impedance

$v_{arc}(t)$ = arc voltage in time domain

$I_F(t)$ = fault point current

$I_{Farc}(t)$ = fault point arc current

$K_{arc}(t)$ = arc cyclogram constant

$V_{farc}(t)$ = total arc voltage at fault point

$V_{fss}(t)$ = pre-fault voltage at fault point

$V_{ffarc}(t)$ = superimposed arc voltage at fault point

P_1, P_2, V_1, V_2 = power, voltage, current at any two points

I_1, I_2 for defining Decibels

YTSM = close mode impedance of stack tuner

YSM = close mode output impedance of stack tuner

YTM = open mode impedance of stack tuner

YOM = open mode output impedance of stack tuner

YNC = close mode gain of stack tuner

YNO = open mode gain of stack tuner

20

VpPSC,VpQSC = sending end, receiving end modal voltages:

              earth mode, mode 1, mode 2 if $p = 0,1,2$

$SI(p,q)$ $= Q^{-1}$ matrix if $p = 1,2,3$ and $q = 1,2,3$

$VPS(p,q)$, = SE,RE phase voltage matrix if $p = 1,2,3$

$VQS(p,q)$ and $q = 1$

VpPFC,VpQFC = SE,RE modal voltages in frequency domain:

              earth mode, mode 1, mode 2 if $p = 0,1,2$

$VPF(p,q)$, = SE,RE phase voltage matrix in frequency

$VQF(p,q)$ domain if $p = 1,2,3$ and $q = 1$

Z_0 = characteristic-impedance matrix

Y_0 = characteristic-admittance matrix

B = charge-coefficient matrix

R = series resistance matrix per unit length

X = series-reactance matrix per unit length

d_{ij} = distance between conductors i and j

D_{ij} = distance between conductor i and image of j

Θ_{ij} = angle substended at conductor i by images of

              i and j

ϵ = permittivity

CHAPTER 1

INTRODUCTION

1.1 Literature survey

A literature survey of modern trends of high voltage
transmission line protection and the effect of the electric
arc in power system applications has been performed:

1.1.1 Modern trends in HV transmission line protection

Conventional schemes [1,2] for EHV protection using pilot
relays, distance and/or directional over current relays are
very well known. Early forms of directional comparison
relays and the later- developed phase comparison relays are
commonly used. These schemes, together with distance
relays employ non-unit measurements and they lack the
advantages of inherent discrimination for external faults.
Carrier aided protection schemes are commonly used as pilot
schemes. These schemes are known as unit-type and provide
the best discrimination against external faults. For
these, the carrier communication link has to be highly
reliable and secure. In order to attain reliability and
security of this type of protection, a continuous
monitoring of the communication channel is necessary which
makes the scheme relatively expensive.

As these schemes operate on power frequency, these are liable to maloperate during initial disturbance of the system due to the transient effect if sufficient filtering or time delay is not provided. But this delay may cause damage and system instability, and therefore ultra-high-speed fault clearance has been warranted [3,5]. With this view many experts have been investigating new concepts of protection of EHV transmission lines and it is worth mentioning the idea of Johns [6] to develop a method which is capable of measuring accurately a signal from a window of information for a fraction of one period of power frequency without increasing significant delays due to extensive filtering. Johns [7] also claims that further reduction in overall fault clearance time has to be concentrated on fast speed protection schemes rather than operating times of circuit breakers. Later Johns [8] developed a new method of distance protection using Finite Transform Technique for UHS tripping. Other distance schemes using filtering and curve-fitting techniques [9,10] have been developed which have half power cycle detection time.

In order to further improve detection times many authors [11-17] have used non-power frequency components in the fault signals. Chamia [11] uses the change in voltage and current signals to determine the direction of the fault. This relay is being commercially used. Takagi [12-15] computes travelling waves at both ends and uses their difference to detect an internal fault. Dommel [16] derives a travelling wave discriminant whose co-ordinates

at two ends of the line decides the operation of the relay. Johns [17] derives a sequence in which forward and reverse travelling waves exceed given thresholds to determine the direction of the fault. Vitins [18] describes a distance scheme based on the wave equation. Swift [19] gives a spectral analysis of post-fault signals which determine a dominant frequency component with a period of twice the propagation time from source to the fault. Crossley [20] describes a distance scheme using a correlation technique to measure the distance to the fault.

All unit-type schemes based on travelling waves developed so far need carrier communication link for discrimination against external faults. At present there is no such non-unit type of scheme which has features of unit type of protection. Mehdi [21] describes a non-unit scheme having features of unit-type of protection which uses processing of a fault generated current waveform. Such a scheme has limitations of response time of current transformers. For discrimination purposes, wave-traps on the primary side of the transmission line have been used. Normally, any change in, or application of equipment to the primary side is not appreciated. Later Johns [22] has postulated and described the principles of a new scheme in which the high frequency fault noise is detected in switched stack-tuning circuits. This work was the starting point for the work of this thesis and the author has performed extensive investigations into this techniquein order to lay the foundation for a practicable design of the hardware necessary for its impletation.

1.1.2 Consideration of electric arcs in EHV Protection

It is a known fact that most faults on transmission lines involve arcing or some other discharge. The voltage drop across the arc is generally much smaller than the transmission line voltages and does not affect the operation of the relay which normally works on the steady state fault current. It is only the current which can affect the operation. Arcing faults in low voltage distribution systems have been studied by many authors [23 - 26]. Consideration of arc resistance in distance schemes [27 - 30] has been used for a long time and the arc has been taken into account as a linear resistance. Many authors [31-37] have studied static characteristics of electric arcs. Strom [31] has investigated the dynamic arc characteristics of a long arc at atmospheric pressure and has found that the characteristic follows different paths for increasing and decreasing current, calling it an arc-cylogram. It is also found that the arc characteristics do not repeat for every successive cycle. Brown [38] has also investigated the dynamic characteristics but for low current. Brown [38], Eaton [39], Slepian [40] have studied the arc extinction mechanism. Eaton [39] has found that the arc extinction may result from two causes: (1) following a current zero, the recovery voltage across the arc terminals fails to reach a value equal to the dielectric strength of the arc path; (2) the arc length is increased by the wind (or

25

otherwise) at such a rate that the voltage required to maintain the positive column of the arc is greater than that which can be supplied by the current. Slepian [40] has studied the factors for extinguishing the A.C. arc at a current zero: (1) the rate of recovery of the voltage across the arc, (2) the ability of the arcing medium to recover the dilectric strength. If the rate of recovery of the voltage across the arc exceeds the rate at which the arcing medium recovers dielectric strength, the arc will persist. Slepian also shows that the arc hystersis cylogram repeats only if the voltage across the arc is such that the time for which the arc current remains at zero following voltage reversal is sufficiently small to ensure that the arc is re-established without an appreciable restriking voltage i.e. negligible arc deionization occurs during zero current time. Where this is not a case, a significant reignition voltage has to be developed before the arc cylogram is attained. Recently, studies of arc characteristics in secondary arc application has gained importance and the work of Fukunishi [41]' for extinction of long secondary arcs is important. Johns [42 - 43] gives an expression for the reignition voltage and arc modelling with the reignition effect is possible. Cornick [44] has studied the power system transients caused by arcing faults considering weak and strong arc currents.

These transients may have high frequency components and their detection for protection application has not been previously considered. In the present study, methods have been developed for simulating the effect of electric arcs

on the high frequency components of the fault generated noise have been studied and their application for protection purposes is discussed.

1.2 Objective of the thesis

Distance and/or directional over-current schemes are non unit-type schemes and lack the advantages of discrimination for external or reverse faults. Similarly carrier aided pilot schemes are unit-type schemes which have advantages of discrimination for external fault but depend upon the reliability of the communication systems. With this view, the objective of the present thesis is to investigate a new principle of a non-unit-type scheme having advantages of unit-type schemes. The principle is based on the travelling wave phenomena and has been postulated by Johns [22]. Basically, whenever a disturbance occurs on a transmission line, travelling waves travel in all directions and it is possible to detect these travelling wave components of voltages and currents at both ends of the transmission line without application of any communication link. To detect these travelling wave components generated due to fault, a signal of a particular band of frequencies has to be detected and to processed to establish the scheme.

Since most faults involve arcing or any other kind of discharge, studies of the effect of electric arcing on these fault-generated travelling wave components of a particular band of frequencies have to be performed. In

order to study the effect of higher frequency components of the arc e.g. 300 kHz for long observation time e.g. few cycles, it is also the objective of this thesis to optimise the computer program for system simulation due to limited capacity of the memory: 12 M byte of the computer Gould 9095, available at the City University, London.

It is well known that the arc voltage which is much smaller than the transmission line voltage, may repeat for a few power cycles following the instant of fault inception. This arc voltage may have high frequency components near the zero crossing of the arc voltage waveform. An extremly important aim of the thesis is also to detect such components repeating every half a cycle of the power frequency.

Further, schemes based on travelling wave phenomena have been considered failures for zero degree of fault inception angle. But if it is possible to detect the above travelling wave components of high frequency at zero degree of fault inception angle, perhaps it could be a success for the schemes based on travelling waves to operate on zero degree fault inception angle. With this view, it is also the aim of the scheme to detect high frequency arc voltage components at zero degree fault inception angle repeating every half a cycle of the power frequency.

These aims can be categarically stated as below:

1. To develop computational models of transmission line end source systems incorporating the equipment reported by Johns [22].

2. To investigate its performance and establish whether further work as its implementation is worthwhile.

3. To develop a means of incorporating arc models into the system simulation and prove their validity.

4. To investigate the extent to which the performance is affected by arcing fault conditions.

5. To refine the design of the equipment and, if necessary to propose means of improving the system developed for the stack tuner circuits and the signal processing means.

1.3 Structure of the thesis

This thesis has been structured on the basis of twelve chapters. The first chapter of the thesis has been devoted to the introduction of the thesis describing literature survey, objective of the thesis and structure of the thesis. Chapter 2 to Chapter 8 describe theoretical concepts and experimental results to establish the objectives of the thesis. Synopses of each of these chapters is described later in this section. Chapter 9 is devoted to the conclusion of the thesis. Chapter 10 is devoted to suggesstions for the future work. Chapter 11

lists out references for the thesis. Chapter 12 is an appendix in five sections: (A) power line carrier , (B) stack tuner frequency response data, (C) calulation of transmission line basic parameters, (D) program for band pass filter, (E) simulated test results of the arc cyclogram.

1.3.1 Chapter 2 synopsis

Chapter 2 describes theoretical concepts, operational principles, and design aspects of the basic scheme.

1.3.2 Chapter 3 synopsis

Chapter 3 is devoted to work regarding digital simulation of the stack tuner, transmission line, stack tuner with transmission line and for the output of the stack tuner.

1.3.3 Chapter 4 synopsis

Chapter 4 describes: (1) comparison of fault responses at tuner frequencies of 300, 200, 100, 100 - 300, 10 - 90 kHz, (2) establishment of the principle based on internal and reverse fault responses, (3) effect of different fault inception angles i.e. 90, 60, 30, 15, 5, 0 degrees, (4) effect of different source capacities i.e. 1 GVA at each end, 99 GVA at each end, 5 GVA at sending end and 20 GVA at receiving end.

1.3.4 Chapter 5 synopsis

Chapter 5 is devoted to simulation techniques of the (1, -2, 1) modal component and describes the results on the basis of the (1, -2, 1) modal component responses for: (1) establishment of the principle, (2) detailed signal processing, (3) single phase to earth fault results at different points on the transmission line i.e. 1 km, 25 km, 50 km, (3) other faults i.e. single phase to earth fault at phase A, phase B, phase C, three phase fault, two phase fault.

1.3.5 Chapter 6 synopsis

Chapter 6 is devoted to investigation of the scheme considering bus bar capacitance. Simulated test results for various tests have been included: (1) establishment of the principle, (2) effect of different fault inception angles i.e. 90, 60, 30, 15, 5, 2, 0 degrees, (3) effect of different source capacities: 1 GVA, 50 GVA, 90 GVA at both ends.

1.3.6 <u>Chapter 7 synopsis</u>

Chapter 7 is devoted to studies relating to an electric arc. This chapter describes digital simulation techniques of the electric arc model considering the reignition effect. Later the chapter describes the digital simulation techniques of the superimposed arc voltages of the transmission line system.

1.3.7 <u>Chapter 8 synopsis</u>

Chapter 8 is devoted to the simulated test results considering the effect of an electric arc. Various test results are: (1) discrimination feature of the scheme, (2) advantages of electric arc at zero degree fault inception angle, (3) different arc lengths i.e. 2 meter, 20 meter, 40 meter, (4) arc effect repeating every half a cycle.

CHAPTER 2

THEORETICAL ASPECTS OF THE NEW SCHEME

This chapter describes the theoretical aspects of the proposed scheme:

2.1 Principle of the scheme

A fault on the power line produces wideband noise [45]. This noise has been considered a nuisance, e.g. it can interfere with carrier signalling equipment [46,47]. In the proposed principle this noise has been used for protection application. Various methods could be used to apply this principle, but in the scope of present work only the method of processing the noise through high frequency capacitance stack-tuning circuits at the ends of the protected circuit has been discussed. In most applications the coupling capacitor C_C forms part of the capacitor voltage transformer (CVT) which is required to provide 50/60 Hz low voltage for metering and protection purposes. The stack tuner can be arranged to short circuit or open circuit any high frequency signals induced by a fault. The gain of the tuner can be arranged high in short circuit mode NC and low in open circuit mode NO. At the moment if these short and

33

open ciruit arrangements of the tuner circuit can be considered as a switch S_S at the sending end SE or S_R at the receiving end RE in short and open mode respectively, the principle can be explained with reference to Figure 2.1 as below:

S_S and S_R are normally open and are closed if a reverse fault is detected through a local directional detector DD inhibiting the tripping at local end. If this reverse fault occurs at SE, switch S_S will be closed due to reverse fault and would restrict any in-band components from reaching RE thereby, even though the switch is in open mode at RE, inhibiting tripping at RE. In-band is referred to as the high frequency band of the tuner. If directions with reference to Figure 2.1 can be defined as forward at sending end SE and receiving end RE for in-zone fault F_2, then, for an out of zone fault at say F_1, SE would see F_1 as reverse and RE would see F_1 as forward. Now to detect these directions any type of high speed directional detector DD based on locally derived parameters e.g. distance protection / directional comparision relay or any other device can be used. For in-zone fault at F_2 the inband signals remain at both ends causing tripping at SE and RE.

2.1.1 Consideration of the bus bar capacitance

In the HV transmission line system, many lines terminate at single bus-bar which responds for effective capacitance

between the bus-bar and the earth. This capacitance does not affect the power frequency signals due to very high impedance but terminate the line at any high frequency signals due to low impedance. The value of the capacitance may vary from line to line but a typical value of 0.1 micro-farad has been considerd for the present scope of the work. Under such circumtances, the only possible way of receiving the in band frequency signals is by providing the impedance of the comparable value of the stack tuner circuit. Therefore the stack tuner switch has been maintained in the normally closed, NC position for the internal faults as shown in Figure 2.2. For the reverse fault at F_1 the stack tuner switch has to be operated to open NO position by the contact of a DD switch inhibiting the tripping at the SE as shown in Figure 2.3. In the reverse fault condition, the high frequency signals are short circuited effectively through the low impedance of the bus bar capacitive circuit at SE and can not reach the RE inhibiting the tripping at the RE.

2.2 Block-diagram representation

In general, the fault can be of any type and therefore it is necessary to combine the output of each stack tuner in such a way that a composite signal can be formed. A convenient way of combining the outputs involves the use of aerial mode components of propagation , and the 1, 0, -1 and 1, -2, 1 mode distribution approximations are particularly convenient. Figure 2.2 shows more details of

the precise arrangement used for a 1, -2, 1 combination.

The above arrangement ensures that any fault combination can be readily detected and it also ensures:

(1) any remote low level sources e.g., radio transmitters, do not cause interference with the operation of the scheme because any such remote source generally causes common-mode-signals to be induced in the power line and the 1, -2, 1 combination clearly causes such signal cancellation,

(2) to reduce the in-band signal detected by the healthy circuit following a fault on an adjacent circuit in double circuit or parallel feeder applications.

The output of the summation process of Figure 2.4, the tuned voltage (V_F), is fed to an auto-correlator to strengthen the signal. The output of the auto-correlator V_A is fed to a level detector which is set to pick up any signals present which lie above a threshold voltage V_T i.e. , the output of the level detector is such that $V_D = 1$, $|V_A| > V_T$ and $= 0, |V_A| < V_T|$. The threshold voltage is set so that any noise in V_F (generated by the tuner) and V_A (generated by the auto-correlator) is effectively ignored. The threshold can also be used to control the sensitivity of the equipment to system faults. Estimating the threshold value after auto-correlating the signal improves discrimination against external faults due to strengthen of the signal.

The decision logic circuit of Figure 2.4 receives the

signal V_D and the forward/reverse signals generated by the local directional detector DD. It is arranged to assert tripping of the local circuit breaker according to internal or reverse fault. As mentioned previosly, the local DD reverse signal is used to trigger the operation of switch S to NC mode in the stack tuning circuit as shown in Figure 2.1 or to NO mode as shown in Figure 2.3 for the case of the effective bus bar capacitance. This description of the signal processing is based on the theoretical concepts only. The signal processing used in this thesis has been described later in other chapters.

2.3 **Operational aspects**

The operation of the scheme has been illustrated in Figure 2.5. Figure A is for an internal fault and Figure B is for a reverse fault at SE. V_F, V_D, TF, TR, trip are the tuned voltage signal of the summation process, the level detector output signal, the forward direction signal of the directional detector, the reverse direction signal of the directional detector, the tripping signal based on the logic respectively. These are shown high or low at the SE or the RE according to internal or reverse fault conditions. Now triping can take place only when V_F and TF both are high (shown by 1) and triping has been shown by 1. For the reverse fault condition TR is high shown by 1 and tripping cannot take place shown by low (0). For the internal fault condition, V_F and TF are high and tripping will take place at both ends SE and RE. For a reverse fault

condition at SE, the signal TR is high and tripping cannot take place. At RE, V_F is low(0), TF is high and therefore tripping cannot take place at RE. Internal fault has been shown nearer to RE so DD at RE is expected to operate earlier than DD at SE as shown in Figure 2.5. Similarly reverse fault is nearer to SE and DD at SE is expected to operate earlier than DD at RE as shown in Figure 2.5.

If relatively slow DD is used, pulse stretching of the main signal may be required. A care is required to the extent, a pulse can be stretched as it may loose the security of the system for reverse faults.

When the bus bar capacitance is effective, the operational principle has been explained in Figure 2.6. Figure A shows the internal fault condition and Figure B shows the reverse fault condition. Based on the decision logic input of V_D, T_F, T_R, the output trip signal can be seen 0 for the reverse fault condition and 1 for the internal fault condition. If DD is relatively slow, the pulse stretching may be required.

2.4 **Design consideration [46,47]**

Figure 2.7 shows a typical circuit to tune with the stack tuning capacitance C_C at 300 kHz in such a way that the impedance presented to the flow of in-band high frequency components is small with high gain (approximate to closure of S_S and S_R, NC in Figure 2.1) or very large with relatively low gain (approximate to open of S_S and S_R, NO). With switch S closed operated through DD switch, the

circuit provides high gain output voltage V_O in NC condition which is proportional to the in-band system voltage. The values of the components in Figure 2.7 can also be used to adjust the band receptability relative to any carrier signalling channels (if these are used) to avoid any interference. The centre frequency can be adjusted to suit the application and, if no carrier signalling is used , there is virtually no restriction on the band of receptability. With switch S open, the stack tuner provides low gain to distinguish with the condition of S closed. If V_1 is the line voltage and V_O is the stack tuner output voltage, the gain is V_O/V_1. This design is based on the theoretical concepts only. The design circuit used in this thesis has been described later in Chapter 3.

SENDING

RECEIVING END

F2 (Internal Fault)

Coupling capacitor C_C
(typically 2000 pf)

F1 (Reverse Fault)

STACK TUNER
IN OPEN MODE

S_S

S_R

FORWARD

FORWARD
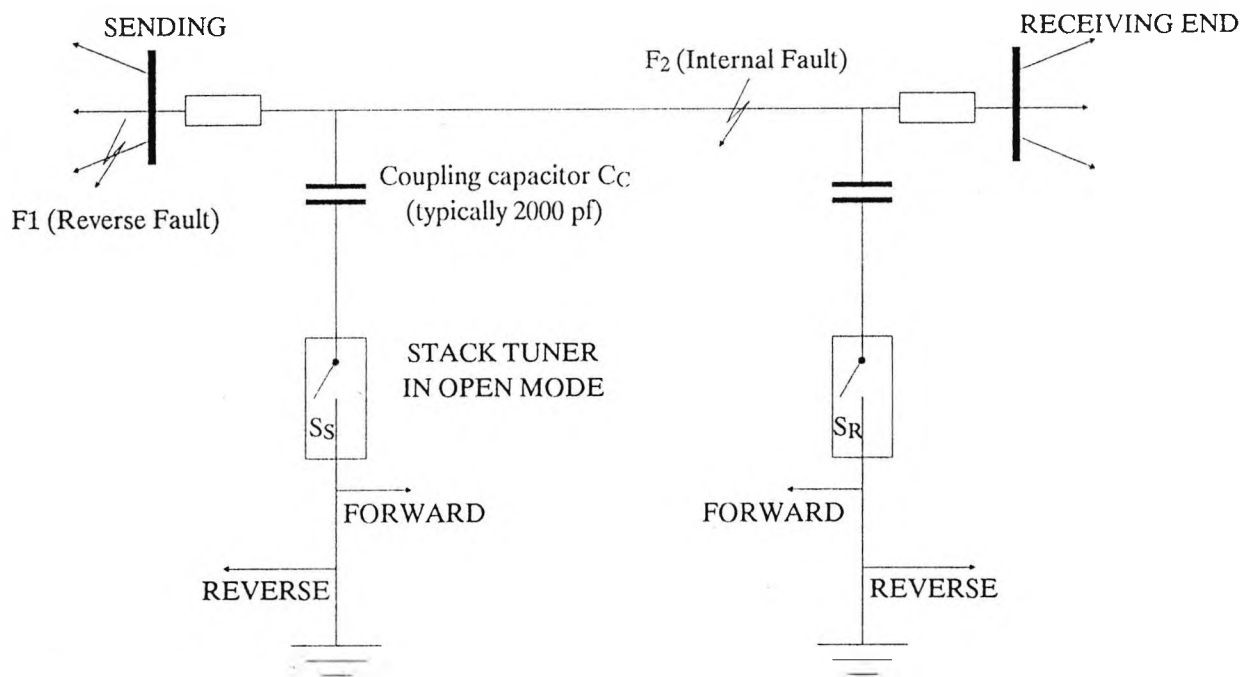
REVERSE

REVERSE

Figure   2.1   ARRANGMENT SHOWING STACK-TUNER AS A SWITCH AND
              FAULT DIRECTIONS FOR REFERENCE
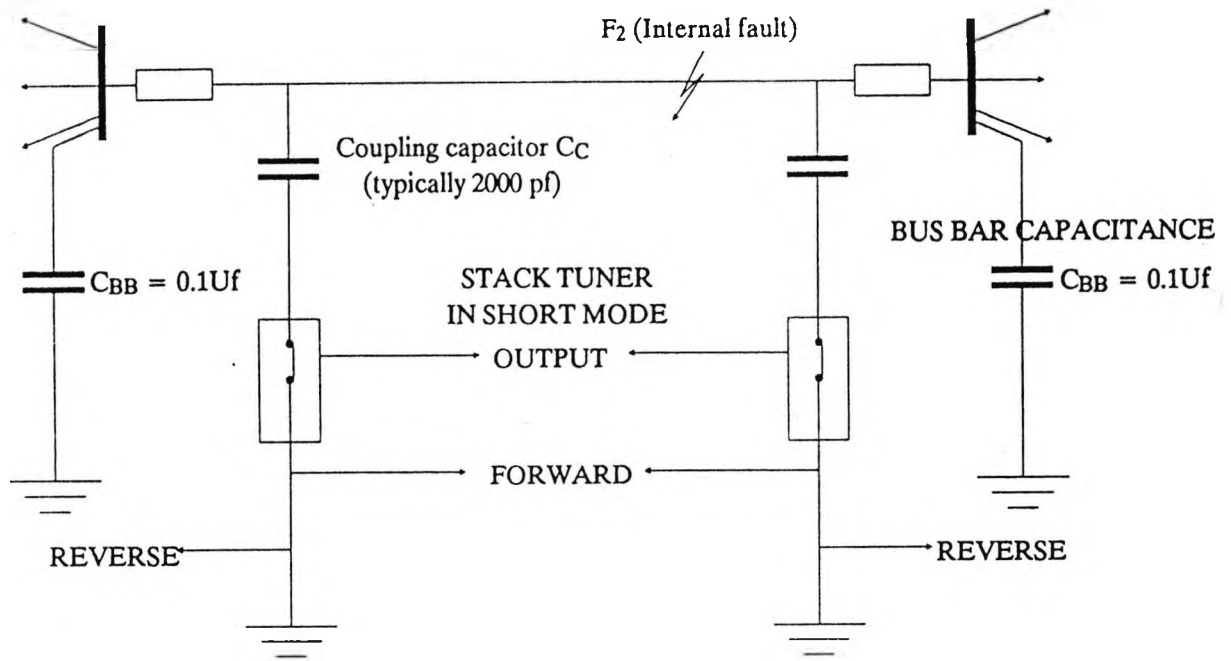
Figure 2.2 ARRANGMENT CONSIDERING
BUS - BAR CAPACITANCE FOR INTERNAL FAULT
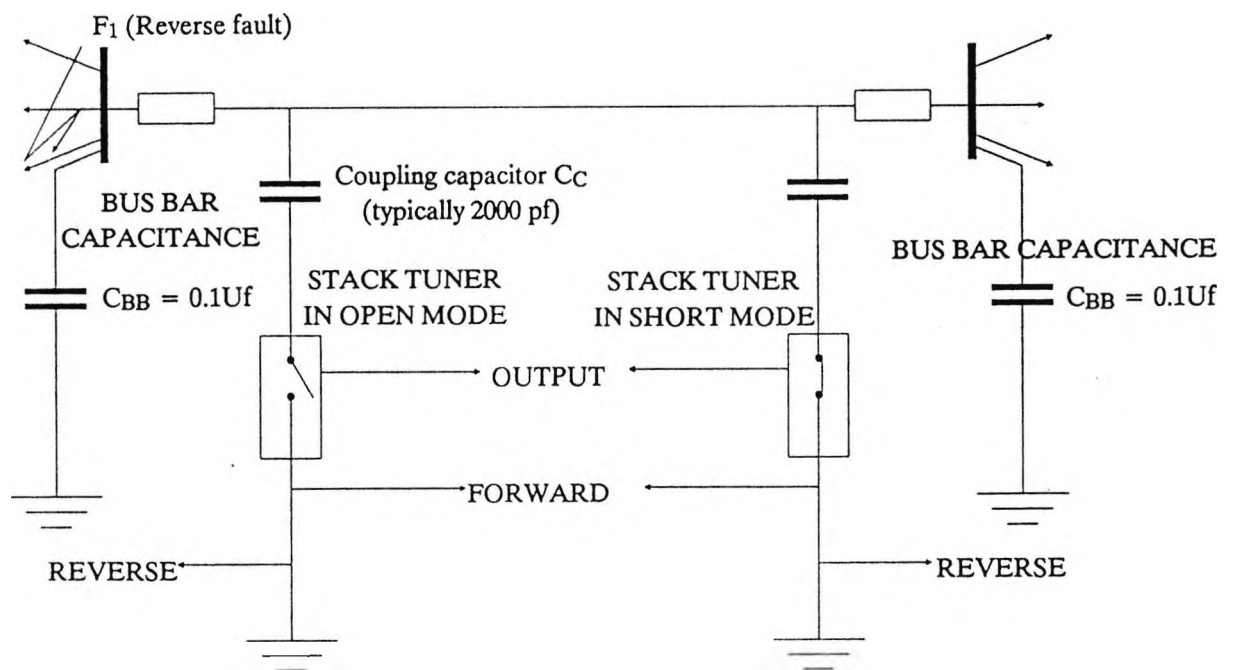
Figure 2.3 ARRANGMENT CONSIDERING BUS BAR
CAPACITANCE FOR REVERSE FAULTS
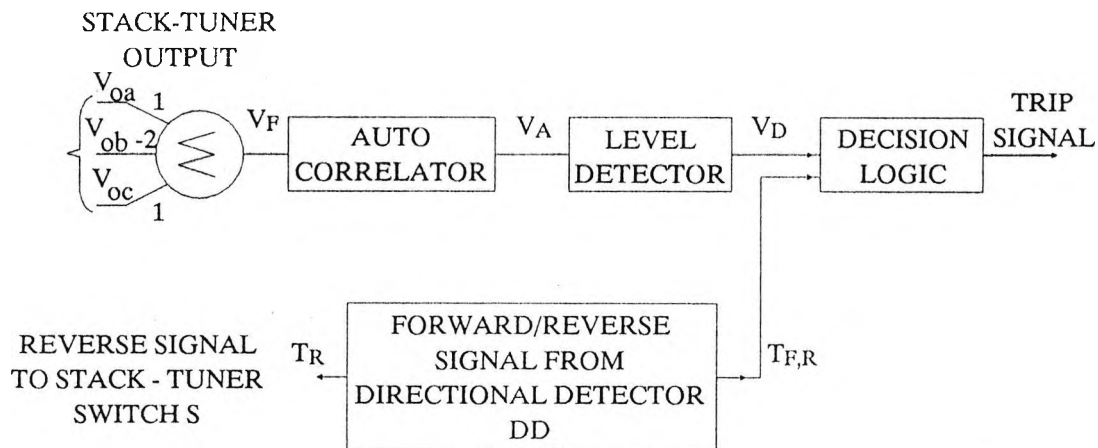
Figure 2.4 BLOCK DIAGRAM REPRESENTATION FOR SIGNAL
PROCESSING
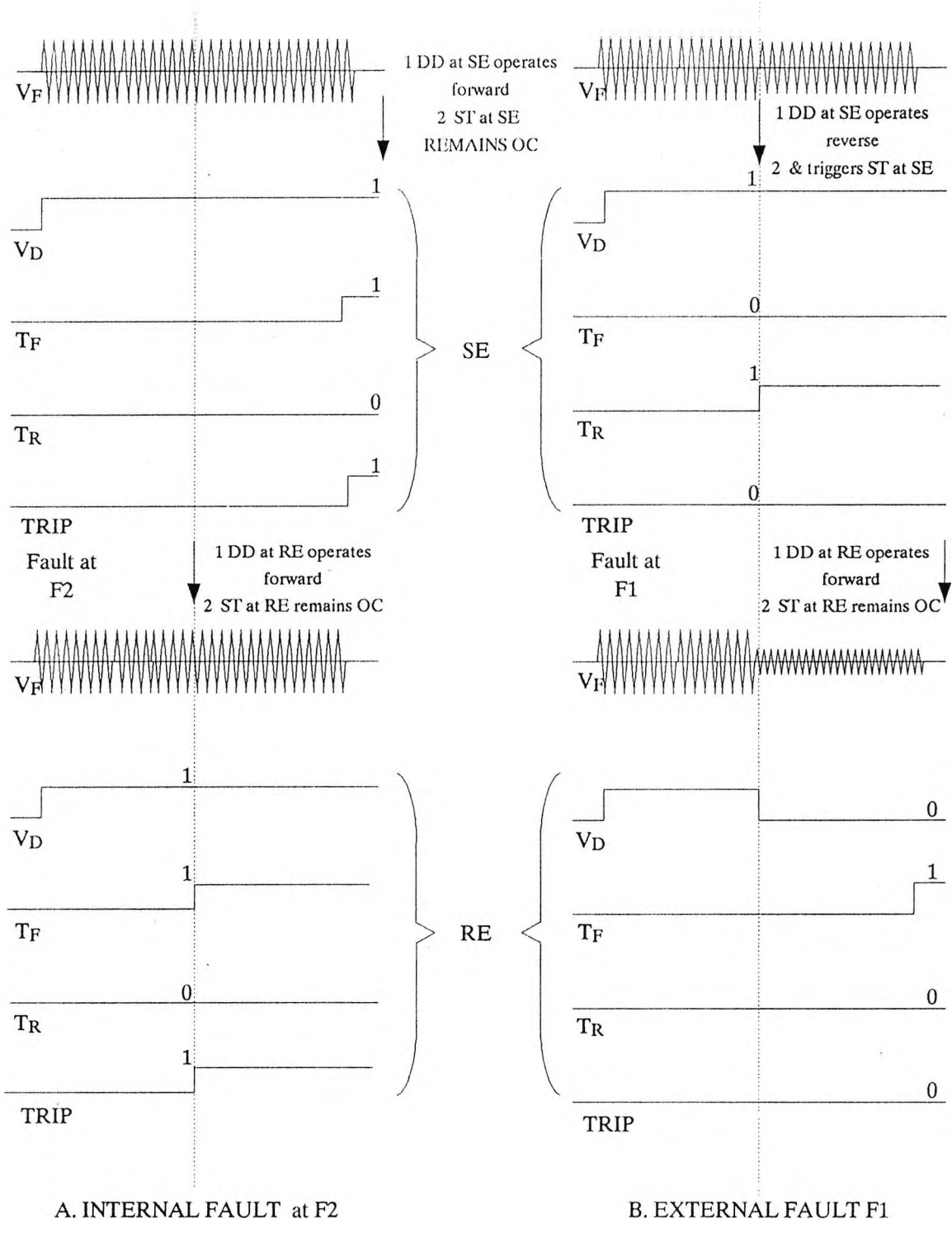
A. INTERNAL FAULT at F2   B. EXTERNAL FAULT F1

Figure   2.5 OPERATIONAL PRINCIPLES OF THE SCHEME
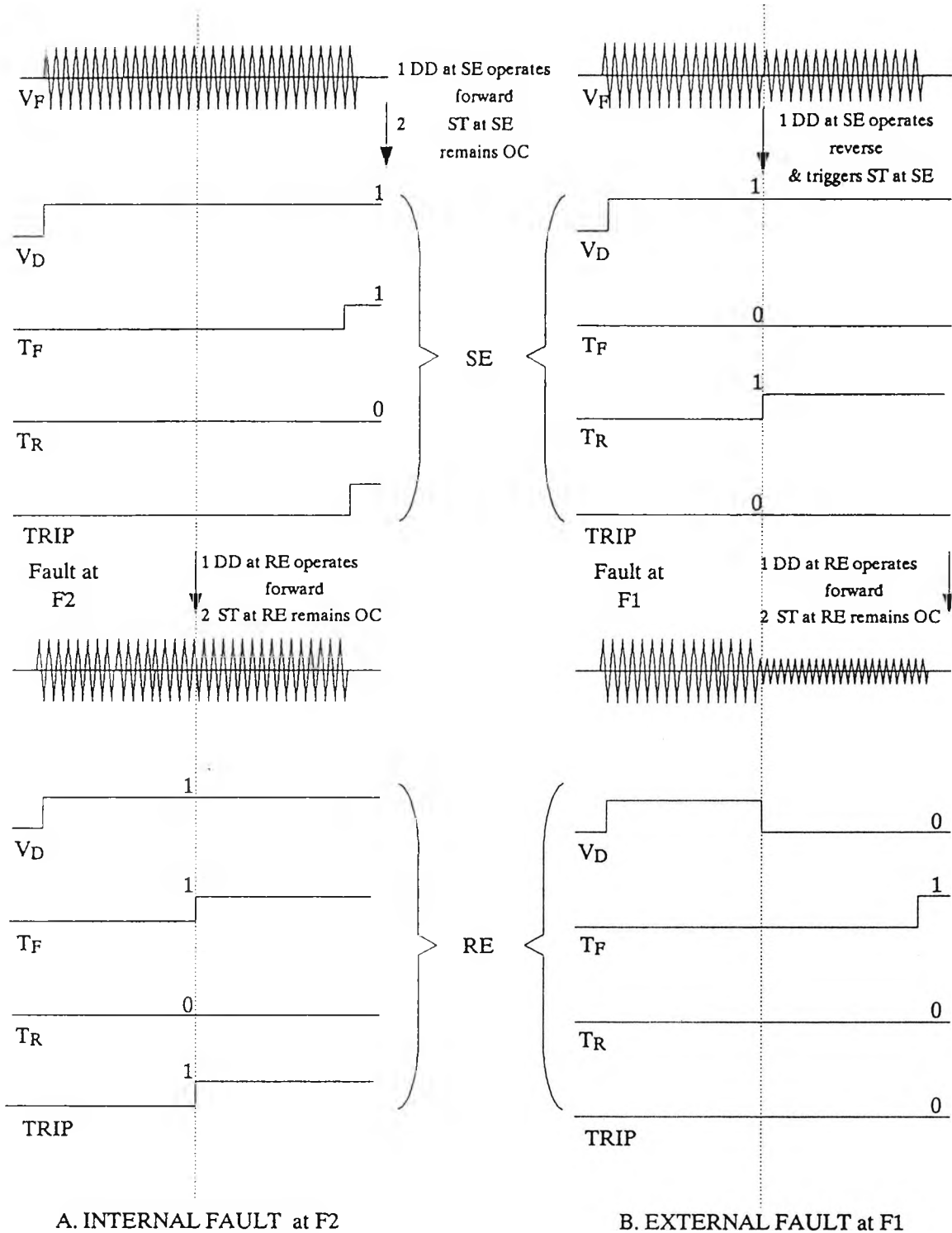
Figure 2.6 OPERATIONAL PRINCIPLE OF THE SCHEME CONDIDERING

BUS BAR CAPACITANCE

IMPEDANCE

CC = 2000 pf

V_1 (TOTAL LINE VOLTAGE)

S

V_0

GAIN = V_0 / V_1
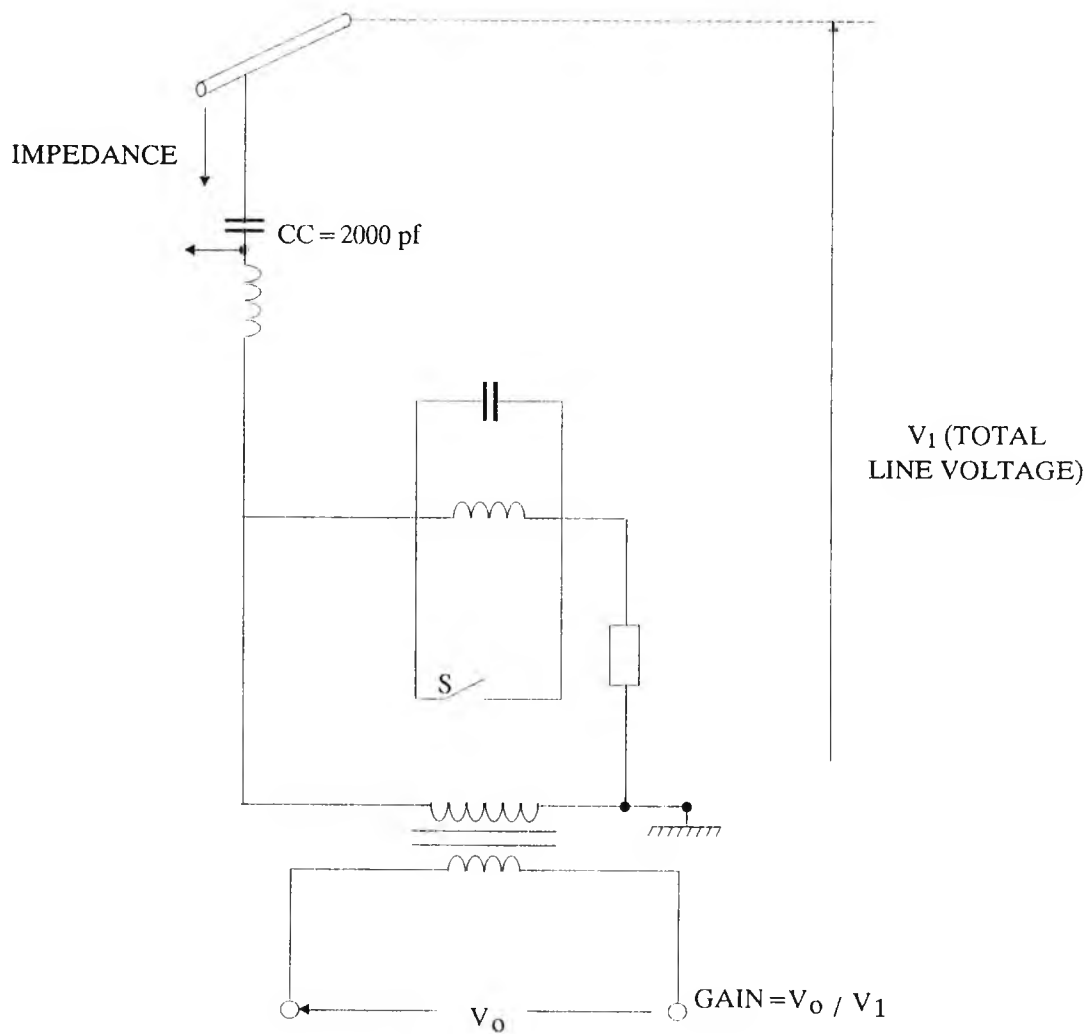
Figure 2.7 STACK TUNER CIRCUIT

CHAPTER 3

DIGITAL SIMULATION OF TRANSMISSION LINE SYSTEM

This chapter describes the digital simulation of the
transmission line and the stack tuner in the following
sections:

3.1 Design, digital simulation and frequency response of the stack tuner

Primary application of a coupling capacitor to the
transmission line is very well known for measuring the line
voltages for metering and protection applications. Another
application of the capacitor is known for tuning with the
line tuner for carrier communication purposes. Application
of the coupling capacitor to match the line tuner for
protection purposes is unknown so far and in the absence of
such information, the circuits based on carrier
communications have been studied and taken for reference
[28,48] to develop a line tuner for protection
applications.

40

3.1.1 Frequency range

Power line carrier generally operates over the band of frequencies between 30 and 300 kHz. These frequencies can be coupled to and transmitted over power lines with relatively small loss. Below 30 kHz, line coupling become impractical and above 300 kHz, the line losses are higher and radiation into space may interfere with licensed space. In U.K. the range is between 70 and 500 kHz.

3.1.2 Modes of operation

The power line carrier signal may use on-off, frequency-shift, or single-side band (ssb)operation. The on-off signal is used to block-tripping in an unfaulted line section; frequency-shift operation is used either for blocking or transfer-tripping. When functions are combined on an ssb channel, audio tones are used to modulate the carrier, thus providing the relaying intelligence.

3.1.3 Line coupling

The power-line phase conductor is used to transmit the carrier signal between power stations. Many protective relaying carrier channels use single-phase-to-ground coupling, which requires only one set of coupling equipment at a line terminal. Phase to phase coupling may be used to improve dependability. It offers a better chance of getting a signal through an internal fault when the channel

41

is used for a transfer-trip relaying system. In Britain, it is usual to use phase-to-phase transmission [48].

A conventional stack tuner circuit used in Britain is shown in Figure 3.1. C_1 and C_4 are parts of a coupling capacitor to provide tapping for voltage measurement. L_1 is a series-tuning coil. L_2 and C_2 form a parallel-tuned circuit and connected to the primary of the isolating transformer. This isolating transformer is used for impedance matching. The parallel tuned circuit provides a high impedance path to high frequency signals and low impedance path to 50 Hz voltage of the line. The carrier equipment is connected across this parallel tuned circuit. L_3 and C_3 is also a parallel tuned circuit known as a line trap which provides low impedance at 50 Hz and high impedance at carrier frequencies to avoid short circuiting of the carrier signals through low impedance of the bus bar capacitance. The complete circuit of a phase-to-phase coupling is shown in Figure 3.2. Figure 'a' shows layout of the coupling equipment. Figure 'b' shows the actual circuit. Figure 'c' shows the derived equivalent circuit assuming that the bus bar capacitance is effectively an high frequency short-circuit.

It can be seen that this circuit has the form of a π-section band-pass filter, the band is fairly wide as shown in Figure 3.3. The frequency band is selected by varying line-trap capacitance C_3, series inductance L_1 and L_2, C_2 of a parallel tuned circuit. Using values of line trap inductance of 200 µH and an h.v. capacitance of 2000 pF,

42

the bands used on 132 kV and 275 kV are shown below:

Band	Mid-band frequency kHz	Band Width kHz
A	95	82-110
B	140	110-180
C	200	145-255
D	340	194-600
E	180	90-132
F	152	116-196

In the case of a 400 kV system, using line-trap inductance of 100 uH and coupling capacitor of 2000 pF, the bands are shown as below:

Band	Mid-band frequency kHz	Band width kHz
1	75.5	70-81
2	87.5	80-95
3	99.5	90-110
4	112	100-125
5	125	110-140
6	138	120-158
7	151	130-175
8	179	150-214
9	225	180-280
10	353	250-500

3.1.4 <u>Design principle of the coupling equipment</u>

<u>3.1.4.1 132 kV and 275 kV systems</u>: Upto 275 kV systems, bus bar capacitance can be assumed as a short circuit at high frequencies and can be based upon the filter theory. The equivalent circuit is as shown in Figure 3.4. R_O is the line characteristic-impedance. If the line characteristic-impedance is matched with the carrier transmitter impedance, then the transmitter impedance is also R_O. Two shunt tuning circuits and one series tuning circuit have the same resonant frequency, f_O (angular frequency, w_O) which is also a mid-band frequency. C_S and L are fixed values of the coupling capacitor and the line trap inductance. C_S is half the value of the coupling capacitor and L is twice the value of the line trap inductane due to phase-to-phase coupling. The mid-band frequency is varied by the shunt capacitors C and the series tuning coil L_1. L_1 is twice of the value of the inductance of the series tuning coil. For correct matching,

$$R_O = (L_1)^{1/2} / 2C \qquad (3.1)$$

$$\text{but} \quad w_O^2 = 1/L_1 C_S = 1/L C \qquad (3.2)$$

$$\text{hence } R_O = (1/w_O^2 C_S)^{1/2} \times w_O^2 L/2 = (L)^{1/2} /2 C_S \quad (3.3)$$

For 132 kV and 275 kV systems, R_O is equal to 450 Ohm if line trap inductance is 200 μH and coupling capacitor is 2000 pF.

Now it can be shown that

$$\text{Bandwidth} \quad f = 1 /\pi (2 L_1 C)^{1/2} \quad\quad\quad (3.4)$$

$$\text{or} \quad f = \pi f_o^2 \sqrt{2LC_s} \quad\quad\quad (3.5)$$

It is also known that $\quad f = f_2 - f_1$

and $f_o = \sqrt{f_1 f_2}$ \quad\quad\quad\quad\quad\quad\quad\quad\quad (3.6)

The frequency bands obtained have been listed earlier.

3.1.4.2 **400 kV equipment** :In this system, bus bar capacitance is taken into account. The circuit arrangement and the equivalent circuit are shown in figures 'a' and 'b' of Figure 3.5. Now the line-trap and the bus bar capacitance (total impedance Z_T) are considered in terms of controlled loss on the coupling equipment.
It can be seen that the coupling filter is an L section band pass, and Z_T varies according to frequency and the bus bar capacitance.
In order to study the effect of the bus bar capacitance which may cause high attenuation peaks in the the pass band, a simple arrangement has been shown in Figure 3.6, ignoring attenuation of the coupling filter in the pass band.
Frequency response of a parallel tuned circuit for resistance R_T and reactance X_T has been shown in Figure 3.7.

45

In the pass band of the equipment, the reactive component of the line trap may resonant with the capacitance of the bus bars which varies over a wide range depending on particular switching conditions. Such resonance is a series resonance and if the circuit is a low loss circuit, the resulting value of the resistance R_T across the line impedance R_O is low and loss of power can be found considerable.

To avoid such a situation, a damping is provided in the line trap delibrately so that the resistive component is always relatively high in the pass band. If series resonance takes place, the resulting resistance across the line is sufficiently high to limit the loss of power to an acceptable level e.g. fifty percent reduction in power input to the line. This is a reason for considering bus bar capacitance and line trap as a controlled insertion loss rather than an integral element of the filter.

If a 50 percent power loss is assumed, insertion resistance of the line trap can be expressed in terms of the line impedance as below using a simple circuit shown in Figure 3.8:

h.f.voltage on the line without considering R_T is

$$V_1 = E/2 \qquad\qquad (3.7)$$

The voltage on the line with R_T is

$$V_2 = [E/2] \, R_T / \, (R_T + R_O/2 \,) \qquad\qquad (3.8)$$

46

Ratio of Powers $= 1/2 = (V_2/V_1)^2$ (3.9)

$V_2/V_1 = 1/\sqrt{2}$ (3.10)

$[E/2 . R_T/ (R_T + 1/2 R_O)]/ (E/2) = 1/\sqrt{2} = R_T/ (R_T + (R_O/2))$ (3.11)

So $R_T = 1.24 R_O$ (3.12)

This represents a lower limit of R_T. The higher value can be decided on the basis of the bandwidth. It can be shown that that the maximum bandwidth is available when $R_T = 2$ times the lower limit i.e. 2.48 R_O. If R_T is more or less than the optimum value, bandwith may be lost as shown in Figure 3.9.

Using the optimum value of this R_T the bandwidth available for phase to phase coupling can be expressed as

$f = 2 \pi f_O L/ R_T$ (3.13)

where L is the inductance of the line trap

$R_T = 1.24 R_O$ (3.14)

R_O = Characteristic impedance of the line

also $f = f_2 - f_1$ (3.15)

and $f_O = \sqrt{f_1 f_2}$ (3.16)

47

With a view to increase the bandwidth, additional damping can be provided by adding another series resonant circuit tuned to f_o and the damping resistance as shown in Figure 3.10.

With this arrangement, the bandwith can be increased to twice the earlier value with simple damping line trap as shown in Figure 3.11.

The bandwidth so obtained is normally smaller than the bandwidth obtained with the filter theory applied for 132 kV and 275 kV systems.

Manufactured Data

Manufactured data of the Power Carrier System of the Westinghouse Electric Corporation, USA are described in Appendix A for reference purposes. These include data of the line traps, the coupling capacitor, the line tuner, the drain coil, the coaxial cable and the power line characteristics.

3.1.5 Design of the stack tuner for protection applications

As shown in Figure 3.12, the basic circuit arrangement consists of three parts: (1) series resonance low impedance path as a short circuit, (2) directional detector (dd) switch (as described in Chapter 2.4) in close mode as a short circuit to provide low impedance path to the primary of the output transformer, (3) a parallel resonance high impedance path as an open mode when dd switch is open. With reference to Figure 3.13, the coupling capacitor CS is

48

assumed to be fixed. For series resonance of a selected mid band frequency f_o, the parameters: series inductance CL for case (1), quality factor Q_c of the coil, equivalent resistance RS can be evaluated in a sequence. Another resistance RSP is evaluated based on the stack tuner close mode gain. The typical value of the close mode gain is assumed to be 90 percent. The 'gain' has been defined earlier in Figure 2.7 as the tuner output voltage divided by the line to earth voltage. In this case, RS represents the component loss of the main coil CL and RSP represents the primary impedance of the transformer for the output voltage in the short mode. For case (2), the dd switch provides low impedance to the primary of the output transformer when closed. For case (3), a parallel tuned circuit tuned to mid band frequency f_o provides high impedance to the primary of the output transformer when dd switch is opened. The capacitor CP is assumed equal to the capacitor CS. Similarly, the inductance CLP is assumed equal to the inductance CL. Now quality factor of the coil, Q_c for a parallel tuned circuit can be evaluated. Knowing Q_c, a parallel equivalent resistance, RP, is evaluated. With a view to match the output impedance with the input impedance in the open mode, it is necessary to provide an equivalent resistance RS1 = RP as shown in Figure 3.13. Finally, in order to provide minimum circuit resistance in the short circuit mode, the switch S (operated by a directional detector dd as referred earlier) is arranged to short circuit the parallel resonance circuit and the resistance RS1.

3.1.6 Digital simulation of the stack tuner

The equivalent circuit of the stack tuner in close mode is shown in Figure 3.14. This shows impedance of the circuit, YTSM (with reference to line). Total input voltage V_{IN} across YTSM and impedance YSM proportional to output voltage V_{OUT} are also shown. Now gain can be simulated as below:

$$\text{GAIN} = V_{OUT}/V_{IN} = YSM/YTSM \qquad (3.17)$$

(absolute value for frequency response)
GAIN in close mode is referred as YNC

$$\text{so, YNC} = (YSM/YTSM) \qquad (3.18)$$

(absolute value for frequency response)
Similarly, equivalent circuit in open mode is shown in Figure 3.15. This shows total impedance YTM, voltage V_{IN}. Output voltage V_{OUT} is also shown. Now gain can be evaluated as below:

$$\text{GAIN} = V_{OUT}/V_{IN} = (YOM/YTM) \qquad (3.19)$$

(absolute value for frequency response)
Gain in open mode is referred as YNO

$$\text{so, YNO} = (YOM/YTM) \qquad (3.20)$$

50

(absolute value for frequency response)

YNC = close mode gain

YNO = open mode gain

YTSM = close mode impedance

YTM = open mode impedance

3.1.7 Frequency response of the stack tuner

Based on the design method, the stack tuner has been designed for different mid band frequencies: 300 ± 2.5 kHz, 200 ± 2.5 kHz, 100 ± 2.5 kHz, 200 ± 100 kHz, 50 ± 40 kHz. For each mid band frequency, the stack tuner has been digitally simulated and the frequency responses for (1) open mode gain YNO, (2) open mode impedance YTM, (3) close mode gain YNC, (4) close mode impedance YTSM are plotted in the frequency range from 1 to 600 kHz. Figure 3.16 shows 'voltage gain' versus frequency response in the open mode and the close mode of the stack tuner (reference Chapter 2). Figure 3.17 shows the open mode impedance versus frequency response of the stack tuner for mid frequencies of 300±2.5 kHz, 200±2.5 kHz, 100±2.5 kHz. Figure 3.18 shows the close mode impedance versus frequency response of the stack tuner for mid frequencies of 300±2.5 kHz, 200±2.5 kHz, 100±2.5 kHz. Figure 3.19 shows impedance versus frequency response in the open mode and the close mode of the stack tuner for mid frequencies of 200±100 kHz and 50±40 kHz. Frequency response characteristics have been found to be excellent as desired for the satisfactory performance of the whole scheme. The close mode gain has

been found to be 0.9. The open mode gain has been found to be 0.5. These values of the voltage gain can be varied subject to selection of the components and the design requirements. Simulated values for a case of mid frequency of 300 ± 2.5 kHz tuner are shown in Appendix B.

3.2 Digital simulation of the transmission line

3.2.1. Basic theoretical concept

A system voltage steady state equation can be expressed as

$$\frac{d^2 \bar{V}}{dx^2} = ZY\bar{V} \tag{3.21}$$

Based on the theory of natural mode developed by Wedepohl [49] , a solution to Equation 3.21 can be transformed into a number of independent differential eqations of the form:

$$\bar{V} = \exp(-\Phi x)\bar{V}_i + \exp(\Phi x)\bar{V}_r \tag{3.22}$$

where $\Phi = Q \Gamma Q^{-1}$

Using a method of matrix transformation leading to diagonalisation, it is easy to calculate the surge impedance and hyperbolic functions, e.g.:

$$Z_O = Q \, \Gamma^{-1} \, Q^{-1} \, Z \tag{3.23}$$

and $\cosh (\Phi x) = Q \cosh (\Gamma x) \, Q^{-1}$ (3.24)

3.2.2 <u>Selection for a two port transfer matrix representation or a two-port nodal admittance matrix:</u>

A faulted transmission system up to the fault point(distance x from the fault point) can be represented by the two port matrix formation as shown in Figure 3.20 either impedance matrix (A_1, B_1, C_1, D_1) as in Equation 3.25 or the admittance matrix $(A_{y1}, -B_{y1}, B_{y1}, -A_{y1})$ as in Equation 3.26.

$$\begin{bmatrix} \bar{V}_S \\ \bar{I}_S \end{bmatrix} = \begin{bmatrix} A_1 & B_1 \\ C_1 & D_1 \end{bmatrix} \begin{bmatrix} \bar{E}_{fS} \\ \bar{I}_{fS} \end{bmatrix} \tag{3.25}$$

where $A_1 = \cosh (\Phi x)$ $B_1 = \sinh (\Phi x) Z_O$

   $C_1 = Y_O \sinh(\Phi x)$

   $D_1 = Y_O \cosh(\Phi x) Z_O$, and

   $\Phi = Q \, \Gamma \, Q^{-1}$

$$\begin{bmatrix} \bar{I}_S \\ \bar{I}_{fS} \end{bmatrix} = \begin{bmatrix} A_{y1} & -B_{y1} \\ B_{y1} & -A_{y1} \end{bmatrix} \begin{bmatrix} \bar{V}_S \\ \bar{E}_{fS} \end{bmatrix} \tag{3.26}$$

where $A_{y1} = Y_O \coth(\Phi x)$

   $B_{y1} = Y_O \operatorname{cosech}(\Phi x)$

   $Y_O = [Z]^{-1} \, Q \, \Gamma \, Q^{-1}$

One main advantage of Equation 3.25 is that if the transmission system has different sections, it is easy to calculate voltage or currents at either end of the line simply by process of multiplication of the matrices e.g.:

$$\begin{bmatrix} \bar{V}_S \\ \bar{I}_S \end{bmatrix} = \begin{bmatrix} A_1 & B_1 \\ C_1 & D_1 \end{bmatrix} \begin{bmatrix} A_f & B_f \\ C_f & D_f \end{bmatrix} \begin{bmatrix} A_2 & B_2 \\ C_2 & D_2 \end{bmatrix} \begin{bmatrix} \bar{V}_R \\ \bar{I}_R \end{bmatrix} \qquad (3.27)$$

But, when dealing with the network impedances or admittances matrix, this form may not be very useful. The other difficulty can arise because of overflow during the evoluation of $(e^{\Phi x})$ in cosh Φx and sinh Φx at higher frequencies. Since these difficulties are avoided in nodal admittance matrix, this particular method has been chosen for this thesis.

3.2.3 Fault transient modelling

Consider a single phase transmission line as shown in Figure 3.21 having a fault at point (F) and two end sources P and Q.

By using the theory of superimposition, the fault can be considered as a voltage generator equal and opposite to the steady-state voltage at the instant of the fault inception, t = 0. It can be represented as:

$$v_f(t) = v_{fs}(t) + v_{ff}(t) \qquad (3.28)$$

54

where $v_f(t)$ is the total voltage at point F. $v_{fs}(t)$ is prefault steady state voltage and $v_{ff}(t)$ is the superimposed voltage in the time domain.

$$v_{ff}(t) = 0 \ , \ t < 0$$
$$= -v_{fs}(t) \ , \qquad t \geq 0 \qquad\qquad (3.29)$$

In general, the prefault steady state voltage at the fault point can be expressed as

$$v_{fs}(t) = \hat{V}_{fs} \cdot \sin(w_o t + \Theta_{fs}) \qquad\qquad (3.30)$$

where the phase angle Θ_{fs} determine the point-on-the prefault waveform of the steady state voltage at which the fault occurs. The voltage $v_{ff}(t)$ can be assumed to exist in an unenergised system. By using the Heavyside Theorem, it can be expressed as:

$$v_{ff}(t) = -\hat{V}_{fs} \sin(w_o t + \Theta_{fs}) h(t) \qquad\qquad (3.31)$$

or $v_{ff}(t) = -\hat{V}_{fs}(\sin w_o t \cos \Theta_{fs} + \cos w_o t \sin \Theta_{fs}) h(t)$

$$\qquad\qquad (3.32)$$

Now, by applying the Laplace Transform, Equation 3.32 becomes:

$$v_{ff}(s) = -\hat{V}_{fs} \frac{w_o \cos \Theta_{fs}}{s^2 + w_o^2} + \frac{s \sin \Theta_{fs}}{s^2 + w_o^2} \qquad\qquad (3.33)$$

This is the basic form of equation which is responsible for the fault transient modelling and has been used in this work.

3.2.4 Frequency spectrum

Now, reconsider Equation 3.33 as $v_{ff}(t)$ is finite for the condition $t \geq 0$, and can be written as:

$$\tilde{V}_{ff}(jw) = \tilde{V}_{ff}(s) \qquad (3.34)$$

$$\text{if } s = jw$$

$$\text{or } \tilde{V}_{ff}(jw) = \hat{V}_{fs}\frac{w_o \cos \Theta_{fs}}{w^2 - w_o^2} + \frac{jw \sin \Theta_{fs}}{w^2 - w_o^2} \qquad (3.35)$$

This represents a continuous function of frequency. The full spectrum is carried out through a Fast Fourier Transform Routine.

3.2.5 Determination of the time varying components

With a view to determine the time varying voltage, the Inverse Fourier Transform may be used. The total superimposed voltage can be expressed as;

$$v_{ff}(t) = 1/2 \int_{-\infty}^{\infty} \tilde{V}_{ff}(jw) e^{jwt} \, dw \qquad (3.36)$$

Now, substituting value of $\tilde{V}_{ff}(jw)$ from Equation 3.35 to Equation 3.36 and can be written as:

$$v_{ff}(t) = 1/2\pi \int_{-\infty}^{\infty} \frac{w_o \cos \Theta_{fs} + jw \sin \Theta_{fs} \, e^{jwt} \, dw}{(w^2 - w_o^2)} \qquad (3.37)$$

56

Earlier it has been seen [49] that these time varying components are not readily available as divergence occurs and leads to distortion. However, it has been found that a satisfactory result can be obtained using a Modified Fourier Transform Technique and can be expressed as:

$$f(t) = REAL \frac{e^{\alpha t}}{\pi} \int_0^\Omega f(w - j\alpha) e^{jwt} \sigma \, dw \qquad (3.38)$$

The finite range of integration gives rise to Gibbs Oscillation, and this can be overcome by introducing the factor

$$\sigma = \sin(\pi w/\Omega)/(\pi w/\Omega) \qquad (3.39)$$

In addition, a frequency shift constant 'α' is introduced to ensure numerical stability when the integral is evaluated digitally. Ω is truncation frequency.

3.2.6. Steady state calculation

Pre-fault voltages and currents can be related by

$$\begin{bmatrix} \bar{V}_{Ss} \\ \bar{I}_{Ss} \end{bmatrix} = \begin{bmatrix} A_1 & B_1 \\ C_1 & D_1 \end{bmatrix} \begin{bmatrix} A_2 & B_2 \\ C_2 & D_2 \end{bmatrix} \begin{bmatrix} \bar{V}_{Rs} \\ \bar{I}_{Rs} \end{bmatrix} = \begin{bmatrix} A & B \\ C & D \end{bmatrix} \begin{bmatrix} \bar{V}_{Rs} \\ \bar{I}_{Rs} \end{bmatrix}$$

$$(3.40)$$

The sending end current before the fault is given by

57

$$\bar{I}_{Ss} = [C - D B^{-1} A] [\bar{V}_{Rs}] + D B \bar{V}_{Ss} \qquad (3.41)$$

and, the steady state value $\dot{V}_{fs}$ is given by

$$\bar{V}_{fs} = [A_2 - B_2 B^{-1} A] \bar{V}_{Rs} + B_2 B^{-1} \bar{V}_{Ss} \qquad (3.42)$$

Solution for the above equations is obtained at power frequency. The voltages and currents are calculated in the phaser form and converted directly in the time domain. It does not involve inverse transform.

3.2.7. Analysis of superimposed voltages for internal faults

Considering the homogeneous sections of the transmission line in Figure 3.22, the following equations can be written as:

$$\begin{bmatrix} \bar{I}_{Sf} \\ \bar{I}_{fSf} \end{bmatrix} = \begin{bmatrix} A_{y1} & -B_{y1} \\ B_{y1} & -A_{y1} \end{bmatrix} \begin{bmatrix} \bar{V}_{Sf} \\ \bar{E}_{ff} \end{bmatrix} \qquad (3.43)$$

and

$$\begin{bmatrix} \bar{I}_{fRf} \\ \bar{I}_{Rf} \end{bmatrix} = \begin{bmatrix} A_{y2} & -B_{y2} \\ B_{y2} & -A_{y2} \end{bmatrix} \begin{bmatrix} \bar{E}_{ff} \\ \bar{V}_{Rf} \end{bmatrix} \qquad (3.44)$$

Considering Equation 3.43 :

$$\bar{I}_{Sf} = A_{y1} \bar{V}_{Sf} - BY1 \bar{E}_{ff} \qquad (3.45)$$

and,

58

$$\bar{I}_{fSf} = B_{y1} \, \bar{V}_{Sf} - A_{y1} \, \bar{E}_{ff} \tag{3.46}$$

$$\bar{V}_{Sf} = -Z_{SS} \, \bar{I}_{Sf} \tag{3.47}$$

using Equation 3.47 and Equation 3.45

$$[Z_{SS}^{-1} + A_{y1}] \, \bar{V}_{Sf} = B_{y1} \, \bar{E}_{ff} \tag{3.48}$$

using Equation 3.48 and Equation 3.46

$$\bar{E}_{ff} = [\, B_{y1} \, \{ (Z_{SS}^{-1}) + A_{y1} \}^{-1} B_{y1} - A_{y1} \,]^{-1} \cdot \bar{I}_{fSf} \tag{3.49}$$

now, considering the section from the fault location to the receiving end, a relationship between $\bar{I}_{fRf}$ and $\bar{E}_{ff}$ can be obtained:

using Equation 3.44

$$\bar{I}_{fRf} = A_{y2} \, \bar{E}_{ff} - B_{y2} \, \bar{V}_{Rf} \tag{3.50}$$

$$\bar{I}_{Rf} = B_{y2} \, \bar{E}_{ff} - A_{y2} \, \bar{V}_{Rf} \tag{3.51}$$

but,

$$\bar{V}_{Rf} = Z_{SR} \cdot \bar{I}_{Rf} \tag{3.52}$$

using Equation 3.52 and Equation 3.51

$$[(Z_{SR})^{-1} + A_{y2}] \, \bar{V}_{Rf} = B_{y2} \cdot \bar{E}_{ff} \tag{3.53}$$

59

now, using Equation 3.53 and Equation 3.50

$$\bar{E}_{ff} = [\ A_{y2} - B_{y2} \ \{ \ (Z_{SR})^{-1} + A_{y2}\}^{-1} \ B_{y2}]^{-1} . \ \bar{I}_{fRf} \qquad (3.54)$$

Considering any general earth fault at the fault location, the following relationship can be deduced:

$$\bar{E}_{ff} = \bar{V}_{ff} + Rf [\ \bar{I}_{fSf} - \bar{I}_{fRf} \ ] \qquad (3.55)$$

where Rf is a diagonal matrix representing the fault resistance in each phase.

now, using Equation 3.54 and Equation 3.49

$$[\ \bar{I}_{fSf} - \bar{I}_{fRf} \ ] = [\{ \ B_{y1}(Z_{SS}^{-1} + A_{y1})^{-1} . B_{y1} - A_{y1}\} -$$
$$\{ \ A_{y2} - B_{y2} \ ((Z_{SR})^{-1} + A_{y2})^{-1} \ B_{y2} \ \} \ ]. \ \bar{E}_{ff}$$
$$(3.56)$$

Finally, substituting Equation 3.56 into Equation 3.55 :

$$\bar{V}_{ff} = [\ \{ \ (\ B_{y1} \ (\ Z_{SS}^{-1} + A_{y1})^{-1} \ B_{y1} - A_{y1} \ ) -$$
$$(\ A_{y2} - B_{y2} \ ((Z_{SR})^{-1} + A_{y2})^{-1} \ B_{y2} \ ) \ \} - Rf \ ] \ .$$
$$[\ \bar{I}_{fSf} - \bar{I}_{fRf} \ ] \qquad (3.57)$$

3.2.8. <u>Evaluation of superimposed voltages currents at the</u>
       <u>relaying points</u>

When the relay is located at the sending end, voltage $\bar{V}_{Sf}$
and current $\bar{I}_{Sf}$ can be evaluated as follows : using

60

Equation 3.48

$$\bar{V}_{Sf} = [(Z_{SS}^{-1}) + A_{y1}]^{-1} B_{y1} \bar{E}_{ff} \qquad (3.58)$$

substituing this equation in Equation 3.45

$$\bar{I}_{Sf} = [A_{y1} \{ (Z_{SS}^{-1}) + A_{y1} \}^{-1} B_{y1} - B_{y1}] . \bar{E}_{ff} \quad (3.59)$$

Similarly, when the relay is located at the receiving end, voltage $\bar{V}_{Rf}$ and current $\bar{I}_{Rf}$ can be evaluated as follows : using Equation 3.53

$$\bar{V}_{Rf} = [(Z_{SR}^{-1}) + A_{y2}]^{-1} . B_{y2} \bar{E}_{ff} \qquad (3.60)$$

substituing this equation in Equation 3.51

$$\bar{I}_{Rf} = [B_{y2} - A_{y2} \{ (Z_{SR}^{-1}) + A_{y2} \}^{-1} . B_{y2}] . \bar{E}_{ff} \qquad (3.61)$$

3.2.9 <u>Analysis of main source network models</u>:

The digital simulation for the main source is based upon selecting the short-circuit level arbitrarily at the terminating bus bars. Neglecting any capacitance effect, a simplified model (see Figure 3.23) has been used as follows:

$$\bar{E}_{Sa} = \bar{I}_{Sa} . Z_{S1} + (\bar{I}_{Sa} + \bar{I}_{Sb} + \bar{I}_{Sc}) . Z_{Sn} + V_{Sa} \qquad (3.62)$$

$$\text{or } \bar{E}_{Sa} = \bar{I}_{Sa} . (Z_{S1} + Z_{Sn}) + \bar{I}_{Sb} . Z_{Sn} + \bar{I}_{Sc} . Z_{Sn} + V_{Sa} \qquad (3.63)$$

similarly,

$$\bar{E}_{Sb} = \bar{I}_{Sa} \cdot Z_{Sn} + \bar{I}_{Sb}(Z_{S1} + Z_{Sn}) + \bar{I}_{Sc} \cdot Z_{Sn} + \bar{V}_{Sb} \qquad (3.64)$$

$$\bar{E}_{Sc} = \bar{I}_{Sa} \cdot Z_{Sn} + \bar{I}_{Sb} \cdot Z_{Sn} + \bar{I}_{Sc} \cdot (Z_{S1} + Z_{Sn}) + \bar{V}_{Sc} \qquad (3.65)$$

In matrix form,

$$
\begin{bmatrix} \bar{I}_{Sa} \\ \bar{I}_{Sb} \\ \bar{I}_{Sc} \end{bmatrix}
=
\begin{bmatrix} (Z_{S1} + Z_n) & Z_{Sn} & Z_{Sn} \\ Z_{Sn} & (Z_{S1} + Z_{Sn}) & Z_{Sn} \\ Z_{Sn} & Z_{Sn} & (Z_{S1} + Z_{Sn}) \end{bmatrix}
\begin{bmatrix} \bar{V}_{Sa} \\ \bar{V}_{Sb} \\ \bar{V}_{Sc} \end{bmatrix}
\qquad (3.66)
$$

In a general form, it can be stated as:

$$
\begin{bmatrix} \bar{E}_S \\ \bar{I}_S \end{bmatrix}
=
\begin{bmatrix} U & Z_{SS} \\ 0 & U \end{bmatrix}
\begin{bmatrix} \bar{V}_S \\ \bar{I}_S \end{bmatrix}
\qquad (3.67)
$$

Where $[Z_{SS}]$ is the source impedance matrix of diagonal elements $(Z_{S1} + Z_{Sn})$ and off-diagonal elements of (Z_{Sn}). These elements are calculated as:

$$SCL = 3. |V_L| \cdot I_{sc} = \frac{\sqrt{3} \; |V_L|^2}{\sqrt{3} \; |Z_{S1}|}$$

$$\text{or } Z_{S1} = |V_L|^2 / SCL \qquad (3.68)$$

But,

62

$$Z_{S1} = R_{S1} + jwL_{S1} = R_{S1} + j X_{S1} \qquad (3.69)$$

By knowing the X/R ratio of the sending and receiving end sources at power frequency, elements of Equation 3.68 can be found out. This ratio is of the order of 30-300.

The neutral source impedance (Z_{Sn}) is calculated using both positive phase sequence (Z_{S1}) and zero phase sequence (Z_{S0}) impedances for the circuit of Figure 3.23, where

$$Z_{S0} = Z_{S1} + 3 Z_{Sn}$$

Hence, $Z_{Sn} = Z_{S1} \{ (Z_{S0}/Z_{S1}) - 1 \}/3 \qquad (3.70)$

Various parameters like short circuit level (SCL), (X/R) ratio at power frequency, (Z_{S0}/Z_{S1}) ratio, system line voltage V_L are input data for the computer program and used for this simulation.

3.2.10. Fault-simulation studies

For simulating and studying the high frequency transients, a 400 kV, 3-phase (a, b, c) 100 km long transmission line with sources of 5 GVA at the sending end (SE) and 20 GVA at the receiving end (RE) has been considered. A phase to earth fault has been considered in the phase-a at a distance of 50 km from the SE and the fault induced transients have been studied in the faulted phase-a and the healthy phases b and c. The data for the vertical configuration of the conductors (shown in Figure 3.24) are:

1) phase conductors 4 x 54/7/0.33 cm with 0.305 m bundle spacing, 2) earth wire 54/7/0.33 cm, 3) earth resistivity 100 Ohm meter. The phase angle which determine the fault at the pre-fault waveform is 90 degree. The frequency shift constant 'α'(reference Equation 3.38) has been critically adjusted to a value of 1000 to get satisfactory waveforms. In the present study, the sampling frequency (SF) of 819.2 kHz has been used. The fault observation time is 5 msec with the number of samples of 4096. The fault observation time of 5 msec is appropriate for the present study as most transients die in this period.

Figure 3.25 and Figure 3.26 show the fault responses in the faulted phase a and the healthy phases b and c with the sampling frequency of 6.4 kHz at the sending end (SE) and the receiving end (RE). Figure 3.27 and Figure 3.28 show the responses with 819.2 kHz of the sampling frequency. The pre-fault time is only 10 micro-seconds which is not visible in the fault response of 5 msec. A delay of about 0.18 msec is clearly shown in Figure 3.25 to Figure 3.28. This delay can be confirmed due to the travelling time of the fault induced travelling waves. Assuming the speed of the travelling wave is nearly same as the speed of the light i.e. 300 km per second, then the time taken by the travelling wave to travel a distance of 50 km is about 0.17 msec. Figure 3.27 and Figure 3.28 indicate clearly the high frequency components which are not visible in Figure 3.25 and Figure 3.26. The fault induced transients can be seen in all the phases. The peak value of the transients in the faulted phase has been found to be about twice the

peak value of the transients in the healthy phases.

3.3 <u>Digital simulation of stack tuner with transmission line</u>

When sources are earthed at the two ends of the transmission line, the source impedance can be considered in parallel with the stack-tuner impedance. The arrangement of the transmission line, the end sources, and the stack-tuner has been shown in Figure 3.29. A technique for digital simulation of the end sources is explained in Section 3.2.

Admittance matrix for stack tuner circuit Y_{ST} can be written as:

$$\begin{bmatrix} Y_{ST} & 0 & 0 \\ 0 & Y_{ST} & 0 \\ 0 & 0 & Y_{ST} \end{bmatrix} \qquad (3.71)$$

Y_{ST} = 1/YTSM for close mode (reference Chapter 3.1.7)

Y_{ST} = 1/YTM for open mode (reference Chapter 3.1.7)

where YTSM and YTM are short mode and open mode impedances of the stack tuner.

If Y_{S1} = 1 / Z_{S1} and Y_{Sn} = 1 / Z_{Sn} in Equation 3.66,

the admittance matrix for the source can be written as:

$$
\begin{bmatrix}
(Y_{Sn1}) & Y_{Sn} & Y_{Sn} \\
Y_{Sn} & (Y_{Sn1}) & Y_{Sn} \\
Y_{Sn} & Y_{Sn} & (Y_{Sn1})
\end{bmatrix}
\tag{3.72}
$$

where $Y_{Sn1} = \dfrac{Y_{S1} \cdot Y_{Sn}}{Y_{S1} + Y_{Sn}}$

Since source and stack tuner have been assumed in parallel for the digital simulation purposes, elements of both matrices can be added for the combined admittance purpose shown as below:

$$
\begin{bmatrix}
(Y_{Sn1}+Y_{ST}) & Y_{Sn} & Y_{Sn} \\
Y_{Sn} & (Y_{Sn1}+Y_{ST}) & Y_{Sn} \\
Y_{Sn} & Y_{Sn} & (Y_{Sn1}+Y_{ST})
\end{bmatrix}
\tag{3.73}
$$

If $(Y_{Sn1}+Y_{ST}) = Y_{TT}$ as total admittance, the above matrix can be written as below:

$$
\begin{bmatrix}
Y_{TT} & Y_{Sn} & Y_{Sn} \\
Y_{Sn} & Y_{TT} & Y_{Sn} \\
Y_{Sn} & Y_{Sn} & Y_{TT}
\end{bmatrix}
\tag{3.74}
$$

Now inverting all the elements of this matrix, impedance matrix can be re-written as:

$$
\begin{bmatrix}
Z_{TT} & Z_{Sn} & Z_{Sn} \\
Z_{Sn} & Z_{TT} & Z_{Sn} \\
Z_{Sn} & Z_{Sn} & Z_{TT}
\end{bmatrix}
\tag{3.75}
$$

Equation 3.66 can be re-written as:

$$
\begin{bmatrix}
\bar{I}_{Sa} \\
\bar{I}_{Sb} \\
\bar{I}_{Sc}
\end{bmatrix}
\begin{bmatrix}
Z_{TT} & Z_{Sn} & Z_{Sn} \\
Z_{Sn} & Z_{TT} & Z_{Sn} \\
Z_{Sn} & Z_{Sn} & Z_{TT}
\end{bmatrix}
\begin{bmatrix}
\bar{V}_{Sa} \\
\bar{V}_{Sb} \\
\bar{V}_{Sc}
\end{bmatrix}
\tag{3.76}
$$

Now this source impedance matrix which includes the impedance of the stack tuner in close or open mode as the case may be, can be used as explained in Chapter 3.2.

3.3.1 <u>Fault simulation studies</u>

Figure 3.30 and Figure 3.31 are the transient responses with the tuned circuit at SE and RE respectively. When these responses are compared with the responses of Figure 3.27 and Figure 3.28, it can be seen that there is no difference in the waveforms. This study concludes that the stack tuner does not affect the fault induced transient responses and can be used successfully for detecting the high frequency components of the fault induced transients in a particular frequency bandwidth.

3.4 **Digital simulation of the bus bar capacitance and stack tuner with the transmission line**

When the bus bar to earth capacitance and the tuned circuit both are considered, the simplified arrangement can be shown as in Figure 3.32. When sources are earthed at the two ends of the transmission line, all the three circuits: the source, the tuned circuit and the bus bar to earth impedances can be considered in parallel. Alternatively, the admittances of all the three circuits can be added directly. Admittance matrix for the bus bar to earth admittance can be written as:

$$
\begin{bmatrix}
Y_{CB} & 0 & 0 \\
0 & Y_{CB} & 0 \\
0 & 0 & Y_{CB}
\end{bmatrix}
\tag{3.77}
$$

where Y_{CB} is bus bar to earth admittance.

The source admittance matrix considering the tuned circuit admittance and the bus bar to earth admittance can be written as below after combining all the three admittances i.e. matrices (3.73) and (3.77):

$$
\begin{bmatrix}
(Y_{Sn1} + Y_{ST} + Y_{CB}) & Y_{Sn} & Y_{Sn} \\
Y_{Sn} & (Y_{Sn1} + Y_{ST} + Y_{CB}) & Y_{Sn} \\
Y_{Sn} & Y_{Sn} & (Y_{Sn1} + Y_{ST} + Y_{CB})
\end{bmatrix}
\tag{3.78}
$$

If $(Y_{Sn1} + Y_{ST} + Y_{CB}) = Y_{TT}$ as total admittance, the above matrix is of the form of Matrix (3.74). Now inverting all the elements of this matrix, the impedance matrix is of the form of Matrix (3.75), and Equation (3.76) can be established.

3.41 <u>Simulated test results</u>

Figure 3.33 and Figure 3.34 show the transient responses with the tuner and the bus bar capacitance. A negligible amount of the phase shift has been noticed. The magnitude has been also affected but the effect is negligible. The transmission system and the fault location are same as in Section 3.2.10.

3.5 <u>Digital simulation of output of the stack tuner</u>

From Chapter 3.1.7, gain in closed mode, YNC is

$$YNC = V_{OUT} / V_{IN} = YSM / YTSM \qquad (3.79)$$

and gain in open mode, YNO is

$$YNO = V_{OUT} / V_{IN} = YOM / YTM \qquad (3.80)$$

YNC and YNO are in the 'phasor form'.
Voltages at the relaying points can be called as sending end (SE) and receiving end (RE) voltages. These are in two

components: (1) steady state, (2) superimposed. For pre
fault voltages, steady state voltage as simulated in
Equation (3.42) is multiplied by YNC for voltages in close
mode and by YNO for voltages in open mode. These can be
written as below:
For close mode,

$$\bar{V}_{fs}\text{new} = (\bar{V}_{fs}) \text{ YNC} \qquad\qquad (3.81)$$

For open mode,

$$\bar{V}_{fs}\text{new} = (\bar{V}_{fs}) \text{ YNO} \qquad\qquad (3.82)$$

For post fault calculations, only superimposed components
have been taken into account due to interest of high
frequency components. These are calculated using Equation
(3.52) at SE and Equation (3.62) at RE as below:
For close mode,

$$\bar{V}_{Sf}\text{newc} = (\bar{V}_{Sf}) \text{ YNC at SE} \qquad\qquad (3.83)$$

$$\bar{V}_{Rf}\text{newc} = (\bar{V}_{Rf}) \text{ YNC at RE} \qquad\qquad (3.84)$$

For open mode,

$$\bar{V}_{Sf}newo = (\bar{V}_{Sf}) \text{ YNO at SE} \tag{3.85}$$

$$\bar{V}_{Rf}newo = (\bar{V}_{Rf}) \text{ YNO at RE} \tag{3.86}$$

These evaluations are in frequency domain. The superimposed voltages in time domain are evaluated using Modified Fourier Transform Technique as given by Equation (3.38).
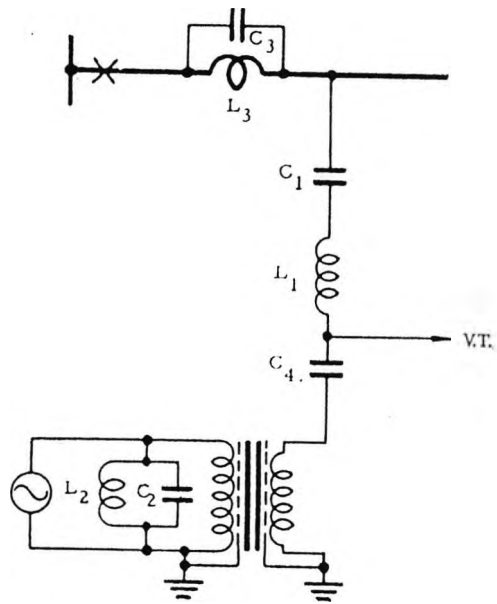
Figure 3.1 A CONVENTIONAL STACK TUNER
CIRCUIT
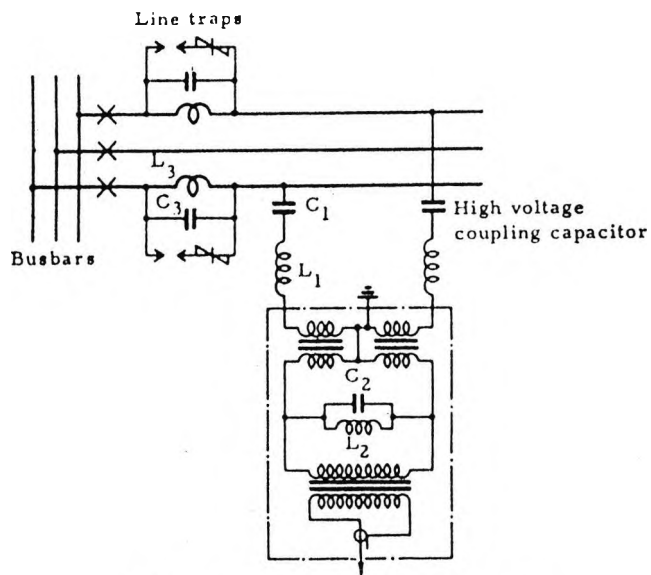
'a' Phase to phase coupling equipment
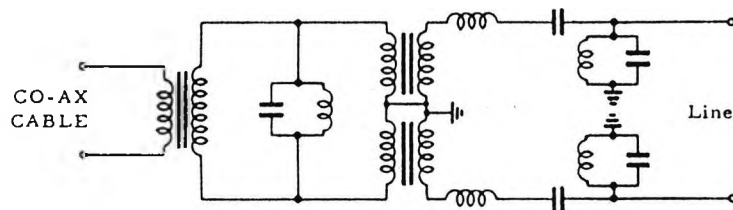
'b' Actual Circuit
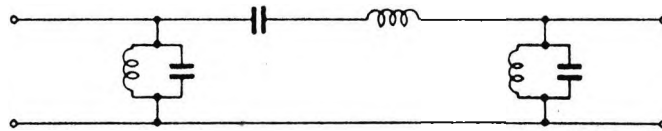
'c' Simplified Circuit

Figure 3.2 PHASE TO PHASE COUPLING EQUIPMENT REGARDED AS BAND PASS FILTER
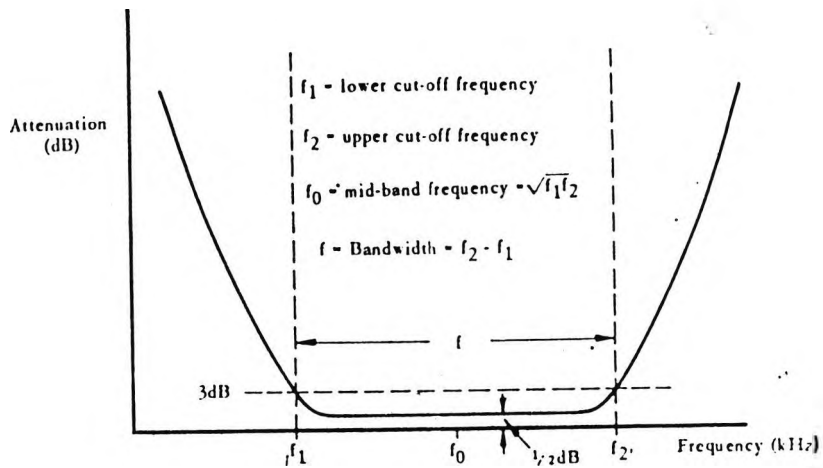
Figure 3.3 **WIDE BAND ARRANGEMENT IN A BAND PASS FILTER**
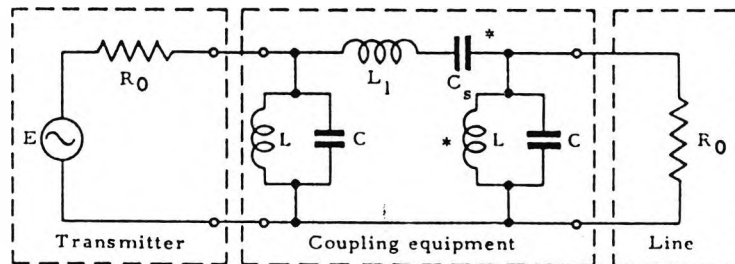
Figure 3.4 **EQUIVALENT CIRCUIT OF THE LINE UPTO 275 kV SYSTEM**

Trans-
mitter   Coupling equipment   Line trap and   Line
local busbar
impedance
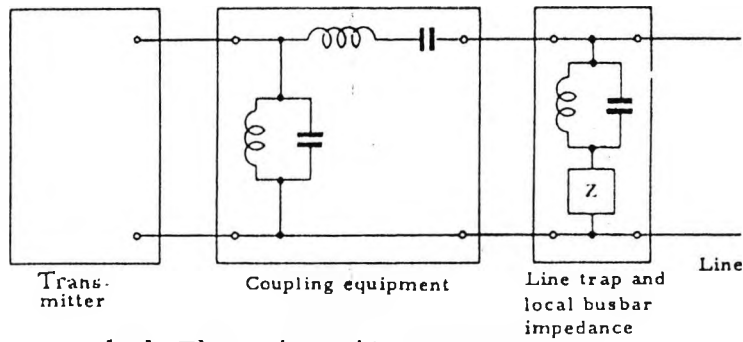
'a' The circuit arrangement

This can be shown as:

Transmitter   Coupling   Line trap   Line.
equipment   and local
busbar
impedance
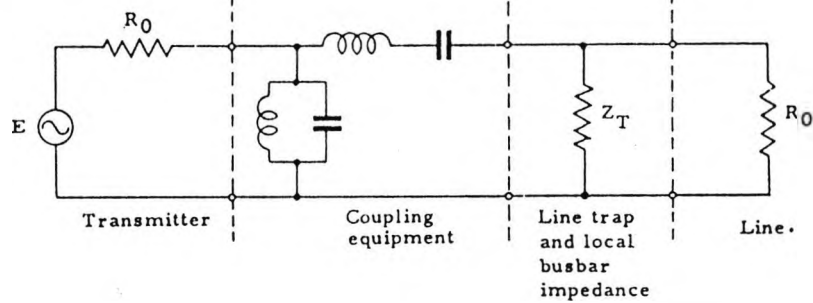
'b' The equivalent circuit

Figure 3.5 PHASE TO PHASE COUPLING FOR A
400 kV SYSTEM
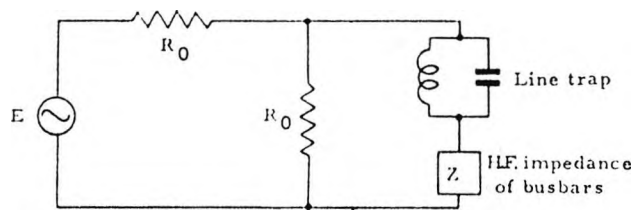
Figure 3.6 A SIMPLE ARRANGEMENT OF FIGURE 3.5
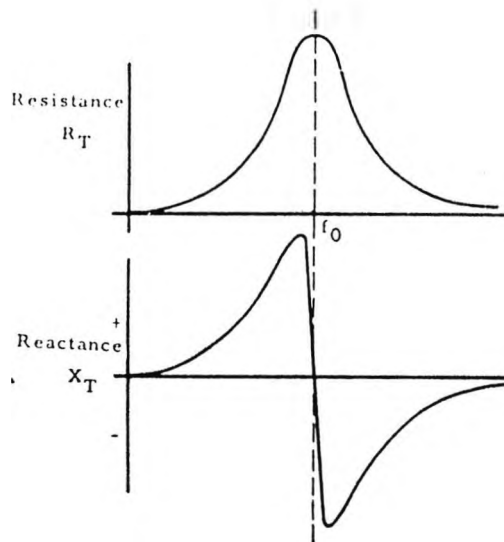
Figure 3.7 FREQUENCY RESPONSE OF A PARALLEL
TUNED CIRCUIT
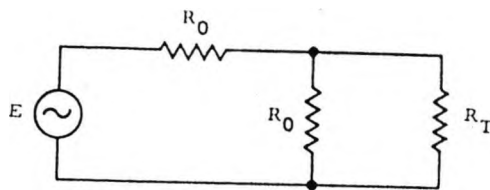
Figure 3.8 SIMPLIFIED CIRCUIT FOR CALCULATION OF R_T
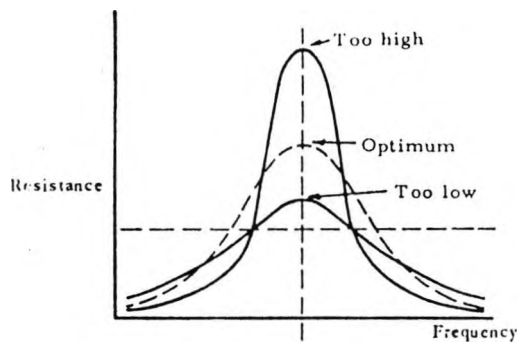
Figure 3.9 EFFECT OF R_T ON BANDWIDTH

Line trap   Damping circuit

C   L   L'   C'   R' = 1.24 R_0

$$\omega_0^2 = \frac{1}{LC} = \frac{1}{L'\,C'}$$
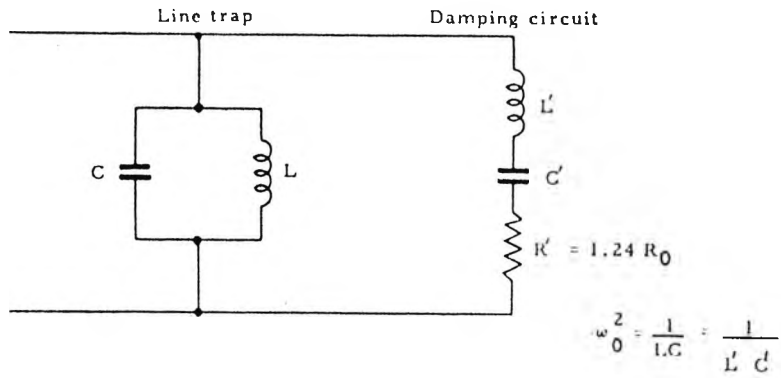
Figure 3.10 ADDITIONAL DAMPING ARRANGEMENT

Resistance

Simple damped trap — 2.48 R_0

1.24 R_0

Trap with additional damping

Δf Frequency
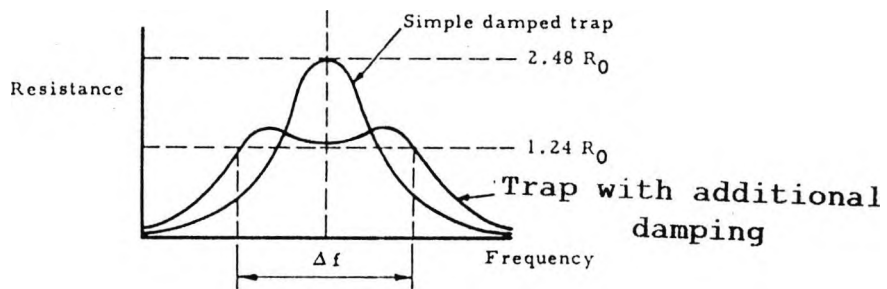
Figure 3.11 EFFECT ON BANDWIDTH DUE TO
ADDITIONAL DAMPING

Line

1   h.f.
low impedance
circuit

2   3   h.f.
high impedance
circuit

Low impedance short circuit switch
S operated by dd
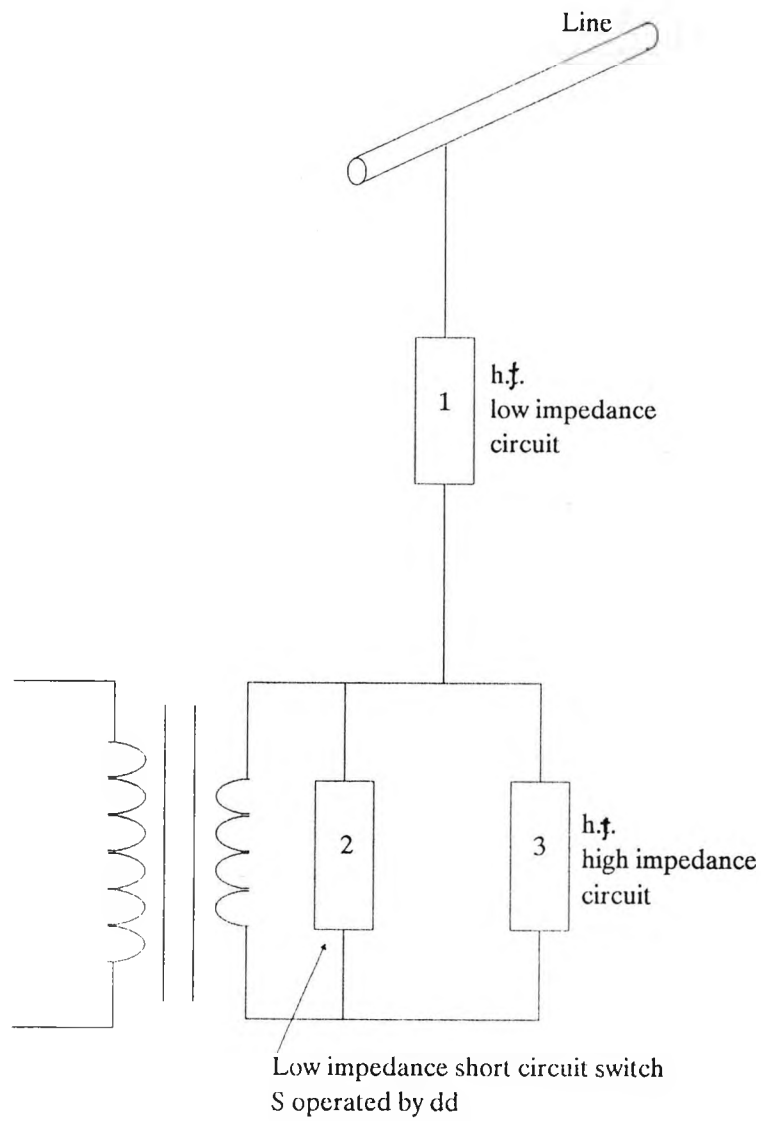
Figure 3.12 BASIC CIRCUIT ARRANGEMENT
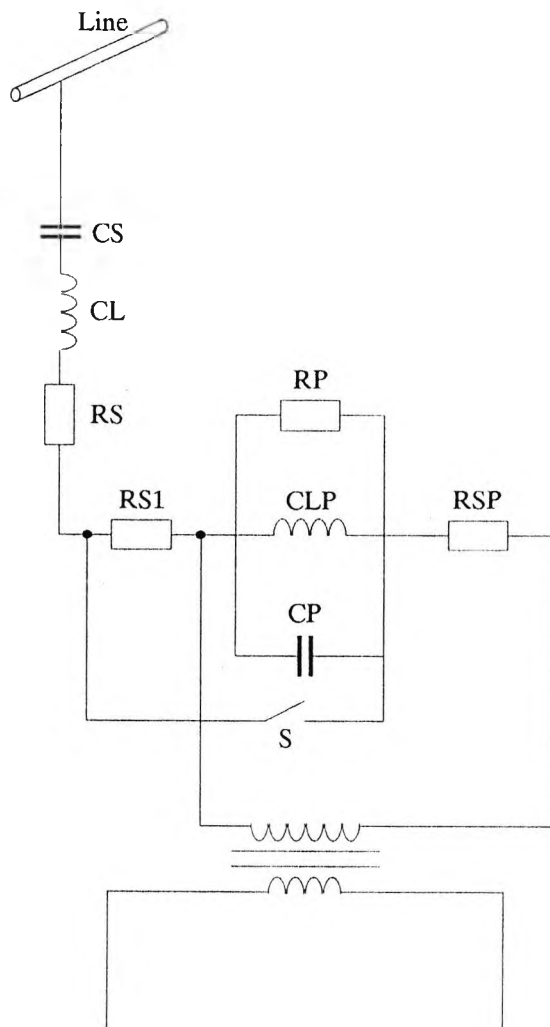
Figure 3.13 CIRCUIT DIAGRAM OF THE TUNER

Line

V_{IN}
Total impedance
$YTSM$

V_{OUT}

Y_{SM}

$$\text{GAIN} \atop (\text{YNC}) = \frac{V_{OUT}}{V_{IN}} = \frac{YSM}{YTSM}$$
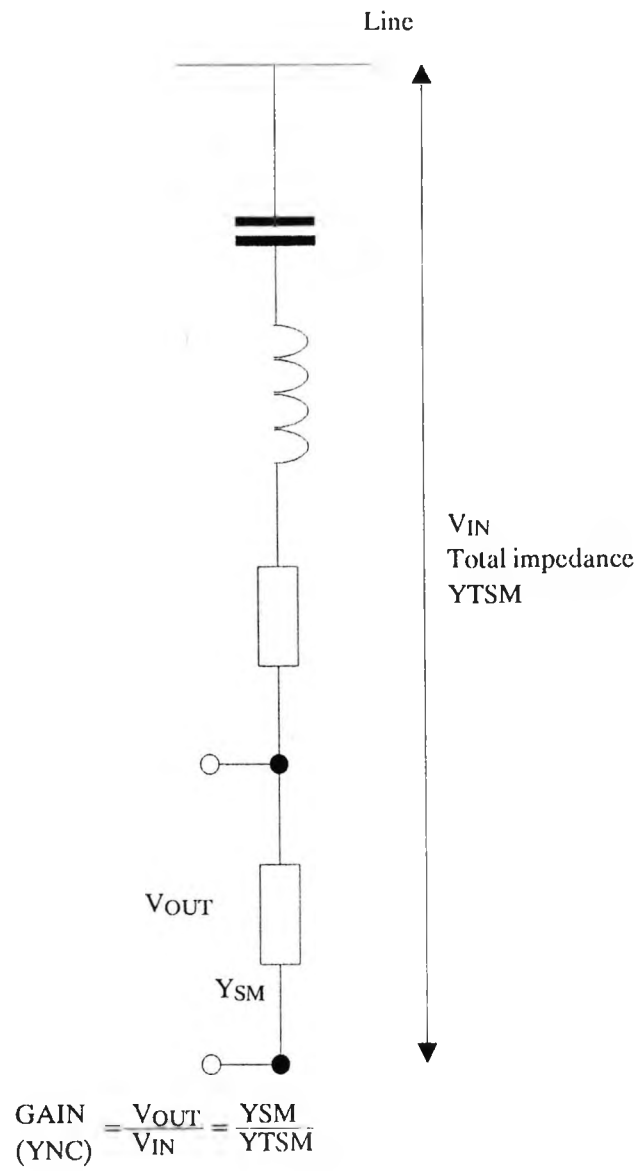
Figure 3.14 <u>EQUIVALENT CIRCUIT IN CLOSE MODE</u>

Line

V_{IN}
Total impedance
YTM

V_{OUT}

YOM
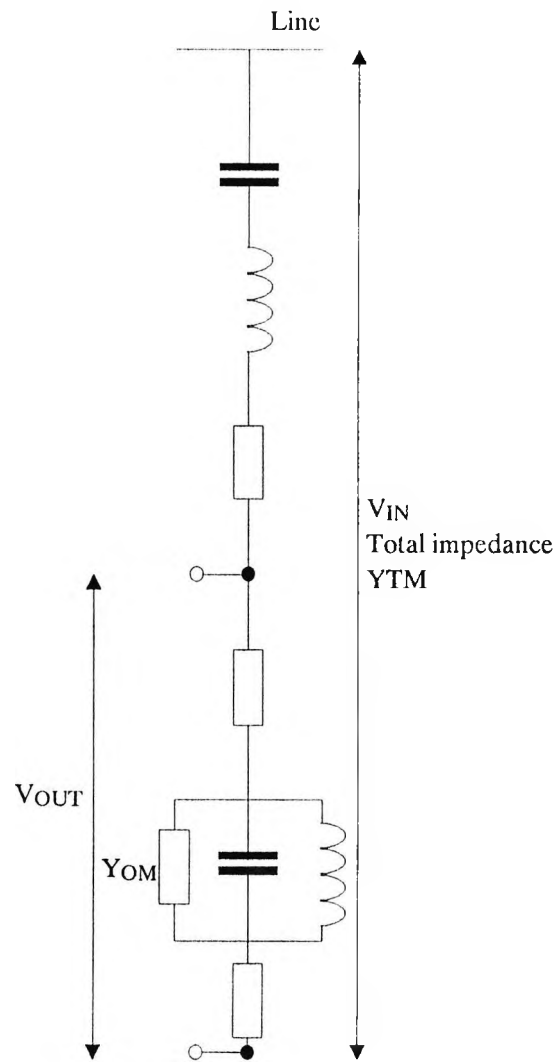
$$\text{GAIN} \atop (\text{YNO}) = \frac{V_{OUT}}{V_{IN}} = \frac{YOM}{YTM}$$

Figure 3.15 EQUIVALENT CIRCUIT IN OPEN MODE
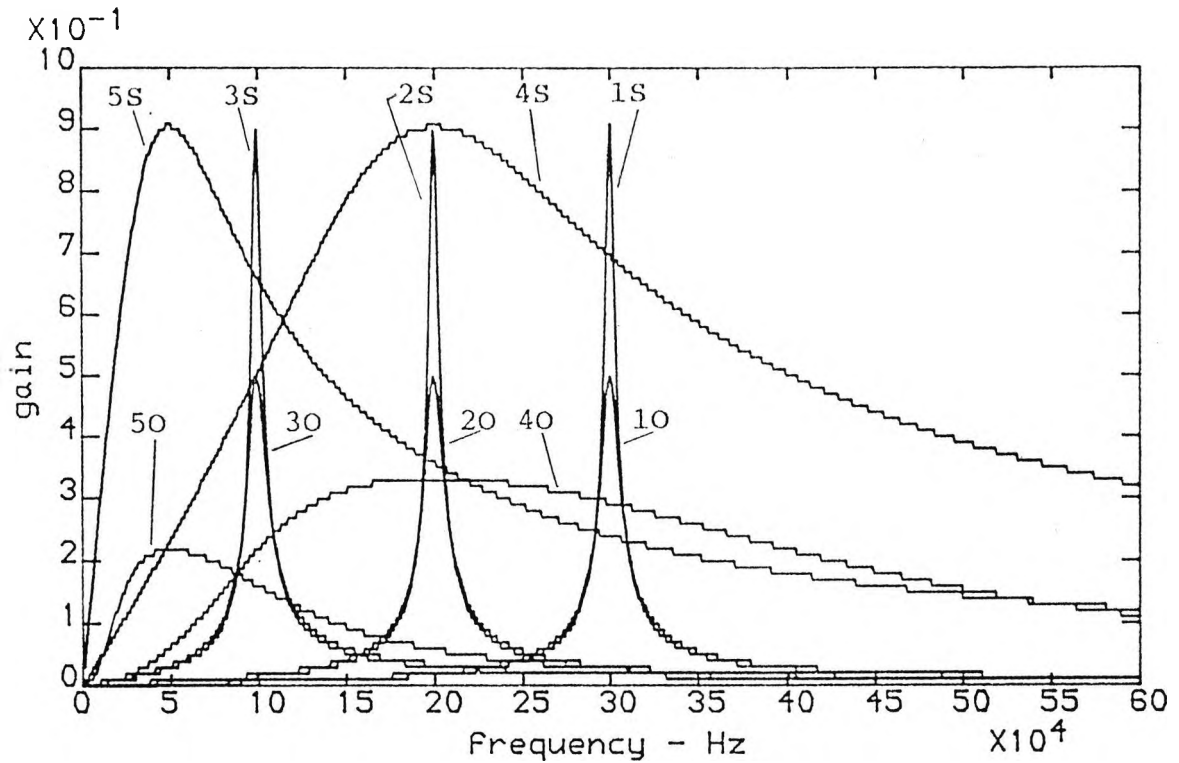
```
1S:  SHORT MODE, MID-FREQ 300±2.5 kHz
1O:  OPEN MODE, MID-FREQ 300±2.5 kHz
2S:  SHORT MODE, MID-FREQ 200±2.5 kHz
2O:  OPEN MODE, MID-FREQ 200±2.5 kHz
3S:  SHORT MODE, MID-FREQ 100±2.5 kHz
3O:  OPEN MODE, MID-FREQ 100±2.5 kHz
4S:  SHORT MODE, MID-FREQ 200±100 kHz
4O:  OPEN MODE, MID-FREQ 200±100 kHz
5S:  SHORT MODE, MID-FREQ 50±40 kHz
5O:  OPEN MODE, MID-FREQ 50±40 kHz
```

Figure 3.16 <u>GAIN Vs FREQUENCY CHARACTERISTICS</u>
<u>OF THE STACK TUNER</u>
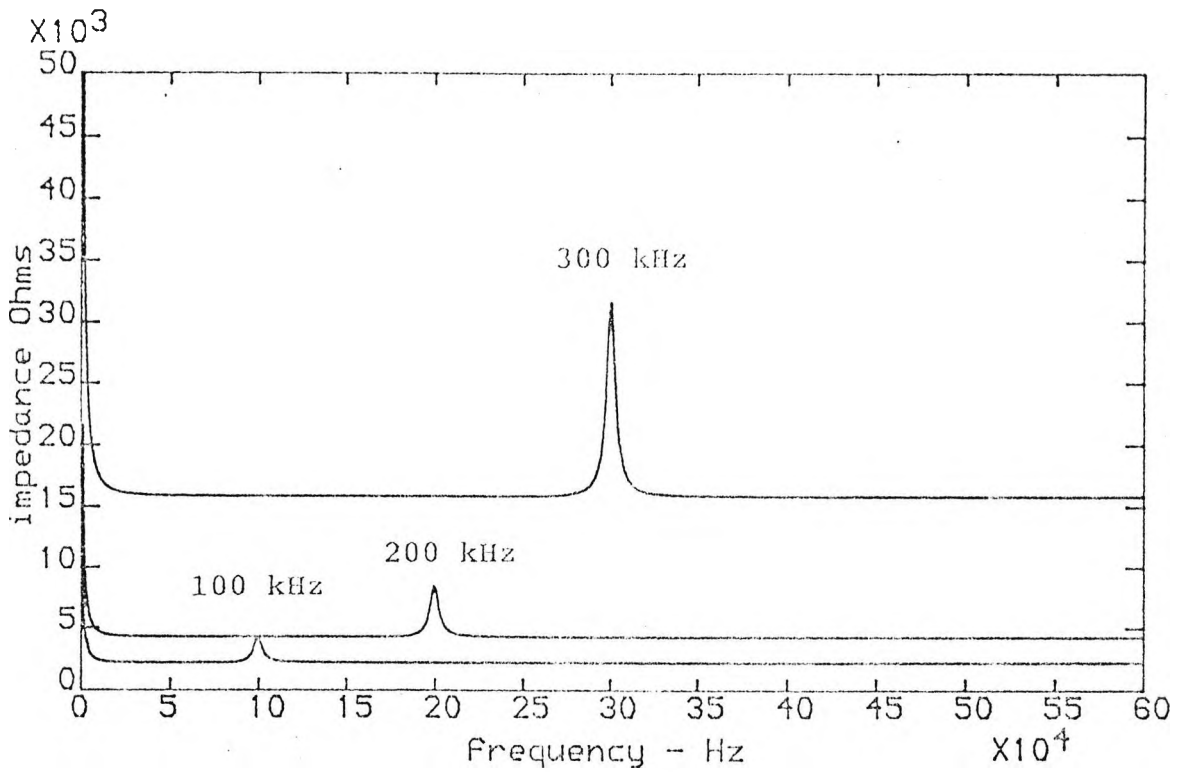
Figure 3.17   OPEN MODE IMPEDANCE CHARACTERISTICS OF
              THE STACK TUNER AT 300, 200, 100 kHz
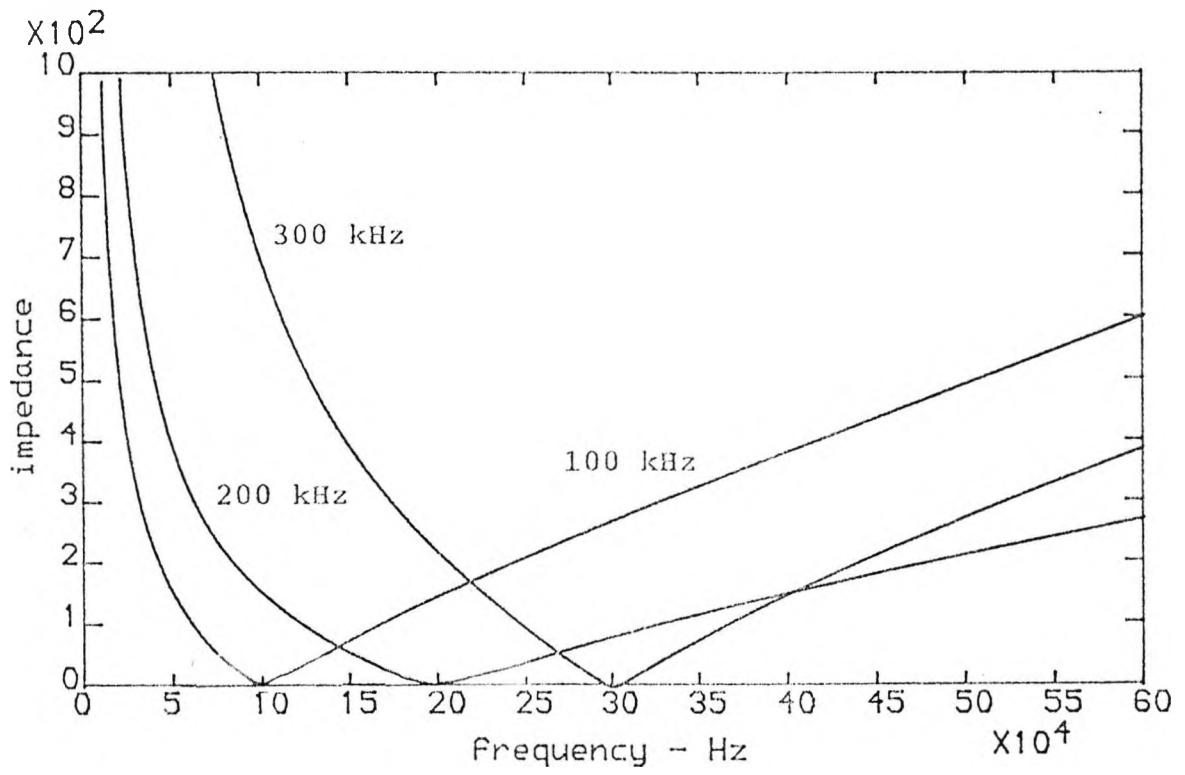
Figure 3.18 SHORT MODE IMPEDANCE CHARACTERISTICS OF THE STACK TUNER AT 300, 200, 100 kHz
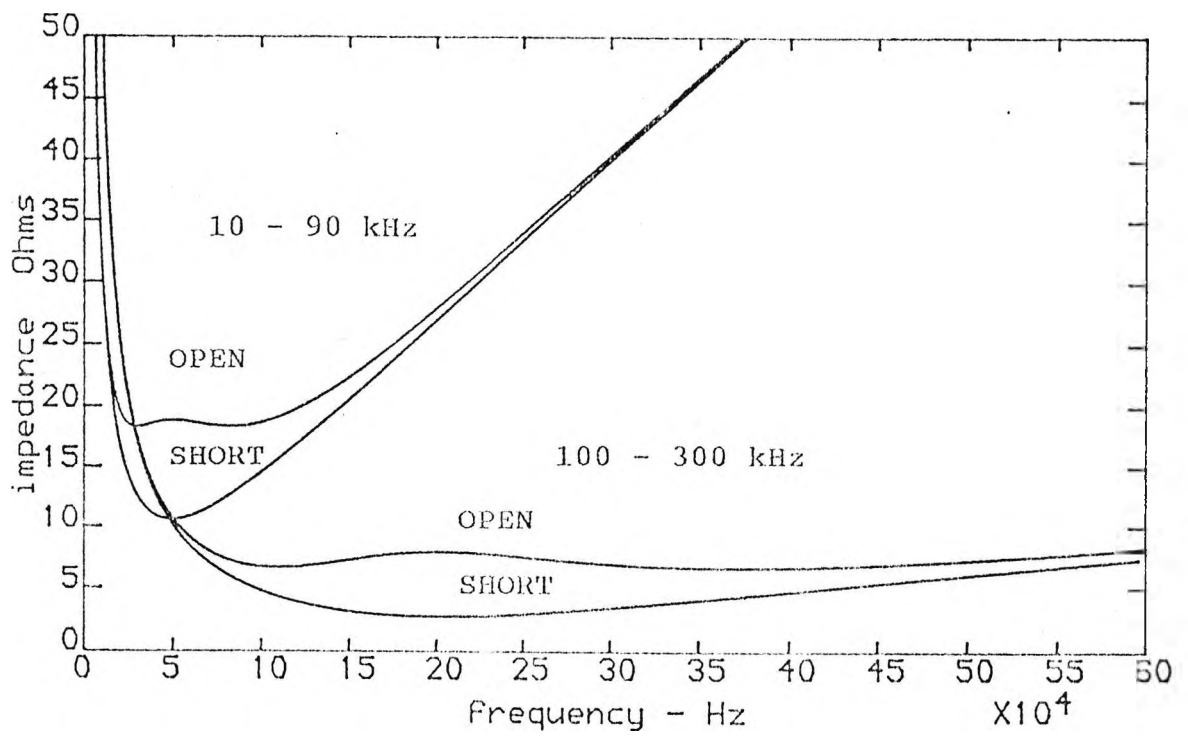
Figure 3.19   OPEN / SHORT MODE IMPEDANCE CHARACTERISTICS
OF   THE STACK TUNER FOR 100 - 300,
10 -   90 kHz
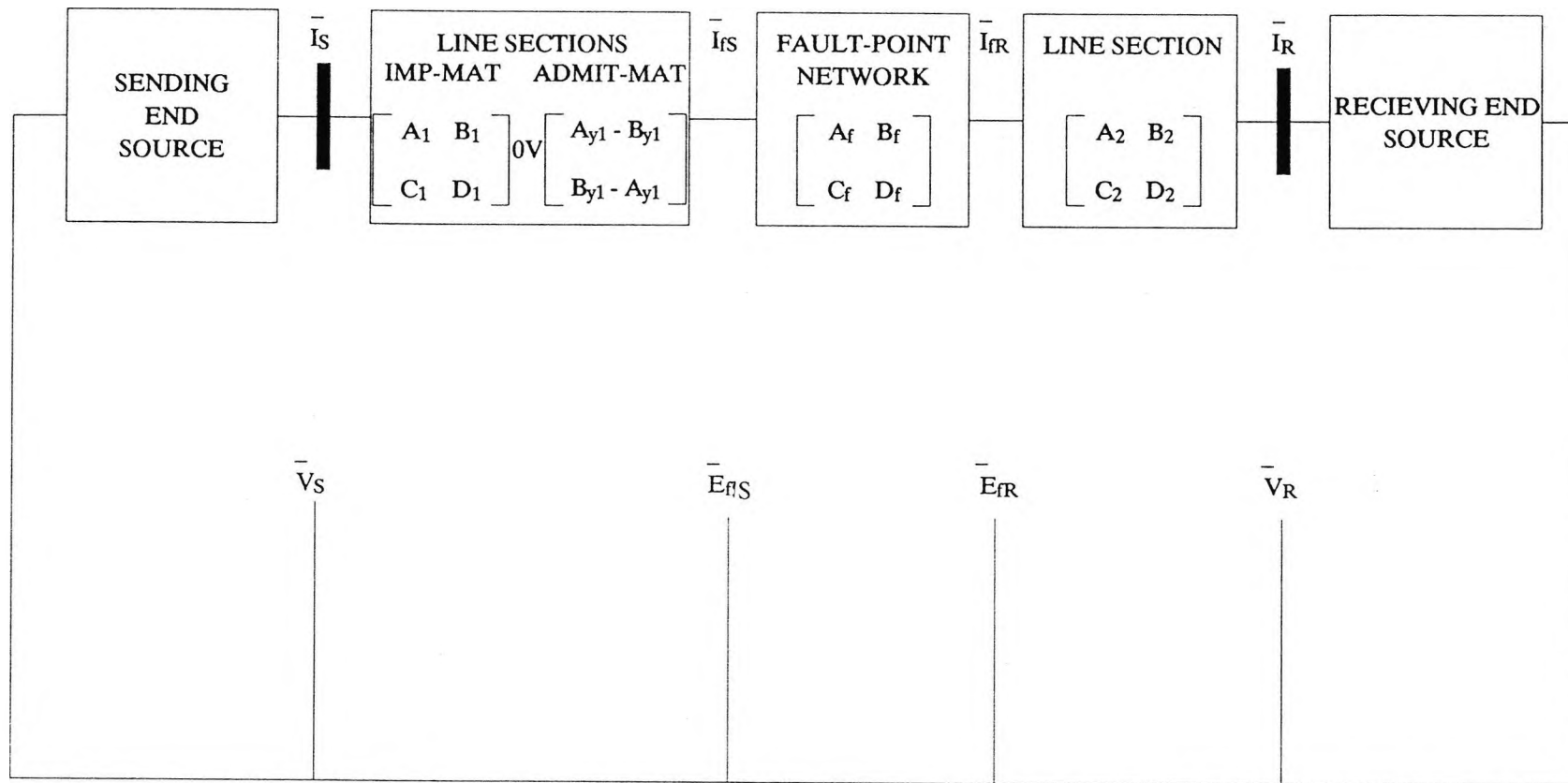
Figure 3.20 TRANSMISSION LINE RERESENTATION BY THE 2-PORT

MATRIX FORMATION
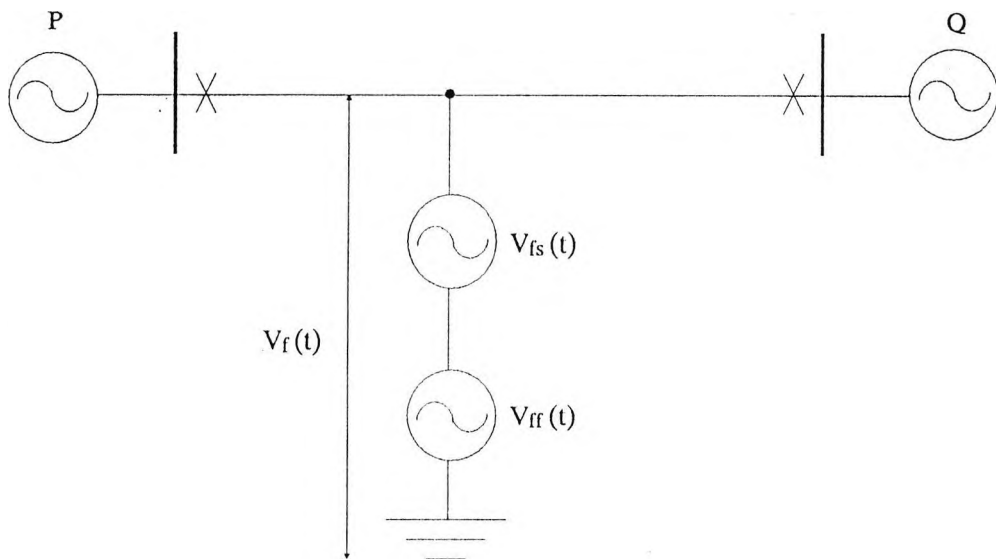
Figure 3.21 REPRESENTATION OF THE FAULTED TRANSMISSION LINE
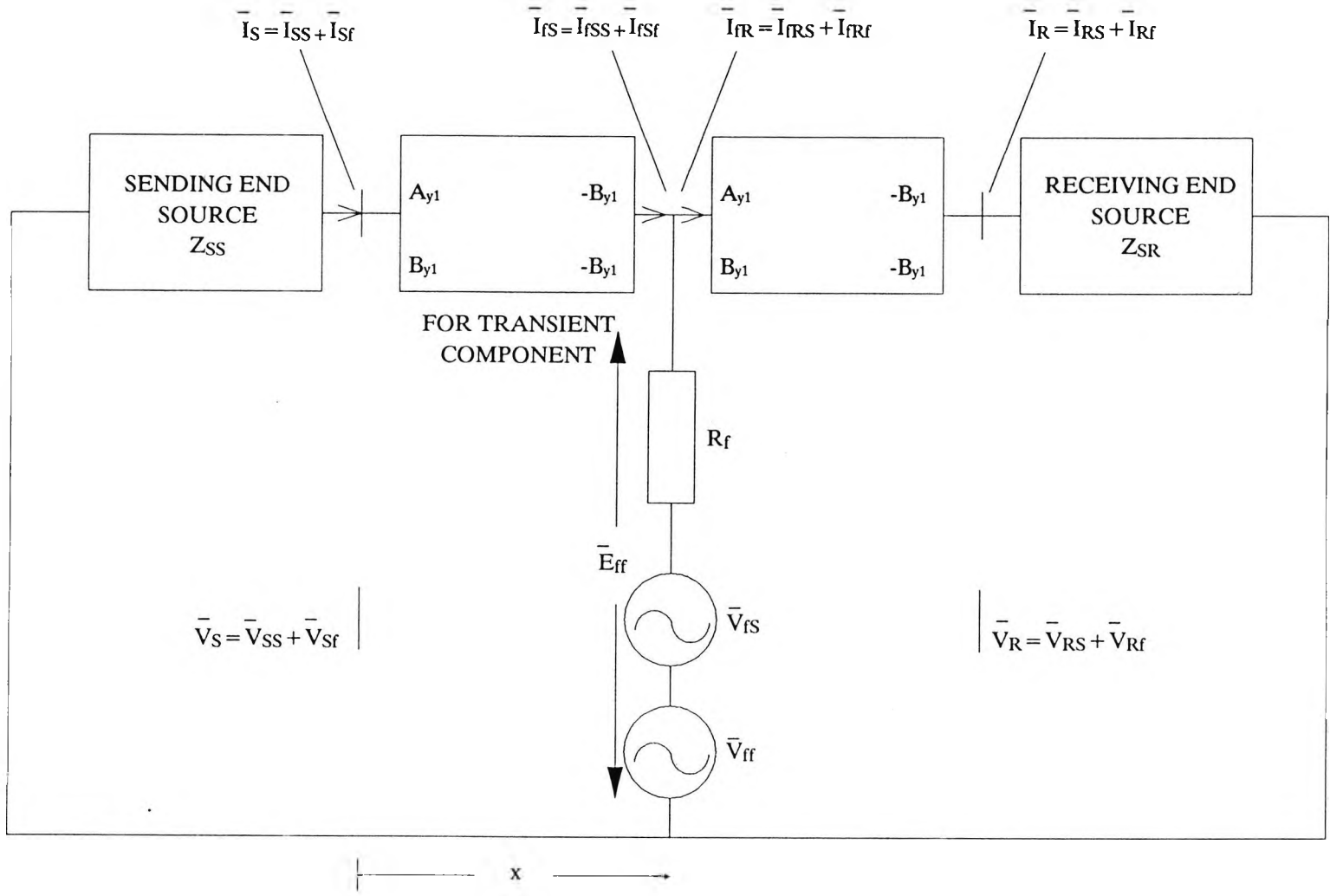
Figure 3.22   REPRESENTATION OF THE TRANSMISSION LINE WITH

CONSIDERATION OF AN INTERNAL FAULT AT

DISTANCE X FROM SENDING END
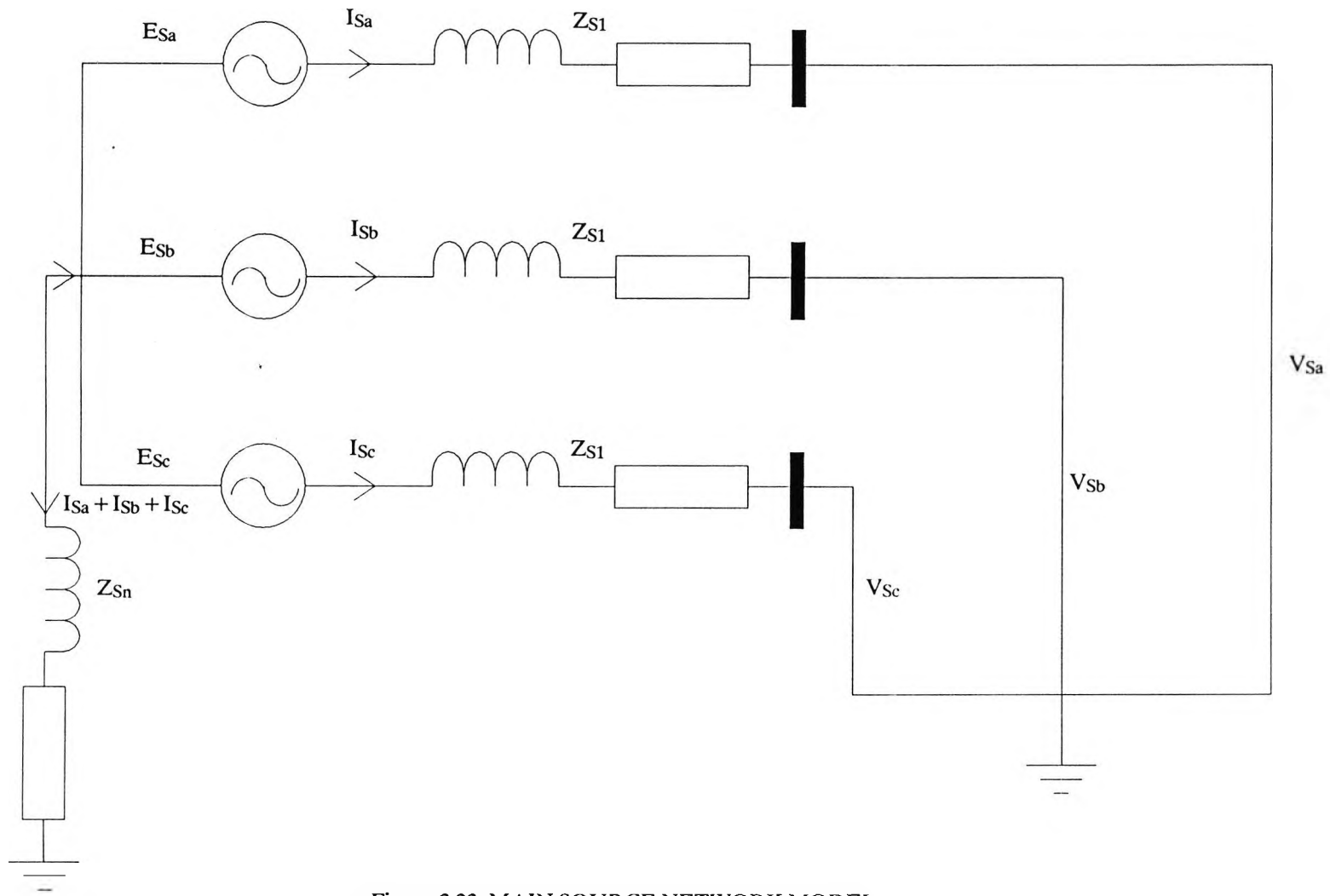
Figure 3.23 MAIN SOURCE NETWORK MODEL
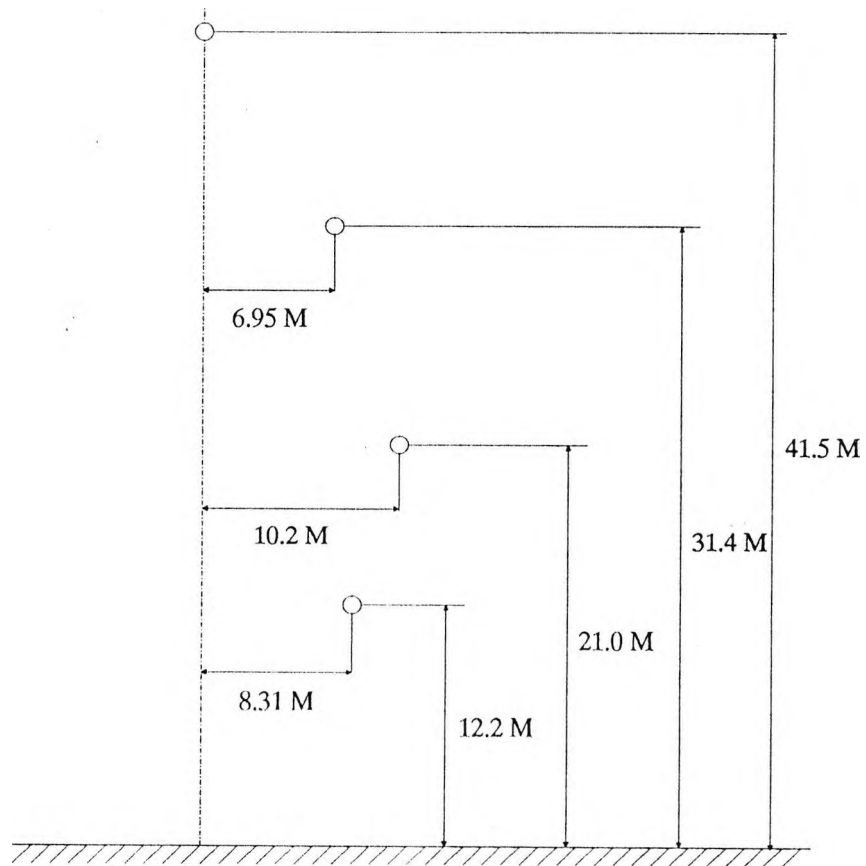
Figure 3.24   LINE CONFIGURATION
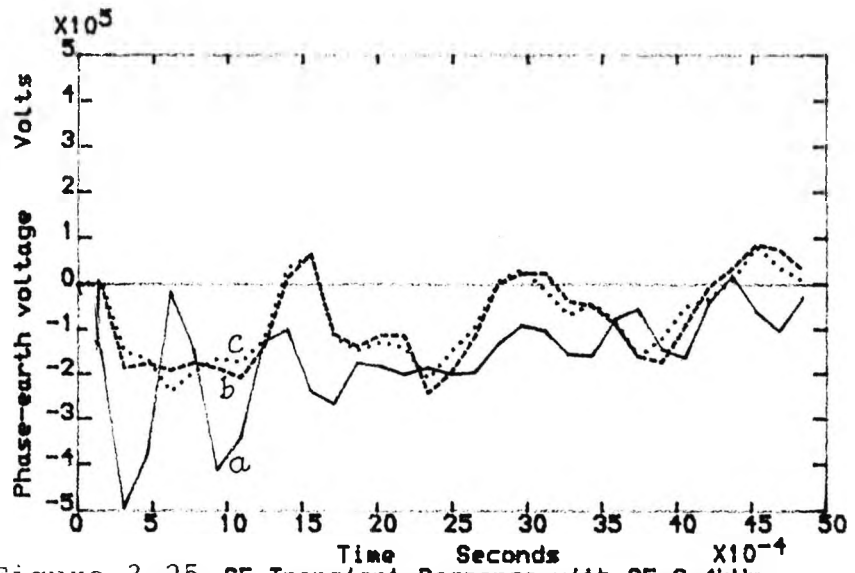
Figure 3.25 SE Transient Response with SF 6.4kHz
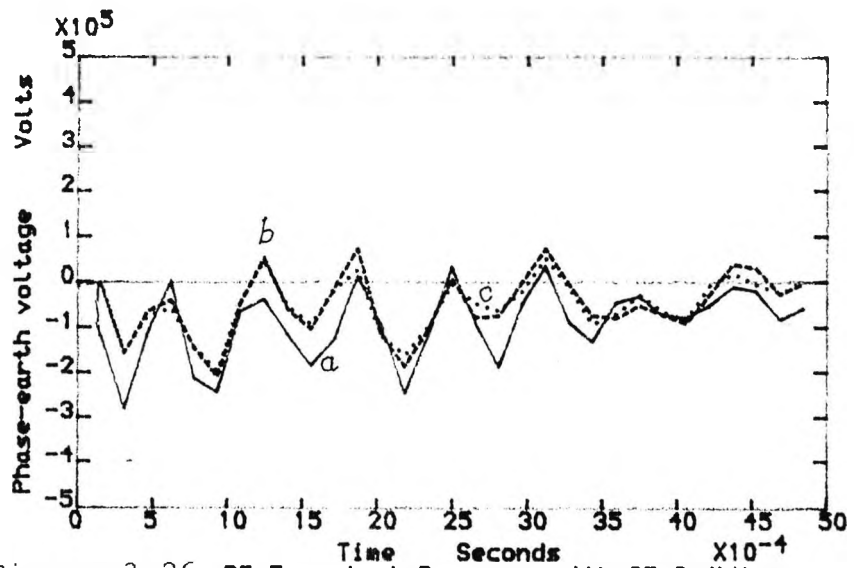
Figure 3.26 RE Transient Response with SF 6.4kHz
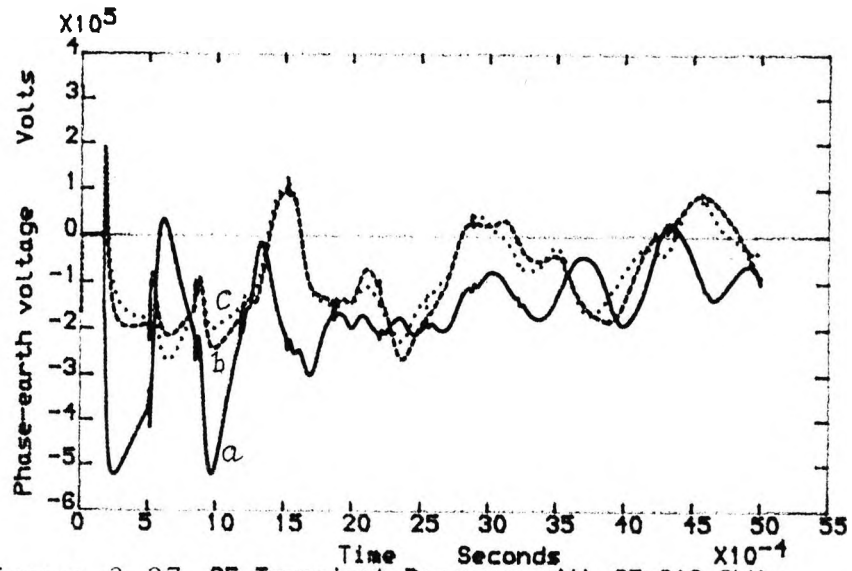
Figure 3.27 SE Transient Response with SF 819.2kHz
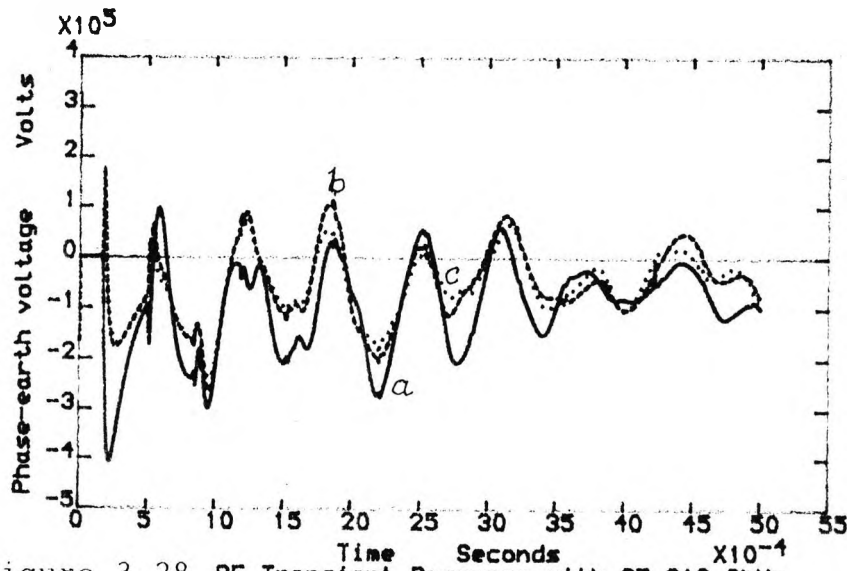
Figure 3.28 RE Transient Response with SF 819.2kHz
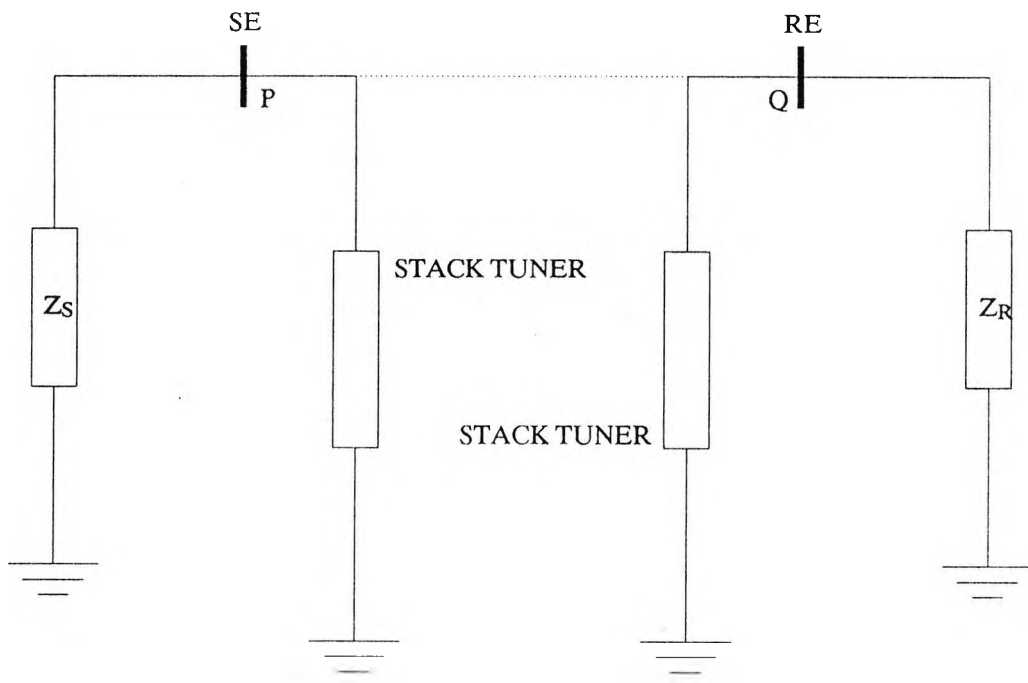
Figure 3.29 REPRESENTATION OF STACK TUNER WITH
TRANSMISSION LINE
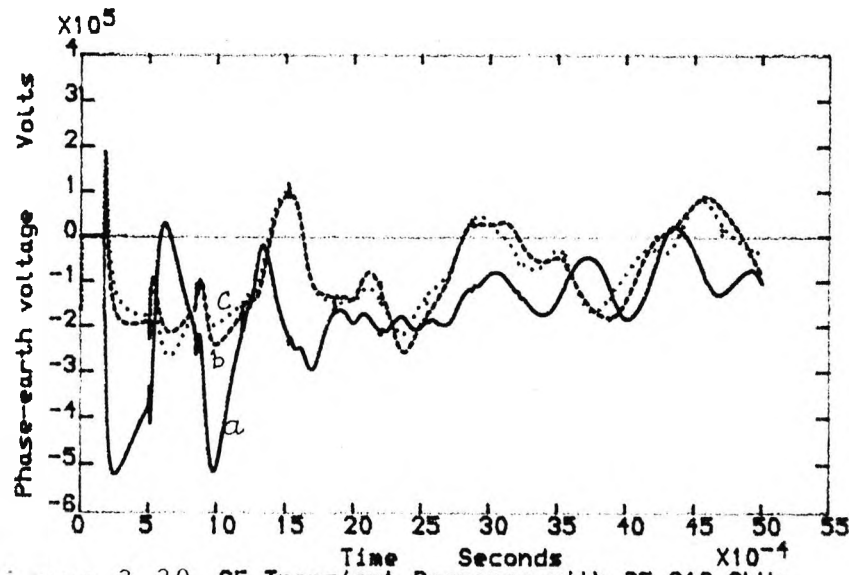
Figure 3.30 SE Transient Response with SF 819.2kHz
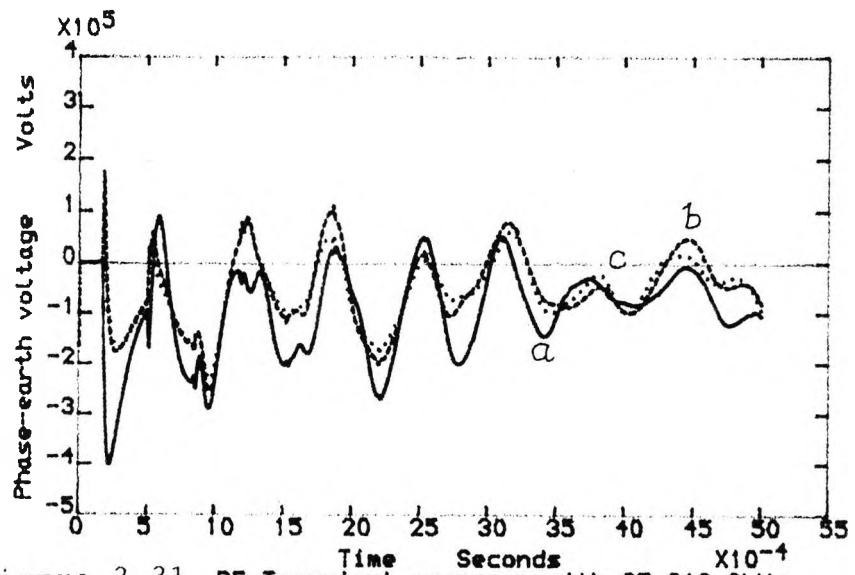
Figure 3.31 RE Transient response with SF 819.2kHz
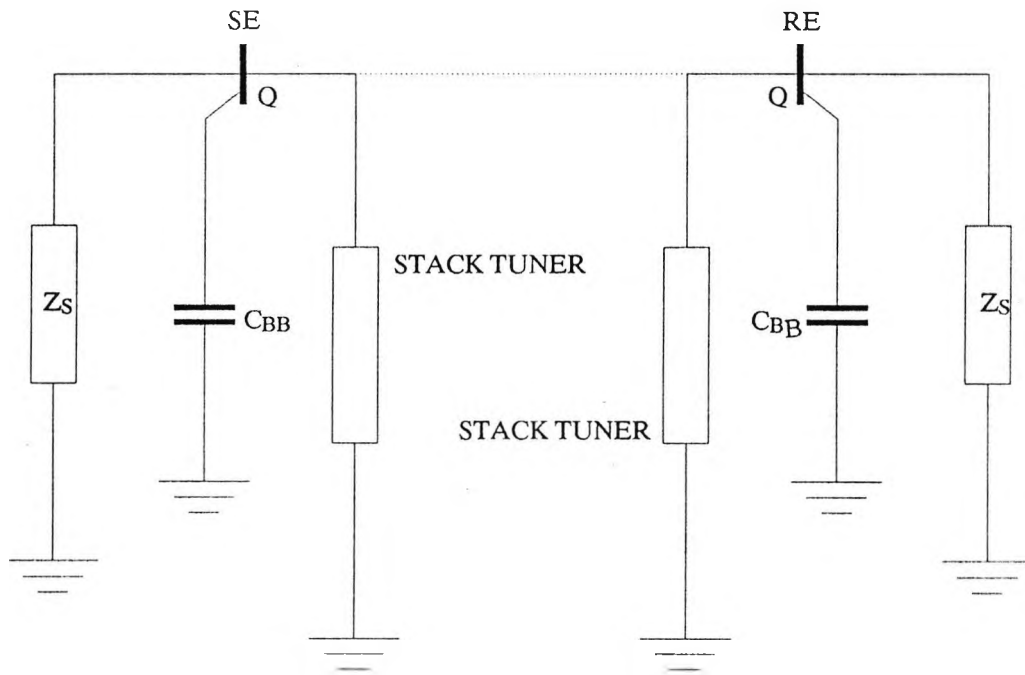
Figure 3.32   REPRESENTATION OF STACK TUNER WITH TRANSMISSION
LINE CONSIDERING BUS BAR CAPACITANCE
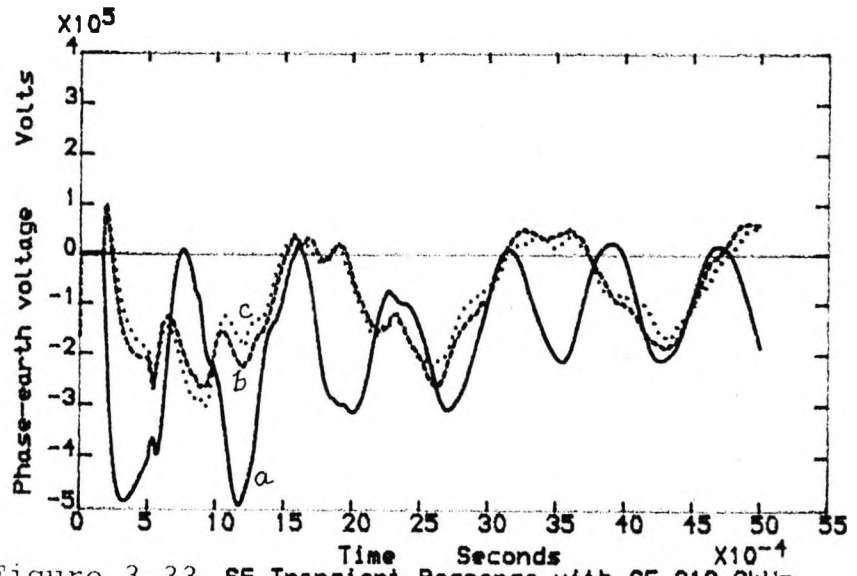
Figure 3.33 SE Transient Response with SF 819.2kHz
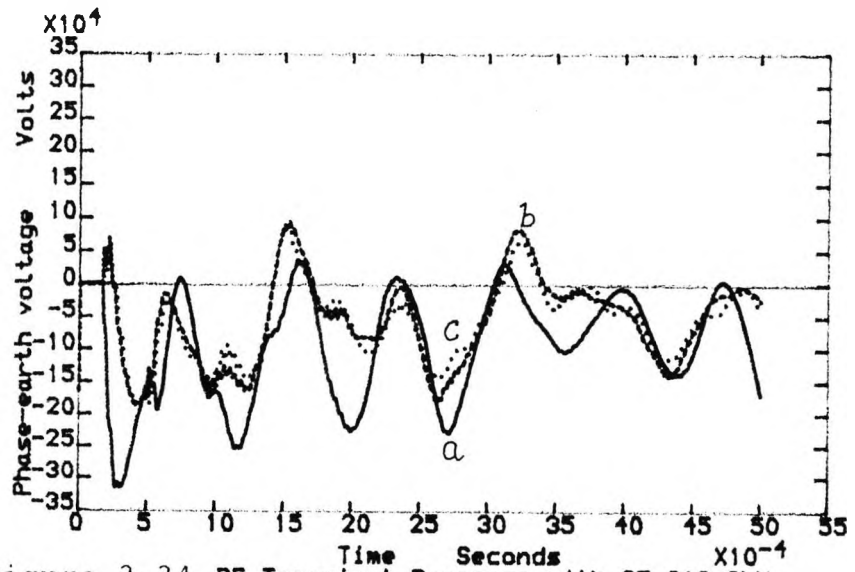
Figure 3.34 RE Transient Response with SF 819.2kHz

CHAPTER 4

INVESTIGATIONS BASED ON STACK-TUNER-OUTPUT-RESPONSES
OF THE FAULTED PHASE ONLY

This chapter investigates the stack tuner output (Figure 3.14 and Figure 3.15) responses of the faulted phase only at both ends of the transmission line. Firstly, simulated tests have been performed for different mid-frequencies of the stack tuner and then a particular mid-frequency has been selected based on the response and the design criterion. The establishment and the evaluation of the basic principle of the scheme have been described. The signal processing scheme used for investigations in this chapter is explained. Application of the auto-correlation technique in the signal processing has been highlighted. In the scheme (reference Chapter 2) which is to be investigated, a directional detector, DD has been used for the purpose of the discrimination of the reverse fault simply by detecting the direction of the fault. This directioal detector will have certain operating time delay. In the present scheme of the signal processing, this time delay has been taken in to consideration.

As it is a well known fact that the travelling wave based schemes are failures for the faults at lower inception angle, the fault responses at different fault inception angles of the voltage waveform have been investigated. The effect of diffent source capacities has been also investigated.

For all the simulated tests, the stack tuner has been considered in the open mode. In reverse fault condition only, the stack tuner has been simulated in normally close mode at the sending end, SE, only. For all the cases, a single phase to earth fault has been considered at 1 km from the SE of a 100 km long 400 kV transmission line with end sources of 5 GVA at SE and 20 GVA at RE. Time of fault-observation is 600 micro-seconds. The sampling frequency is 853.33 kHz. The fault inception angle of the voltage is 90 degrees. The performance of the simulated tests have been described on the basis of the positive peak value of the response during the post-fault observation time. Later few results are based on the fault-observation time of 5 msec.

4.1 Fault response at mid-frquency of 300±2.5 kHz, 200±2.5 kHz, 100±2.5 kHz, 200±100 kHz, 50±40 kHz of the stack tuner and selection of an appropriate tuner mid-frequency

Figure 4.1 shows the fault responses at various mid-frequencies of the stack tuner: 300±2.5 kHz, 200±2.5 kHz, 100±2.5 kHz, 200±100 kHz, 50±40 kHz at SE and RE. It can be seen that the peak value of the response at mid-frequency

73

of 100±2.5 kHz of the stack tuner is about twice of the peak value of the response at the mid-frequency of 200±2.5 kHz of the stack tuner. Similarly, the peak response at the mid-frequency of 200±2.5 kHz has been found to be about twice of the peak response at the mid-frequency of 300±2.5 kHz at the sending end, SE. This fact can be established theoretically as below:

A technique of the digital simulation of the superimposed component of the voltage at the fault-point has been explained in Chapter 3.2.3 and Chapter 3.2.4. Equation (3.35) for the superimposed component of the voltage in the frequency domain is -

$$\bar{V}_{ff}(jw) = \hat{V}_{fs} \frac{w_o \cos \Theta_{fs}}{w^2 - w_o^2} + \frac{jw \sin \Theta_{fs}}{w^2 - w_o^2} \qquad (4.1)$$

In this expression, Θ_{fs} is the phase angle which determine the point-on-the pre-fault waveform of the steady state voltage at which the fault occurs.

For the case of the fault inception angle $\Theta_{fs} = 90$ degree, there is an extreme limit of the voltage, called as voltage maximum fault, $\bar{V}_{ffMAX}$ which is given by

$$\bar{V}_{ffMAX}(w) = \hat{V}_{fs} \frac{w}{w^2 - w_o^2} \qquad (4.2)$$

where 'w_o' is power frequency in radians and 'w' is frequency in radians. When $w = w_o$, $\bar{V}_{ffMAX}$ is infinite.

74

In the present case, mid frequencies of the stack tuner are being considered in the range of 100 to 300 kHz which is of course very much greater than the power frequency and the above Equation (4.2) can be simplified as

$$\bar{V}_{ffMAX}(w) = \hat{V}_{fs} \frac{1}{w} \tag{4.3}$$

for different mid-frequemcies: (1) 100 kHz, $w = 2\pi 10^5$, (2) 200 kHz, $w = 2\pi X2X10^5$, (3) 300 kHz, $w = 2\pi X3X10^5$, and above relation (4.3) can be written as for (1) of 100 kHz as

$$\bar{V}_{ffMAX}(w) = C_V / 1 \tag{4.4}$$

for (2) of 200 kHz as

$$\bar{V}_{ffMAX}(w) = C_V / 2 \tag{4.5}$$

for (3) of 300 kHz as

$$\bar{V}_{ffMAX}(w) = C_V / 3 \tag{4.6}$$

where C_V is a voltage constant $= \hat{V}_{fs} / 2\pi X10^5$

equations (4.4) and (4.5) establish that the $\bar{V}_{ffMAX}(w)$ for the mid-frequency of 100 kHz is twice of the $\bar{V}_{ffMAX}(w)$ for the mid-frequency of 200 kHz. Similarly equations (4.5) and (4.6) establish that the $\bar{V}_{ffMAX}(w)$ for the mid-frequency of 200 kHz is 1.5 times the $\bar{V}_{ffMAX}(w)$ for the

mid-frequency of 300 kHz.

The peak values of the response for other mid-frequencies of 200±100 kHz and 50±40 kHz have been found very small in comparison to the responses for other mid-frequencies. Therefore, these two mid-frequencies (200±100 kHz and 50±40 kHz) have not been considered for the simulated tests. Based on the peak values of the fault response, the mid-frequency of 100±2.5 kHz can be selected for the stack tuner. But, the value of the capacitance of the coupling capacitor (reference Chapter 2.1) has been assumed constant and a larger value of the inductance of the stack tuning coil is required for resonance at the mid-frequency of 100±2.5 kHz in comparison to the mid-frequency of 300±2.5 kHz. This will result in increase of the size and the cost of the equipment. Therefore, the mid-frequency of 300±2.5 kHz of the stack tuner has been selected for all the simulated tests in this thesis.

4.2 Establishment of the new principle

Figure 4.2a shows the voltage waveforms at the stack tuner output in NO, NO mode at both ends SE and RE for an internal fault at peak voltage for phase 'a' to earth fault. Figure 4.2b shows the voltage waveforms at the stack tuner output in NC, NO mode at the ends SE and RE for reverse fault (external fault). A positive peak voltage of 300 Volts at RE in Figure 4.2b has been found in comparison to 800 Volts at RE in Figure 4.2a. At SE, the positive peak voltages are 7000 Volts and 3500 Volts for

internal and reverse faults. In such a case, if a threshold voltage of the level detector (reference Chapter 2.2: assuming the faulted phase signal from the output of the stack tuner goes direct to the level detector) corresponding to a positive peak of about 400 Volts can be arranged, then discrimination at the RE for reverse fault is possible. At the SE, the discrimination for reverse fault is taken care by the directional detector, DD (reference Chapter 2.2). In such a case, the decision logic (Figure 2.2) inputs are $V_D = 1$, $T_F = 1$, $T_R = 0$ at SE and RE for internal faults which results in a TRIP = 1, signal at the output of the decision logic. Similarly for the reverse fault, the decision logic inputs are $V_D = 1$, $T_F = 0$, $T_R = 1$ at SE which results in a signal, TRIP = 0 and prevents the tripping at the SE. Also at RE for the reverse fault, the decision logic inputs are $V_D = 0$, $T_F = 1$, $T_R = 0$ which results in a TRIP = 0, signal and prevents the tripping at RE. With this criterion, the scheme has been established at least in principle. Detailed investigation on the basis of the signal processing (reference Chapter 2.2) is carried out later on. These results are based on the post-fault observation time of 600 micro-seconds. If the operating time of the directional detector, dd, typically say 1 msec is considered, it is necessary to study the fault responses at least for a quarter cycle to establish the scheme satisfactorily. With this view, Figure 4.3 shows the fault responses for a post-fault time of 5 msec. It can be seen from the responses in Figure 4.3 that the fault response repeats after a

77

particular time and reduces in magnitude each time when it repeats. This particular time of repeat corresponds to the time taken by the travelling-wave to travel a distance between the fault point and the end of the transmission line i.e. SE or RE. Using the same criterion as in Figure 4.2 for the internal and the reverse faults based on the positive peak responses, a discrimination has been found to be possible and, the scheme at least in principle has been established satisfactorily.

4.3 Signal processing and investigations of the signals

Figure 4.4 shows the block representation of the signal processing which has been used for investigation purposes in this chapter. The output of the stack tuner, V_F is sent to an auto-correlator block. The output signal of the auto-correlator, V_A is sent to another block 'DD operating delay'. Now the signal V_A is delayed by the operating time of the DD i.e. T_{DD}. In the present investigation, this delay T_{DD} has been taken as 1 ms which is a typical value. This delayed signal is X. This signal X is squared and integrated with time in another block for the purpose of deciding the level of the signal. This signal is y. This y signal is sent to another block, called as the level detector. In this block, the signal y is compared with a threshold value and the output V_D is sent to another block 'Decision logic' which also receives a signal $T_{F,R}$ from the directional detector. If both the signals are 1, the trip signal is sent for the tripping of the local breaker.

The principle of the auto-correlation has been described as below:

The discrete cross-correlation function $P_{xy}(T)$ measures the correlation between sections of sampled signal x and the delayed signal y as a function of the delay T

$$P_{xy}(T) = 1/N \sum_{k=1}^{N} x(k\delta t + T) . y(k\delta t) \qquad (4.7)$$

where k = 1,2,-----N

   δt = sampling time

if T = mδt where m can vary from 0 to N-1 , then N values of P_{xy} can be found out.

The correlation function $P_{xy}(T)$ shows the similarity between two waveshapes as a function of the time shift between them. Maximum output of the correlation function indicates the best match between the waveshapes.

Now if signal y is the signal x i.e. the signal 'x' is being correlated against itself then the technique is called an auto-correlation technique and the auto-co rrelation function can be written as:

$$P_{xx}(T) = 1/N \sum_{k=1}^{N} x(k\delta t + T) . x(k\delta t) \qquad (4.8)$$

where k = 1,2,----N

   δt = sampling time

if $T = m\delta t$ where m can vary from 0 to N-1 , then N values of P_{xx} can be found out. $x(k\delta t)$ is known as the window of N samples of the signal x.

The correlation function $P_{xx}(T)$ shows the similarity between two waveshapes as a function of the time shift between them. Maximum output of the correlation function indicates the best match between the waveshapes.

Depending upon the value of the 'm' in the expression $T = m\delta t$, the signal 'x' can be started from any sampling point for the purpose of the auto-correlated response. If there are 100 sampling points in a signal 'x'and 'm'is 51, then the signal 'x' can be auto-correlated with the signal 'x' after a delay of half the signal time. If 'm' = 0, the signal 'x' can be auto co-rrelated with the same signal 'x' without any delay provided window $x(k\delta t)$ is available. This means that first half of the signal 'x' can be auto-correlated with the second half of the same signal 'x' if m = 51. The choice for selection of 'm' depends upon the duration and waveform of the signal.

In the present case, the application of the auto-correlation technique is being investigated for the purpose of the increase in the discrimination factor (explained later in this section) and the effect of the DD operating time has not been considered on the fault responses. With this view, Figure 4.5 shows the auto-correlated responses for all the signals shown in Figure 4.3. For these responses 'm' is 0 as explained above and the response V_A

is only for a period of 2.4 msec which is about half the signal time, and has been considered sufficient for the purpose of investigation. The delay T_{DD} due to the operating time of the directional detector, DD, is clearly shown in Figure 4.5. The response after a delay, T_{DD} is 'x' as shown in Figure 4.5. These signals 'x' are squared and integrated with respect to time and the responses are called 'y' which are shown in Figure 4.6. It can be seen that the factor of discrimination has been improved to about 30. Now these signals are processed to a level detector whose threshold value V_T (reference Chapter 2) can be set to a value larger than the value corresponding to the response 'y' at the receiving end in the reverse fault condition. As explained in Chapter 2, the output of the level detector, V_D is processed to a 'logic gate'which also receives a signal from the directional detector, dd. The output of the 'logic gate' gives a tripping signal for the internal faults only.

4.4 Effect of different fault inception angles of the voltage

A technique of the digital simulation of the superimposed component of the voltage at the fault-point has been explained in Chapter 3.2.3 and Chapter 3.2.4. Equation (3.35) for the superimposed component of the voltage in the frequency domain is being re-written as below:

$$\bar{V}_{ff}(jw) = \hat{V}_{fs}\frac{w_o \cos \Theta_{fs}}{w^2 - w_o^2} + \frac{jw \sin \Theta_{fs}}{w^2 - w_o^2} \qquad (4.9)$$

In this expression, Θ_{fs} is the phase angle which determine the point-on-the pre-fault waveform of the steady state voltage at which the fault occurs. In Equation (4.9), there are two extreme conditions for Vff(jw): (1) a minimum, $\bar{V}_{ffMIN}(w)$ corresponding to the value of $\Theta_{fs} = 0$, and (2) a maximum, $\bar{V}_{ffMAX}(w)$ corresponding to the value of $\Theta_{fs} = 90$ degree which can be written as

$$\bar{V}_{ffMIN}(w) = \hat{V}_{fs}\frac{w_o}{w^2 - w_o^2} \qquad (4.10)$$

and

$$\bar{V}_{ffMAX}(w) = \hat{V}_{fs}\frac{w}{w^2 - w_o^2} \qquad (4.11)$$

where 'w_o' is the power frequency in radians and 'w' is the frequency in radians. Equation (4.11) is same as Equation (4.2) explained earlier. When $w = w_o$, $\bar{V}_{ffMAX}(w)$ and $\bar{V}_{ffMIN}(w)$ are infinite. But, when $w \gg w_o$, above equations (4.9), (4.10), (4.11) can be simplified as below:

$$\bar{V}_{ff}(w) = \frac{\hat{V}_{fs}}{w} \sin \Theta_{fs} \qquad (4.12)$$

$$\bar{V}_{ffMIN}(w) = \hat{V}_{fs}\frac{1}{w^2} \qquad (4.13)$$

and

82

$$\bar{V}_{ffMAX}(w) = \hat{\bar{V}}_{fs} \frac{1}{w} \qquad\qquad (4.14)$$

It can be seen from the equations (4.13) and (4.14) that $\bar{V}_{ffMAX}(w)$ is 'w' times the $\bar{V}_{ffMIN}(w)$. This means that the response at zero voltage point-on-wave faults can be improved by selecting a lower value of the mid-frequency of the stack tuner. Equation (4.12) gives the fault responses for various values of the Θ_{fs}, and is proportional to the value of the $\sin \Theta_{fs}$ for a particular voltage of the transmission system and a particular mid-frequency of the stack tuner as shown below:

Θ_{fs}	$\sin \Theta_{fs}$
90	1
80	0.984
70	0.939
60	0.866
50	0.766
45	0.707
40	0.642
30	0.5
20	0.342
15	0.258
10	0.173
5	0.087
1	0.017

This shows that the response at 1 degree voltage point-on-wave faults is reduced to 1.7 percent of the response at 90 degree voltage point-on-wave faults at higher mid-frequencies of the stack tuner.

Figures 4.7a, b, c, d, e, f show the stack tuner output responses for different point-on-wave faults of the voltage: (1) 90 degree, (2) 60 degree, (3) 30 degree, (4) 15 degree, (5) 5 degree, and (6) 0.

A table as below shows (1) the positive peak responses at sending end, SE, (2) its percentage of the maximum voltage point-on-wave fault, (3) the positive peak response at the receiving end, RE, (4) its percentage of the maximum voltage point-on-wave faults, (5) calculated value of the $\sin \Theta_{fs}$ from the above table, and (6) its percentage of the maximum voltage point-on-wave fault for different point-on-wave faults: 90, 60, 30, 15, 5, and 0.

TABLE

Θ_{fs}	$\bar{V}_{ff}$(SE) (Volts)	%	$\bar{V}_{ff}$(RE) (Volts)	%	$\sin\Theta_{fs}$	%
90	7000	100	800	100	1	100
60	6000	85.7	700	87.5	0.866	86.6
30	3500	50	400	50	0.5	50
15	1800	25.7	200	25	0.258	25.8
5	600	8.5	70	8.7	0.087	8.7

84

This table shows a good agreement between the calculated values and the simulated test results. Now Equation (4.12) can be used as a useful tool for designing the scheme and to find out the point-on-wave of the voltage for which the scheme can operate satisfactorily from the discrimination point of view for reverse fault conditions. For example, the positive peak voltages at RE in Figure 4.2a is 800 Volts and in Figure 4.2b is 300 Volts which is 37.5 percent of 800 Volts. If a margin of safety of 12.5 percent is considered then for a total value of 50 percent, point-on-wave of the voltage of 30 degree can be considered safely for the operation of the scheme as the value of sin Θ_{fs} = sin 30 = 0.5 i.e. 50 percent. This concludes that the scheme can work satisfactorily up to 30 degree of the fault inception angle of the voltage. The performance of the scheme can be improved for operation at lower value of the Θ_{fs} either by reducing the output voltage gain of the stack tuner in the open mode, NO, or by increasing the gain in the short mode, NC (reference Chapter 3.1.5 and Chapter 3.1.6) depending on the design of the stack tuner circuit. Regarding the performance of the scheme at zero voltage point-on-wave faults, the simulated test results have been shown in the Figure 4.7f and it can be seen that the value of the response is so low that the scheme can not discriminate under reverse fault conditions. This fact has been established earlier from the equations (4.12) and (4.13) theoretically as the the $\bar{V}_{ffMAX}(w)$ is 'w' times the $\bar{V}_{ffMIN}(w)$. According to Mehdi [21], zero voltage point-on-wave faults are relevent to theory, but in practice modern

EHV systems have very high impulse insulation levels which causes almost all flashovers to occur near voltage maximum. However another method of improving the performance of the scheme at a lower value of the Θ_{fs} or zero voltage point-on-wave faults will be discussed later considering arcing faults.

## 4.5 **Effect of different source capacities**

The newly developed scheme is based on the detection of the high frequency signals (300 kHz in the present case) from the fault generated noise at the ends of the transmission line. Whenever a fault or disturbance occurs on the transmission line, the voltage and current waveforms travel from the point of the disturbance to the ends of the transmission line due to a well known travelling wave phenomena. As the scheme is based on the detection of the voltage signals, only voltage waveforms have been considered in this thesis. Depending on the distance of fault from the end, the voltage signal is attenuated due to losses in the line. When the voltage signal reaches to the end of the line, part of the signal is reflected towards the fault and a part of the signal is refracted towards the source which is again reflected towards the fault, and the process cotinues until the voltage signal fully dies out. The refracted component of the signal depends upon the well known refracted coefficient of the transmission line which is given by:

$$R_r = 2 Z_O / (Z_O + Z_L) \qquad\qquad (4.15)$$

where Z_O is the surge impedance of the line and Z_L is the source impedance. This source impedance varies depending on the capacities of the sources connected at the ends of the transmission line. Therefore the high frequency signals at the ends depend on the source capacities. With this aim, the newly developed scheme has been digitally simulated and tested for satisfactory operation with different source capacities.

The surge impedance, Z_O of the transmission line under the scope of this thesis has been calculated and found to be of the order of 370 Ohm. Based on the conventional values of the source capacities: 5 GVA to 30 GVA, the source impedance, Z_L may vary from 32 Ohm to 5 Ohm for a 400 kV line, and, the corrosponding refracted coefficient, R_r varies from 1.86 to 1.98. With a view to study the performance of the simulated tests under extreme conditions, the simulated tests have been carried out with source capacities (1) 1 GVA at both ends, (2) 99 GVA at both ends, (3) 5 GVA at the sending end, SE, and 20 GVA at the receiving end, RE. The results of these simulated tests are shown in Figure 4.8. It can be seen in Figure 4.8 that there is no appreciable difference in the responses at both the ends.

Therefore, it can be concluded that the newly developed scheme can be used satisfactorily for different combinations of source capacities for the particular system considered in this thesis.
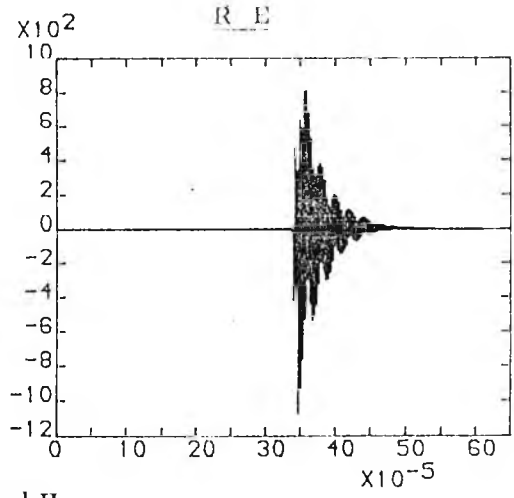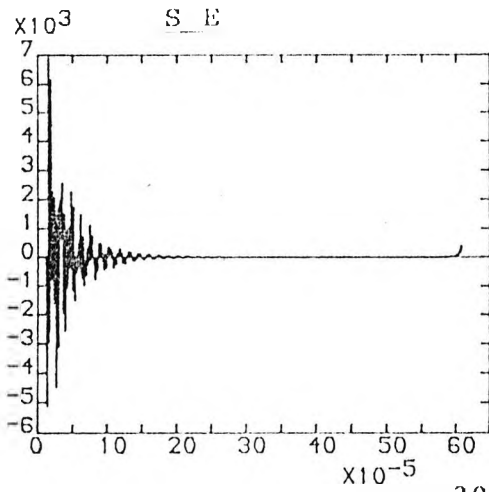
a: 300±2.5 kHz
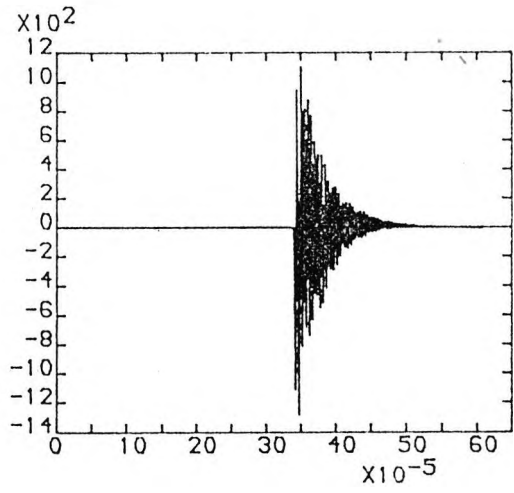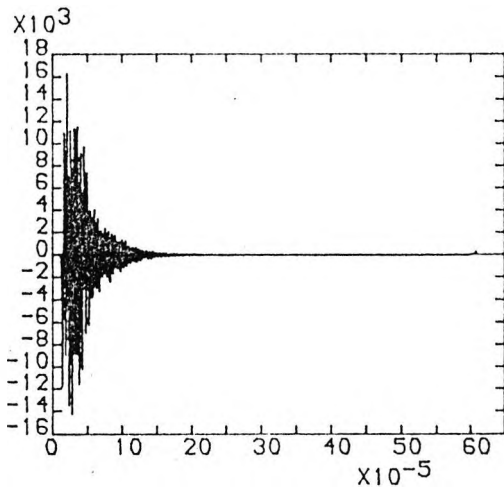
b: 200±2.5 kHz
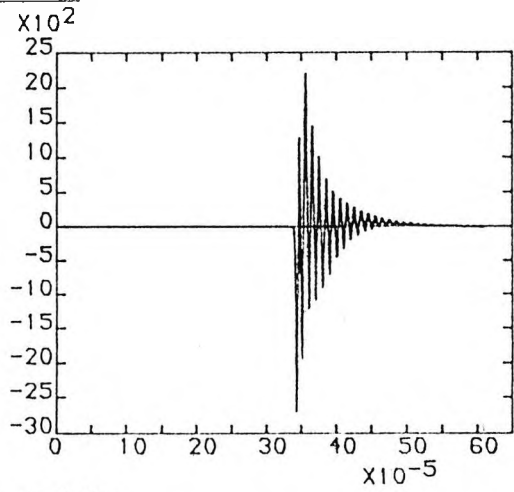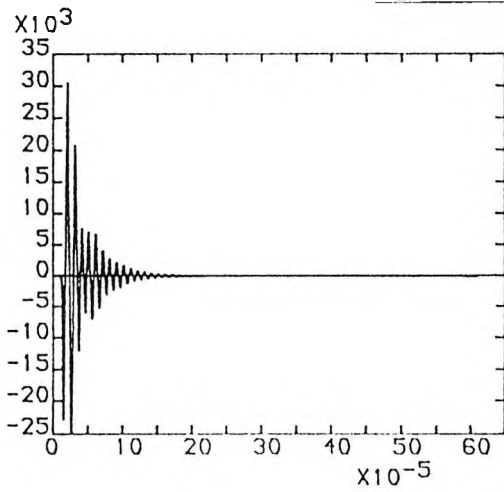
c: 100±2.5 kHz

X axis: TIME - Seconds
Y axis: VOLTAGES - Volts
(TUNER OUTPUT)

Figure 4.1   FAULT RESPONSES AT DIFFERENT
FREQUENCIES

Cont.
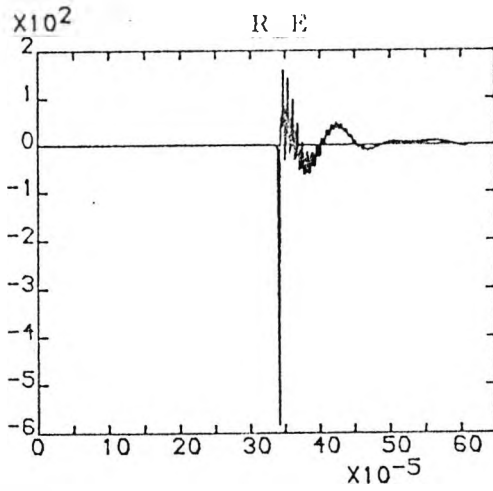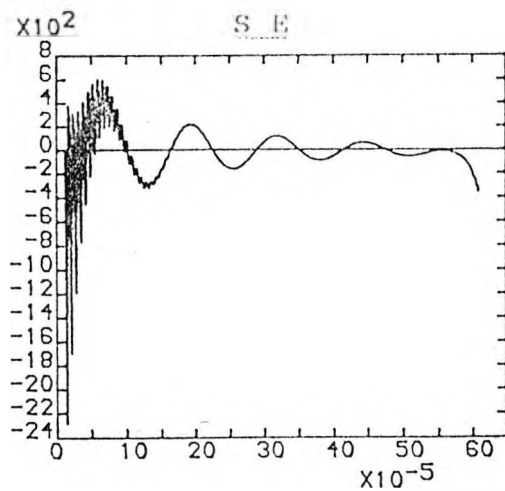
d: 200±100 kHz
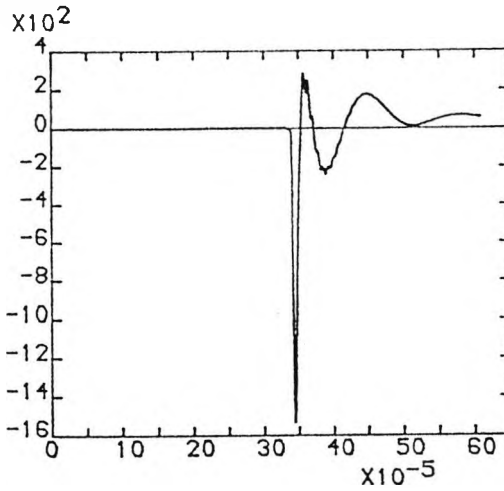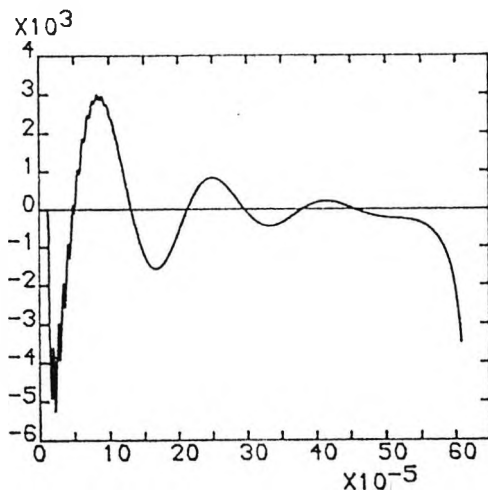
e: 50±40 kHz

X axis: TIME - Seconds
Y axis: VOLTAGES - Volts
(TUNER OUTPUT)

Figure 4.1   FAULT RESPONSES AT DIFFERENT
FREQUENCIES
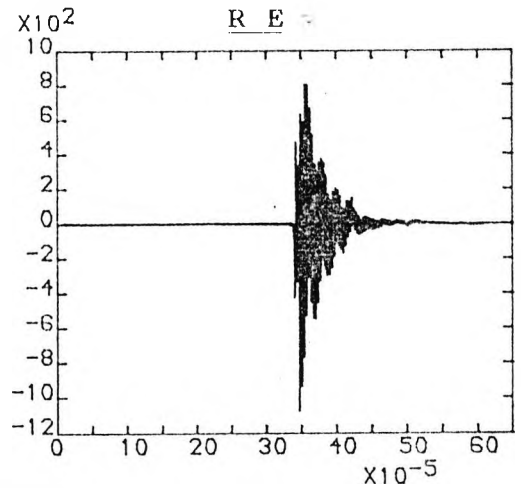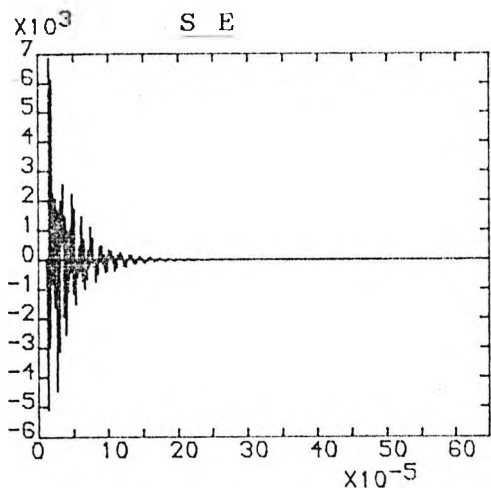
a: Internal fault
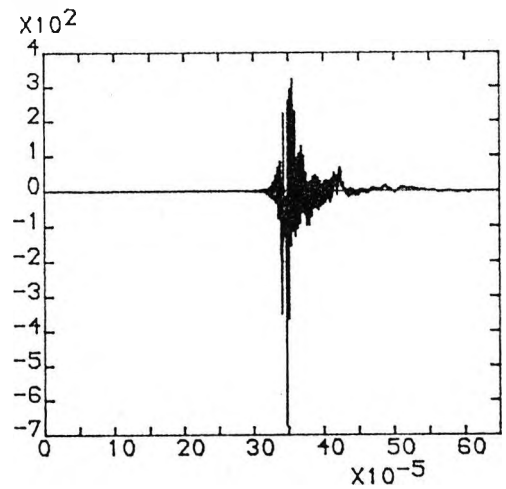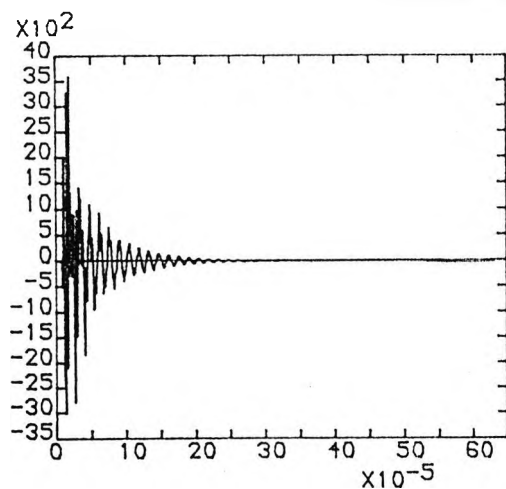
b: Reverse fault

a: Internal fault

VD=1,TF=1
TR=0,TRIP=1

VD=1,TF=1
TR=0,TRIP=1

b: Reverse fault

VD=1,TF=0
TR=1,TRIP=0

VD=0,TF=1
TR=0,TRIP=0

X axis: TIME - Seconds
Y axis: VOLTAGES - Volts
(TUNER OUTPUT)
Figure 4.2   ESTABLISHMENT OF THE PRINCIPLE
(STACK-TUNER MID-FREQUENCY 300±2.5 kHz)
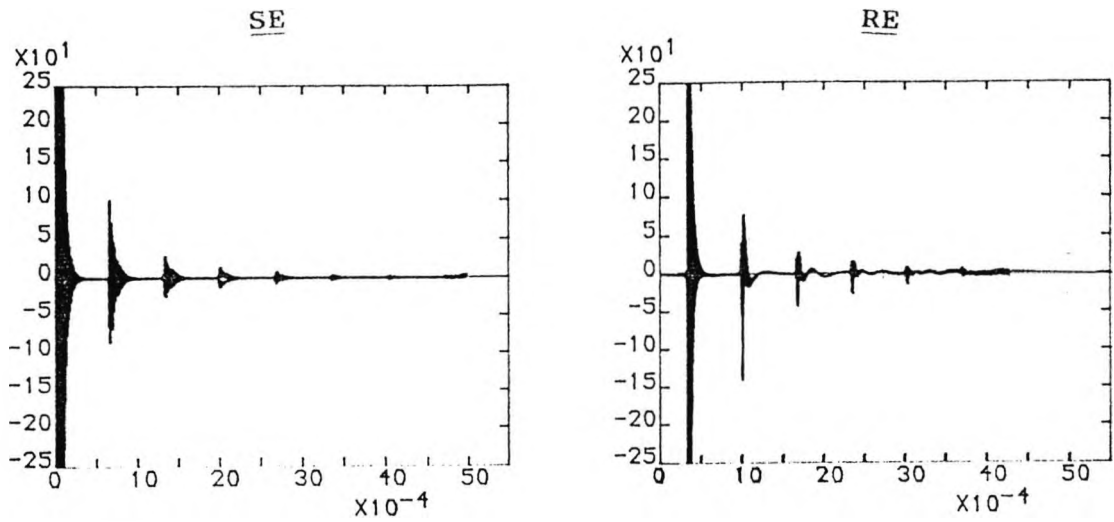
SE   RE

a: Internal Fault
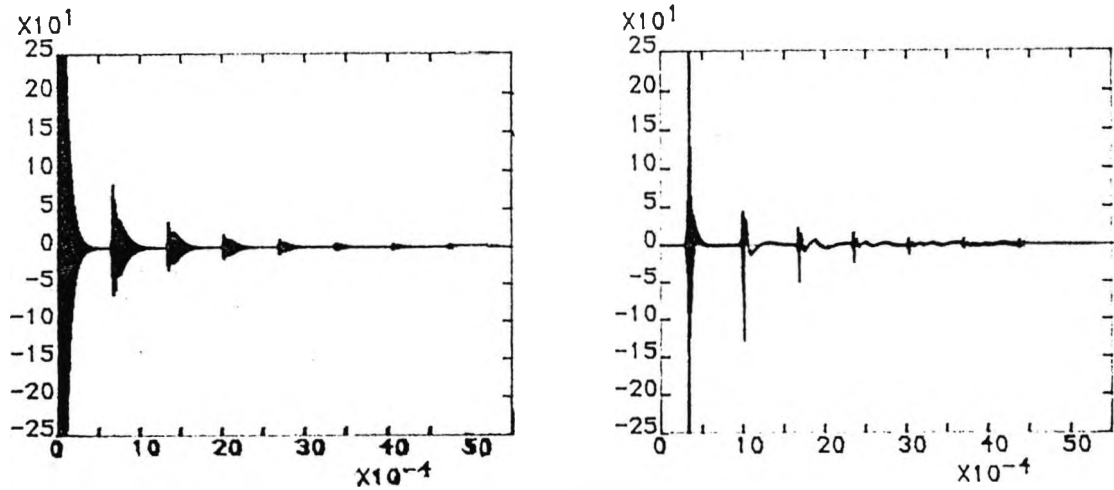
b: Reverse Fault

X-Axis: TIME-Seconds
Y-Axis: TUNER OUTPUT VOLTAGE- Volts

Figure 4.3 DISCRIMINATION TEST BASED ON RESPONSES FOR 5
MILLI-SECONDS (STACK-TUNER MID-FREQUENCY
300±2.5 kHz)

STACK-TUNER OUTPUT — V_F → [AUTO CORRELATOR] — V_A → [DD OPERATING DELAY] — χ → [$\int \chi^2 dt$] — y → [LEVEL DETECTOR] — V_D → [DECISION LOGIC]

REVERSE SIGNAL TO STACK - TUNER SWITCH S ← T_R — [FORWARD/REVERSE SIGNAL FROM DIRECTIONAL DETECTOR DD] — $T_{F,R}$ →

TRIP SIGNAL
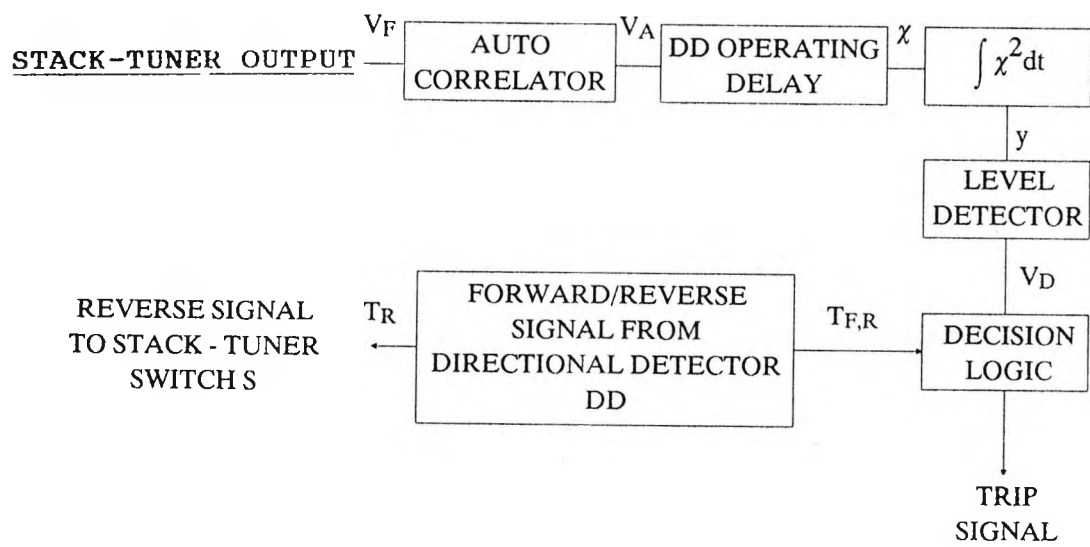
Figure 4.4 BLOCK DIAGRAM REPRESENTATION FOR SIGNAL PROCESSING

SE   RE
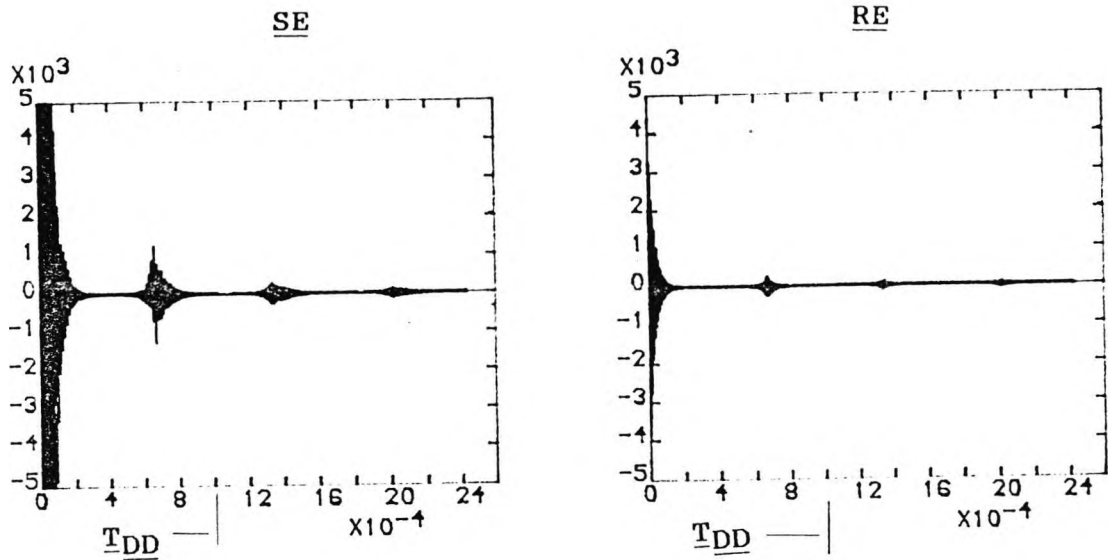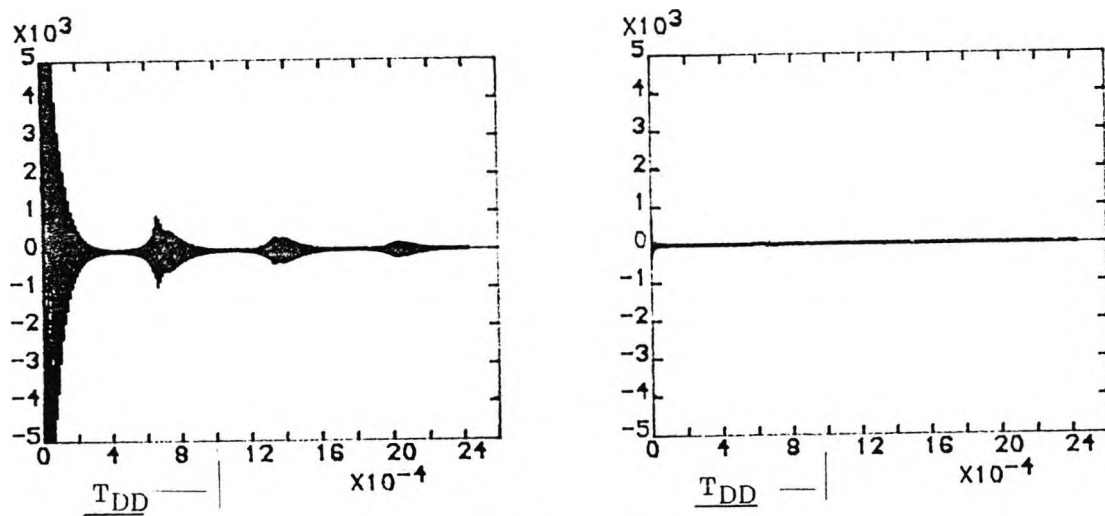
a: Internal Fault

b: Reverse Fault

X-Axis: TIME–Seconds
Y-Axis: AUTO-CORRELATED SIGNAL VOLTAGE
V_A/OR SIGNAL 'X' AFTER DELAY T_{DD}-Units

(DELAY DUE TO $x(k\delta t)$ NOT CONSIDERED – REF. CHAPTER 4.3)

Figure 4.5 AUTO-CORRELATED RESPONSES OF FIGURE 4.3
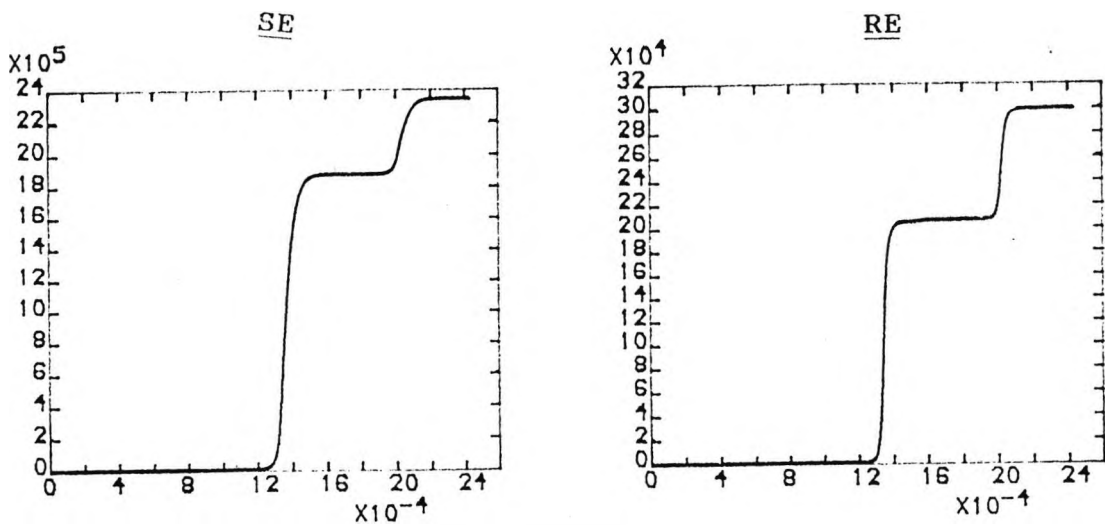
a: Internal Fault

y=1, TF=1
TR=0, TRIP=1

y=1, TF=1
TR=0, TRIP=1

y=1, TF=0
TR=1, TRIP=0

y=0, TF=1
TR=0, TRIP=0
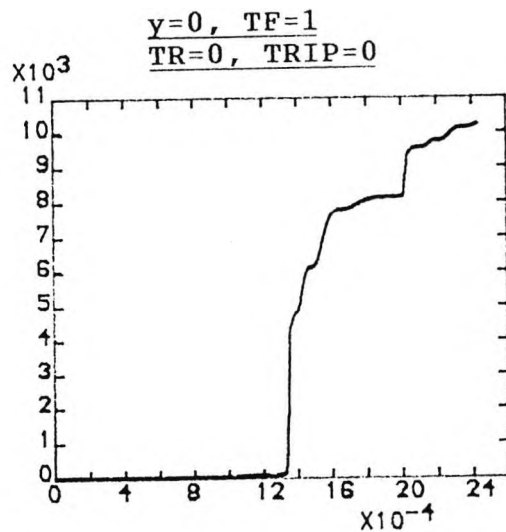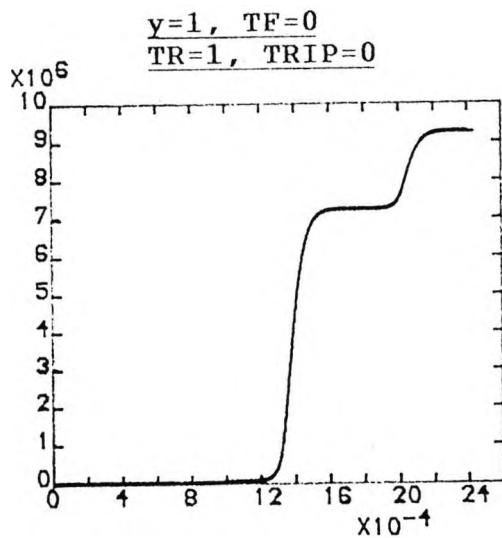
b: Reverse Fault

X-Axis: TIME-Seconds
Y-Axis: RESPONSE 'y' VOLTAGE- Units

Figure 4.6 RESPONSES 'y' FOR DISCRIMINATION TEST
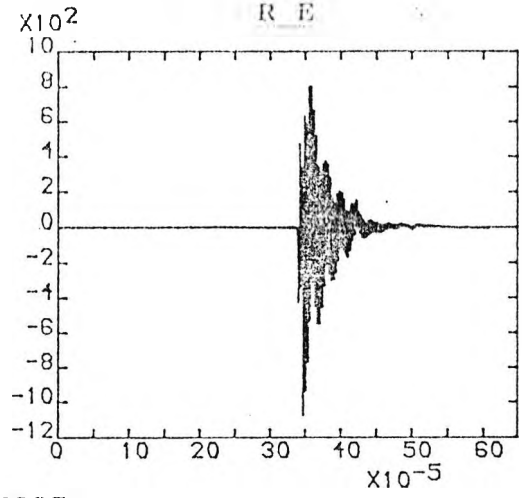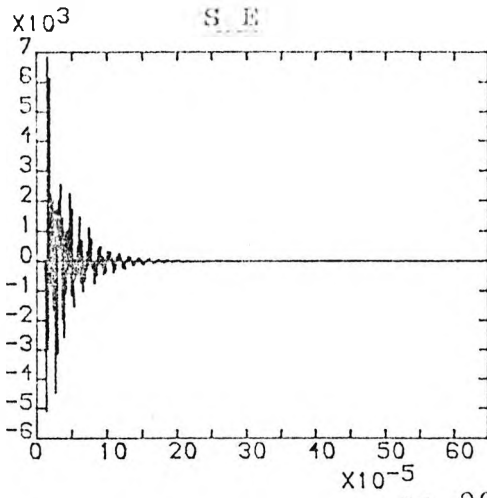
a: 90 Degrees
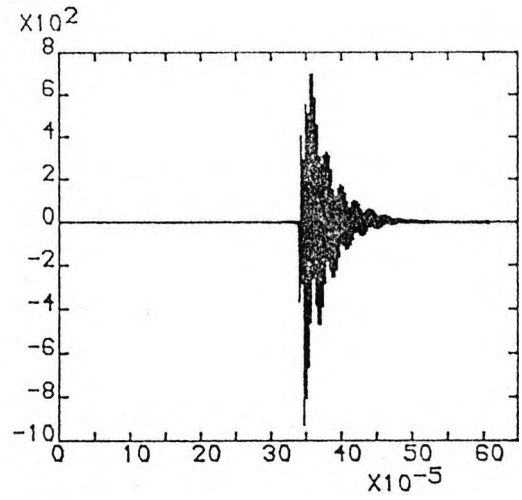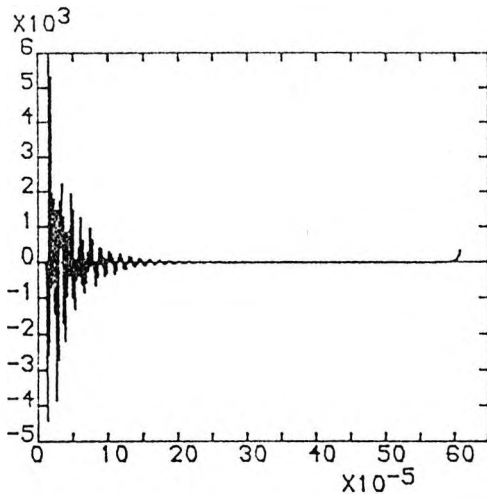
b: 60 Degrees
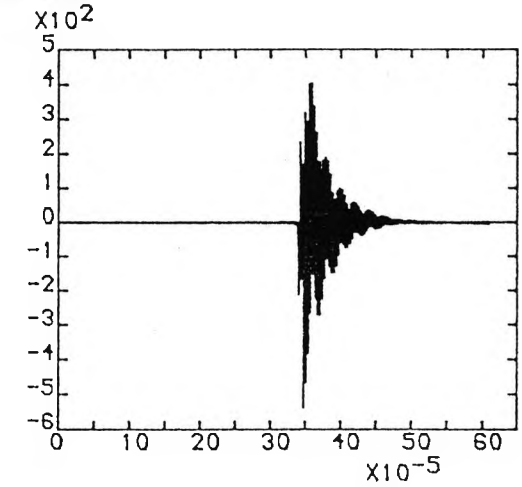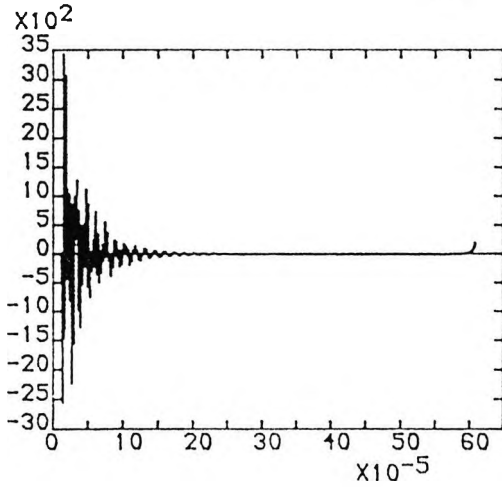
c: 30 Degrees

X axis: TIME - Seconds
Y axis: VOLTAGES - Volts
(TUNER OUTPUT)

Figure 4.7   EFFECT OF DIFFERENT   FAULT
INCEPTION ANGLES

Cont.
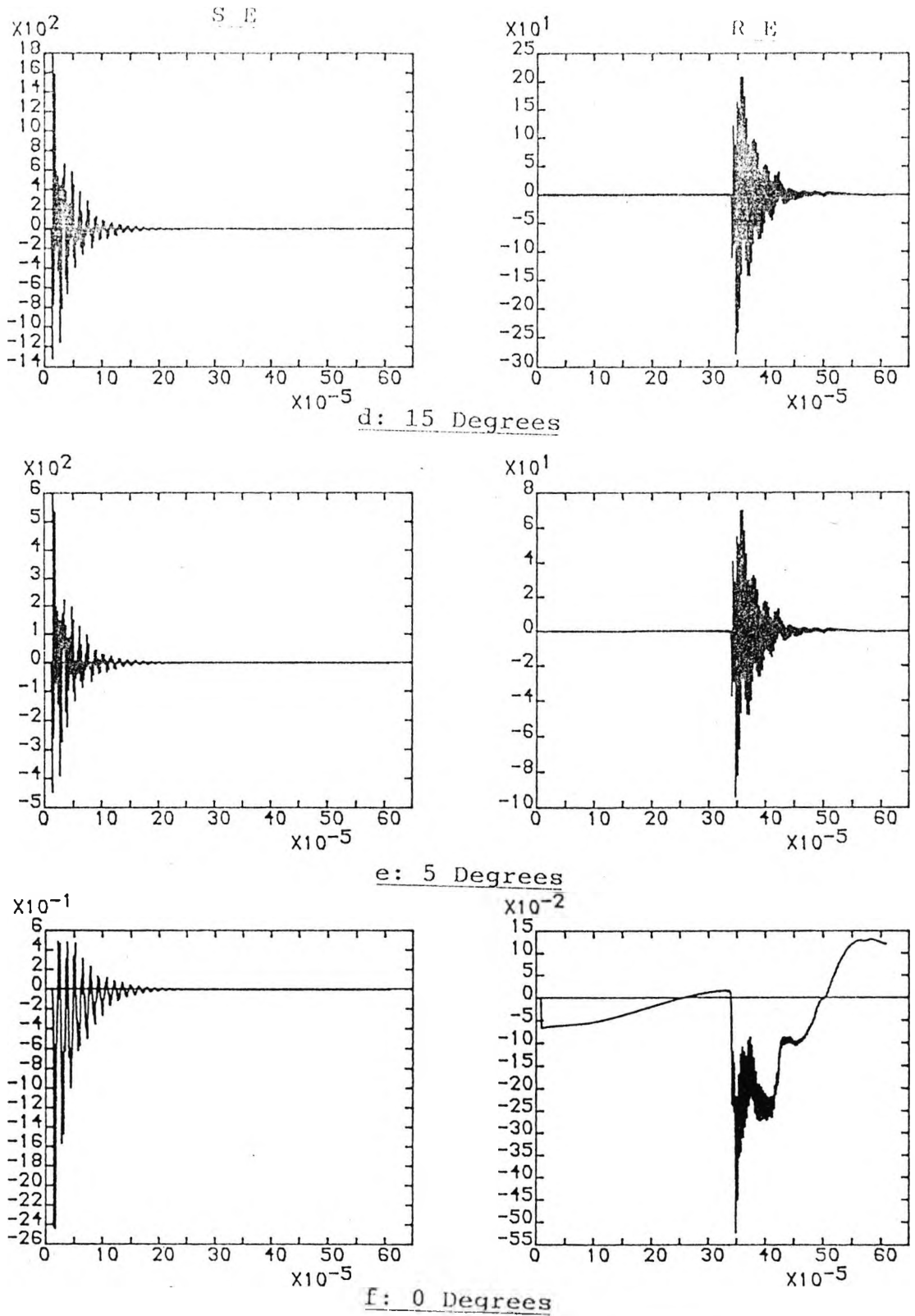
S E   R E

d: 15 Degrees

e: 5 Degrees

f: 0 Degrees

X axis: TIME - Seconds
Y axis: VOLTAGES - Volts
(TUNER OUTPUT)

Figure 4.7   EFFECT OF DIFFERENT FAULT
INCEPTION ANGLES
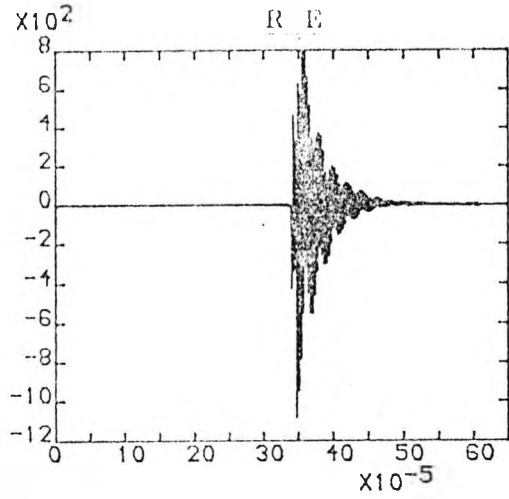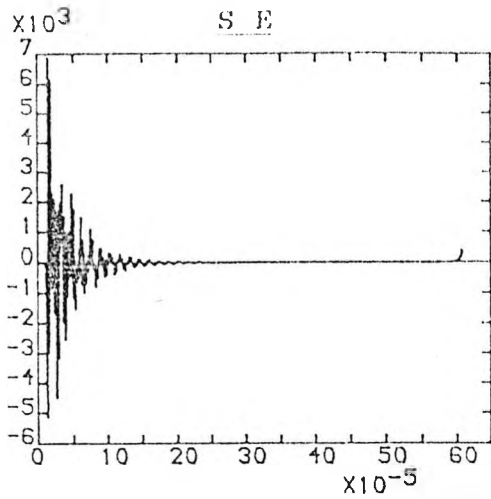
a: 1 GVA at both ends
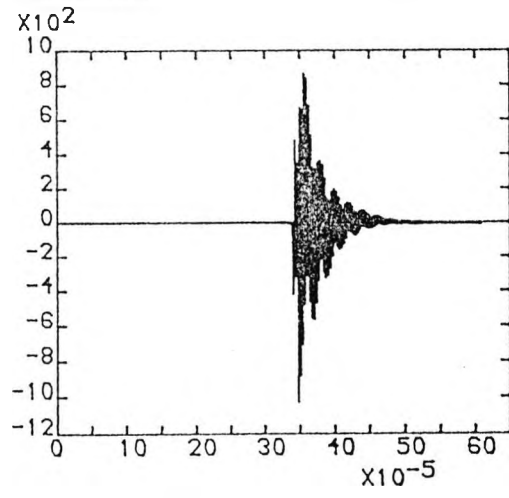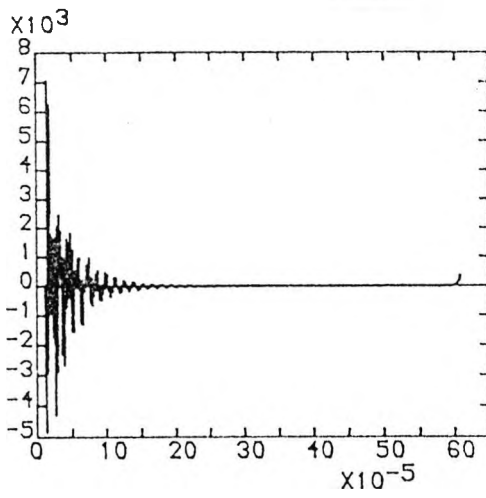
b: 99 GVA at both ends
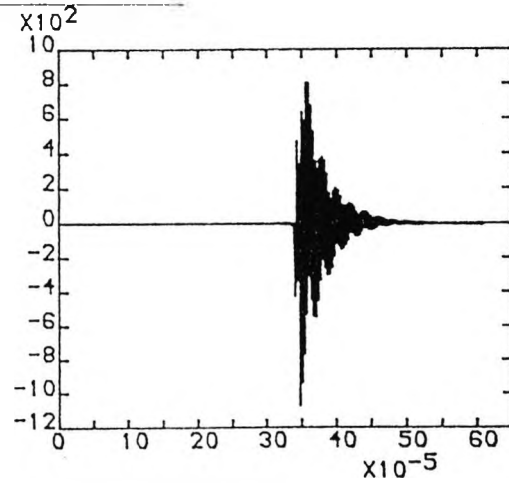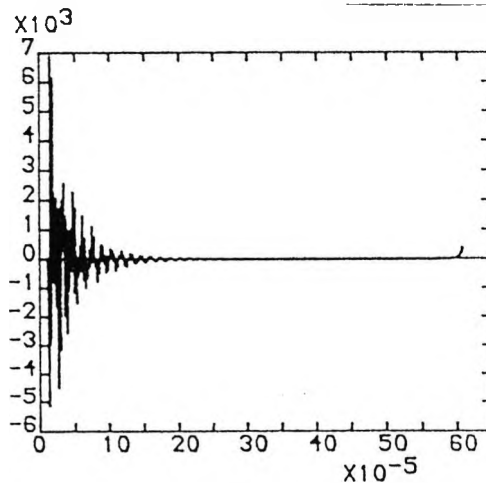
c: 5 GVA at SE and 20 GVA at RE

X axis: TIME - Seconds
Y axis: VOLTAGES - Volts
(TUNER OUTPUT)

Figure 4.8   EFFECT OF DIFFERENT   SOURCE
CAPACITIES

CHAPTER 5

NATURAL MODES OF PROPAGATION, DIGITAL SIMULATION AND SIMULATED TEST RESULTS

This chapter describes the natural modes of propagation and its application to get a composite signal to establish the basic principle of the scheme and to detect any kind of fault. A technique for the digital simulation of the natural modes has been explained. Further, various simulated test results of the new scheme (reference Chapter 2) based on the composite signal using natural modes of propagation have been discussed.

5.1 NATURAL MODES OF PROPAGATION

This section describes: (1) a theoretical concept of the natural modes of propagation, (2) application of the natural modes of propagation in the Power Line Carrier System, (3) application of the natural modes of propagation for Power System Protection purposes.

5.1.1 <u>THEORETICAL CONCEPT OF THE NATURAL MODES OF PROPAGATION</u>

It is a well known fact that a multi-conductor line can be represented in terms of the phase variables: voltages and currents as in Equation (3.26) of Chapter 3 using Admittance Matrix Method. Equation (3.26) is being re-written for a transmission line of length 'l' with sending end and receiving end voltages and currents as below:

$$
\begin{bmatrix} \bar{I}_S \\ \bar{I}_R \end{bmatrix} = \begin{bmatrix} A_{y1} & -B_{y1} \\ B_{y1} & -A_{y1} \end{bmatrix} \begin{bmatrix} \bar{V}_S \\ \bar{V}_R \end{bmatrix} \tag{5.1}
$$

where $A_{yi} = Y_O \coth(\Phi l)$

$\qquad B_{yi} = Y_O \operatorname{cosech}(\Phi l)$

$\qquad Y_O = [Z]^{-1} Q \, \Gamma \, Q^{-1}$

$\bar{V}_S$, $\bar{I}_S$ are the sending end voltages and currents.

$\bar{V}_R$ and $\bar{I}_R$ are the receiving end voltages and currents.

Y_O is the surge admittance.

Γ is $\sqrt{ZY}$ where Z is the impedance matrix and Y is the admittance matrix of the line.

The solution of Equation (5.1) needs evaluation of Φ. In the evaluation of Φ, a numerical difficulty has been

89

noticed in general. For this purpose, diagonilisation of matrix is suggested so that the function can be obtained directly from the eigen value matrix 'Γ'. If $Γ^2$ is the diagonal eigen value matrix then it follows from

$$Z Y = Q Γ^2 Q^{-1} \qquad (5.2)$$

that the relevant matrices used in the two port equations for example, can be evaluated by the theory of matrix functions leading to

$$Φ = Q Γ Q^{-1} \qquad (5.3)$$

Q being a matrix of eigenvectors in which each column corresponds to an eigenvalue of ZY. The diagonalisation leads to the concept of natural modes of propagation.

5.1.1.1 Modal voltages [52]

Consider the semi-infinite line of length x, propagation takes place according to the equation

$$V = e^{-Γx} . V_i \qquad (5.4)$$

90

where V_i is an incident voltage vector. Furthermore finding the eigenvalues and eigenvectors of

$$V = Q e^{-\Gamma x} Q^{-1} V_i \qquad (5.5)$$

and introducing the variables v and v_i such that

$$v = Q^{-1} V \qquad (5.6)$$

and $v_i = Q^{-1} V_i,$ (5.7)

it follows that

$$v = e^{-\Gamma x} v_i \qquad (5.8)$$

But $e^{-\Gamma x}$ is diagonal indicating that each element of v can be considered to the mutual exclusion of all other elements. For any such element, it is possible to think in terms of a single phase line characterised by the corresponding element of 'Γ', there being as many such lines as there are distinct values of 'Γ'.

A solution in terms of each component voltage is exactly

analogous to the solution of a single line problem. Each component voltage is associated with its own propagation constant Γ_k where for

$$\Gamma_k = \alpha_k + j\,\beta_k,$$

α_k and β_k define attenuation and phase shift constants per unit length respectively. The latter also defines phase velocity such that $u_k = w\,/\,\beta_k$ where w is frequency in radians.

The concept of component voltages leads to the simple interpretation that at any point x the actual voltage vector may be considered as being composed of a number of components, the relative distribution of voltage corresponding to a given component being defined by a particular column of Q, known as the modal matrix. These columns in turn define <u>natural modes of propagation</u>. Thus if one of the natural modes is generated at one end of a multiconductor line it will propagate without changing its voltage distribution but it will of course be attenuated and shifted in phase. If the initial voltage vector does not correspond to a particular mode, the vector V at any point x will not have the same relative distribution as V_i. In general there are as many modes as there are effective conductors. As an example, consider a three phase horizontal line for which the eigen vector or mode distribution matrix Q is given by

$$Q = \begin{bmatrix} 1 & 1 & 1 \\ 1 & 0 & -2 \\ 1 & -1 & 1 \end{bmatrix} \qquad (5.9)$$

Then from $Q^{-1} = \begin{bmatrix} \dfrac{1}{3} & \dfrac{1}{3} & \dfrac{1}{3} \\ \dfrac{1}{2} & 0 & -\dfrac{1}{2} \\ \dfrac{1}{6} & -\dfrac{1}{3} & \dfrac{1}{6} \end{bmatrix}$ (5.10)

it follows that when the centre conductor is energised from a unit voltage source with the remaining conductors short circuited

$$v_i = Q^{-1} V_i = Q^{-1} \begin{bmatrix} 0 \\ 1 \\ 0 \end{bmatrix} = \begin{bmatrix} \dfrac{1}{3} \\ 0 \\ -\dfrac{1}{3} \end{bmatrix} \qquad (5.11)$$

so that it may be seen that the initial voltage vector is composed of 1/3 of mode 1, zero mode 2 and -1/3 mode 3. i.e.

93

$$V_i = Q \, v_i = \begin{array}{c} \text{Phase} \\ a \\ b \\ c \end{array} \overset{\begin{array}{ccc} \text{Mode} \\ 1 & 2 & 3 \end{array}}{\begin{bmatrix} 1 & 1 & 1 \\ 1 & 0 & -2 \\ 1 & -1 & 1 \end{bmatrix}} \begin{bmatrix} \dfrac{1}{3} \\ 0 \\ -\dfrac{1}{3} \end{bmatrix}$$

$$= \frac{1}{3} \underset{\text{Mode 1}}{\begin{bmatrix} 1 \\ 1 \\ 1 \end{bmatrix}} - \frac{1}{3} \underset{\text{Mode 3}}{\begin{bmatrix} 1 \\ -2 \\ 1 \end{bmatrix}} \qquad (5.12)$$

and at any point x

$$V = e^{-\Gamma 1 x} \underset{\text{Mode 1}}{\begin{bmatrix} \dfrac{1}{3} \\ \dfrac{1}{3} \\ \dfrac{1}{3} \end{bmatrix}} - e^{-\Gamma 3 x} \underset{\text{Mode 3}}{\begin{bmatrix} \dfrac{1}{3} \\ -\dfrac{2}{3} \\ \dfrac{1}{3} \end{bmatrix}} \qquad (5.13)$$

where $\Gamma 1$, $\Gamma 3$ are propagation constants for Mode 1, Mode 3. Moreover, from the attenuation constants associated with the three modes, typically 10 dB/km, 0.1 dB/km and 0.01 dB/km respectively at power line carrier frequencies, it is seen that the attenuation of modes 1 and 3 are in the ratio 1000/1. In consequence, for matched conditions say at a point x = 87 km the arrival voltage has the distribution of mode 3 modified in magnitude by

94

$$\frac{1}{3} e^{(-0.01 \times (87/8.7))} = \frac{1}{3} e^{-0.1} \qquad (5.14)$$

(since 1 Np = 8.7 dB) assuming that mode 1 voltage received can be neglected because of its high attenuation. As a result an appreciable part of the arrival power is contained on the two conductors which in the first instance had no signal coupled to them.

5.1.1.2 <u>Perfectly Transposed Three Phase Line</u>[52]

For a perfectly transposed, and therefore balanced line, the modes correspond to the positive, negative and zero sequence components. If a_s is the operator for the symmetrical components then

$$Q = \begin{bmatrix} 1 & 1 & 1 \\ 1 & a_s^2 & a_s \\ 1 & a_s & a_s^2 \end{bmatrix} \qquad (5.15)$$

and $\quad K = Q^{-1} = \frac{1}{3} \begin{bmatrix} 1 & 1 & 1 \\ 1 & a_s & a_s^2 \\ 1 & a_s^2 & a_s \end{bmatrix} \qquad (5.16)$

It is known in this case that the propagation constant of the zero sequence mode is greater than that of the balanced sequences. This is due to the presence of the earth, i.e. a perfectly transposed line having a voltage distribution

95

corresponding to the zero sequence component must be coupled electromagnetically to the earth return path exclusively. On the other hand the balanced or aerial modes are characterised by their independence of earth effects. This results in the zero phase sequence impedance being greater than the positive and negative, these latter two being equal (as are the propagation constants).

In practice a line is not transposed perfectly. For a single circuit horizontal line the eigenvector matrix can have the form:

$$
Q = \begin{array}{c} \\ a \\ b \\ c \end{array}
\begin{array}{ccc} \text{Phases} & 1 & 2 & 3 \end{array}
\begin{bmatrix} 1 & 1 & 1 \\ 1 & 0 & -2 \\ 1 & -1 & 1 \end{bmatrix}
\qquad (5.17)
$$

and in this case the propagation constants (velocity and attenuation) are different as shown in Table 5.1 and to some degree depend upon earth effects. Mode 1 being highly dependent on earth effects, has a zero sequence characteristic and for this reason is often referred as the Earth Mode. Mode 2 even though it appears balanced, depends upon conductor height above ground and the separation between outer conductors but is less affected by the presence of the earth. In the extreme case of an infinite separation between outer conductors, these conductors can be considered as independent systems with separate earth return paths, whereas for a separation very much less than conductor height above ground, little electromagnetic coupling between the conductors and earth

exists. similar reasoning applies to Mode 3 but because of its more balanced nature, its propagation constant is generally less than that of Mode 2. This is particularly so at high frequencies. For Mode 3, smaller separation between adjacent conductors is more important than the separation between the outers.

It may be noted that modes having the lower velocities of propagation are also those with the highest attenuation. This is shown in Table 5.1 which gives typical values of velocity and attenuation for single and double circuit horizontal and vertical lines.

5.1.2 APPLICATION OF THE NATURAL MODES OF PROPAGATION IN POWER LINE CARRIER COMMUNICATION

For many years, the application of power-line-carrier was empirical. Lines were relatively short, and attenuation was usually well within the dB rating of the transmitter and receiver. Line attenuation was measured after the equipment was installed, if at all. Ocasionally, inexplicable anomalies were noted. Often utilities discovered that a carrier channel was coupled to two different phases at opposite ends of the line, and that this combination gave the best received signal level. It was also noted that the rate of attenuation (dB/mi) on a short line was apparently higher than on a long line. At that time, these observations were simply accepted and used.

With the introduction of long EHV lines, however, it became necessary to predict carrier performance accurately, even before the line was built. Modal analysis provides such an approach. It is a mathematical tool similar to the symmetrical components technique used for analyzing unbalanced faults on three-phase power system at 50 or 60 Hz. Like its power counterpart, modal analysis is a practical system whose components or 'modes' can be electrically generated and measured separately.

If a given carrier-frequency power were applied to a single conductor line, the power level would decrease exponentially with distance. At a distance of about 10 miles, approximately 1 percent of the input power would be present. Such a system would obviously be impractical for a power-line carrier channel. If the same input power were fed into one phase conductor of a three-phase horizontal line, however, the 1-percent signal can be obtained from any of the phase conductor at a distance of about 250 mi. Thus, it is apparent that, even though only one conductor is energized, the other two phase wires play an important part in the propagation of carrier energy. Indeed, modal theory is based on the premise that there are as many independent 'modes' of propagation on a multiconductor line as there are conductors involved in the propagation of energy.

There are five characteristics of natural modes:

a. Any set of phase-conductor currents or voltages existing at any point on a lossy, reflection-free three-phase line can be resolved into three sets of natural-mode components.

b. At any point on a line, the mode components must add up to the actual phase quantities. Also, the total power derived from phase currents and voltages must be equal to the sum of mode powers.

c. The ratio of mode voltage to mode current (the 'mode characteristic impedance') is constant on each phase conductor.

d. Each mode propagates with a specific attenuation per unit length and a specific velocity of propagation.

e. A set of phase components corresponding to one mode only cannot be resolved into other modes. The modes are independent, and there is no inter-mode coupling on a uniform line.

There are three modes of propagation which are being described as per the convention of the Westinghouse Electric Corporation, USA (Power Carrier Equipment manufacturer). These conventions are also as per IEEE publications. Mode 3 is a high attenuation mode which is propagated on all three phases with ground return. Because of its high attenuation, mode 3 can be neglected beyond about 10 miles from the transmitter.

Mode 2 is a medium-attenuated mode that is propagated on one outside phase and returns on the other outside phase. There is no mode 2 current in the center phase. Mode 2 losses are higher and more frequency-dependent than mode 1

losses.

Mode 1 is the least attenuated of the three modes, and makes carrier channels possible on long EHV lines. The energy is propagated on the two outer phases and returns on the center phase. Mode 1 attenuation is the lowest, and the least frequency-dependent.

In Section 5.1.1, Mode 3 and Mode 1 have been described as Mode 1 and Mode 3 respectively.

5.1.2.1 **Modal quantities on an EHV Three-phase Line**

Modal analysis has been most generally applied to a horizontally spaced, single-circuit, three-phase EHV line with two overhead static wires 'g' (Figure 5.1). Grounded at each tower, the static wires do not generate any transmission modes. The three modes present on such a system are shown in Figure 5.2. Coefficients p and q are the center-phase mode coefficients for modes 1 and 3, respectively, and depend on the line under study. The value of 'q' will vary from about 1.1 to 1.3; p can range from about -1.6 to -1.9. Modal calculations and field tests on a 40-mile, 500-kV line, provided with reflection-free termination gave the 'p' and 'q' values and mode impedance values listed in Table 5.2.

Values of attenuation coefficients and relative phase velocity for the three modes are shown in Table 5.3. Data shown are for lines from 345 to 765 kV.

5.1.3 <u>APPLICATION OF THE MODAL CONCEPT FOR PROTECTION</u> <u>PURPOSES</u>

Application of the Modal Concept for calculation of superimposed components of the voltages and currents in a transmission line system has been described in Section 5.1.1. Application of the Modal Concept in carrier applications has been described in Section 5.1.2. In this section, application of the Modal Concept has been described for protection purposes. When a disturbance or a fault occurs on a transmission line, voltages and currents (which include superimposed components) in different phases can be found at both ends of a transmission line. These voltages and currents are used for relaying applications. Normally three protection eqipments will be required for a three phase system which is generally an un-economic proposal. In case of radio-interference, signals can be coupled to all the phases, and the protection equipment may mal-operate. With these considerations, it is proposed to combine the three phase output signals in a suitable 'mode', and the advantages can be described as below:

1. economical,

2. provides a composite signal to detect any kind of fault (phase to earth, phase to phase, etc.) using a single protection equipment,

3. cancels the signals due to other sources of noise, e.g. radio-interference.

Since the earth-mode does not cancel signals due to other sources of noise e.g. radio interference, application of

the earth mode has not been considered. Only (1,0,-1) Mode and (1,-2,1) Mode have been considered.

5.2 DIGITAL SIMULATION TECHNIQUE OF (1,0,-1) MODE AND (1,-2,1) MODE FOR PROTECTION APPLICATION

Theoretically, a relationship between the phase voltages and the modal voltages can be expressed as

$$v = Q^{-1} V \tag{5.18}$$

where v is the modal voltages in the matrix form (1,3), V is the phase voltages in the matrix form (1,3) and Q is the eigen vector in the matrix form (3,3) for a three- phase single circuit line. This can be expressed as

$$
\begin{bmatrix} v_0 \\ v_1 \\ v_2 \end{bmatrix} =
\begin{bmatrix} a & a & a \\ a & 0 & -a \\ a & -2a & a \end{bmatrix}
\begin{bmatrix} V_a \\ V_b \\ V_c \end{bmatrix}
\tag{5.19}
$$

where V_0, V_1, V_2 are the Earth Mode, Aerial Mode 1, and Aerial Mode 2 respectively. 'a' is a coefficient of inverse of the eigen vector matrix Q. V_a, V_b, V_c are phase voltages for the Phase 'a', Phase 'b', Phase 'c' respectively.

Steady State Modal Voltages

For the purpose of the digital simulation of the pre-fault steady state voltages, Equation (5.19) can be expressed as below at the sending end, say P (reference Chapter 2)

$$
\begin{bmatrix} V0PSC \\ V1PSC \\ V2PSC \end{bmatrix} = \begin{bmatrix} SI(1,1) & SI(1,2) & SI(1,3) \\ SI(2,1) & SI(2,2) & SI(2,3) \\ SI(3,1) & SI(3,2) & SI(3,3) \end{bmatrix} \begin{bmatrix} VPS(1,1) \\ VPS(2,1) \\ VPS(3,1) \end{bmatrix} \tag{5.20}
$$

and at the receiving end Q (reference Chapter 2)

$$
\begin{bmatrix} V0QSC \\ V1QSC \\ V2QSC \end{bmatrix} = \begin{bmatrix} SI(1,1) & SI(1,2) & SI(1,3) \\ SI(2,1) & SI(2,2) & SI(2,3) \\ SI(3,1) & SI(3,2) & SI(3,3) \end{bmatrix} \begin{bmatrix} VQS(1,1) \\ VQS(2,1) \\ VQS(3,1) \end{bmatrix} \tag{5.21}
$$

Alternatively, euuations (5.20) and (5.21) can be written as

$$
\begin{bmatrix} VpPSC \end{bmatrix} = \begin{bmatrix} SI(p,q) \end{bmatrix} \begin{bmatrix} VPS(p,q) \end{bmatrix} \tag{5.22}
$$

$$
\begin{bmatrix} VpQSC \end{bmatrix} = \begin{bmatrix} SI(p,q) \end{bmatrix} \begin{bmatrix} VQS(p,q) \end{bmatrix} \tag{5.23}
$$

where SI(p,q) denotes Q^{-1} matrix if p = 1,2,3 and q = 1,2,3. VpPSC and VpQSC denote Sending End 'P'and Receiving End 'Q' Modal Voltages: Earth Mode (1,1,1), Mode 1 (1,0,-1) and Mode 2 (1,-2,1) if p = 0,1,2. VPS(p,q) and VQS(p,q) are Sending End 'P' and Receiving End 'Q' phase voltages for Phase 'a', Phase 'b' and Phase 'c' if p = 1,2,3 and q = 1.

From the equations (5.20) and (5.21), Mode (1,0,-1) voltages at Sending End 'P' and Receiving End 'Q' can be written as below:

$$V1PSC = VPS(1,1)*SI(2,1) + VPS(2,1)*SI(2,2) +$$
$$VPS(3,1)*SI(2,3) \quad\quad\quad (5.24)$$

$$V1QSC = VQS(1,1)*SI(2,1) + VQS(2,1)*SI(2,2) +$$
$$VQS(3,1)*SI(2,3) \quad\quad\quad (5.25)$$

From the equations (5.20) and (5.21), Mode (1,-2,1) voltages at Sending End 'P' and Receiving End 'Q' can be written as below:

$$V2PSC = VPS(1,1)*SI(3,1) + VPS(2,1)*SI(3,2) +$$
$$VPS(3,1)*SI(3,3) \quad\quad\quad (5.26)$$

$$V2QSC = VQS(1,1)*SI(3,1) + VQS(2,1)*SI(3,2) +$$

$$VQS(3,1)*SI(3,3) \qquad (5.27)$$

Pre-fault steady state modal voltages (1,0,-1) and (1,-2,1) can be found corresponding to each sampling point directly in the time domain at both ends of the transmission line using equations (5.24), (5.25), (5.26), (5.27).

SUPERIMPOSED MODAL VOLTAGES

For the purpose of the digital simulation of the post-fault superimposed voltages, Equation (5.19) can be expressed in the frequency domain as below at the sending end P (reference Chapter 2)

$$\begin{bmatrix} V0PFC \\ V1PFC \\ V2PFC \end{bmatrix} = \begin{bmatrix} SI(1,1) & SI(1,2) & SI(1,3) \\ SI(2,1) & SI(2,2) & SI(2,3) \\ SI(3,1) & SI(3,2) & SI(3,3) \end{bmatrix} \begin{bmatrix} VPF(1,1) \\ VPF(2,1) \\ VPF(3,1) \end{bmatrix} \qquad (5.28)$$

and at the receiving end Q (reference Chapter 2)

$$\begin{bmatrix} V0QFC \\ V1QFC \\ V2QFC \end{bmatrix} = \begin{bmatrix} SI(1,1) & SI(1,2) & SI(1,3) \\ SI(2,1) & SI(2,2) & SI(2,3) \\ SI(3,1) & SI(3,2) & SI(3,3) \end{bmatrix} \begin{bmatrix} VQF(1,1) \\ VQF(2,1) \\ VQF(3,1) \end{bmatrix} \qquad (5.29)$$

Alternatively, equations (5.28) and (5.29) can be written as

$$\left[\text{VpPFC} \right] = \left[\text{SI}(p,q) \right] \left[\text{VPF}(p,q) \right] \qquad (5.30)$$

$$\left[\text{VpQFC} \right] = \left[\text{SI}(p,q) \right] \left[\text{VQF}(p,q) \right] \qquad (5.31)$$

where SI(p,q) denotes Q^{-1} matrix if p = 1,2,3 and q = 1,2,3. VpPFC and VpQFC denote Sending End 'P'and Receiving End 'Q' Modal Voltages: Earth Mode (1,1,1), Mode 1 (1,0,-1) and Mode 2 (1,-2,1) if p = 0,1,2 in the frequency domain. VPF(p,q) and VQF(p,q) are Sending End 'P' and Receiving End 'Q' phase voltages for Phase 'a', Phase 'b' and Phase 'c' if p = 1,2,3 and q = 1 in the frequency domain.

From the equations (5.28) and (5.29), Mode (1,0,-1) voltages at Sending End 'P' and Receiving End 'Q' can be written as below:

V1PFC = VPF(1,1)*SI(2,1) + VPF(2,1)*SI(2,2) +

      VPF(3,1)*SI(2,3)   (5.32)

V1QFC = VQF(1,1)*SI(2,1) + VQF(2,1)*SI(2,2) +

      VQF(3,1)*SI(2,3)   (5.33)

From the equations (5.28) and (5.29), Mode (1,-2,1) voltages at Sending End 'P' and Receiving End 'Q' can be written as below:

V2PFC = VPF(1,1)*SI(3,1) + VPF(2,1)*SI(3,2) +

VPF(3,1)*SI(3,3)   (5.34)

V2QFC = VQF(1,1)*SI(3,1) + VQF(2,1)*SI(3,2) +

VQF(3,1)*SI(3,3)   (5.35)

The above Modal voltages in the frequency domain can be written as a function f (w) where 'w' is frequency in radians. Now to calculate these modal voltages in the time domain, the Modified Fourier Transform Technique has been applied as below:

$$f(t) = REAL \; \frac{e^{\alpha t}}{\pi} \int_{0}^{\Omega} f(w - j\alpha) \; e^{jwt}\sigma \; dw \qquad (5.36)$$

where f(t) is a function of time representing Modal voltages in the time domain. α is a factor to avoid Gibbs oscillations. This factor is expressed as:

$$\sigma = \sin(\pi w/\Omega) / (w\pi/\Omega) \qquad (5.37)$$

In addition, a constant ' α ' is introduced to ensure numerical stability. This constant is known as the frequency shift constant. Ω is the truncation frequency. In time domain, equations (5.32), (5.33), (5.34), (5.35) can be written as below:

107

$$\text{V1PTC} = \text{REAL} \ \frac{e^{\alpha t}}{\pi} \ \int_0^\Omega f(w - j\alpha) \ e^{jwt} \sigma \ dw \qquad (5.38)$$

where $f(w - j\alpha)$ is V1PFC $(w - j\alpha)$

$$\text{V1QTC} = \text{REAL} \ \frac{e^{\alpha t}}{\pi} \ \int_0^\Omega f(w - j\alpha) \ e^{jwt} \sigma \ dw \qquad (5.39)$$

where $f(w - j\alpha)$ is V1QFC $(w - j\alpha)$

$$\text{V2PTC} = \text{REAL} \ \frac{e^{\alpha t}}{\pi} \ \int_0^\Omega f(w - j\alpha) \ e^{jwt} \sigma \ dw \qquad (5.40)$$

where $f(w - j\alpha)$ is V2FFC $(w - j\alpha)$

$$\text{V2QTC} = \text{REAL} \ \frac{e^{\alpha t}}{\pi} \ \int_0^\Omega f(w - j\alpha) \ e^{jwt} \sigma \ dw \qquad (5.41)$$

where $f(w - j\alpha)$ is V2QFC $(w - j\alpha)$

Equations (5.38), (5.39), (5.40), (5.41) give Modal voltages (1,0,-1) and (1,-2,1) at both the ends of the transmission line in the time domain.

5.3 SIMULATED TEST RESULTS

The simulated test results are based on a single phase to earth fault at a distance of 1 km from the sending end (SE) of a 100 km long 400 kV 3-phase transmission line with the end sources of 5 GVA at the SE and 20 GVA at the receiving end (RE). The post-fault observation times are 600 micro-seconds and 5 milli-seconds for different simulated tests. The corresponding sampling frequencies are 853.33 kHz and 819.2 kHz respectively. The fault has been considered at the peak voltage point-on-wave i.e. 90 degree.The internal fault and the reverse or external fault have been considered with reference to Figure 2.1. The fault generated noise signals have been received through the stack tuner circuit as shown in Figure 2.1. The stack tuner circuit has been tuned to the mid-frequency of 300 ± 2.5 kHz and all the simulated test results are based on this mid-frequency of 300 ± 2.5 kHz. The reference for the direction of the fault i.e. forward or reverse is also shown in Figure 2.1. The forward or the reverse fault can be detected by any high speed directional detector device (DD). The operational aspects of the scheme under internal or reverse fault conditions are explained in Figure 2.5. Figure 'A' shows the operatioal aspects at the SE and the RE under the internal fault condition. Figure 'B' shows the operational aspects at the SE and the RE under the reverse fault condition. The stack tuner circuit is arranged either in the normally open mode 'NO' i.e high impedance mode, or the closed mode 'NC' i.e short circuit

mode through a switch 'S' which is operated by the DD as shown in Figure 3.13. Under the internal fault condition, the DD detects the fault as 'forward' at the SE and the RE i.e. the signal T_F as '1'and the signal T_R as '0'. For the internal faults ,the switch 'S' is in the NO mode and is not affected by the DD. The signals V_D corresponding to the fault signal at the SE and the RE are also '1'. '0' or '1' is with reference to a decision logic circuit which gives a tripping signal '1' only when the signals V_D and T_F are '1'. If the fault is at 1 km from the SE of a 100 km long transmission line, the fault response at the SE is instantaneously and at the RE, the fault response is delayed by about 0.4 milli-seconds which is the travelling time of the fault generated travelling wave to reach the RE. If the operating time of the DD is considered as 1 milli-second, then T_F will be available at the SE after a delay of 1 milli-second and at the RE after a delay of 1.4 milli-seconds. Before processing the signal V_D to the decision logic circuit, the signal is processed through a level detector to get the signal '1' or '0'. The level detector detects the level at a particular time, say T_T which is the operating time of the scheme without considering the delay due to the travelling time of the fault generated travelling wave. In such a case the signal T_F from the DD is delayed further by the time T_T - 1 milli-second. If T_T is 2 milli-second, the T_F is delayed further by 1 milli-second. In the reverse fault condition the DD detects the fault as 'forward' at the RE and as 'reverse' at the SE. The signal T_F is '1'at the RE and '0' at the

SE. The signal T_R is '0' at the RE and '1' at the SE. For the reverse faults ,the switch 'S' is in the NO mode at the RE and is not affected by the DD. But at the SE, the NO mode of the 'S' is changed over to the NC mode through a signal from the DD which operates reverse at the SE. This is shown in Figure 2.5 under reverse fault condition. At the SE, the signal V_D is '1', the signal T_F is '0', and the signal T_R is '0' till the stack tuner is under the NO mode. Depending upon the operating time of the DD, the stack tuner changes to the NC mode and provides the signal T_R as '1'. Any way at the SE, V_D is '1' and the T_F is '0', so that the decision logic output for the tripping is always '0'. At the RE, V_D is '1' till the stack tuner at the SE changes over to the NC mode. Once the stack tuner changes to the NC mode at the SE , the signal V_D at the RE becomes '0' due to the short circuiting of the signal at the SE. The signal T_F is '1' at the RE. The signal T_R is '0' at the RE. The decision logic output is always '0'at the RE. Therefore the scheme does not operate under the reverse fault condition. The signal processing of the scheme is explained in Figure 5.3. V_{oa}, V_{ob}, V_{oc} are the output of the stack tuners corresponding to the three phases of the transmission line. These signals have been combined in a suitable Aerial mode (1,0,-1) or (1,-2,1) to get a composite signal, V_F. This signal is passed through a suitable filter i.e. auto-correlator or a band pass filter. The simulated test results have been studied for both the filters: (1) Band Pass Filter of a narrow band width, (2) auto-correlator. The otput signal of this filter is

called, V_X which passes through an 'AND GATE'. The 'AND GATE' also receives a signal from the DD after an operating time delay, say typically 1 milli-second. The output of this 'AND GATE', V_Y does not indicate fault response for this delay of 1 milli-seconds. This delay is increased if the travelling time of the fault generated travelling wave to reach the SE or the RE is taken into account. Now the signal V_Y is squared and integrated with the time. This signal is called as V_Z. This signal V_Z is passed through a level detector whose level is preset. The setting of the level takes into account noise signals due to filter , stack tuner, etc. If the signal V_Z is more than the preset value of the level detector, the output V_D is '1' otherwise the output V_D is '0'. The level of the level detector is set for a particular instant, say typically 2 milli-secods which is agreed as the operating time of the scheme. This has been described earlier in this section. The signal V_D, delayed by about 2 milli-seconds is passed through another 'AND GATE' which also receives the signal T_{FD}. This signal T_{FD} is the signal T_F which is delayed by the time T_D, typically, say an 1 milli-second. This provides total 2 milli-seconds delay for the signal from the DD to match the operating time of the level detector as described earlier. As explained in Figure 2.5, the discrimination for the internal fault and the reverse fault at the SE is looked after by the DD, but at the RE, the discrimination is looked after by the signal of the fault response. So main emphasis of the simulated test results is based on the discrimination of the signals of the fault responses for

the internal and the reverse faults at the RE. This discrimination is also the basis of the preset value of the level detector. However it is to be ensured that the signal at the SE for the internal fault is reasonably much above the preset value of the level detector for the reliable operation of the scheme.

5.3.1 SELECTION OF AERIAL MODE AND FAULT RESPONSE V_F

Figure 5.4 shows the fault responses in the Aerial Mode (1,0,-1) for the internal and the reverse faults at both ends: SE and RE. Figure 5.5 shows the fault responses in the Aerial Mode (1,-2,1) for the internal and the reverse faults at both the ends SE and RE. Based on the positive peak value of the responses at the RE for the internal and the reverse fault, the discrimination factor is about 1.25 for the Aerial Mode (1,0,-1) and 2.5 for the Aerial Mode (1,-2,1). The discrimination factor is defined as the peak response for the internal fault divided by the peak response for the reverse fault. Since the discrimination factor for the Aerial Mode (1,-2,1) is larger than the discrimination factor for the Aerial mode (1,0,-1), the Aerial Mode (1,-2,1) has been selected for the simulated test results. Moreover, Mode (1,0,-1) is independent of the middle phase voltage. This means that the Aerial Mode (1,0,-1) response depends on the two phases only which reduces the reliability of the scheme. Further Aerial Mode (1,-2,1) is mostly used in carrier communication system as

113

it is of a least attenuation. These responses are based on the post fault observation time of 600 micro-seconds. With a view to take consideration of the operating time of the DD, it is necessary to study the fault responses for a period of 5 milli-seconds. Further responses for 600 micro-seconds do not indicate the repeatitive fault responses. The time interval between the responses depends upon the travelling time of the fault generated travelling wave between the fault point and the SE or the RE. Figure 5.6 shows the fault responses for a period of 5 milli-seconds in the Aerial Mode (1,-2,1) for the internal and the reverse faults at SE and RE. It can be seen that the responses are repeating at a definite interval depending upon the travelling time of the fault generated travelling wave between the fault point and the RE or the SE. These responses are V_F with reference to Figure 5.3 of the signal processing. For the purpose of simulating the internal fault, it is to be noted that the stack tuners are in the NO mode at both the ends: SE and RE, and the fault is at a distance of 1 km from the SE. For the purpose of simulating the reverse fault, the stack tuners are in the NC mode at the SE and in the NO mode at the RE with the fault at the same point as for the internal fault i.e. 1 km from the SE. This shows the worst case of the reverse fault as the fault has been considered in the zone of the internal fault. This point of the fault has been chosen under the reverse fault condition to study the discrimination factor under the worst case of the fault. This point of the fault can also be considered as the

114

nearest point of the reverse fault for the purpose of studying the discrimination factor.

Theoretically, reflection coefficient R_1 is given by:

$$R_1 = \frac{Z_L - Z_O}{Z_L + Z_O} \qquad\qquad (5.42)$$

where Z_L is the load impedance and Z_O is the surge impedance of the transmission line.

For an open circuit case (NO), $Z_L \gg Z_O$, and the $R_1 = 1$

For a short mode (NC), $Z_L \ll Z_O$, and the $R_1 = -1$

If the reverse fault is considered at F_2 in Figure 2.1, R_1 is 1 at the RE and -1 at the SE. In such a case, there is an effective component of the superimposed voltage at the RE. But, if the reverse fault is considered at F_1 in Figure 2.1, R_1 is -1 at the SE and the travelling wave is reflected back towards the fault. This ensures that there is no refracted travelling wave towards the RE. In such a case, there is a negligible superimposed voltage at the RE.

5.3.2 BAND PASS FILTER

The output signals of the stack tuner with mid-band frequency of 300 ± 2.5 kHz may have non-band frequency components of very large range i.e. 100 to 500 kHz, and it is necessary to filter these non-band frequency components to improve upon the signals. For this purpose, a band pass filter with a mid-band frequency of 300 ± 5 kHz has been simulated. This filter has the frequency range of only 290

to 310 kHz. This filter filters all frequency components below 290 kHz and above 310 kHz. The frequency response of such a band pass filter is shown in Figure 5.7. The computer program used for the design of the band pass filter has been given in Appendix D. The design details of the band pass filter are also given in Appendix D. For the purpose of running the program, the software package 'SPICE' has been used. Figure 5.8 shows the filtered signals V_X (reference Figure 5.3) for the internal and the reverse fault conditions at the SE and the RE. Figure 5.9 shows the signal V_Y as explained earlier in this section with reference to Figure 5.3. It can be seen that there is zero response for a period of 1 milli-second at the SE for the internal and the reverse fault conditions. This 1 milli-second is considered as a delay due to the operating time of the DD. At RE, the delay is 1.4 milli-seconds for the internal and the reverse faults. This delay includes: (1) 1 milli-second due to the operating time of the DD, (2) 0.4 milli-second due to travelling time of the fault generated travelling wave from the point of the fault to the RE. Figure 5.10 shows the signals V_Z for the internal and the reverse fault conditions at the SE and the RE. The signal V_Z is given by:

$$V_Z(k) = \sum_{k=1}^{N} V_Y^2 (k\delta t) \qquad (5.43)$$

where V_Y is the input signal. k = 1,2,------N where N is total number of the samples. δt is the sampling time for each sample.

It can be seen in Figure 5.10 that the discrimination factor is about 5 at the instant of 2 milli-seconds. It can also be seen that the signal at the SE at the instant of 2 milli-secons for the internal fault is very much greater than the signal at the RE for the reverse fault condition. This ensures the reliable operation of the scheme under the internal fault condition if the level detector is preset according to the signal at the instant of the 2 milli-seconds at RE for the reverse fault condition.

5.3.3 AUTO-CORRELATOR AND ITS SIMULATION TECHNIQUE

The auto-correlation technique gives the filtered response of a signal. It works on the principle that if there is a signal P_X with NS number of samples. A fixed window 'WC' of samples N can be selected from this signal for the purpose of the correlation. The method is based on the principle that the moving window 'WS' of N samples of the signal P_X is selected. The moving window 'WS' starts from the first sample of the signal. The moving window 'WS' is correlated with the fixed window 'WC' and the first sample of the correlated response P_{XX} is calculated. Now the moving window 'WS' moves by the one sample and, the second sample is calculated by correlating the present moving window 'WS' with the fixed window 'WC'. Thus the moving

117

window 'WS'is moved by one sample each time and is correlated with the fixed window 'WC', and the sample of the correlated response is calculated. Mathmatically, it can be explained as below:

$$P_{xx}(T) = \frac{1}{N} \sum_{k=1}^{N} P_x (k\delta t + m\delta t) . P_x (k\delta t) \qquad (5.44)$$

where T = $m\delta t$, m=0,1,2----N_s

k = 1,2,--------N

N_s = number of samples of the signal

N = number of samples of the window

δt = sampling time

This method needs an advance information of the fixed window 'WC' of N samples of the signal P_x, and the correlated response is delayed by the fixed window 'WC'. For this purpose, a method of correlation using a delay of only one sample is used instead of the delay of the complete fixed window 'WC'. In this method, the sample of the correlated response is calculated based on the following equation till the complete fixed window 'WC' becomes available:

$$P_{xx}(T) = \frac{1}{N} \sum_{k=1}^{N} P_x (k\delta t) . P_x (k\delta t) \qquad (5.45)$$

118

where T = kδt

k = 1,2,--------N

So, first N samples of the correlated response are calculated based on the above equation. Once the fixed window 'WC' of N samples is available, the moving window 'WS' of the signal P_x is moved by one sample each time and the correlated response is calculated using the following equation.

$$P_{xx}(T) = \frac{1}{N} \sum_{k=1}^{N} P_x (k\delta t + m\delta t) . P_x(k\delta t) \qquad (5.46)$$

where T = (N+m)δt, m=1,2----N_s-N

k = 1,2,--------N

5.3.4. DESIGN ASPECTS OF THE HARDWARE OF THE AUTO-CORRELATOR AND THE SELECTION OF THE NUMBER OF SAMPLES OF THE FIXED WINDOW

In the present scheme, the principle is based on the detection of high frequency components of the fault generated noise. These high frequency components are in the range of 300 ± 2.5 kHz. In order to detect to these frequency components, a sampling frequency of aleast 605 kHz is required. In the present simulated test results, this sampling frequency is 819.2 kHz which can be

considered nearly 800 kHz for the simplified calculation. In the auto-correlator technique, if there are N samples in the fixed window 'WC'(reference Section 5.3.3) then N numbers of multiplications and additions are required for calculation of the each sample. For example, if there are 25 samples in the fixed window 'WC', then 25 multiplications and 25 additions are required for calculation of the each sample of the auto-correlated response. If the hardware component is selected such that it is capable of carrying the multiplication and the addtion in one instruction, then 25 instructions are required per sample. Since the sampling frequency is 800 kHz, the frequency for each instuction is 25 times 800 kHz i.e. 20000 kHz. This means that the hardware should be capable of carrying 200,000,000 instuctions per second i.e. 20 MIPS (million of instructions per second). A micro-processor hardware upto 5 MIPS are available in general (For example: TMS300). Probably, the micro-processor hardwares of higher MIPS, say typically 40 MIPS are on the way of development. However transputers are commonly used for combination of the micro-processor hardwares if design criterion demands a higher MIPS value. Based on the criterion that the hardware components of 20 MIPS are available, the number of samples of the window 'WS' or 'WC' (reference Section 5.3.3) are considered 25.

5.3.5 <u>SIMULATED TEST RESULTS OF THE AUTO-CORRELATOR</u>

Figure 5.11 shows the auto-correlated output, V_X (reference Figure 5.3) for the internal and the reverse faults at SE and RE. Figure 5.12 shows the response V_Y (reference Figure 5.3) for the internal and the reverse faults at the SE and the RE. These responses show zero response for a period of 1 milli-second at the SE and 1.4 milli-seconds at the RE. The delay of 1 milli-second at SE corresponds to the operation time of the DD. The delay of 1.4 milli-second at the RE takes into account: (1) 1 milli-second for the operating time of the DD, (2) 0.4 milli-second delay due to the travelling time of the fault generated travelling wave from the fault point to the RE. Figure 5.13 shows the response V_Z (reference Figure 5.3). A discrimination factor of about 35 has been found at the instant of 2 milli-second for the internal and the reverse fault at the RE. It can be also seen that the signal at the instant of 2 milli-second at the SE for the internal fault is very much greater than the response at the RE for the reverse fault. This means that if the level detector is preset marginally above the signal at the instant of the 2 milli-second at the RE for the reverse fault, a very reliable operation of the scheme under the internal fault conditions is ensured.

Since the discrimination factor for the auto-correlator is about 35 which is about 7 times greater than the discrimination factor for the band pass filter (reference Section 5.3.2), the auto-correlator has been selected for the purpose of filtering Aerial Mode (1,-2,1) signals.

5.3.6 **ESTABLISHMENT OF THE SCHEME**

Figure 5.14 shows the signals V_F, V_X, V_Y, V_Z for the internal fault and the reverse fault at the RE with reference to Figure 5.6, Figure 5.11, Figure 5.12, and Figure 5.13. These signals have been explained earlier in this section. The only difference is that Figure 5.14 shows the signal V_F and V_X same as in the internal fault condition for a period of 1.4 milli-second. Delay of the 1.4 milli-second takes into account: (1) 0.4 milli-second delay due to the travelling time of the fault generated travelling wave from the fault point to the RE, (2) 1 milli-second delay due to operating time of the DD.

The discrimination factor (value of the signal for the internal fault divided by the value of the signal for the reverse fault at a particular instant) of about 35 has been found which is a very good factor for establishing the principle of the scheme. Figure 5.15 shows the V_F (reference Figure 5.6) and V_Z (reference Figure 5.13) signals for the internal fault at the SE and the RE. It has been found that the values of the signals at the instant, say typically 2 milli-second for both ends: the SE and the RE are much greater than the value of the signal at

122

the RE for the reverse fault (reference Figure 5.14) which ensures the safe reliable operation of the scheme under the internal fault condition. Figure 5.16 shows the signal V_F (reference Figure 5.6) and the signal V_Z (reference Figure 5.13) for the reverse fault at the SE and the RE. In the reverse fault condition, the operation of the scheme at the SE is inhibited due to the reverse signal from the DD as explained earlier i.e. the signal T_F is '0'. At the RE, the operation of the scheme is inhibited due to higher threshold value of the level detector than the signal V_Z i.e. the signal V_D is '0' (reference Figure 5.3). Since both the signals T_F and V_D are required to be '1' for the operation purpose, the operation under the reverse fault condition can not take place. Hence the principle of the scheme has been established successfully.

5.3.7 <u>SIMULATED TEST RESULTS FOR THE FAULT AT 30 DEGREE OF THE VOLTAGE WAVEFORM</u>

When the fault occurs at a lower angle of the voltage waveform, the travelling wave components are much smaller in the magnitude than the fault at 90 degree point-on-wave. Due to this reason, most of the schemes based on the principle of the travelling wave phenomena are considered failures for the faults at lower inception angles. With this view, the simulated test results for the fault at 30 degree of the voltage waveform are shown in Figure 5.17. Figure 5.17 shows the signals V_F, V_Z for the internal fault at the SE and the RE. It can be seen that the V_Z signal at

the RE at the instant of 2 milli-second is about 2 times of the signal at the RE for the reverse fault (reference Figure 5.16) which gives a discrimination factor of 2 for the safe reliable operation of the scheme for faults at 30 degree of the voltage waveform. This can be also seen that the signal V_Z at the SE at the instance of 2 milli-second is much greater than the signal V_Z at the RE for the reverse fault. This ensures the safe and the reliable operation of the scheme for the faults upto 30 degree of the voltage waveform.

5.3.8 MODIFIED SIGNAL PROCESSING SCHEME

In the earlier scheme, the directional detector, DD operating delay of typical 1 ms has been considered after auto-correlating the signal V_F. In the present scheme, the signal V_F is first delayed and then, the signal $V_x(n)$ is auto-correlated as shown in Figure 5.18. If n is the number of samples in the signal V_x, then the auto-correlated output $V_y(n\delta t)$ is given by

$$V_y(n\delta t) = \frac{1}{N} \sum_{k=1}^{N} V_x(k+n)\delta t . V_x(k\delta t) \qquad (5.47)$$

where   n = 1,2----n

k = 1,2,---N

n = number of samples in the signal

N = number of samples in the window.

This auto-correlated signal V_y is processed through another function whose output V_z is given by

$$V_z(n\delta t) = \sum_{k=n-M}^{n} V_y^2 (k\delta t) \hspace{3cm} (5.48)$$

where   M = number of samples corresponding to the signal delay TD which is typically 3 ms,

n = number of samples corresponding to the signal time, say typically 4ms.

In fact this signal is the time integral of the square of the signal V_y in a fixed window of M samples which is fed to a level detector. If the signal V_z is greater than the threshold value (reference Chapter 2) of the level detector, the output of the level detector V_D which is '1', is fed to a decision logic, AND GATE. This AND GATE also receives the signal, T_{FD} from the directional detector, DD after the signal delay TD. If both the signals V_D and T_{FD} are '1', the tripping signal T_S, 1 is sent to the local breaker for tripping.

In the earlier scheme, there has been no arrangement for **resetting of the signal V_z** and the scheme may mal-operate under the reverse fault condition at the receiving end if the scheme has earlier operated for the internal faults. In this scheme, the signal V_y is processed through a window of fixed samples and resets as soon as the window is completed.

Figure 5.19 shows the signals V_x, V_y, V_z for the internal and the reverse faults at the receiving end, RE for the

125

fault at maximum of the voltage. Looking into Figure 5.19c for the reverse fault, a threshold value can be set corresponding to a value of 20×10^6 units. Now looking into Figure 5.19c for the internal fault, the discrimination factor (reference Section 5.3.1) of $50 \times 10^7 / 20 \times 10^6 = 25$ can be noticed. Figure 5.20 shows the signals V_F and V_Z for the internal and the reverse faults at the sending end, SE for the fault at maximum of the voltage. Looking into Figure 5.20b, the discrimination factor for the internal fault is $20 \times 10^8 / 20 \times 10^6 = 100$, and for the reverse fault is $12 \times 10^5 / 20 \times 10^6 = 0.006$. This establishes V_D signal as '1' for the internal fault and '0' for the reverse fault. Figure 5.21 shows the logic conditions of the signals V_D, T_{FD}, and the tripping signal T_S for the internal fault and the reverse fault at the SE and the RE. Figure 5.21A shows the V_D as 1 for the internal fault and 0 for the reverse fault. Figure 5.21B shows the signal T_{FD} as 1 at the SE and the RE for the internal fault and at the RE only for the reverse fault after a delay of 4.4 ms. Figure 5.21C shows the tripping signal T_S as '1' for the internal faults and '0' for the reverse fault. This establishes the principle. Figure 5.22 shows the signals V_X and V_Z for the internal fault at both ends, SE and RE for the fault at 30 degree of the voltage. The discrimination factors have been found to be $13 \times 10^7 / 20 \times 10^6 = 6.5$ at SE and $30 \times 10^6 / 20 \times 10^6 = 1.5$ at RE. This ensures the safe operation of the scheme for fault at 30 degree of the voltage.

5.3.9 SIMULATED TEST RESULTS FOR FAULTS AT DIFFERENT POINTS OF THE TRANSMISSION LINE

Figure 5.23 shows the fault responses at the SE and the RE for faults at 1 km, 25 km, and 50 km from the SE. The repeatition of the responses at a definite interval is clearly shown. This interval depends upon the distance of the fault from the SE or the RE. These responses are based on the post fault observation time of 600 micro-seconds. For the purpose of the reliable operation of the scheme, these responses are to be compared with the response at the RE under the reverse fault condition (reference Figure 2.5). This is due to the fact that the level of the level detector (reference Figure 5.3) is set above the value of the signal at RE for the reverse fault. For the purpose of the comparison, the signals have been squared and integrated with the time, and these responses are shown in Figure 5.24. Figure 5.25 shows the response for the reverse fault and Figure 5.26 shows the signal which is squared and integrated with time for the reverse fault at the SE and the RE (reference Figure 2.5). Comparison of these responses based on the discrimination factor at the instant of 0.4 milli-second is shown in Table 5.4. This comparison show the safe and the reliable operation of the scheme for all the points (i.e. 1 km, 25 km, 50 km from the SE) of the line.

5.3.10 SIMULATED TEST RESULTS FOR DIFFERENT TYPES OF THE FAULT

Figure 5.27 shows the responses for phase-A fault, phase-B fault, phase-C fault, phase to phase fault, three phase fault. For the purpose of the comparison (reference Section 5.3.9), these responses have been squared and integrated with the time as shown in Figure 5.28. These responses have been compared with the response at the RE for the reverse fault condition for the purpose of the safe and the reliable operation (reference Section 5.3.9). The comparison based on the discrimination factor at the instant of the 0.4 milli-second is shown in Table 5.5. Since the discrimination factor is satisfactory in all the cases, the operation of the scheme under all the fault conditions can be ensured safely and reliably.

```
            g              g
            o              o

      a           b              c
      o           o              o
```
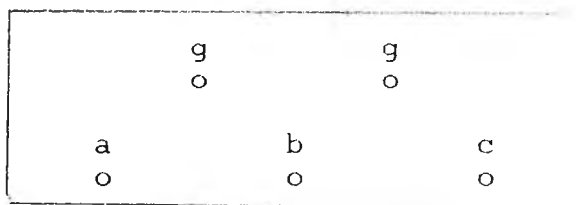
Figure 5.1 **SINGLE CIRCUIT, HORIZONTAL THREE-PHASE EHV LINE CONFIGURATION FOR MODAL ANALYSIS FOR THE PURPOSE OF POWER LINE CARRIER APPLICATION**

| Phase	Mode 3	Mode 2	Mode 1
a	1 →	1 →	1 →
b	q →		p ←
c	1 →	-1 ←	1 →

Figure 5.2 **MODE DISRTIBUTION FOR MODAL ANALYSIS**
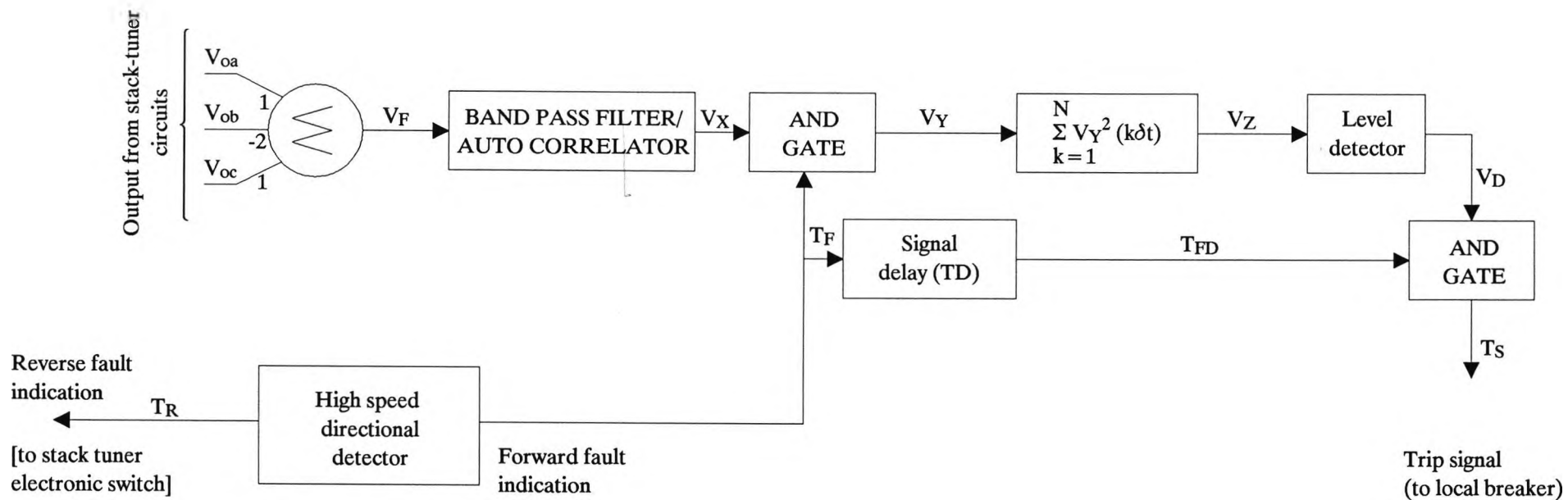
Figure 5.3 <u>BLOCK SCHEMATIC OF RELAY SIGNAL PROCESSING</u>
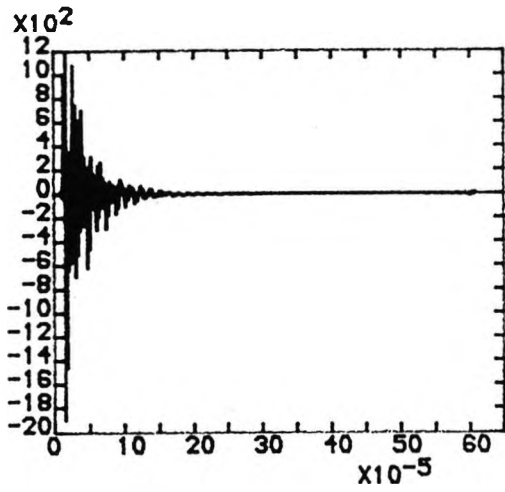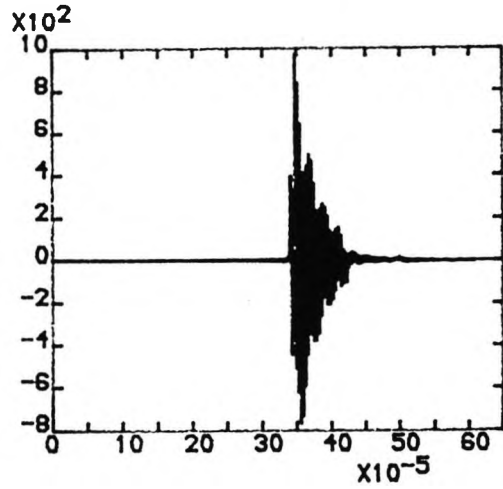
SE   RE
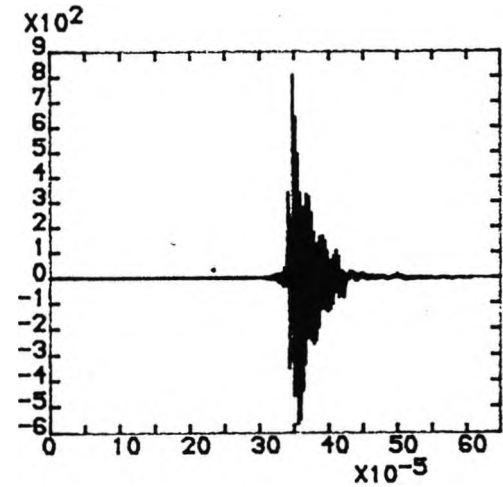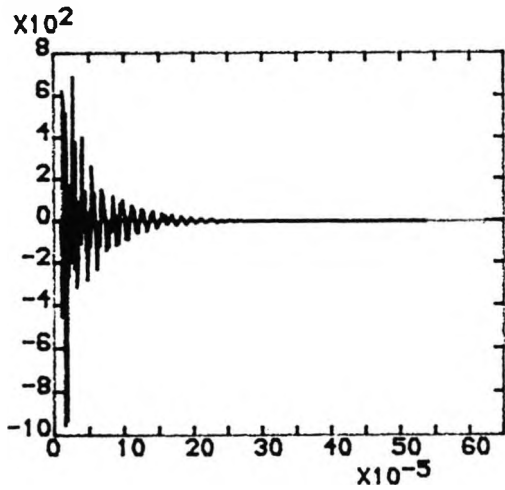

a: Internal fault

b: Reverse fault

X-Axis: TIME-Seconds
Y-Axis: TUNER OUTPUT
        RESPONSE-Volts

Figure 5.4 MODE (1, 0,-1) RESPONSES 'V$_F$ FOR INTERNAL AND
            REVERSE FAULT CONDITIONS
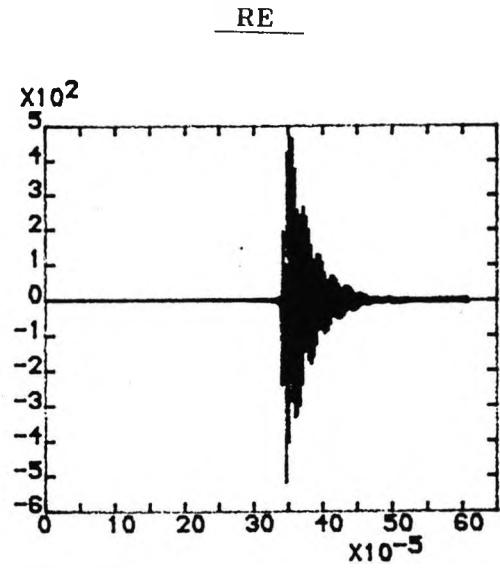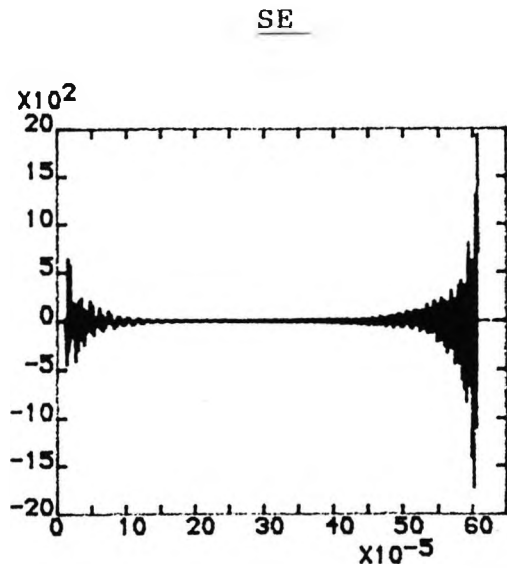
SE   RE
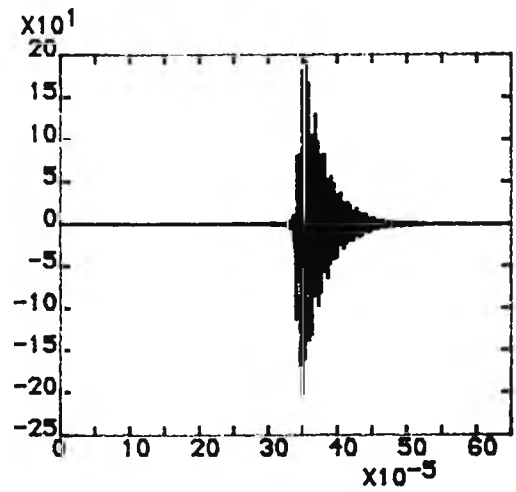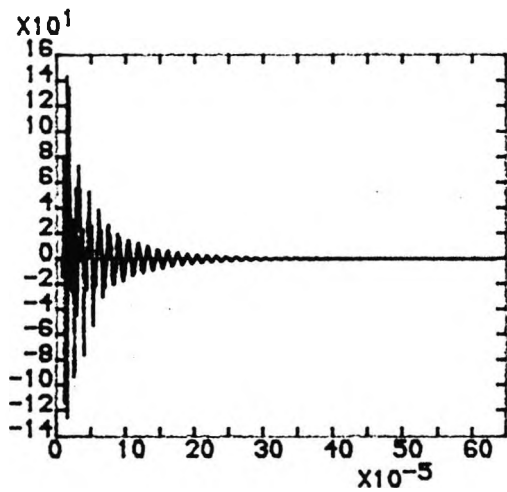
a: Internal fault

b: Reverse fault

X-Axis: TIME-Seconds
Y-Axis: TUNER OUTPUT
RESPONSE-Volts

Figure 5.5 MODE (1, -2, 1) RESPONSES 'V$_F$ FOR INTERNAL AND REVERSE FAULT CONDITIONS
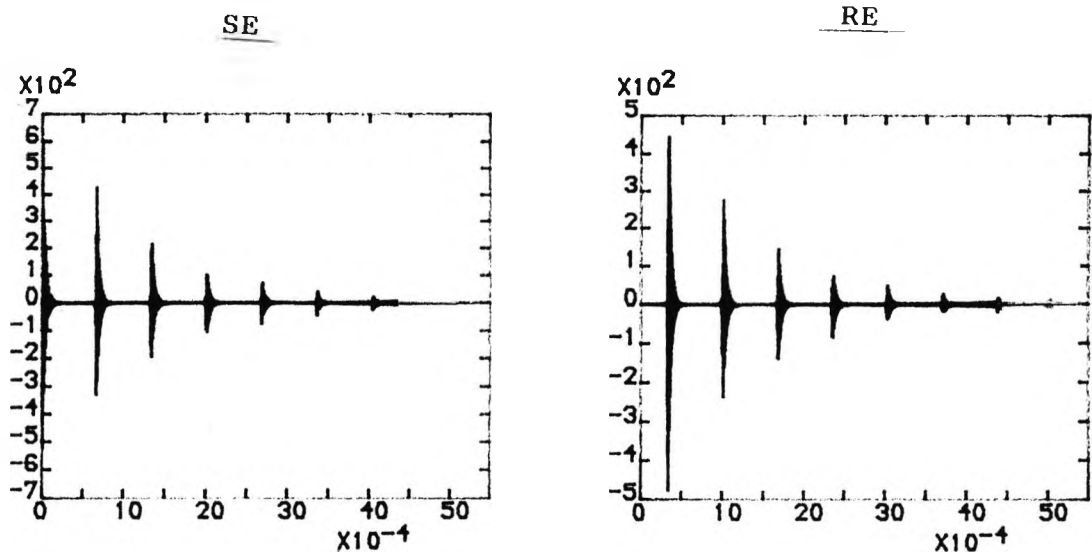
SE   RE
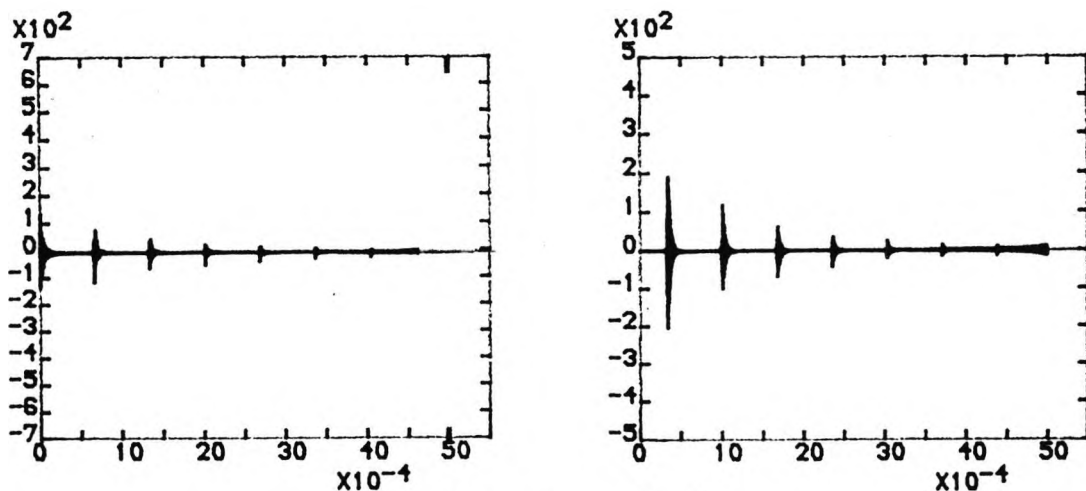
a: Internal fault

b: Reverse fault

X-Axis: TIME-Seconds
Y-Axis: TUNER OUTPUT
    RESPONSE-Volts

Figure 5.6 MODE (1, -2, 1) RESPONSES 'V$_F$' FOR FAULT
OBSERVATION TIME 5 ms UNDER THE INTERNAL AND THE
REVERSE FAULT CONDITIONS
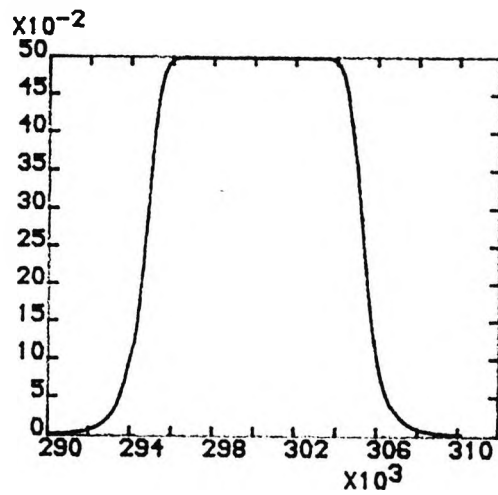
X-Axis: FREQUENCY-Hz
Y-AXIS: GAIN=OUTPUT/INPUT

Figure 5.7 FREQUENCY RESPONSE OF THE BAND PASS FILTER

SE   RE
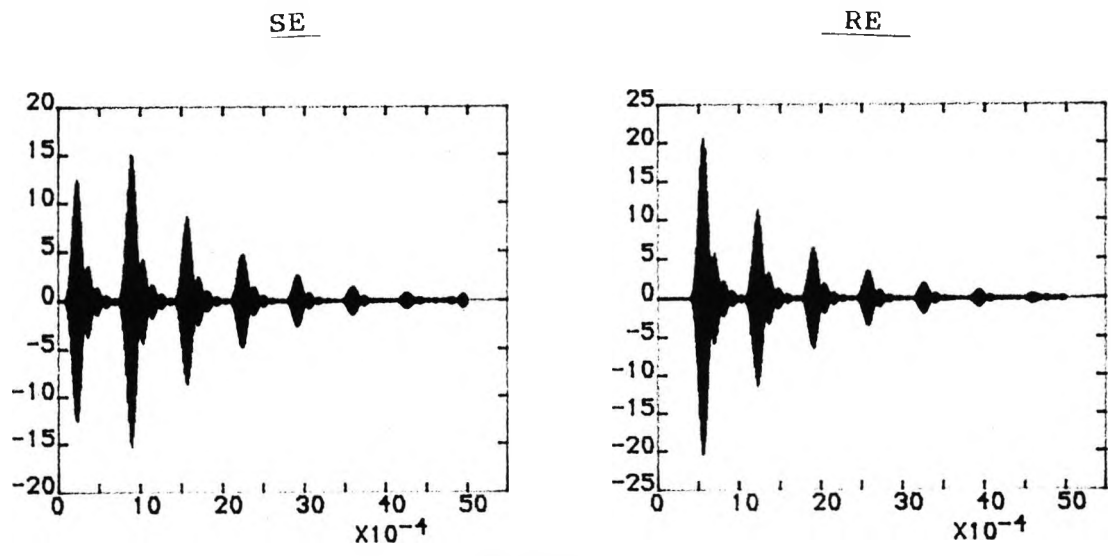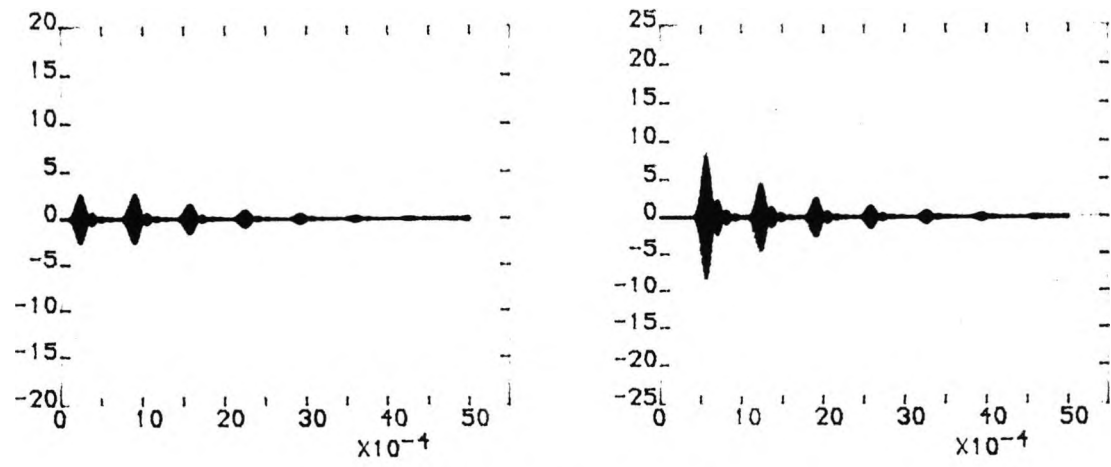
a: Internal fault

b: Reverse fault

X-Axis: TIME-Seconds
Y-Axis: FILTER OUTPUT
        RESPONSE 'V_X-Volts

Figure 5.8 BAND PASS FILTER OUTPUT RESPONSES 'V_X FOR THE
           INTERNAL AND THE REVERSE FAULT

SE   RE
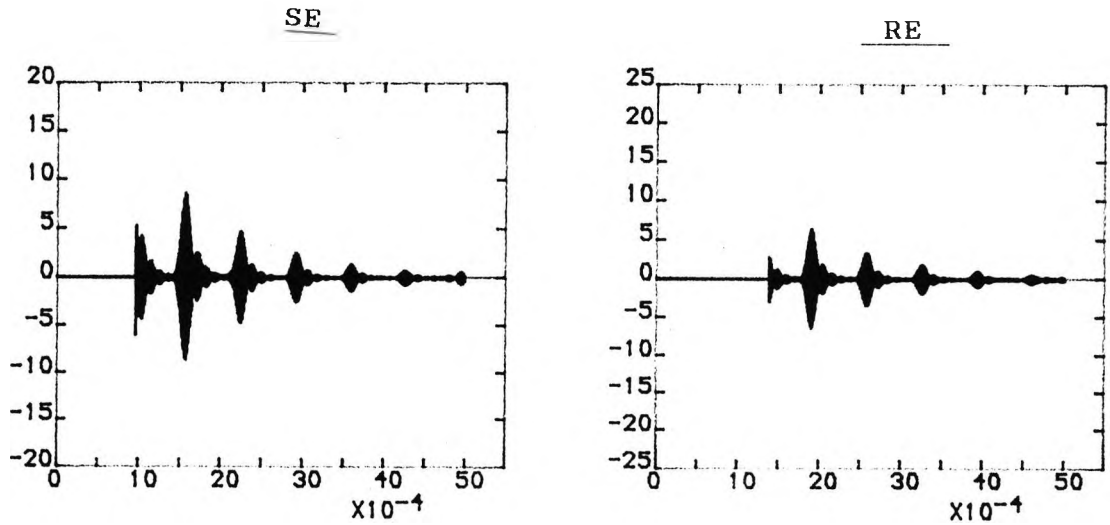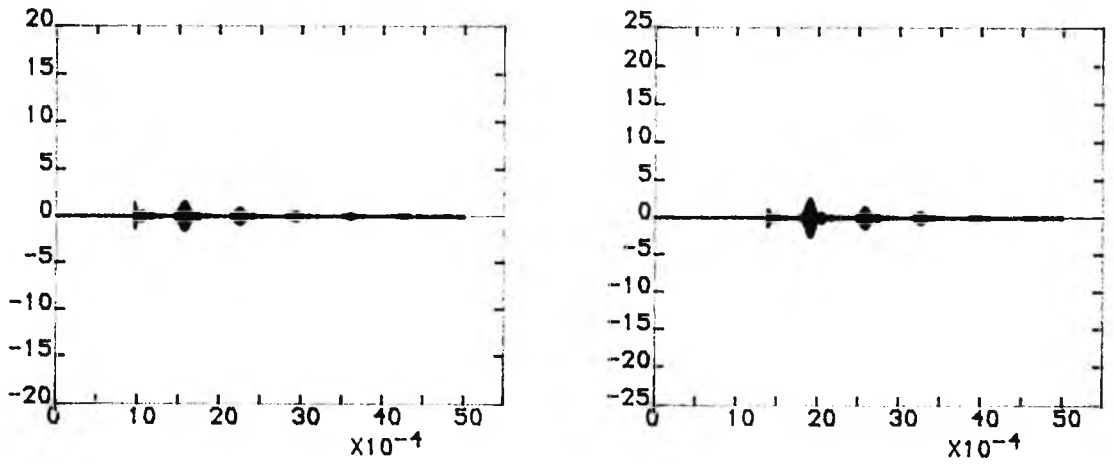
a: Internal fault

b: Reverse fault

X-Axis: TIME-Seconds
Y-Axis: RESPONSE 'V_Y'-Volts

Figure 5.9 RESPONSES 'V_Y' AFTER AN OPERATING DELAY OF THE DIRECTIONAL DETECTOR, DD

SE   RE
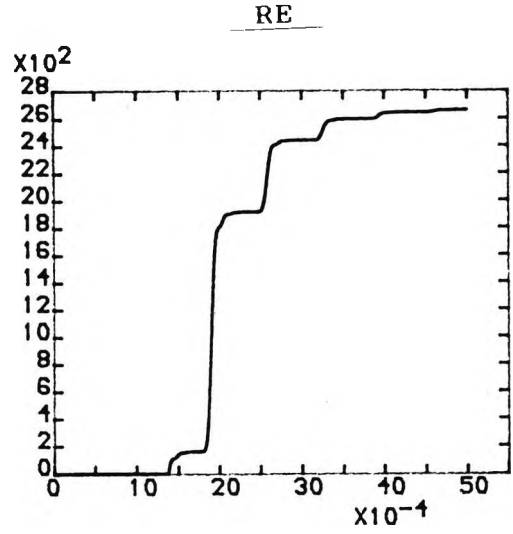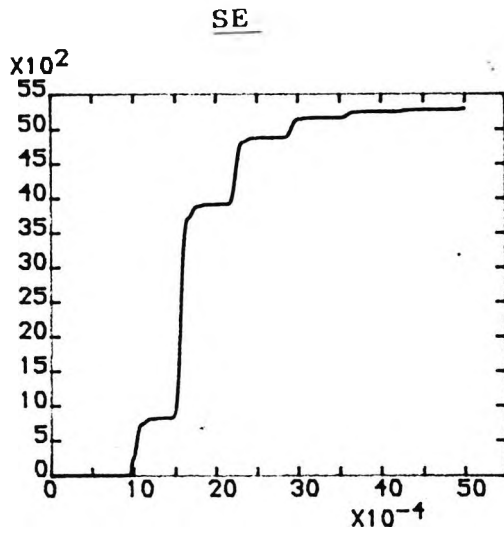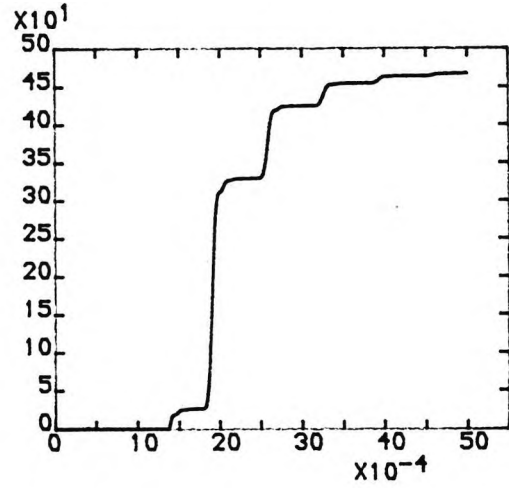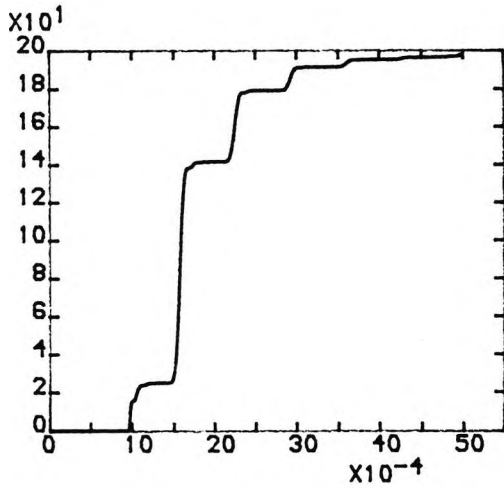
a: Internal fault

b: Reverse fault

X-Axis: TIME-Seconds
Y-Axis: RESPONSE 'V_Z'-Units

Figure 5.10 RESPONSES 'V_Z'UNDER THE INTERNAL AND THE REVERSE FAULT CONDITIONS
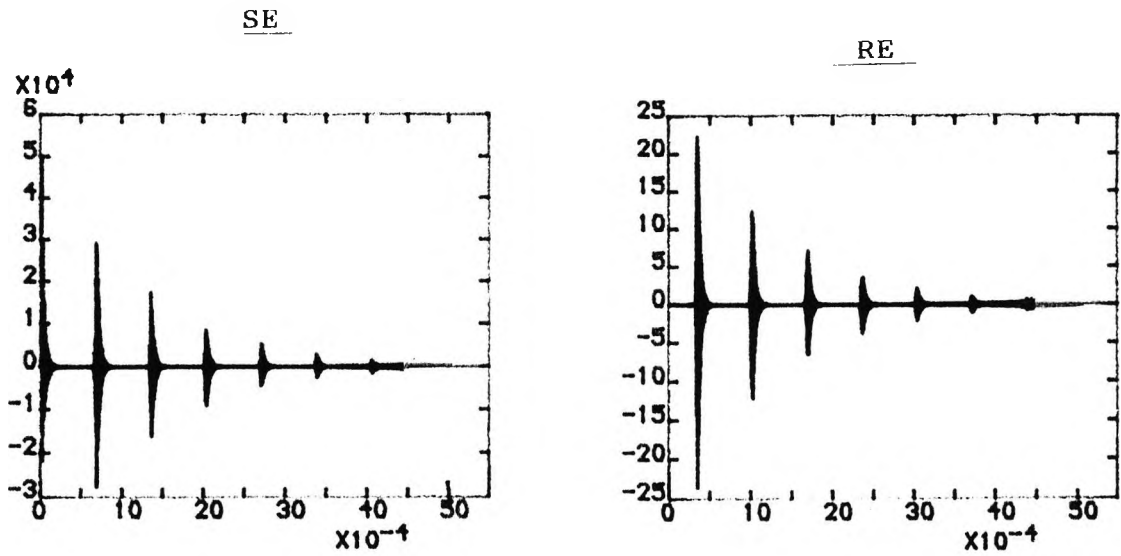
RE
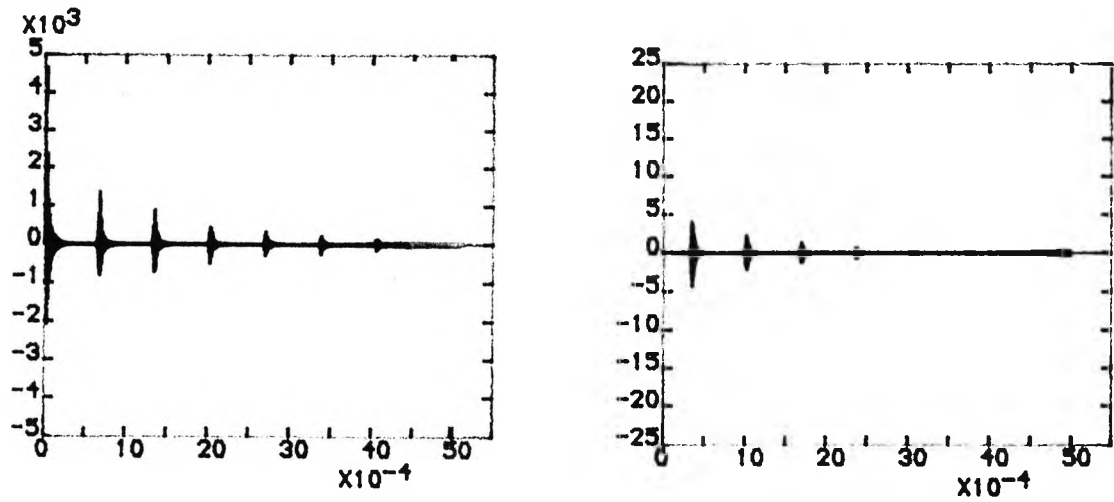
a: Internal fault

b: Reverse fault

X-Axis: TIME-Seconds
Y-Axis: AUTO-CORRELATED
RESPONSE $'V_X'$-Units

Figure 5.11 AUTO-CORRELATED RESPONSES $'V_X'$ UNDER THE
INTERNAL AND THE REVERSE FAULT CONDITIONS
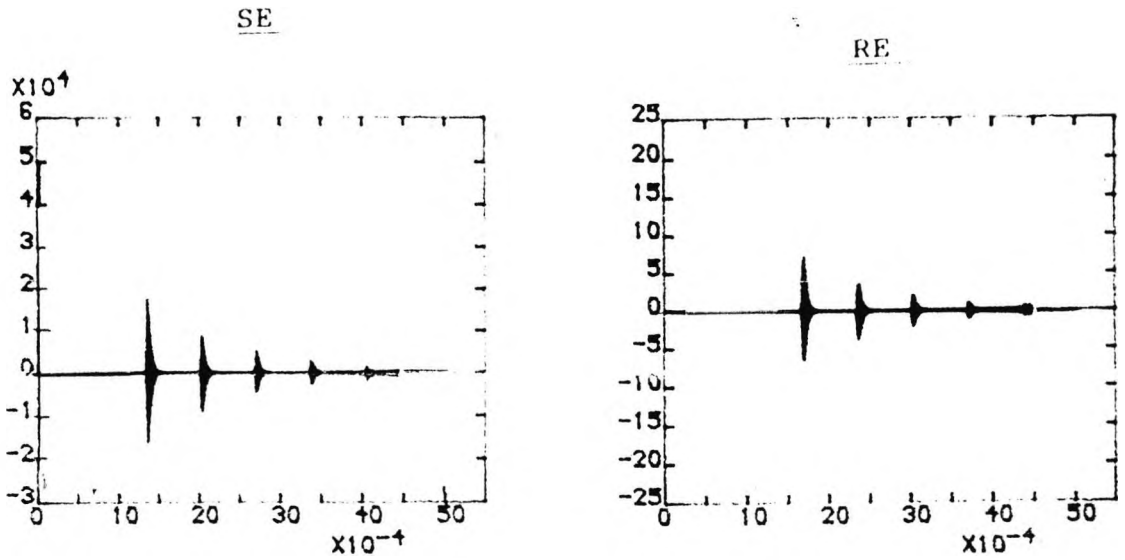
SE

$X10^4$

a: Internal fault

RE
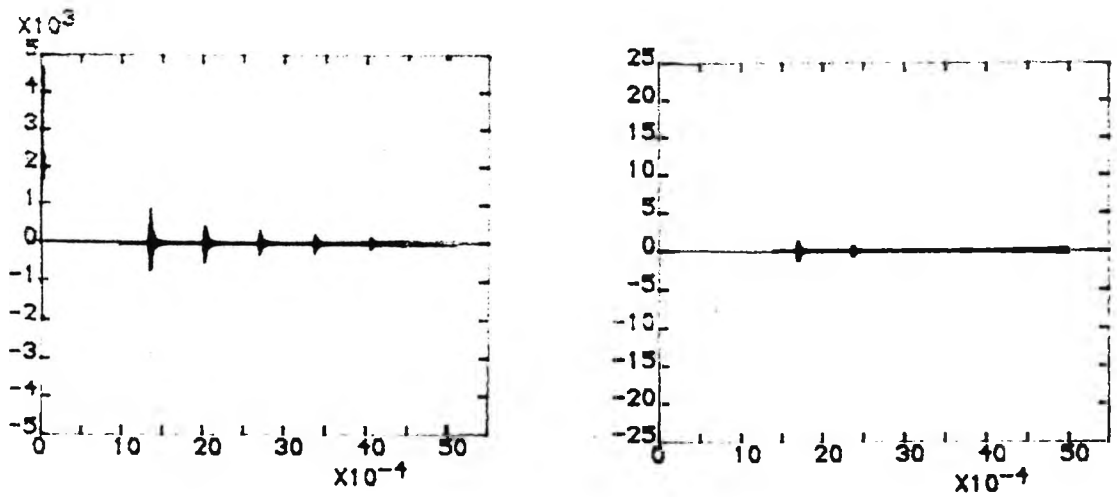
b: Reverse fault

X-Axis: TIME-Seconds
Y-Axis: AUTO-CORRELATED
RESPONSE 'V_X'-Units

Figure 5.12 RESPONSES 'V_X' AFTER AN OPERATING DELAY OF THE DIRECTIONAL DETECTOR,DD

SE   RE

a: Internal fault

b: Reverse fault

X-Axis: TIME-Seconds
Y-Axis: RESPONSE 'V_Z'-Units

Figure 5.13 RESPONSES 'V_Z' UNDER THE INTERNAL AND THE REVERSE FAULT CONDITION

a: Internal fault

V_F V_X V_Y V_Z

b: Reverse fault

X-Axis: TIME-Seconds
Y-Axis: RESPONSE V_F, V_X, V_Y, V_Z-Units
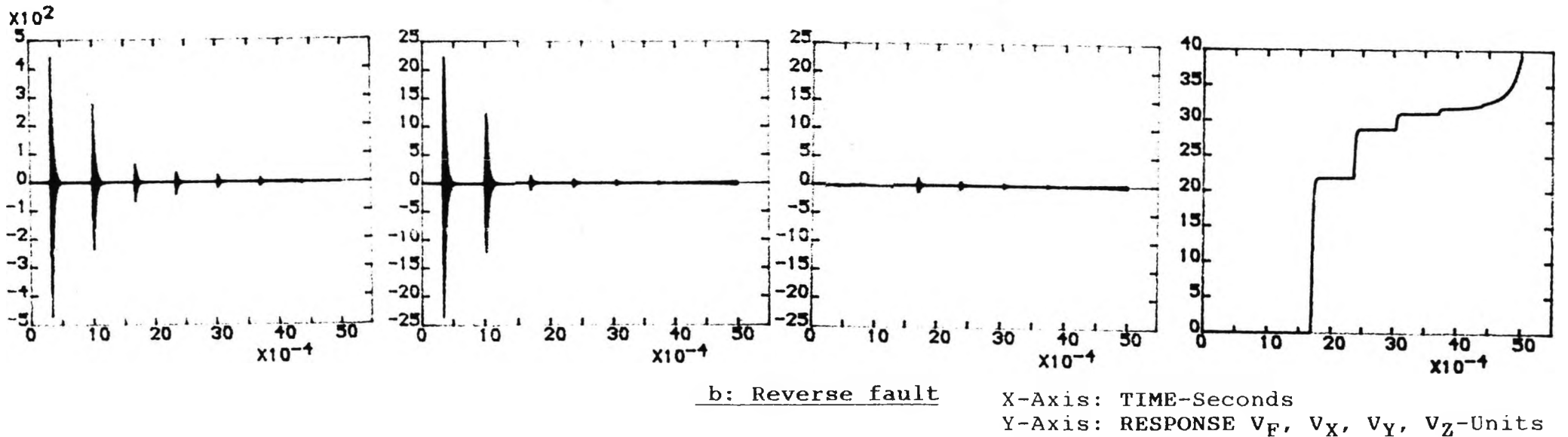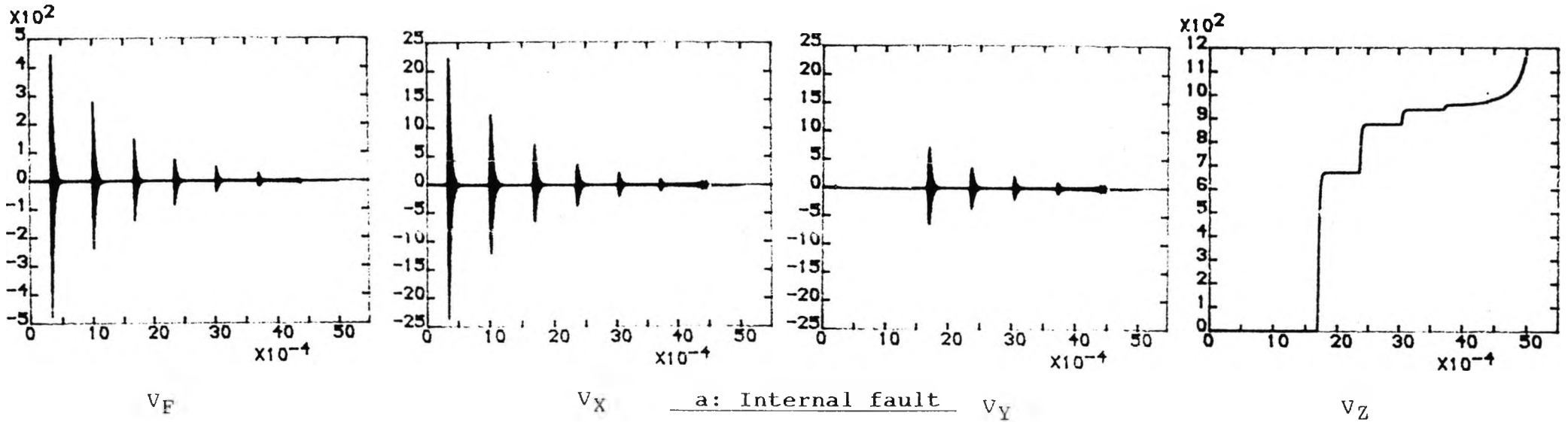
Figure 5.14 SIGNAL RESPONSES V_F, V_X, V_Y, V_Z AT RE FOR THE
INTERNAL AND THE REVERSE FAULT

SE   RE
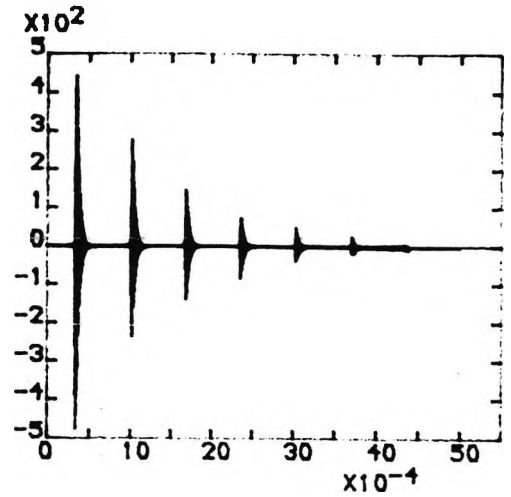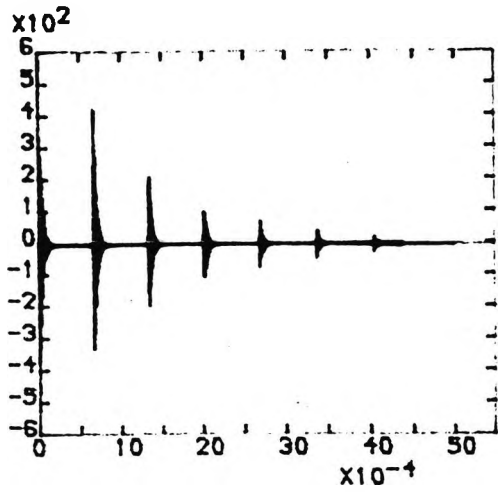
a: Signal 'V$_F$'
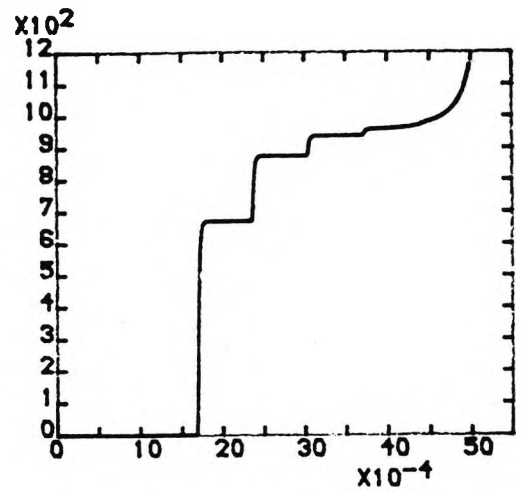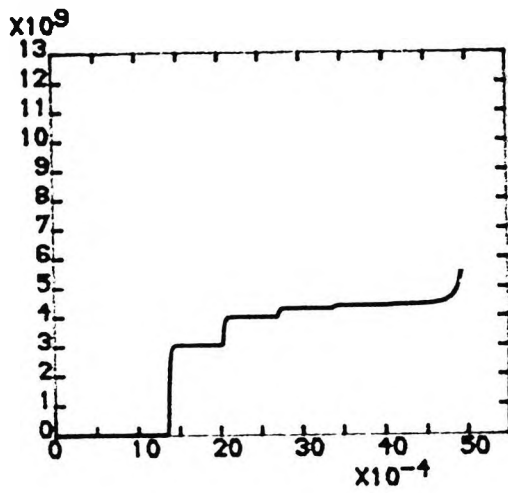
b: Signal 'V$_Z$'

X-Axis: TIME-Seconds
Y-Axis: RESPONSE V$_F$, V$_Z$-Units

Figure 5.15 SIGNAL 'V$_F$' AND 'V$_Z$' FOR THE INTERNAL FAULT
AT V$_{MAX}$

SE   RE
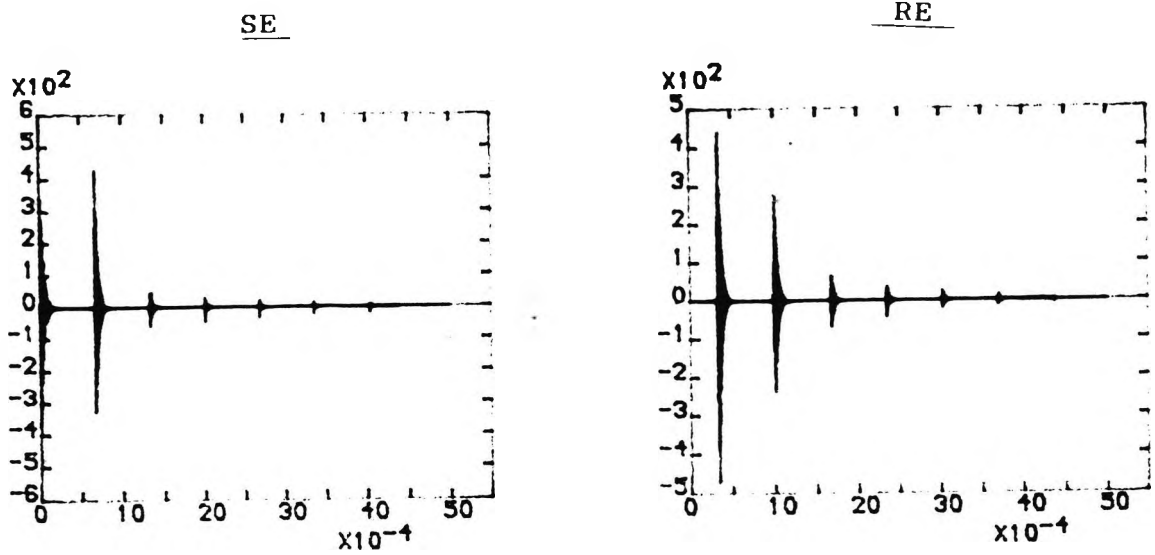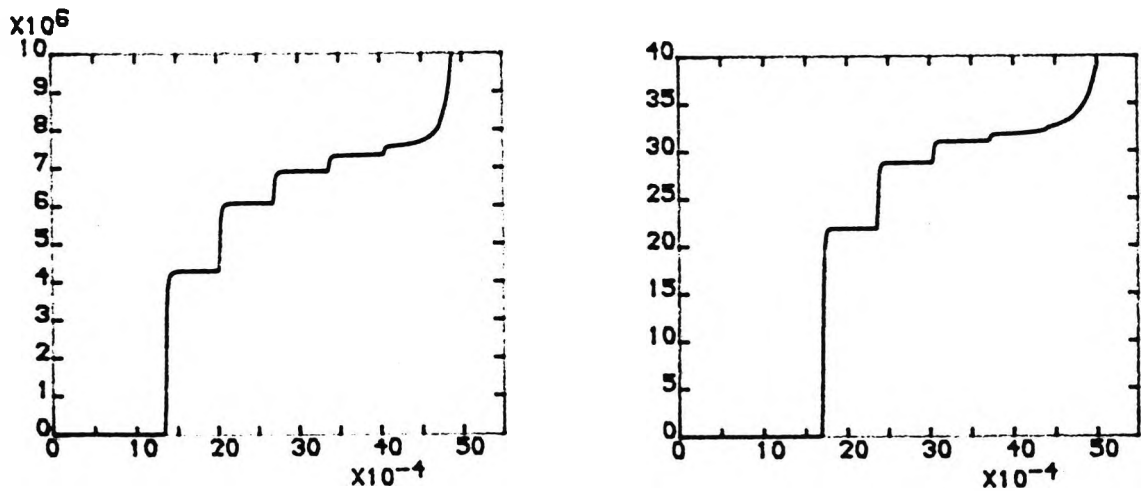
a: Signal 'V_F'

b: Signal 'V_Z'

X-Axis: TIME-Seconds
Y-Axis: RESPONSE V_F, V_Z-Units

Figure 5.16 SIGNAL 'V_F' AND 'V_Z' FOR THE REVERSE FAULT
AT V_MAX
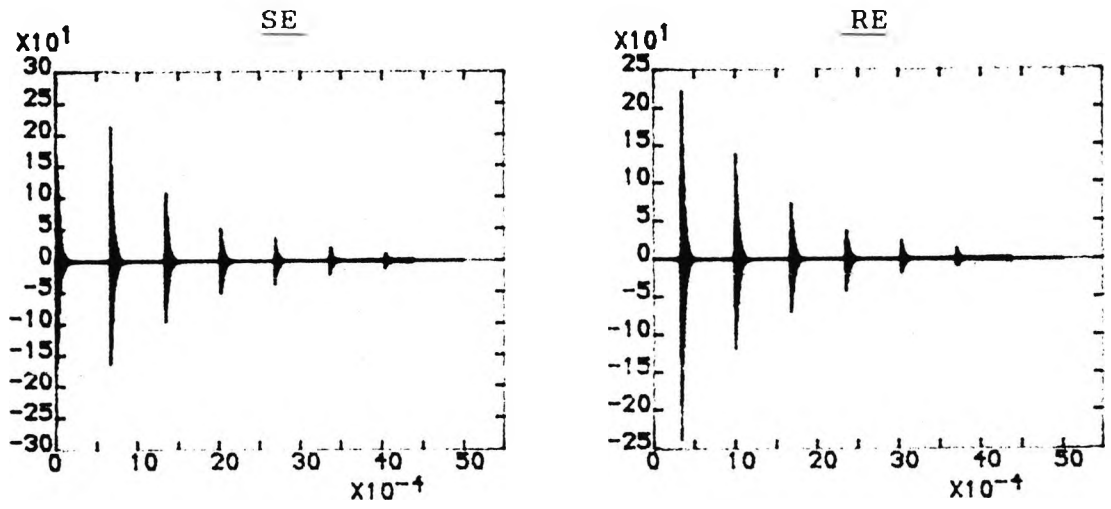
a: Signal 'V$_F$'
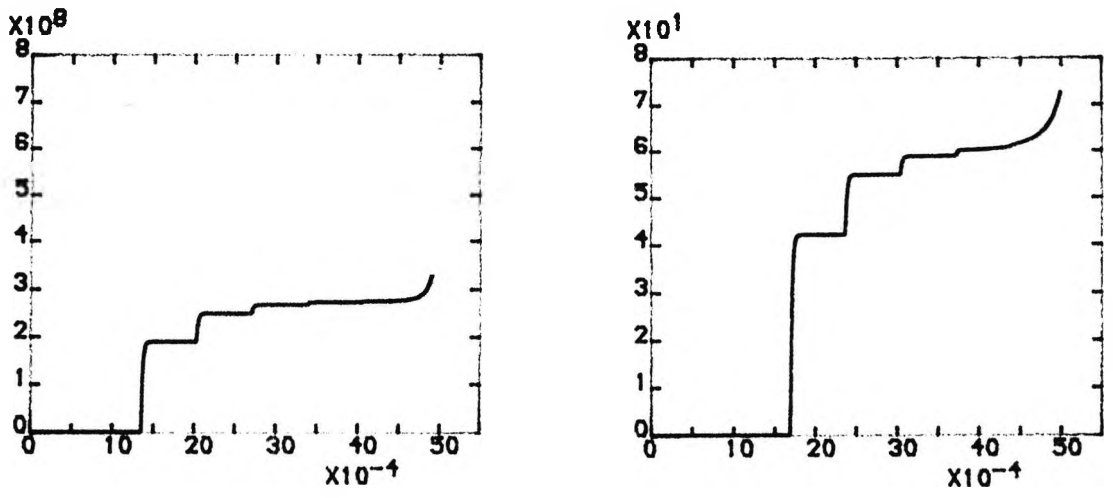
b: Signal 'V$_Z$'

X-Axis: TIME-Seconds
Y-Axis: RESPONSE V$_F$, V$_Z$-Units

Figure 5.17 <u>SIGNAL 'V$_F$' AND 'V$_Z$' FOR THE INTERNAL FAULT AT V$_{30}$ DEGREE</u>
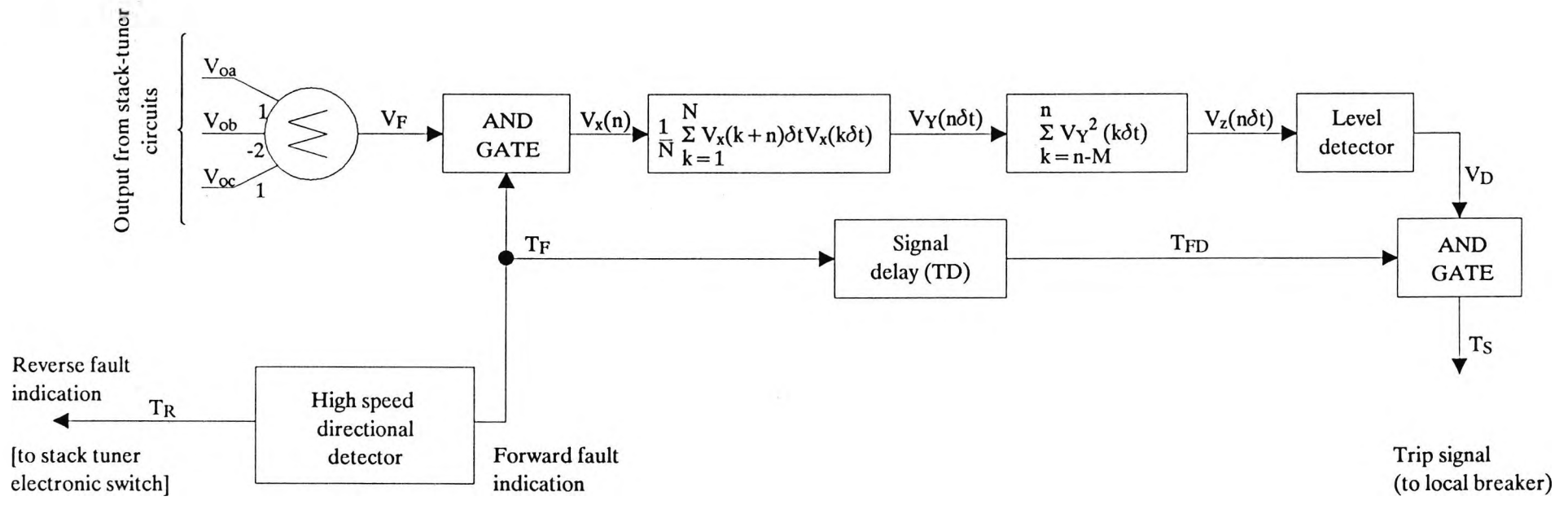
Figure 5.18 MODIFIED SIGNAL PROCESSING SCHEME
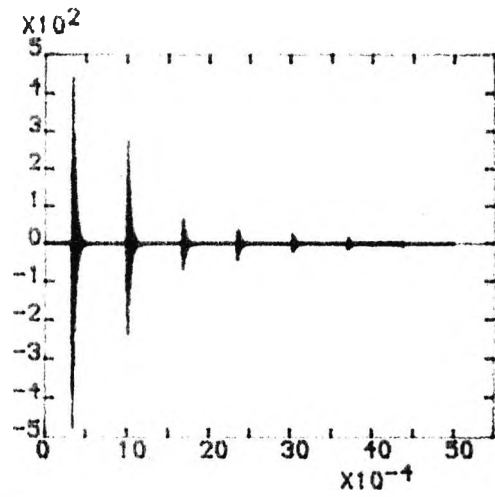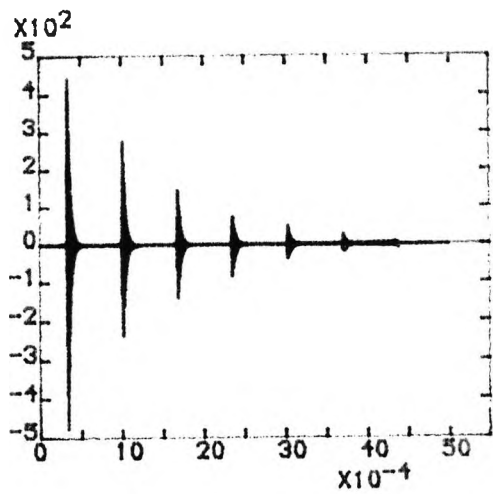
a: Signal 'V_F'
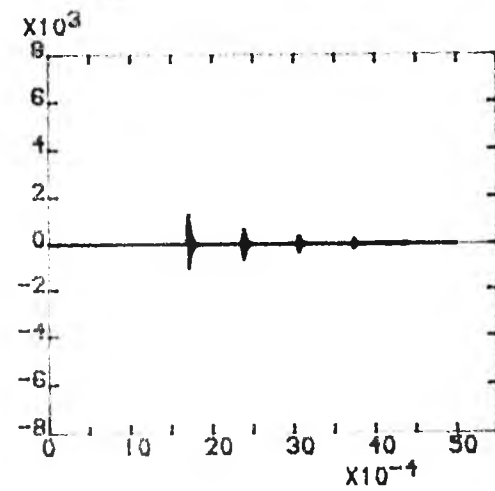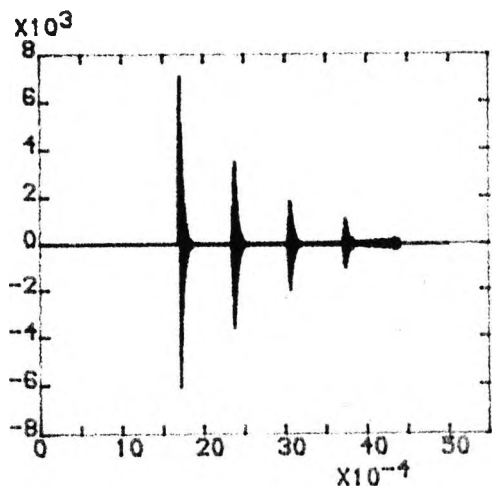
b: Signal 'V_Y'
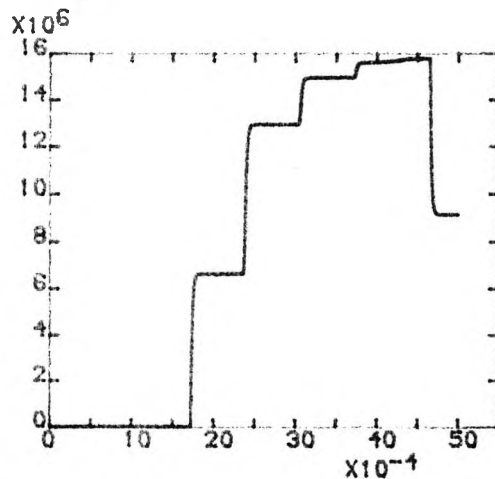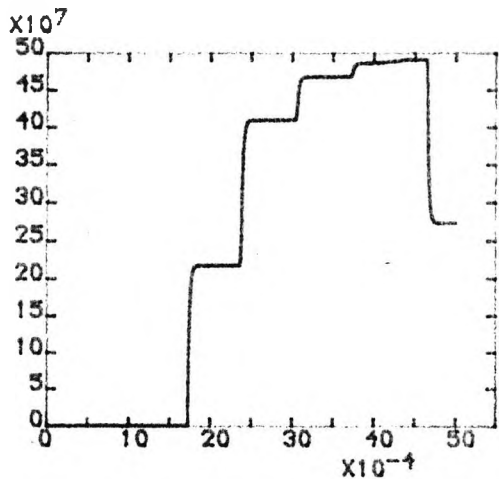
Internal fault   c: Signal 'V_Z'   Reverse fault

X-Axis: TIME-Seconds
Y-Axis: RESPONSE V_F, V_Y, V_Z-Units

Figure 5.19 RESPONSE V_F, V_Y, V_Z FOR THE INTERNAL FAULT AND
THE REVERSE FAULT AT V_{MAX} AT RE

Internal fault   Reverse fault
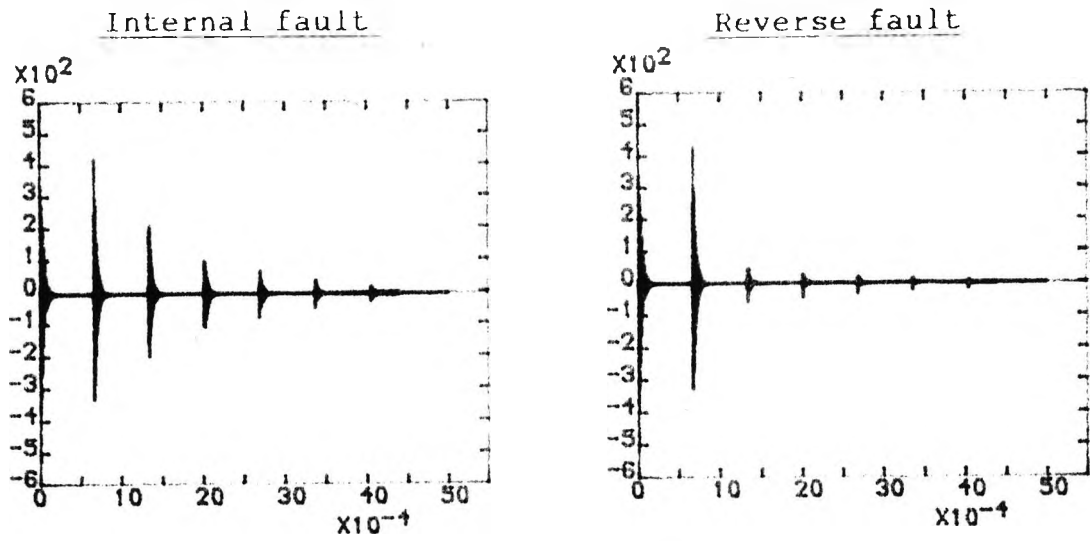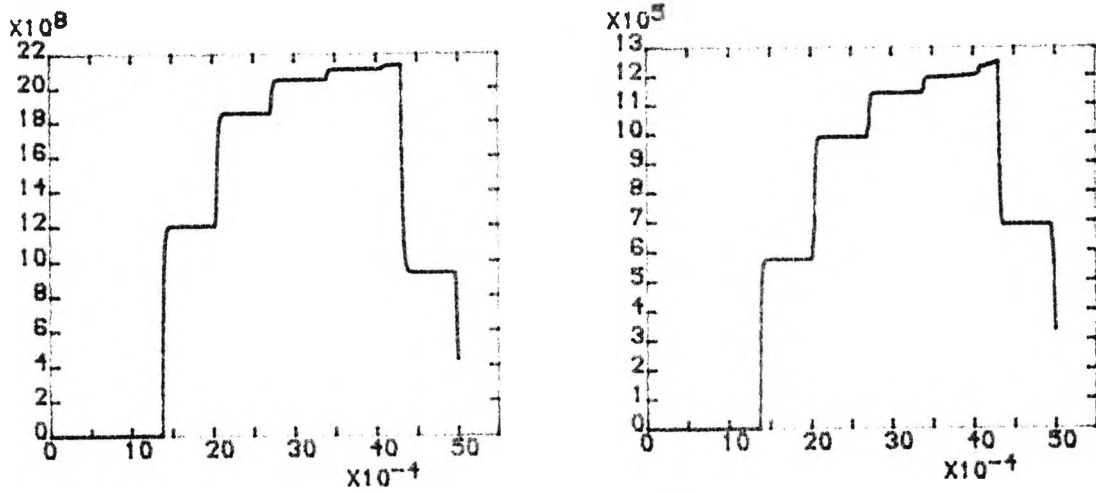
a: Signal 'V_F'

b: Signal 'V_Z'

X-Axis: TIME-Seconds
Y-Axis: RESPONSE V_F, V_Z-Units

Figure 5.20 RESPONSE V_F, V_Z FOR THE INTERNAL FAULT AND
THE REVERSE FAULT AT V_{MAX} AT SE

SE   RE

a. Internal fault
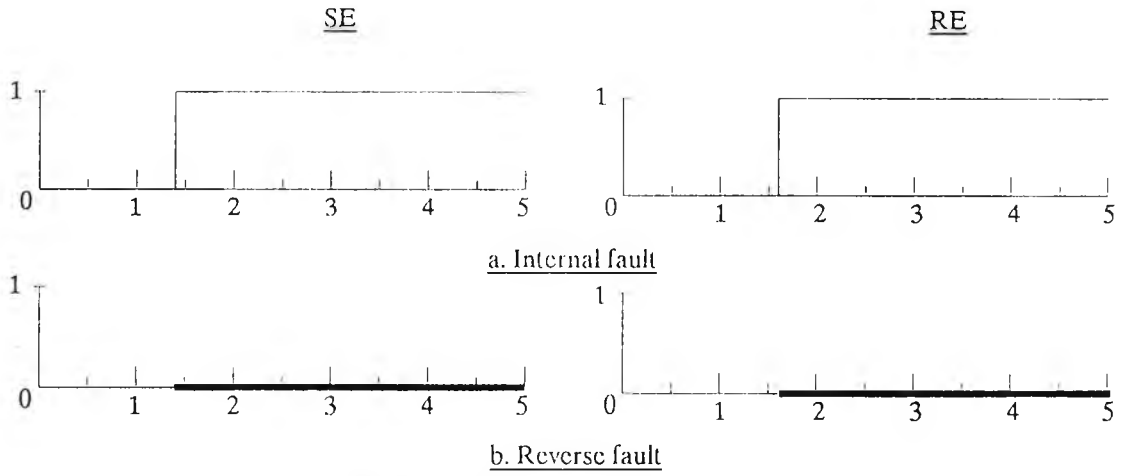
b. Reverse fault

A. Signal V_D, 0 or 1 (1 if $V_Z \geq V_T$, 0 if $V_Z < V_T$. V_T = THRESHHOLD VALUE, 20×10^6 units

a. Internal fault
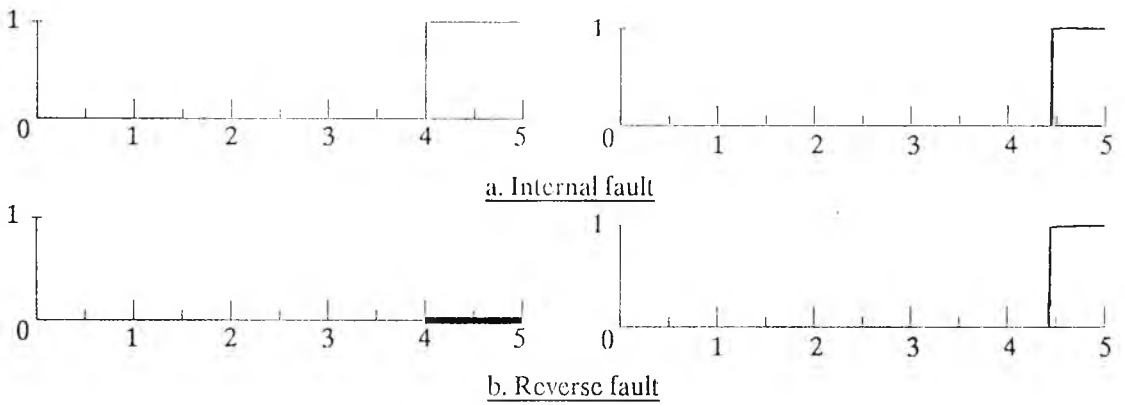
b. Reverse fault

B. Signal T_{FD}, 0 or 1 (1 if forward fault, 0 if reverse fault)

a. Internal fault

b. Reverse fault
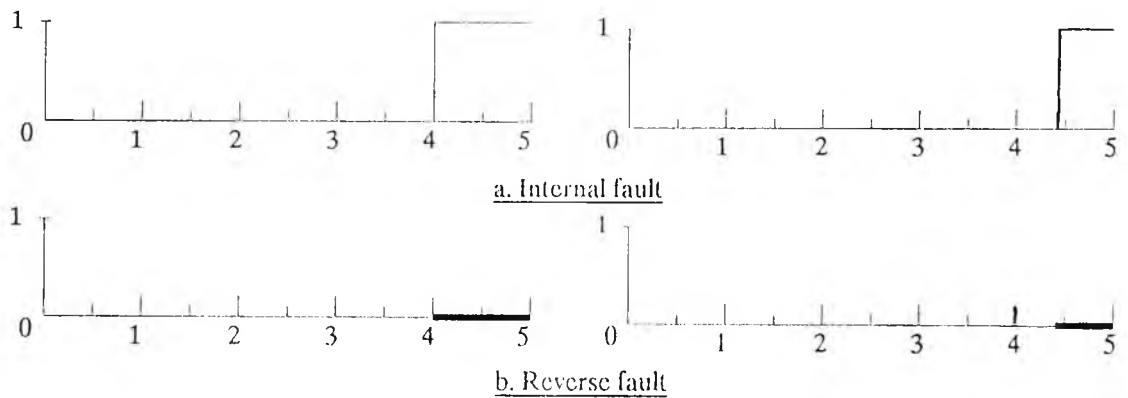
C. Signal trip TS, 0 or 1 (1 if V_D, T_{FD} = 1)

X AXIS; TIME IN mS
Y AXIS; LOGIC CONDITION 1 OR 0

Figure 5.21 SIGNALS V_D, T_{FD} AND TRIP TS AT SE AND RE
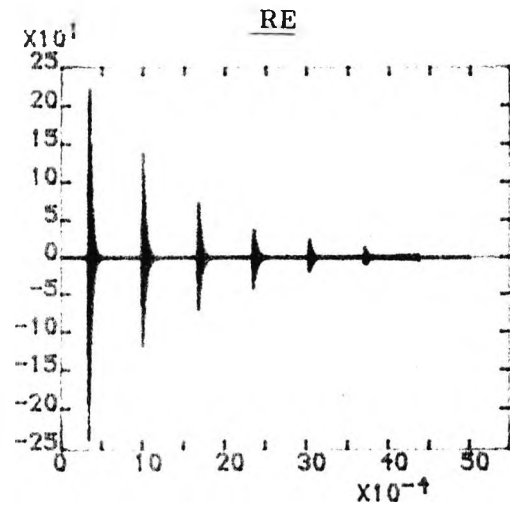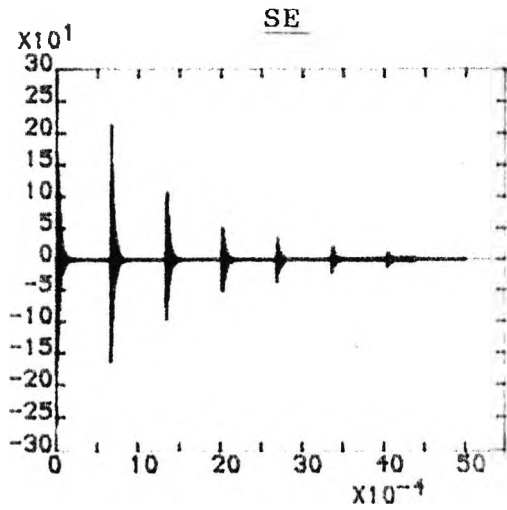
a: Signal 'V$_F$'
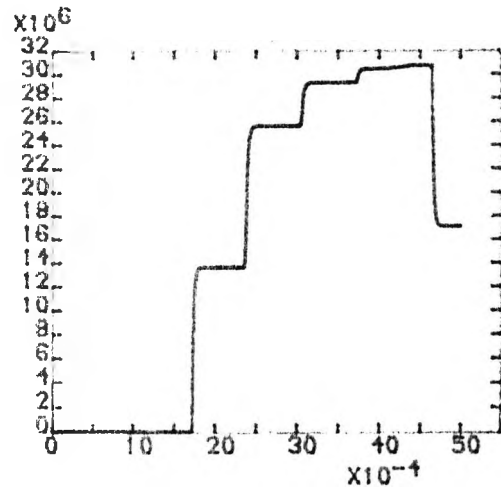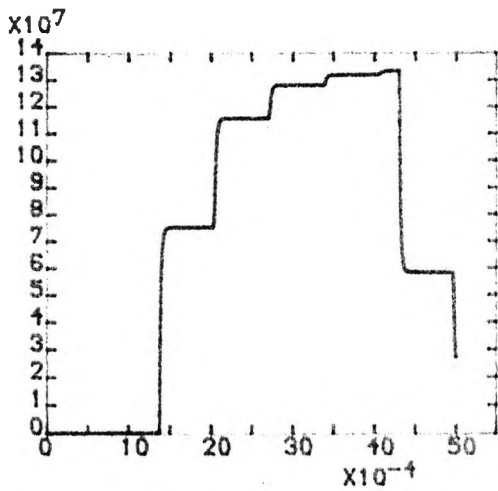
b: Signal 'V$_Z$'

X-Axis: TIME-Seconds
Y-Axis: RESPONSE V$_F$, V$_Z$-Units

Figure 5.22 RESPONSE V$_F$, V$_Z$ FOR THE INTERNAL FAULT AT V30DEGREE AT ENDS SE AND RE
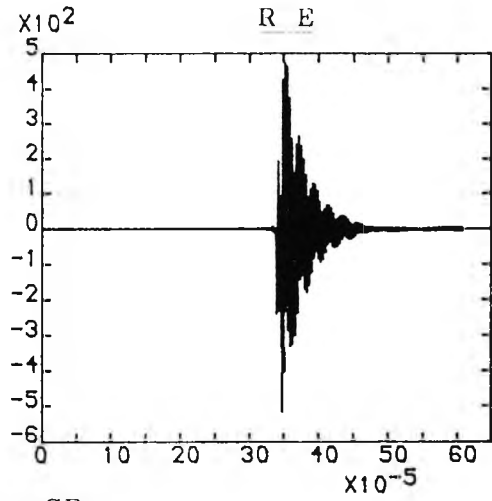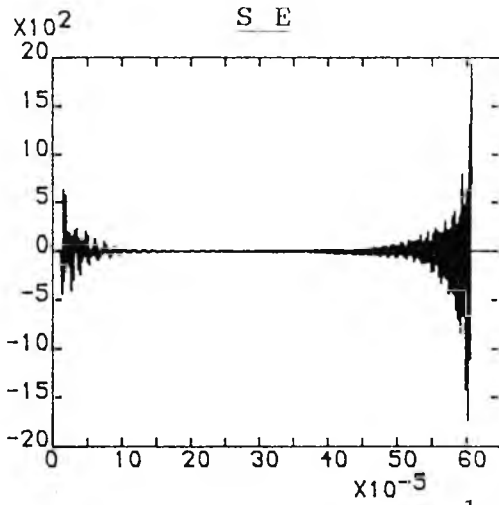
a: 1 km from SE
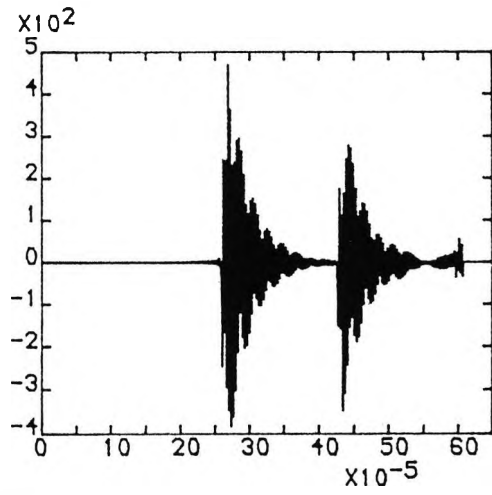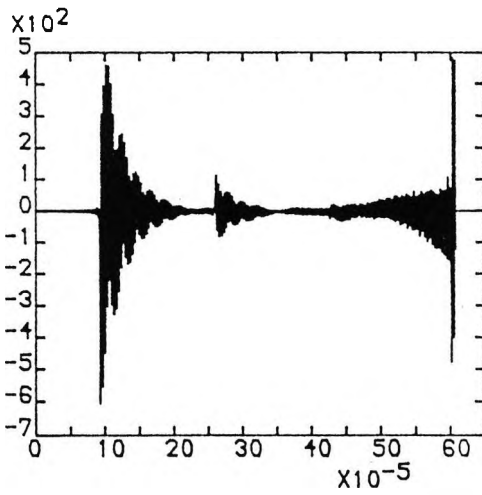
b: 25 km from SE
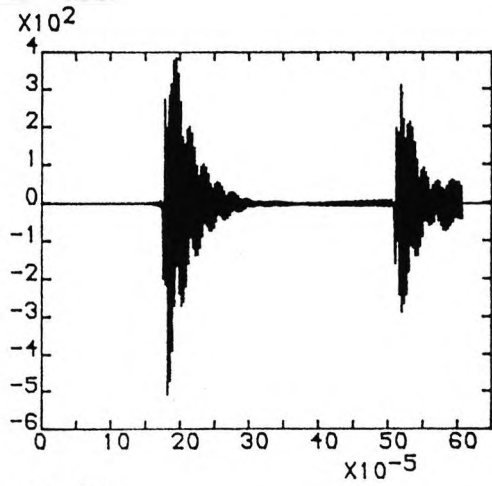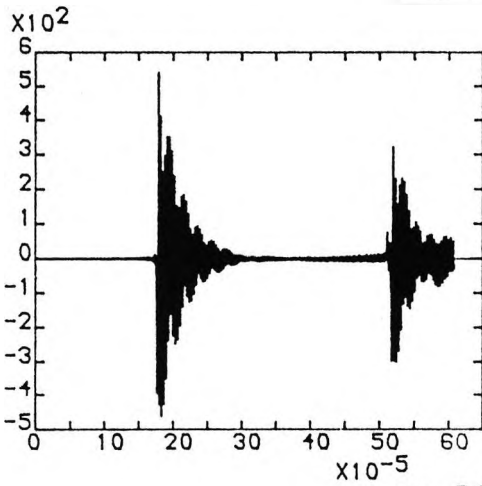
c: 50 km from SE

X axis: TIME - Seconds
Y axis: VOLTAGES - Volts

Figure 5.23   MODAL 2 RESPONSES AT DIFFERENT
POINTS ON THE TRANSMISSION LINE

SE RE
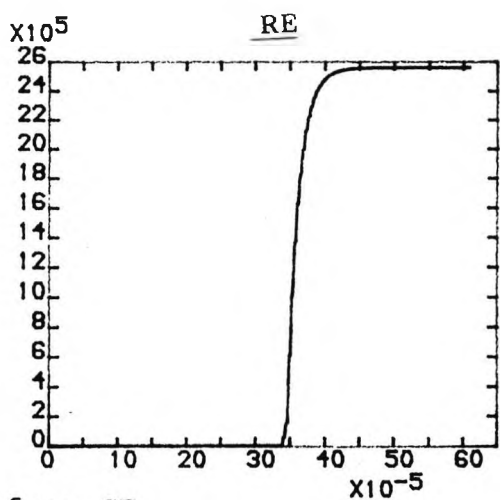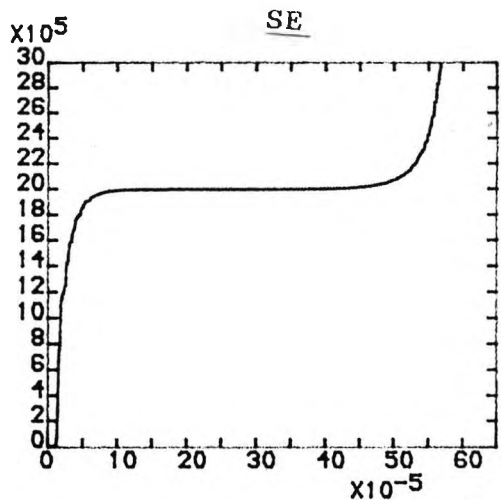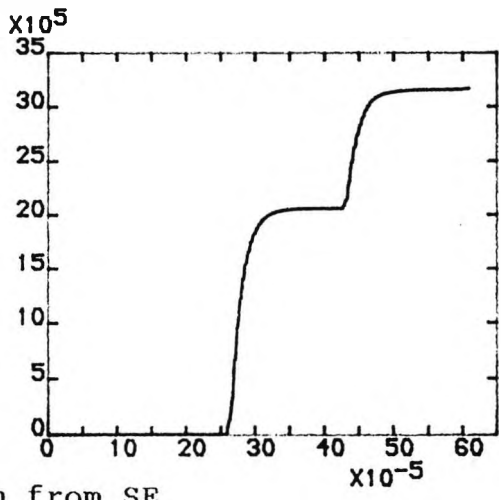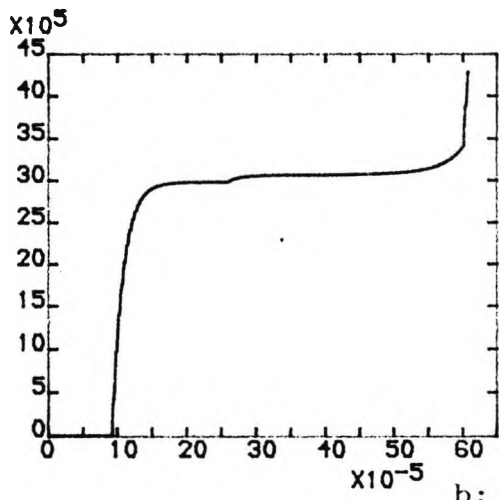
a: 1 km from SE
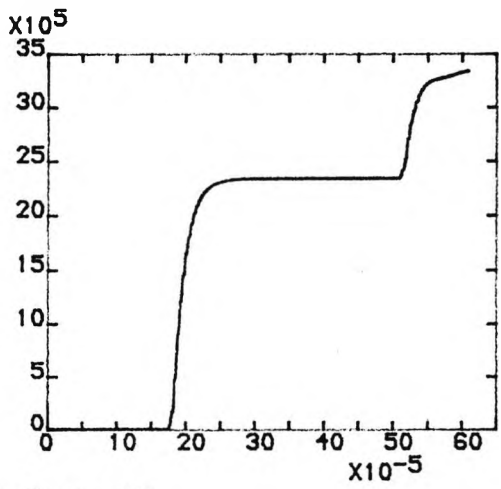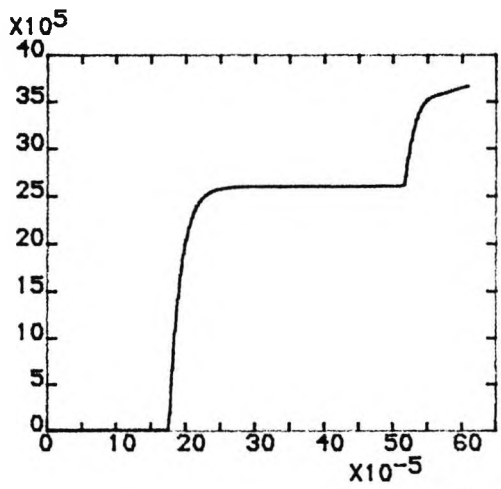
b: 25 km from SE

c: 50 km from SE

X-Axis: TIME-Seconds
Y-Axis: RESPONSE-Units

Figure 5.24 SQUARE AND INTEGRAL WITH TIME OF RESPONSES
CORRESPONDING TO FIGURE 5.23
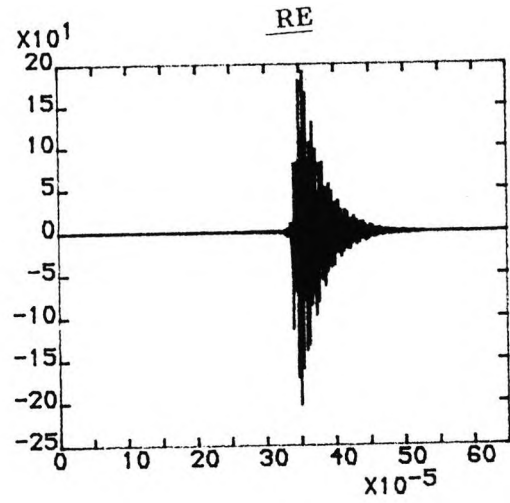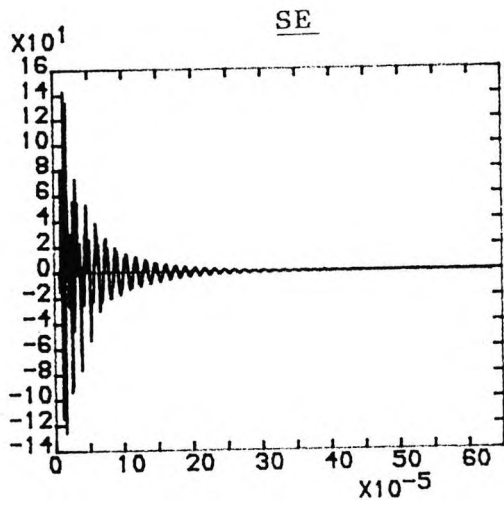
X-Axis: TIME-Seconds
Y-Axis: TUNER OUTPUT RESPONSE-Volts

Figure 5.25 RESPONSE 'V$_F$' IN REVERSE FAULT CONDITION AT V$_{MAX}$
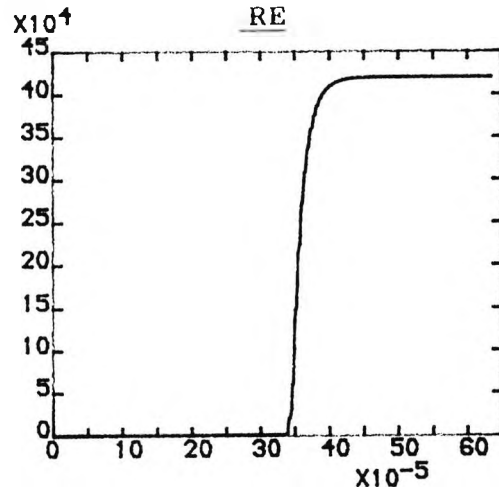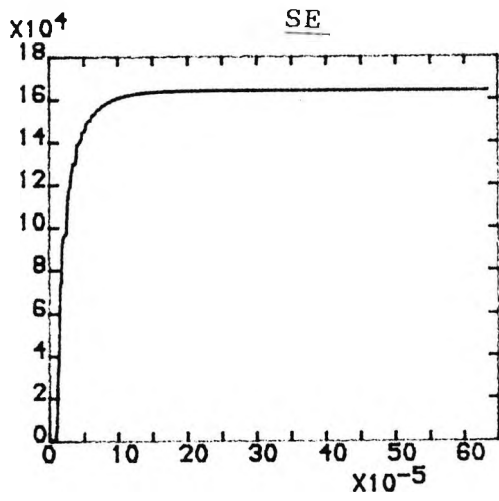
X-Axis: TIME-Seconds
Y-Axis: RESPONSE-Units

Figure 5.26 SQUARE AND INTEGRAL WITH TIME OF RESPONSES
CORRESPONDING TO FIGURE 5.25
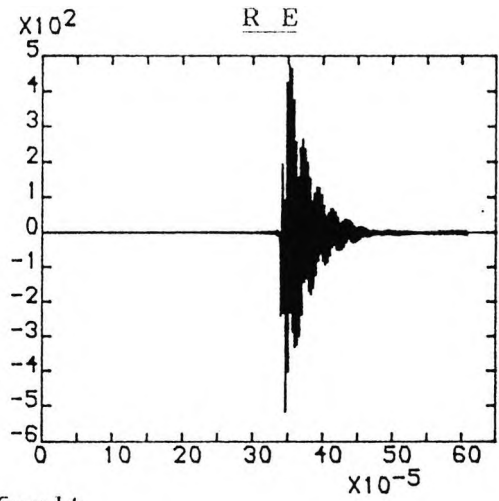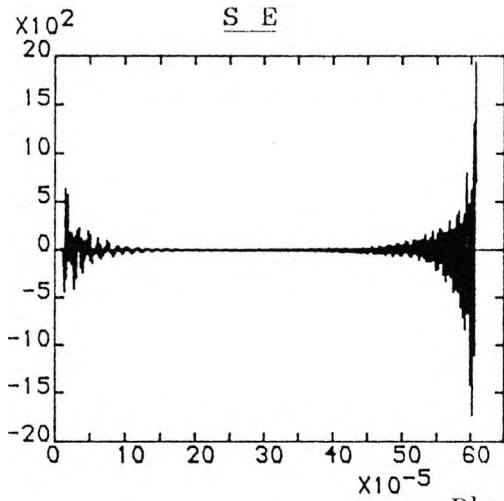
a: Phase A fault
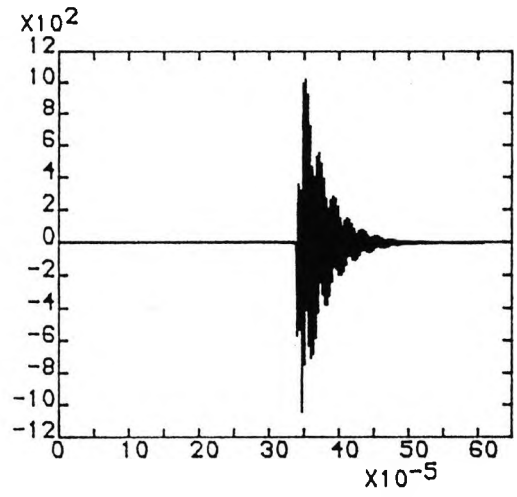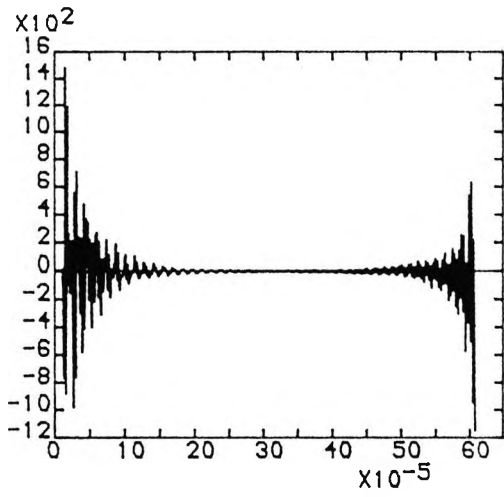
b: Phase B fault
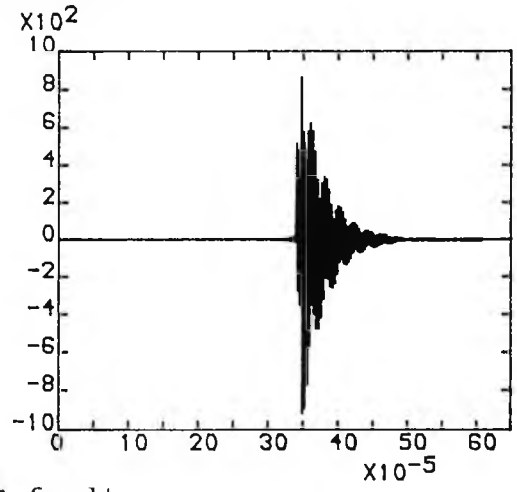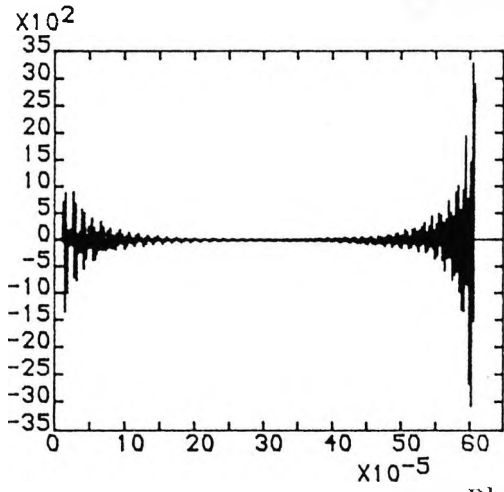
c: Phase C fault

X axis: TIME - Seconds
Y axis: VOLTAGES - Volts
(TUNER OUTPUT)

Figure 5.27   RESPONSES FOR OTHER FAULTS
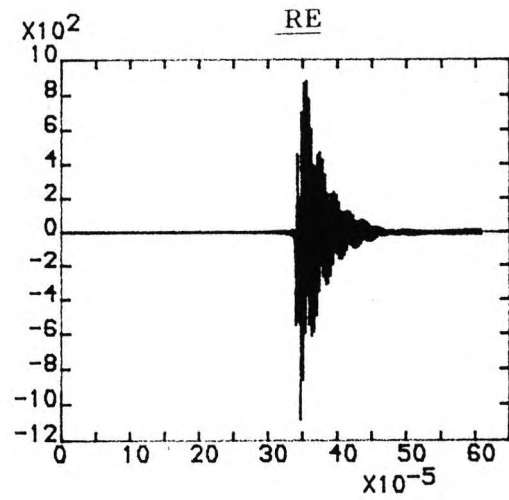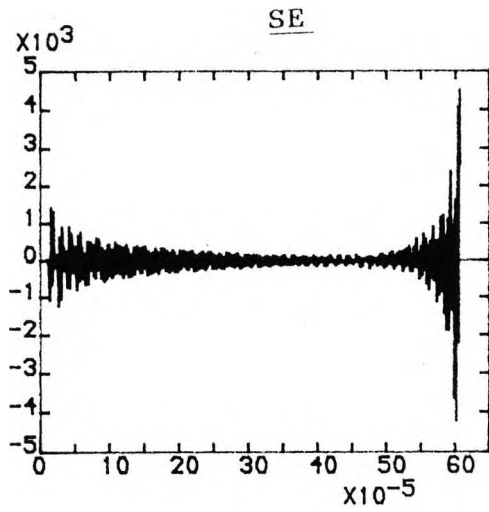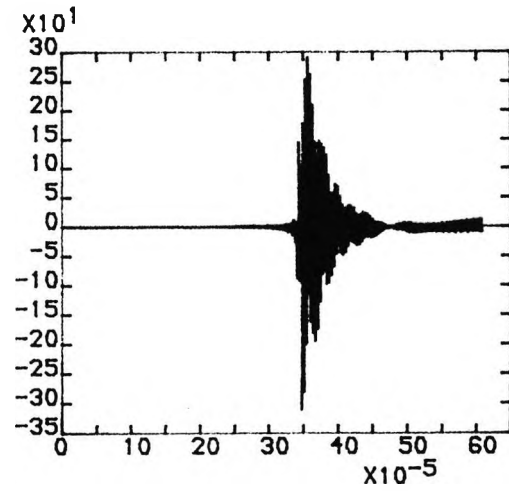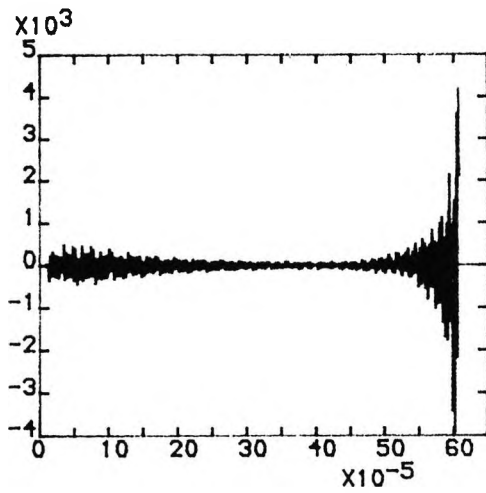
a: 3 Phase fault

b: Phase-Phase fault

X-Axis: TIME-Seconds
Y-Axis: TUNER OUTPUT VOLTAGE-VOlts

Figure 5.27 RESPONSES FOR OTHER FAULTS
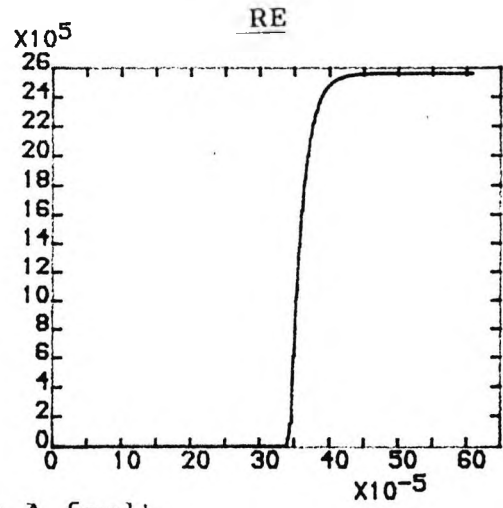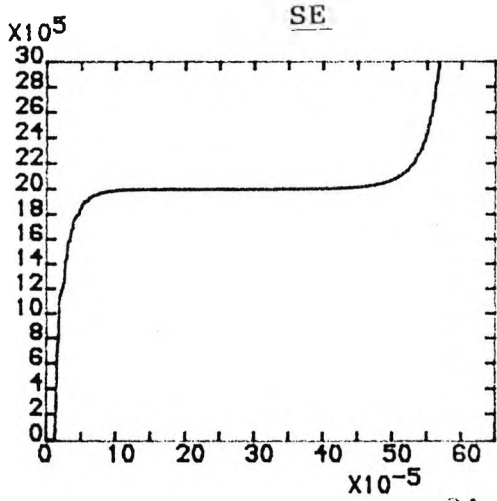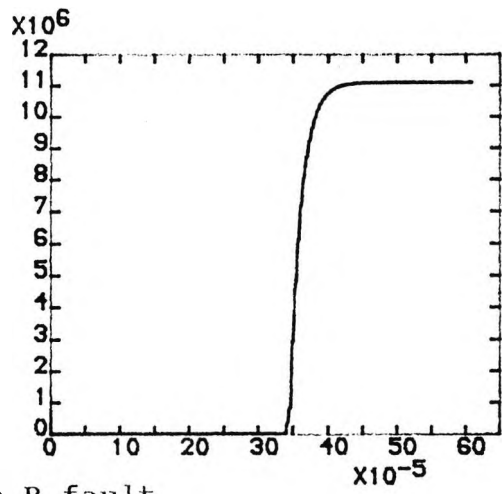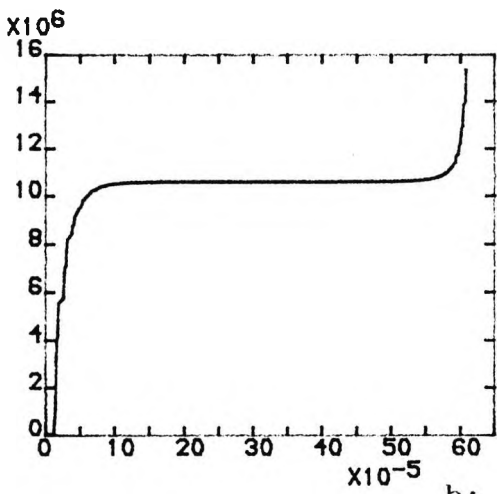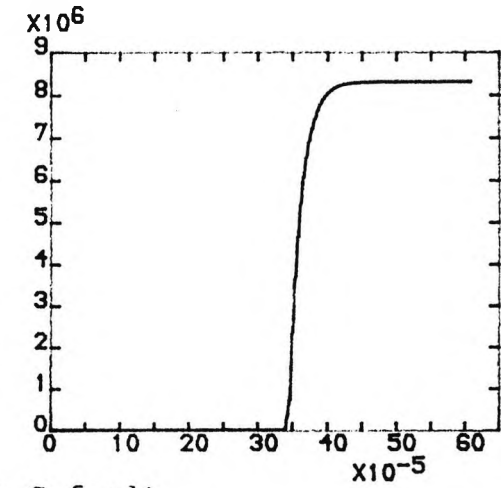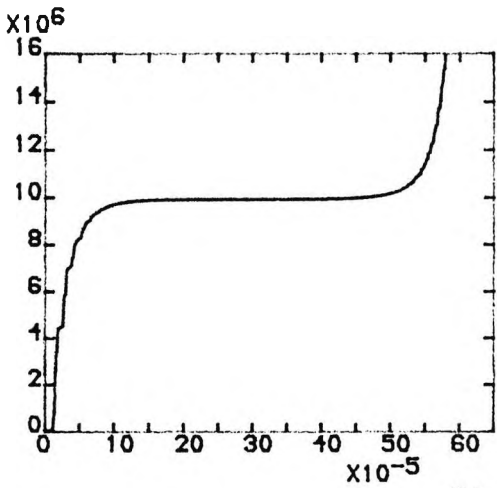
SE RE

a: Phase A fault

b: Phase B fault

c: Phase C fault

X-Axis: TIME-Seconds
Y-Axis: RESPONSE-Units

Figure 5.28 SQUARE AND INTEGRAL WITH TIME OF RESPONSES
CORRESPONDING TO FIGURE 5.27

Cont.
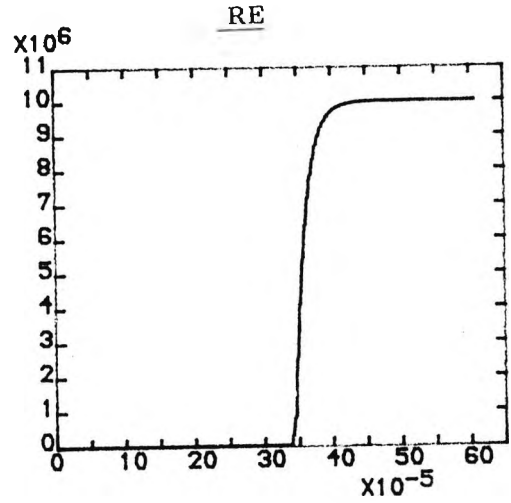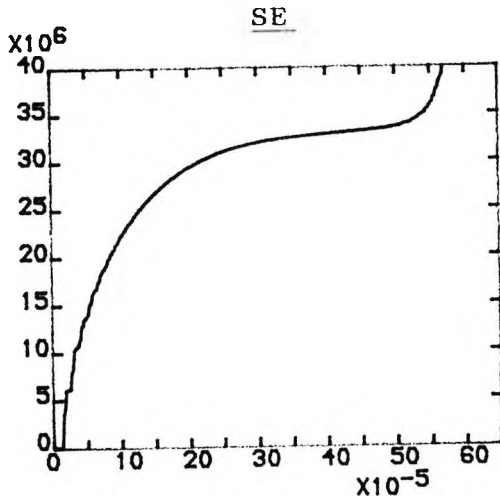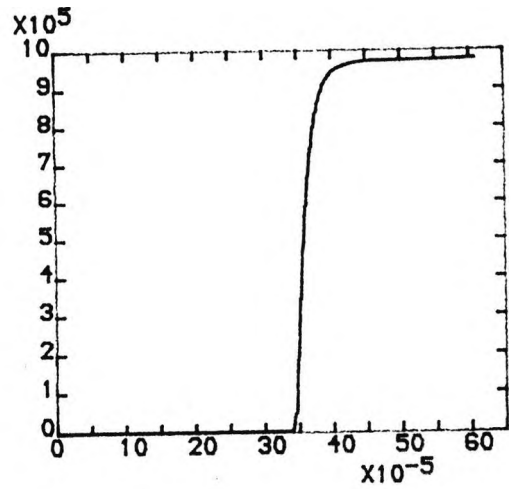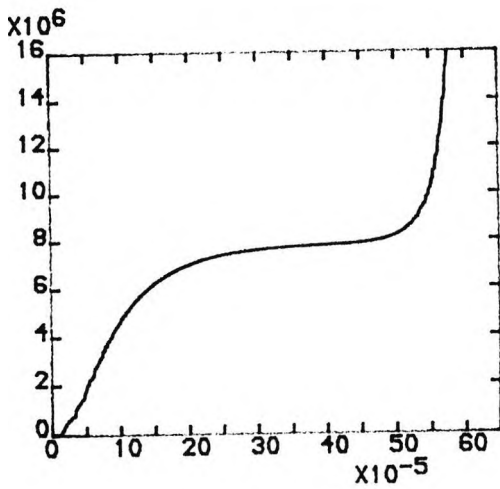
SE

RE

a: 3 Phase fault

b: Phase-Phase fault

X-Axis: TIME-Seconds
Y-Axis: RESPONSE-Units

Figure 5.28 SQUARE AND INTEGRAL WITH TIME OF RESPONSES
CORRESPONDING TO FIGURE 5.27

Table 5.1 MODAL VELOCITIES AND ATTENUATION FOR OVERHEAD LINES (f=100 kHz)

Single Circuit	Horizontal line		Vertical line	
Mode	Velocity km/Sec	Attenuation dB/km	Velocity km/Sec	Attenuation dB/km
1	283395	0.55537	280294	0.64561
2	297392	0.5959	299380	0.02852
3	299402	0.03013	299529	0.02811
Double Circuit				
1	276455	0.9575	272438	1.1842
2	295595	0.0858	298956	0.0351
3	299487	0.0158	299635	0.0099
4	288064	0.3372	294579	0.1209
5	298602	0.0248	299623	0.0132
6	299706	0.0142	299850	0.0094

Table 5.2 **RESULTS OF MODAL ANALYSIS**

Phase	Mode 3	Mode 2	Mode 1
a	1.0	1.0	1.0
b	1.206(q)	0	-1.66(p)
c	1.0	-1.0	1.0
Modal Impedance (Ohms)	379.0	274.0	232.0

Table 5.3 **MODE ATTENUATION AND PHASE VELOCITY**

Mode	Attenuation dB/mi		Phase Velocity relative to Mode 1
	30 kHz	300 kHz	
1	0.01-0.03	0.07-0.009	1.0
2	0.09-0.1	0.4-0.5	0.98-0.995
3	1.5 to 3.0 at 100 kHz		

Table 5.4 **COMPARISON OF RESPONSES 'a' AND DISCRIMINATION FACTOR 'd' FOR FAULTS AT DIFFERENT POINTS OF THE LINE AT THE INSTANT OF 0.4 ms (REF. Figure 5.24) WITH REFERENCE TO THE RESPONSE AT THE RE FOR THE REVERSE FAULT (REF. Figure 5.28)**

Response for reverse fault at RE, 'b' = 40×10^4				
Fault at	SE		RE	
	Response 'a'	Discrimination factor,'d'=a/b	Response 'a'	Discrimination factor,'d'=a/b
1 km	20×10^5	5	25×10^5	6.25
25 km	30×10^5	7.5	20×10^5	5
50 km	25×10^5	6.25	24×10^5	6

Table 5.5 **COMPARISON OF RESPONSES 'a' AND DISCRIMINATION FACTOR 'd' FOR DIFFERENT TYPES OF FAULT AT THE INSTANT OF 0.4 ms (REF. Figure 5.26) WITH REFERENCE TO THE RESPONSE AT THE RE FOR THE REVERSE FAULT (REF. Figure 5.28)**

Response for reverse fault at RE, 'b' = 40×10^4				
Fault Type	SE		RE	
	Response 'a'	Discrimination factor,'d'=a/b	Response 'a'	Discrimination factor,'d'=a/b
Phase'A'	20×10^5	5	25×10^5	6.25
Phase'B'	10×10^6	25	11×10^6	27.5
Phase'C'	10×10^6	25	8.5×10^6	21.25
Three-Phase	32×10^6	80	10×10^6	25
Phase-Phase	8×10^6	20	9.5×10^5	2.4

CHAPTER 6

INVESTIGATION OF THE PRINCIPLE CONSIDERING BUS BAR CAPACITANCE

This chapter investigates the principle as described in Chapter 2 for the transmission line system with effective bus bar capacitance [47]. This bus bar capacitance may vary from line to line depending upon various factors in particular the number of lines terminating at the bus bar. A typical value of 0.1uF has been considered in this chapter for investigation purposes. As explained in Chapter 2, the stack tuner has to be in the normally close mode, NC for the internal faults (reference Figure 2.2) and changeover to the open mode, NO for the external faults as shown in Figure 2.3. The operational principle has been explained in Chapter 2 with reference to Figure 2.6. The digital simulation technique has been explained in Chapter 3. After digital simulation of the stack tuner and the bus bar capacitance, fault responses at the SE and the RE have been studied at the bus bars (primary side of the stack tuner) and have been found to be satisfactorily as described in Chapter 3. In this chapter, fault responses will be investigated at the output (secondary side) of the

stack tuner to establish the principle for faults at the voltage maximum. Further investigations have been carried out for the satisfactory operation of the scheme 1) at lower fault inception angles of the voltage and 2) under the condition of different source capacities. For the simulated test purposes, phase A to earth fault has been considered at 1 km from the SE of a 100 km long 400 kV transmission line with sources of 5 GVA at SE and 20 GVA at RE. The fault observation time is 600 micro-seconds and the sampling frequency is 853.33 kHz. Value of the frequency shift constant α has been adjusted very critically at 1000 or 10000. It has been found that higher the value of α, the response has been found to be satisfactory nearly at the end of the fault response period. At the beginning of the fault response period, the response has been found to be diverge very soon. If the lower value of the α is chosen, the response has been found to be satisfactory at the beginning of the fault response period. At the end of the fault response period, the response has been found to be diverge. In the present study, a lower value of α = 1000 has been chosen for the simulated testing the discrimination feature and a higher value α = 10000 has been chosen for other tests. to get satisfactory responses at the end of the fault response period at the RE. The reason for selecting a satisfactory response at RE is that the discrimination feature of the scheme is decided by the responses at the RE for the internal fault and the reverse fault. The fault responses have been considered for a period of only 600 micro-seconds to establish the basic

130

principle of the scheme. As explained above, with the higher value of α = 10000, at the SE, the divergence of the responses has been found and therefore the responses have been recorded only for a period of half the fault response period i.e. 300 micro-seconds for other tests: different fault inception angles and different source capacities. It has been established earlier that the transients fault responses (bursts) repeats with attenuation (refernce Figure 4.3) at every interval (depending upon the distance of the fault from the bus bar) for a period of about 5 msec. In such a case if the discrimnation for the reverse fault can be established based upon the simulated fault responses for a period of 600 micro-seconds without considering the effect of the operating delay of the directional detector, DD, then the principle based upon the signal processing (reference Chapter 4 and Chapter 5) can be established without any difficulty. The signal processing includes auto-correlation, time delay due to operation of the directional detector, DD, squaring and time integral of the delayed signal for input to the level detector. Based upon the threshold value of the level detector, the output signal V_D (reference Chapter 2) of the level detector is 1 or 0. This signal V_D goes to a decision logic which also gets a signal 1 or 0 from the directional detector for the reverse or the forward fault. When both signals are 1, then only a tripping signal is sent for operation of the local breaker. This signal processing scheme is same as has been explained in the earlier chapters. So in this chapter, the signal

processing of the output of the stack tuner has not been included.

6.1 **Establishment of the principle**

Figure 6.1 shows the fault responses for the internal fault and the reverse fault at the SE and the RE. Figure 6.1a shows the responses for the internal faults and Figure 6.1b shows the responses for the reverse faults. It has been explained earlier that the stack tuners are in the normally close mode at SE and RE for the internal faults and for the reverse fault at F1 (reference Figure 2.1), the stack tuner changes to the open mode. With reference to figures 6.1, the operation can be explained based on the peak voltages of the faulted phase response. Peak voltages have been found to be 6kV at the SE and 3kV at the RE for the internal fault. When considering an external fault, the peak voltages have been found to be 350 Volts at the SE and only 1.5 kV at the RE. This low response at the RE gives an excellent feature of the discrimination of the scheme. With reference to Chapter 2 if the threshold value can be set to a value proportion to say 2 kV, the V_D can be found to be 1 for the internal faults and 0 for the reverse fault at both ends the SE and the RE. For the reverse fault at the RE, V_D is 0. The signal from the directional detector T_F is 1 in all cases except in the case of the reverse fault at the SE. T_F is 0 at the SE for the reverse fault. Since the tripping signal is initiated only when both signals V_D and T_F are 1, it can be confirmed

that the scheme operates satisfactorily for the internal fault and does not operate for the reverse fault. This establishes the principle of the scheme.

6.2 **Effect of different fault inception angles**

Figure 6.2 shows the fault responses for various fault inception angle of the voltage i.e. 0, 2, 5, 15, 30, 60, 90 degrees at the sending end, SE and the receiving end, RE. It has been established in Chapter 4 that the responses are proportional to the value of $\sin\Theta_{fs}$ for a particular voltage of the transmission system and the particular mid-frequency of the stack tuner. where Θ_{fs} is the fault inception angle. If $\bar{V}_{ff}$(SE) is the peak voltage at the SE in Volts and $\bar{V}_{ff}$(RE) is the peak voltage at the RE in Volts, the following table shows (1) Θ_{fs}, (2) the positive peak responses at the SE, (3) its percentage for the fault at the maximum voltage, (4) the positive peak responses at the RE, (5) its percentage for the fault at the maximum voltage, (6) value of $\sin\Theta_{fs}$, (7) its percentage for the fault at the maximum voltage.

TABLE

Θ_{fs}	$\bar{V}_{ff}(SE)$	%	$\bar{V}_{ff}(RE)$	%	$\sin\Theta_{fs}$	%
90	25000	100	25000	100	1	100
60	21000	84	21000	84	0.866	86.6
30	12500	50	12500	50	0.5	50
15	6500	26	6500	26	0.258	25.8
5	2100	8.4	2100	8.4	0.087	8.7
2	900	3.6	900	3.6	0.035	3.5

This table shows a good agreement between the calculated values and the simulated test results. Comparing the positive peak response at the RE for the reverse fault at maximum voltage (Figure 6.1b) and the internal fault at 2 degree point-on-wave fault of the voltage (Figure 6.2f), it can be concluded that the scheme can be used satisfactorily for all faults for the point-on-wave of 2 degrees or more. In general 30 degrres is the very well accepted value as has been evaluated in Chapter 4.

6.3 Effect of different source capacities

Simulated tests have been carried out for (1) 1 GVA at both ends, (2) 50 GVA at both ends, (3) 99 GVA at both ends. Figure 6.3 shows the results for these simulated tests. It has been found that there is no appreciable difference in responses and it can be concluded that the performance of the developed scheme is satisfactory for different source capacities for the transmission line with two sources.
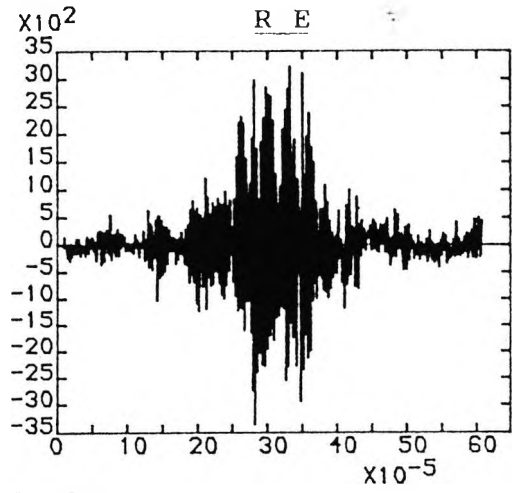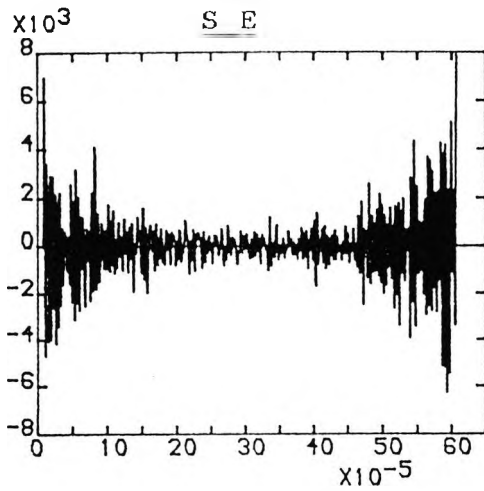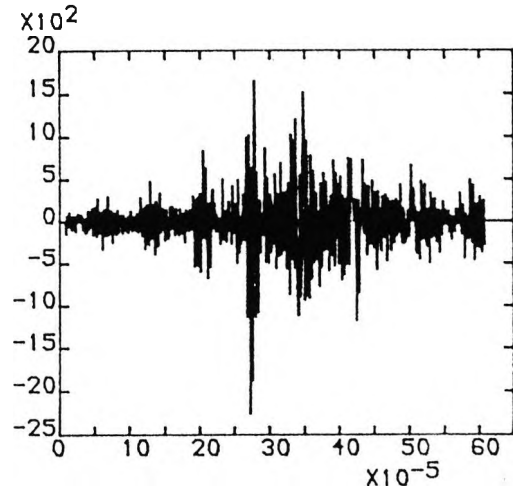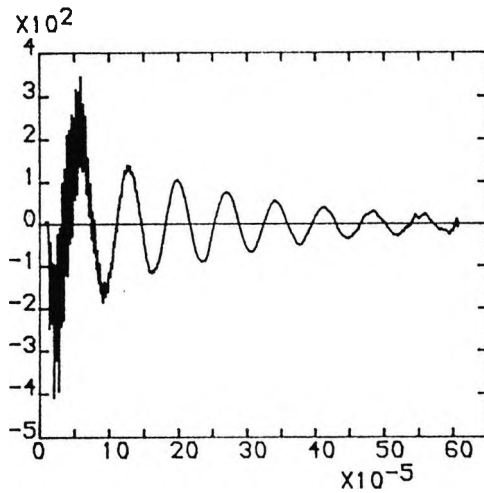
X10³ S E

X10² R E

a: Internal fault

VD=1,TF=1
TR=0,TRIP=1

VD=1,TF=1
TR=0,TRIP=1

X10²

X10²

b: Reverse fault

VD=0,TF=0
TR=1,TRIP=0

VD=0,TF=1
TR=0,TRIP=0

X axis: TIME - Seconds
Y axis: VOLTAGES - Volts

(TUNER OUTPUT)

Figure 6.1   ESTABLISHMENT OF THE PRINCIPLE
CONSIDERING BUS BAR CAPACITANCE
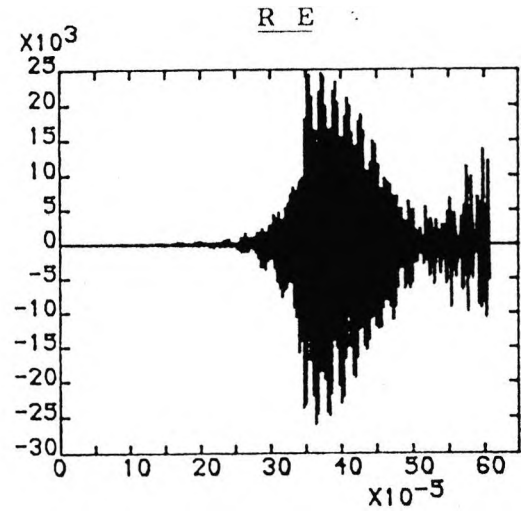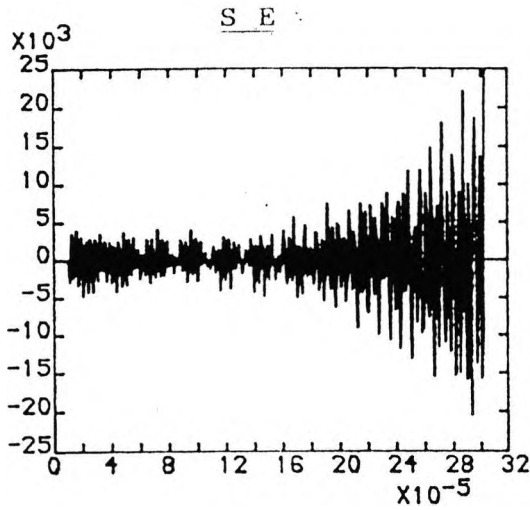
a: 90 Degrees
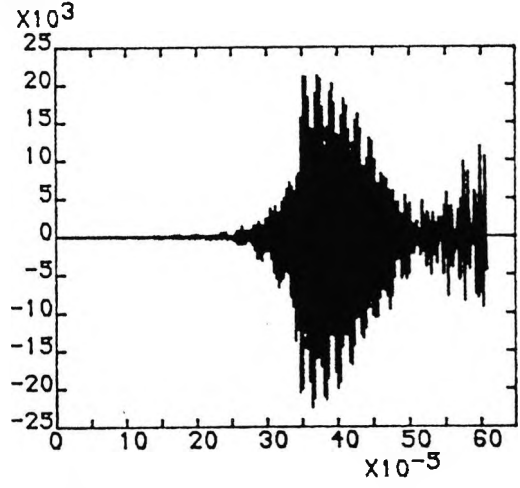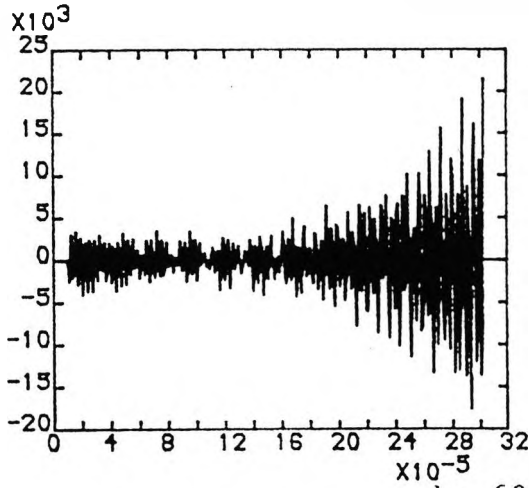
b: 60 Degrees
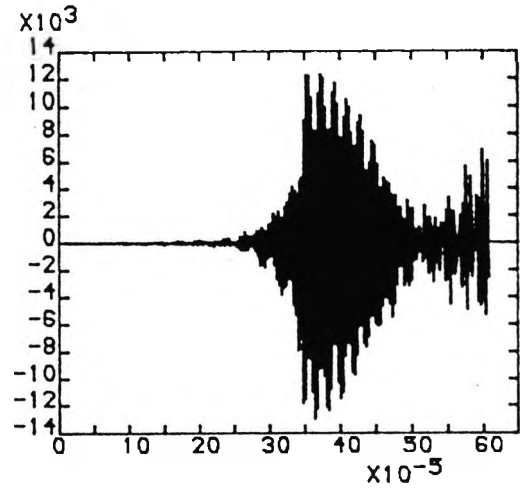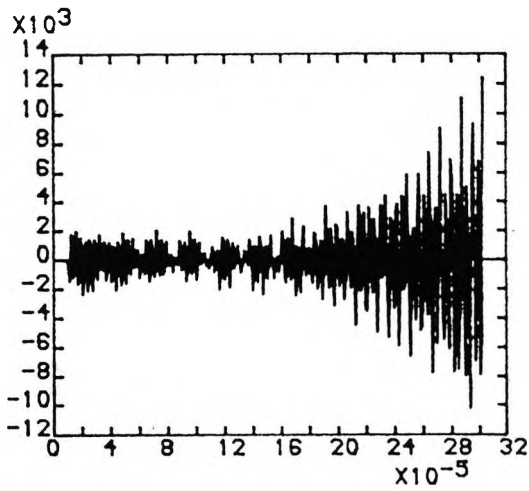
c: 30 Degrees

X axis: TIME - Seconds
(TUNER OUTPUT) Y axis: VOLTAGES - Volts

Figure 6.2   EFFECT OF DIFFERENT FAULT INCEPTION
ANGLES CONSIDERING BUS-BAR CAPACITANCE
Cont.

S E   R E
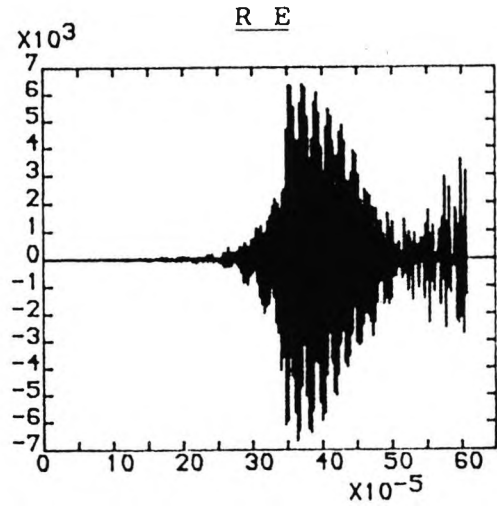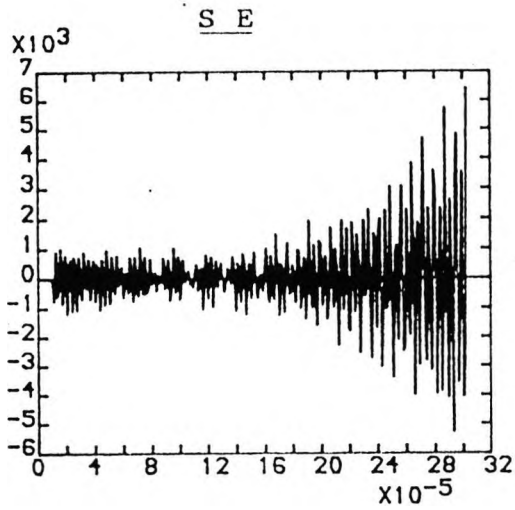
d: 15 Degrees

e: 5 Degrees

X axis: <u>TIME</u> - Seconds
Y axis: <u>VOLTAGES</u> - Volts

(TUNER OUTPUT)

Figure 6.2   <u>EFFECT OF DIFFERENT FAULT INCEPTION ANGLES CONSIDERING BUS-BAR CAPACITANCE</u>
Cont.

S E   R E
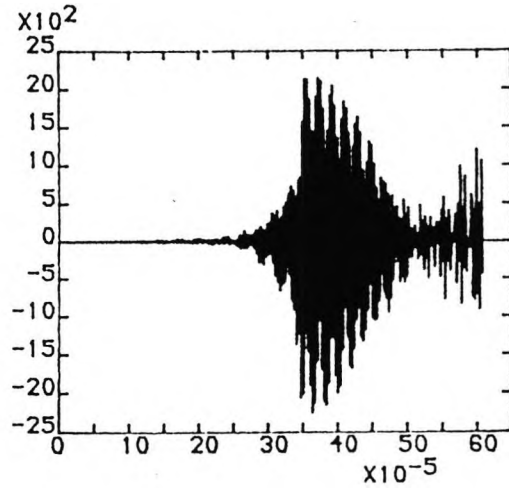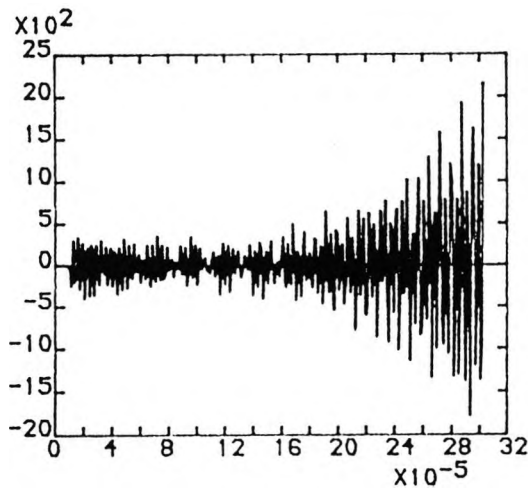
f: 2 Degrees

g: 0 Degree
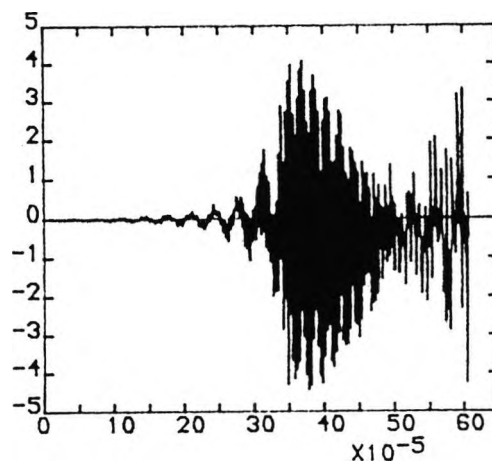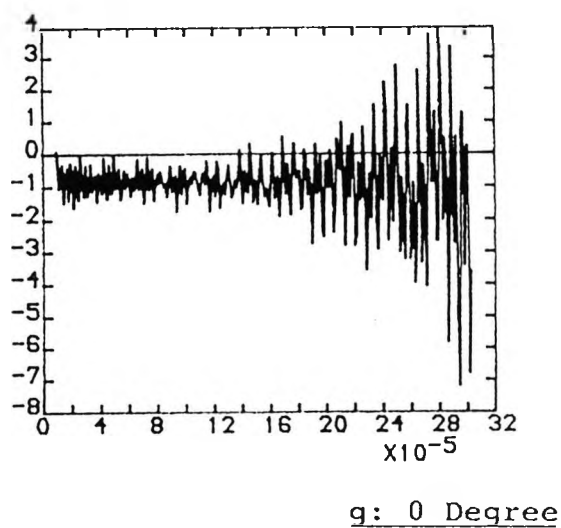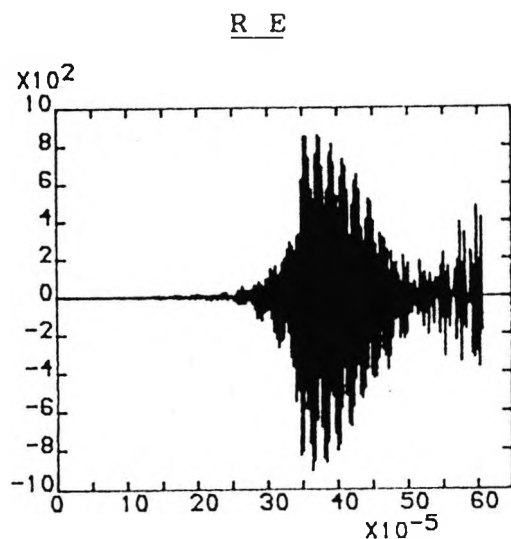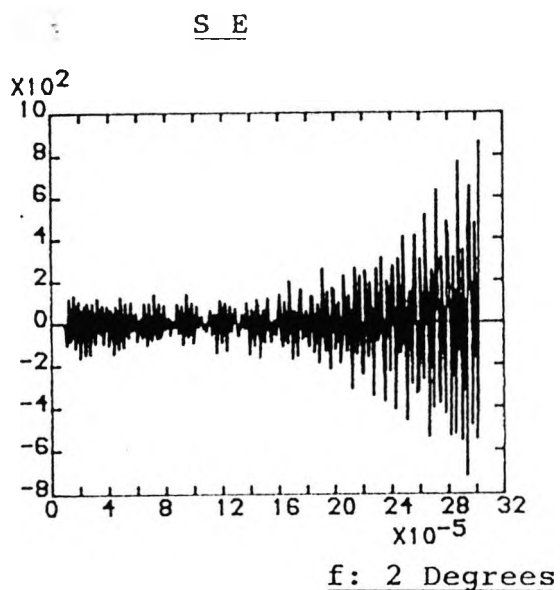
X axis: TIME - Seconds
Y axis: VOLTAGES - Volts

(TUNER OUTPUT)

Figure 6.2 EFFECT OF DIFFERENT FAULT INCEPTION
ANGLES CONSIDERING BUS-BAR CAPACITANCE
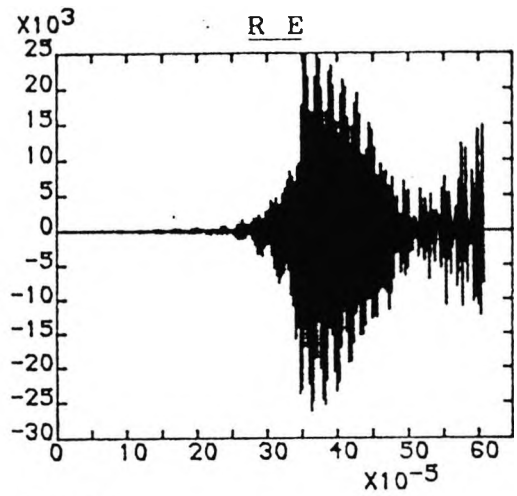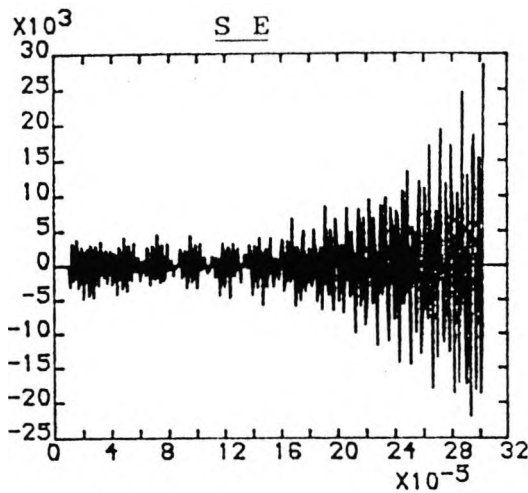
a: 1 GVA at both ends
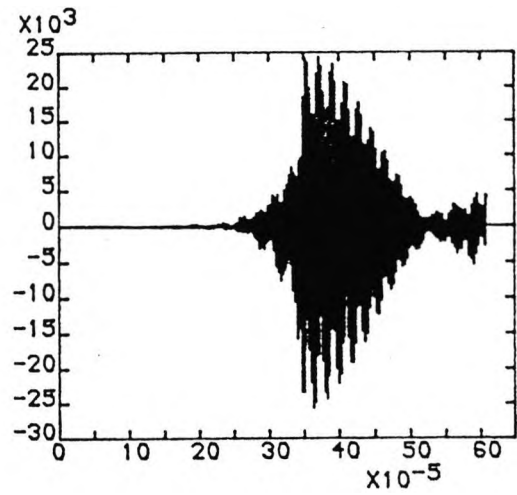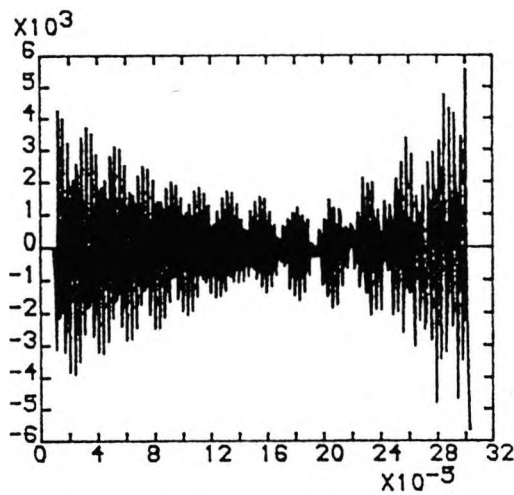
b: 50 GVA at both ends
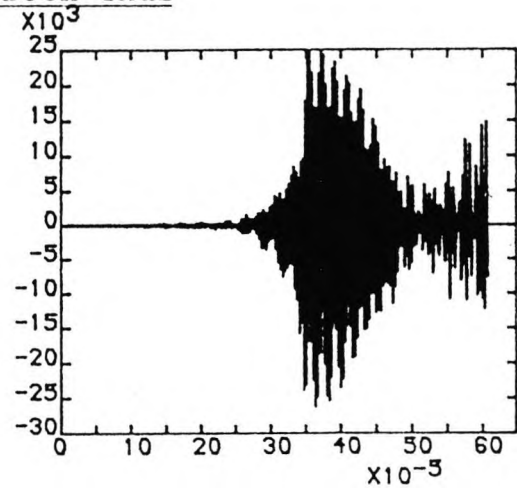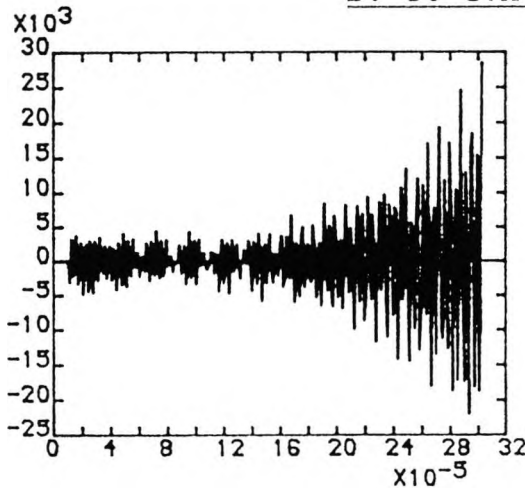
c: 99 GVA at both ends

(TUNER OUTPUT)

X axis: TIME - Seconds
Y axis: VOLTAGES - Volts

Figure 6.3   EFFECT OF DIFFERENT SOURCE CAPACITIES
CONSIDERING BUS-BAR CAPACITANCE

CHAPTER 7

DIGITAL SIMULATION OF ELECTRIC ARC MODEL AND SUPERIMPOSED ARC VOLTAGES

As explained earlier in Chapter 1, most faults on HV
transmission lines involve arcing or some other
intermittent discharge. Arc length may be small or large
but voltage drop across it, is generally very small
relation to transmission system voltages. Typically, for a
20 meter arc length in a 400 kV system, a maximum voltage
drop of 20 kV is expected and does not affect a protection
scheme which normally works on the basis of steady state
fault current. It is only the current which is limited due
to arc resistance and can affect the operation of a relay.
In the new approach of UHS protection due to fault
generated noise, the principle of protection is based on
the detection of a particular frequency band from the high
frequency voltage waveform. In such a scheme, noise due to
other effects in particular arc can not be neglected. With
this aim the present chapter describes the digital
simulation techniques of the arc model and the transmission
system with the arc model.

7.1 Digital simulation of electric arc model [42,43]

The static arc characteristic is very well known. In the present scope of work, the dynamic arc characteristic has been considered due to reversal of current at the power cycle 50Hz or 60Hz. In the dynamic characteristic, the arc does not follow the same path for increasing the current and decreasing the current, and this effect is known as the arc hystersis. Considering Strom's [35] dynamic characteristic, an approximate linearised arc model has been considered for simplification as shown in Figure 7.1. I_p is peak of the steady state arc current in amperes. I_l and I_h are $0.15I_p$ and $0.38I_p$ respectively. V_p is the maximum arc voltage per cm of the arc length which is 10.3 Volts.

The arc cyclogram shown in Figure 7.1 can be obtained repeatedly only if the time for which the current remains zero, is so small that the arc can be reestablished without any appreciable deionization or restriking voltage. Infact the cyclogram shown in Figure 7.1 has negligible reignition voltage. Since the arcing faults may influence the fault generated high frequency waveforms, it is desired to include the effect of reignition voltage to have a reasonably good accuracy in the arc cyclogram modelling. According to Fukunishi [41], the rate at which the reignition voltage increases is a function of the time for which the arc exits. With this view Johns [42] defined the reignition voltage as

$$| V_R(t) | = K(T_e)(t - T_e) \ h(t - T_e) \ kV/Cm \qquad (7.1)$$

where T_e is arc extinguishing time and $K(T_e)$ is the rate of increase of the reignition voltage. Value of $K(T_e)$ has been found to be as 5 V/ms and 15 V/ms for T_e of 0 and 200 ms respectively [53] and the above relationship of Johns [41] can be modified as

$$| V_R(t) | = (5 + 50 \ T_e)(t - T_e) \ h(t - T_e) \ kV/Cm$$

$$(7.2)$$

Figure 7.2 shows the effect of reignition voltage $V_R(t)$ on the arc cyclogram 0, a, b, c, b, 0, a',b',c',b',0, a piecewise linear characteristic VA (voltage - ampere). Following the arc voltage reversal, the arc current is held zero till the arc voltage remains below the reignition voltage given by above equation. When the arc voltage exceeds the re-ignition voltage, the arc voltage follows the arc cylogram. The broken line $'V_R(t) - a'$ shows the lower value of the reignition voltage before following the arc cyclogram. The continuous line $'V_R(t) - a'$ shows the higher value of the reignition voltage before following the arc cyclogram. This arc voltage $\bar{V}_{arc}$ can be evaluated using Thevenin equivalent circuit as shown in Figure 7.3.

$$\bar{V}_{arc} = \bar{E}_T - \bar{I}_{arc} \cdot Z_T \tag{7.3}$$

where $\bar{E}_T$ is Thevenin source voltage at the fault point, $\bar{I}_{arc}$ is the arc current and, Z_T is Thevenin source impedance. In the present work it has been asumed that (1) the time for which the arc current is being held zero, has been assumed to be very small, (2) the reignition voltage shoots up to a value greater than the arc voltage and follows the normal arc cyclogram, (3) the rate of rise of the reignition voltage is proportional to the time from the instant of the fault. Since the arc exits nearly half a cycle all times, $T_e = 0.010$ seconds and the above relationship for the reignition voltage can be simplified as:

$$| V_R(t) | = 5.50 \ t \ h(t) \ kV/Cm \tag{7.4}$$

Now the simulation technique is followed as below:
The simulation techinque is being explained for a positive half cycle o, a, b, c, b, o and it shall follow exactly the same for a negative half cycle o, a', b', c', b', o. Simulation process begins with the comparision of the arc voltage against the reignition voltage for 1 cm length of the arc. Thus the current is held at zero until the arc voltage exceeds the re-ignition voltage. Mathematically,

$$I_{Farc}(t) = 0 \qquad V_{farc}(t) < V_R(t) \qquad (7.5)$$

and when the arc voltage reaches the value $V_R(t)$, Equation (7.6) is applied till the value is reached V_p.

$$V_{farc}(t) = [(V_p - V_R(t))I_{Farc}(t)/0.15I_p + V_R(t)] \qquad (7.6)$$

Now for any current in excess 0f $0.15\ I_p$, the arc voltage assumes a constant value V_p and the arc voltage is given by

$$V_{farc}(t) = V_p \quad , \quad I_{Farc}(t) > 0.15\ I_p \qquad (7.7)$$

Most of the fault current exceeds $0.38\ I_p$. Subsequent reduction in arc current follows the position of arc extinction given by equation (7.8)

$$V_{farc}(t) = [V_p\ I_{Farc}(t)/0.38\ I_p], \quad I_{Farc}(t) < 0.38\ I_p$$
$$(7.8)$$

140

It is important to note that current may reduce before reaching $0.38\ I_p$ for arc extinction and in such case arc voltage and current would be constrained to reach extinction along the line for increasing current where $V_R(t) = 0$. This path can be defined as

$$V_{farc}(t) = [V_p\ I_{Farc}(t)/0.15\ I_p], \quad 0 < I_{Farc}(t) < 0.15\ I_p$$

$$(7.9)$$

The above procedure is repeated again and agian after each extinction. The piecewise linear characteristic is cyclically traversed for both positive and negative half cycles until final extinction occurs when $|V_{farc}(t)|$ remains permanently below the arc reignition voltage $|V_R(t)|$. Appendix E shows the simulated test results for (1) the linearised arc cyclogram, and (2) the linearised arc cyclogram with the reignition effect.

7.2 Digital simulation of superimposed arc voltages of the transmission line

As explained in Chapter 3.2, the fault current $I_F(t)$ at a fault point F as shown in Figure 7.4, can be evaluated. Assuming the fault current as the arc current, it can be written as

$$I_{Farc}(t) = I_F(t) \qquad\qquad (7.10)$$

now using the arc cyclogram simulation, the total arc voltage $V_{farc}(t)$ can be found out and it can be expressed as

$$V_{farc}(t) = K_{arc}(t)\, I_F(t) \qquad\qquad (7.11)$$

where $K_{arc}(t)$ is an arc cyclogram constant. To get more realistic value of the arc voltage, a more realistic value of the arc current is necessary and therefore the arc current has been evaluated considering 0.5 Ohm arc resistance.

It is also known that the arc voltage at the fault point is equal to the sum of steady state voltage $V_{fss}(t)$ and superimposed arc voltage $V_{ffarc}(t)$ which can be expressed as

$$V_{farc}(t) = V_{fss}(t) + V_{ffarc}(t) \qquad\qquad (7.12)$$

Now superimposed arc voltage can be evaluated using following equation:

$$V_{ffarc}(t) = V_{farc}(t) - V_{fss}(t) \tag{7.13}$$

Using the FFT subroutine, the superimposed arc voltage at the fault point can be evaluated in the frequency domain. As explained in Chapter 3, the superimposed arc voltages for all three phases at the sending end P and the receiving end Q can be evaluated. Now using again the FFT subroutine, these superimposed arc voltages at two ends can be evaluated in time domain.
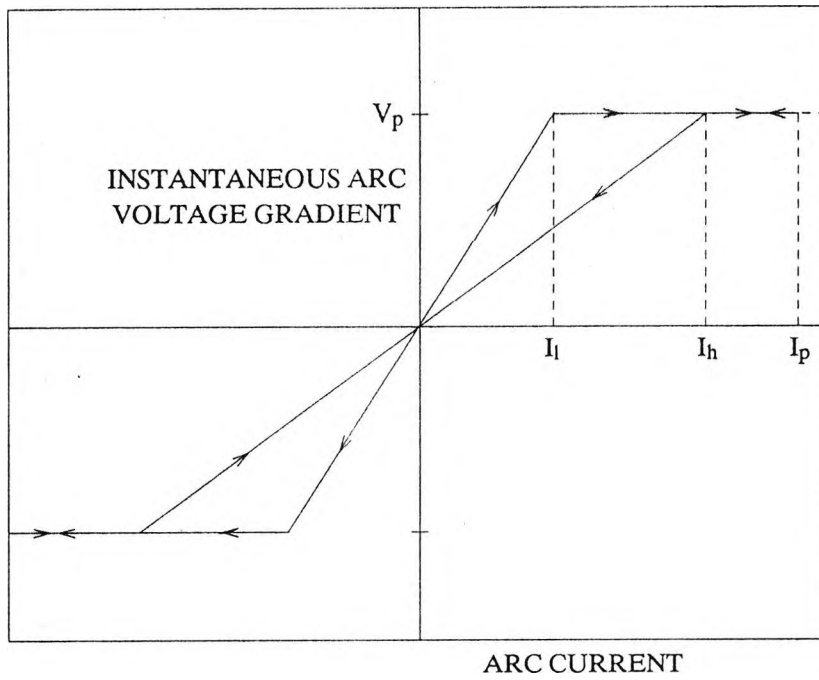
Figure 7.1   APPROXIMATE LINEARISED ARC-CYCLOGRAM
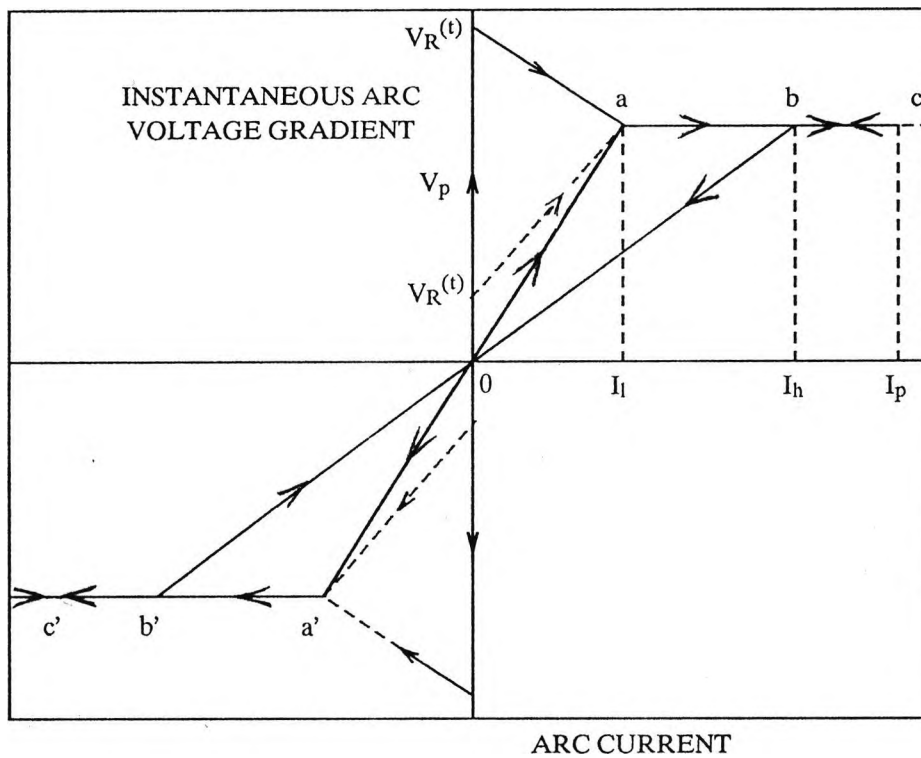
Figure 7.2   APPROXIMATE LINEARISED ARC-CYCLOGRAM WITH
REIGNITION EFFECT
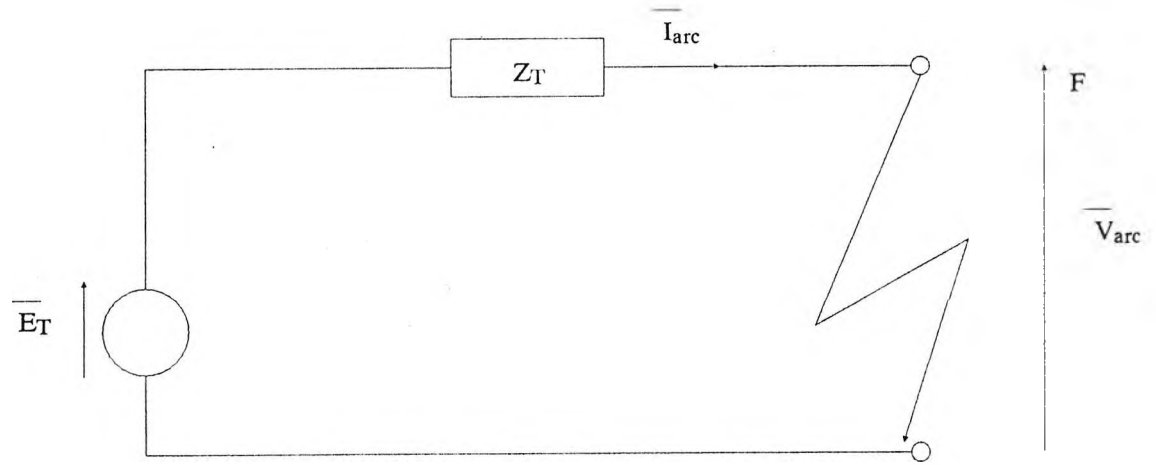
Figure 7.3 THEVENIN EQUIVALENT FAULT POINT CIRCUIT
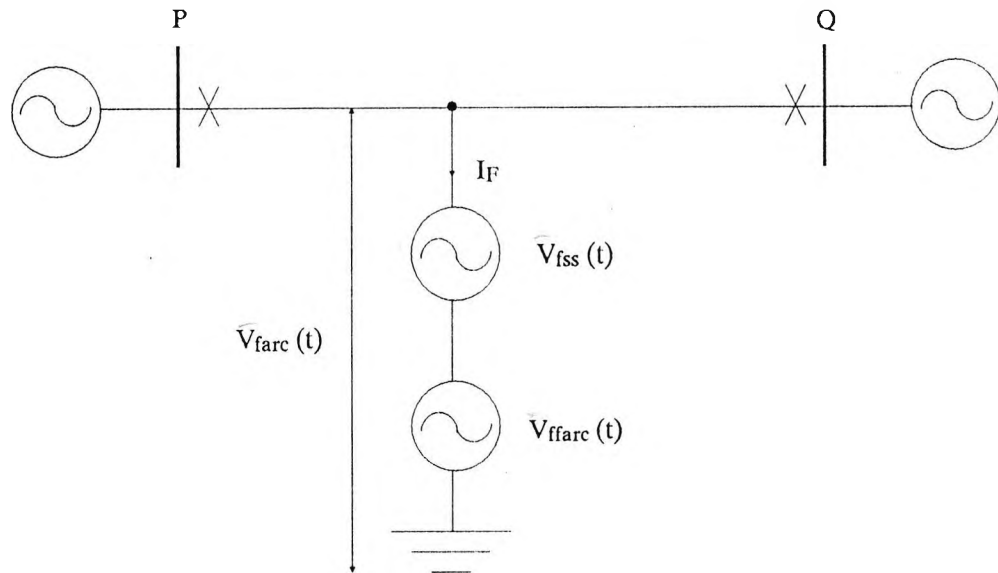
Figure 7.4   REPRESENTATION OF THE FAULTED LINE APPLYING
SUPERIMPOSED ARC VOLTAGE AT THE FAULT POINT

CHAPTER 8

INVESTIGATION OF THE SCHEME BASED ON THE SUPERIMPOSED ARC VOLTAGES

Since most faults involve electric arc, the proposed scheme has to be investigated for the transients due to electric arc. With this view, this chapter investigates the discrimination feature of the scheme with and without effective bus bar capacitance. Other simulated test results include: (1) the performance at zero point-on-wave faults, (2) superimposed arc voltages for different arc lengths, (3) investigation of the superimposed arc voltages (burst) repeating every half cycle.

For simulation of the superimposed arc voltages, a 400 kV 100 km long transmission line with sources 5 GVA at SE and 20 GVA at RE has been considered. Arc has been considered across a 400 kV insulator which is usually 2 meter long. Therefore the arc length of 2 meter has been accounted in the present work. All the simulated results are based on the superimposed voltages of the faulted phase A. Fault has been considered at 1 km from the SE at maximum of the voltage. The stack tuner has been tuned to the mid-frequency of 300 ± 2.5kHz. All fault responses have been

144

studied at the output of the stack tuner. It is worth to mention that the simulation of the fault responses for a period of 5 ms has been found to be possible at the sampling frequency of 820 kHz to detect 300 kHz components with the available computer Gould 9095. In order to investigate the fault response at an interval of half cycle, the computer program has to be optimised for the fault observation time of 13 ms with sampling points of 8192. In order to confirm the repeat feature of the response at every half cycle, it has been found that the fault observation time of about 2 cycles will be desirable. With this objective, the simulated tests have been carried out for the stack tuner mid-frequencies (1) 50 ± 40 kHz to detect 50 kHz components for a period of fault observation time of 40 ms with 4096 sampling points, (2) 100 ± 2.5 kHz to detect 100 kHz components for a period of fault observation time of 40 ms with 8192 sampling points, and, the result has been found to be satisfactory.

8.1 Discrimination feature of the scheme with and without effective bus bar capacitance

Figure 8.1 shows the discrimination feature of the scheme without considering the bus bar capacitance. Figure 8.1.a shows the superimposed arc voltages for the internal fault with stack tuners in open mode NO at both ends, SE and RE (reference Chapter 2). Figure 8.1.b shows the superimposed arc voltages for the reverse fault with stack tuners in the close mode at the SE and in the open mode at

the RE. After studying the responses, it can be concluded that the positive peak at the RE for the reverse fault is 1) about half the positive peak response at the RE for the internal fault, 2) at least eight times smaller than the responses at the SE for the internal fault and the reverse fault. Considering V_F, T_F, T_R, and TRIP with reference to the Chapter 2, it has been found that the TRIP = 0 for the reverse fault and TRIP = 1 for the internal fault at both ends. This has been shown in Figure 8.1. When these responses are compared with the responses of Figure 4.2 (responses without arcing faults), it has been observed that these responses are about twice in magnitude of the responses of Figure 4.2.

Figure 8.2 shows the transient responses considering the effective bus bar capacitance (typically 0.1uF). The stack tuners are in normally close mode for the internal fault. For the reverse fault, the stack tuner at the SE is in the open mode and the stack tuner at the RE is in the close mode (reference Chapter 2). It can be observed that the TRIP =0 for the reverse fault and TRIP=1 for the internal fault at both ends. Figure 6.1 shows the transient responses without considering the arcing faults. In both cases, the frequency shift constant α (reference Chapter 3) is 1000 and the responses can be compared to study the effect of the arcing faults. Comparing the responses of Figure 8.2 and Figure 6.1, it can be concluded that the responses with the arcing faults are about twice of the responses without the arcing faults with the discrimination feature as explained for Figure 8.1. This establishes the

discrimination feature of the scheme for the arcing faults. The signal processing of the scheme has not been included in this chapter as it has been explained earlier.

8.2 Performance at zero point-on-wave faults

It is a well known fact that the faults at zero point-on-wave responds superimposed voltages of nearly zero value due to negligible travelling wave effect and therefore the discrimination for the reverse fault can not be guaranteed below a minimum angle of the fault inception. Under the scope of the present work, as most faults involve the electric arc, it is possible to get superimposed voltages of significant value due to the arc effect. With this view, simulated tests have been carried out (1) without arcing fault (2) with arcing fault as shown in Figure 8.3. Now comparing these results, it can be concluded that the response is improved by ten times with the arcing fault and it is possible to improve the discrimination for the reverse faults. Another significant feature can be seen in Figure 8.4 which shows the repeatitive arc effect (burst) after half a cycle. This effect has given a revolutionary idea in the field of power system protection for the travelling wave relays for the successful discrimination even at zero degree fault inception angle. So far relays based on travelling wave phenomena have been considered a failure.

147

8.3 Superimposed arc voltages for different arc lengths

Figure 8.5 shows the responses for different arc lengths:(1) 2 meters, (2) 20 meters, (3) 40 meters and significant improvement in the responses can be noticed for long arcs. The fault observation time is only 600 micro-seconds to study the effect in the responses due to the different arc lengths.

8.4 Repeatitive arc effect every half a cycle

Figure 8.6 shows the repeatitive feature of the arcing fault response (bursts) at every half cycle. The fault has been considered at the maximum of the voltage. Figure 8.6a shows the responses for the stack tuner mid-frequency of 300 ± 2.5 kHz with the maximum limit of the fault observation time of 13 ms. A burst at an interval of 10 ms i.e. half a cycle can be observed clearly. Figure 8.6b shows the fault responses for the stack tuner mid-frequency of 100 ± 2.5 kHz with the maximum limit of the fault observation time of 40 ms i.e. 2 cycles and the sampling points 8192.

Figure 8.7 shows the fault responses for the stack tuner mid-frequency of 300 ± 2.5 kHz with the maximum limit of the fault observation time of 13 ms but with the arc length of 80 meter. A very clear burst at an interval of 10 ms i.e. half cycle can be observed. Figure 8.6a shows the burst at an interval of half cycle for an arc length of 2 meter only. Comparing the magnitude of the bursts it can

be observed that the positive peak of the burst for 80 meter long arc is 1200 Volts which is about 40 times the positive peak of the burst with 2 meter long arc. It can be concluded that the responses are proportional to the arc length. Figure 8.8 shows the repeating effect of the arcing faults (bursts) at every half cycle. Figure 8.8a shows the responses without the arcing faults and Figure 8.8b shows the responses with the arcing faults. These responses are for the stack tuner mid-frequency of 50 ± 40 kHz for a fault observation period of 2 cycles with the sampling points of 4096. The comparison of Figure 8.8a and Figure 8.8b clearly shows the bursts for the arcing faults repeating every half cycles.

S E   R E

$X10^3$ $X10^2$
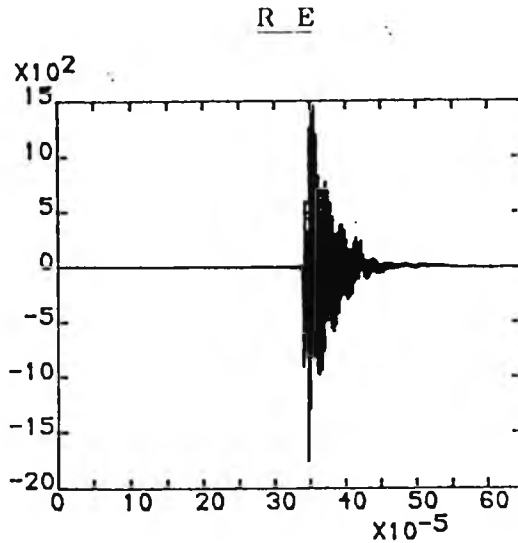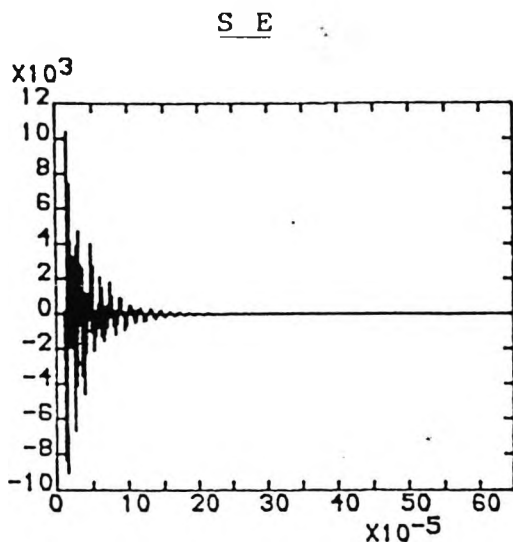
a: Internal fault

VF = 1 , TF = 1   VF = 1 , TF = 1
TR = 0 , TRIP = 1   TR = 0 , TRIP = 1

$X10^3$ $X10^2$
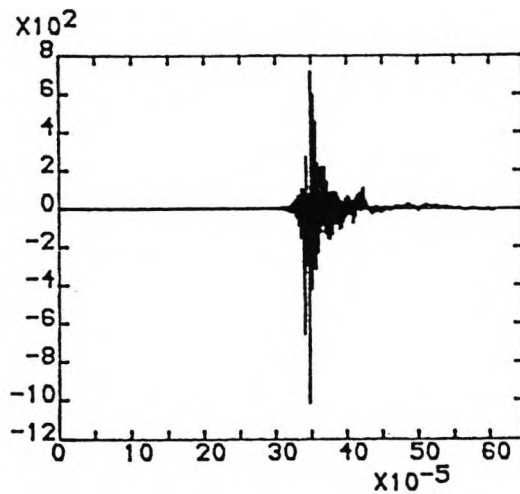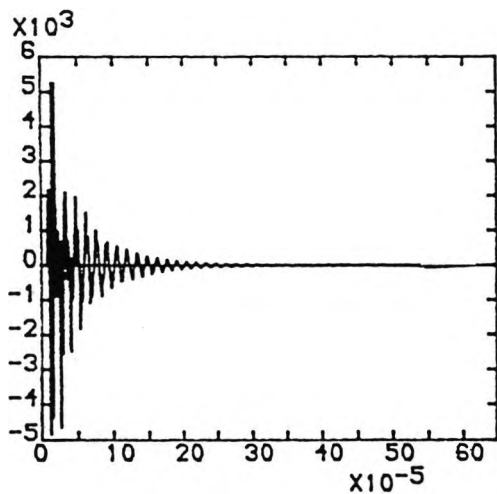
b: Reverse fault

VF = 1 , TF = 0   VF = 0 , TF = 1
TR = 1 , TRIP = 0   TR = 0 , TRIP = 0

X axis: TIME - Seconds
Y axis: VOLTAGES - Volts

(TUNER OUTPUT)

Figure 8.1 DISCRIMINATION TEST FOR REVERSE FAULT
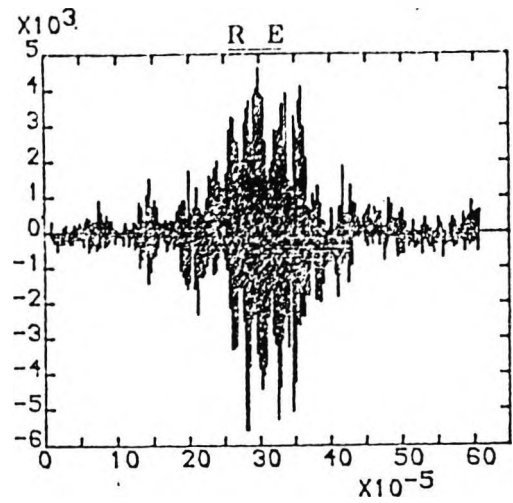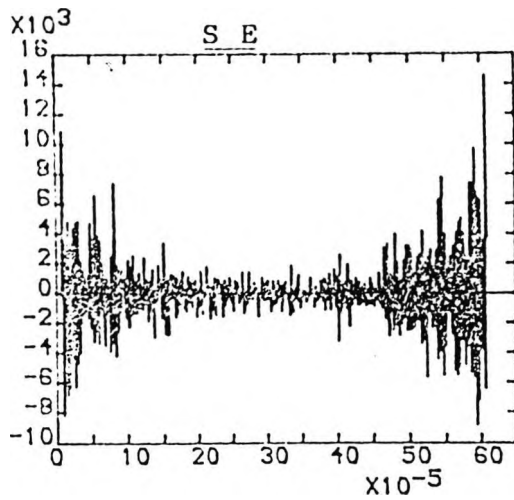
a: Internal fault
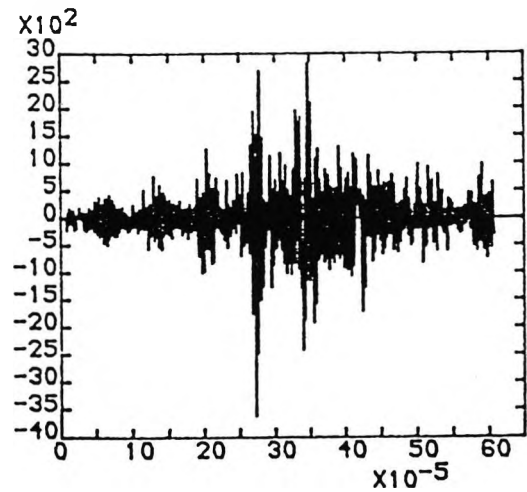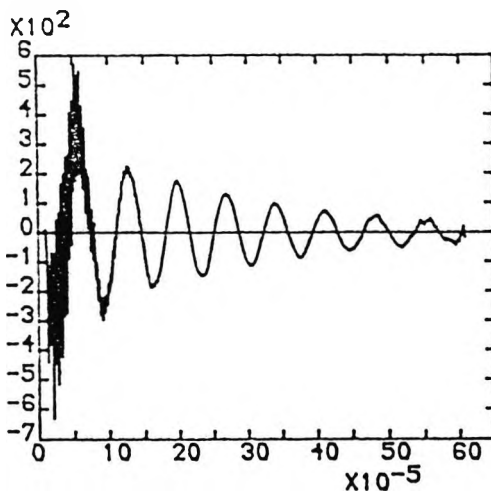
VD = 1 , TF = 1
TR = 0 , TRIP = 1

VD = 1 , TF = 1
TR = 0 , TRIP = 1

b: Reverse fault

VD = 0 , TF = 0
TR = 1 , TRIP = 0

VD = 0 , TF = 1
TR = 0 , TRIP = 0

X axis: <u>TIME</u> - Seconds
Y axis: <u>VOLTAGES</u> - Volts

(TUNER OUTPUT)

Figure 8.2   <u>DISCRIMINATION TEST FOR REVERSE FAULT
CONSIDERING BUS BAR CAPACITANCE</u>
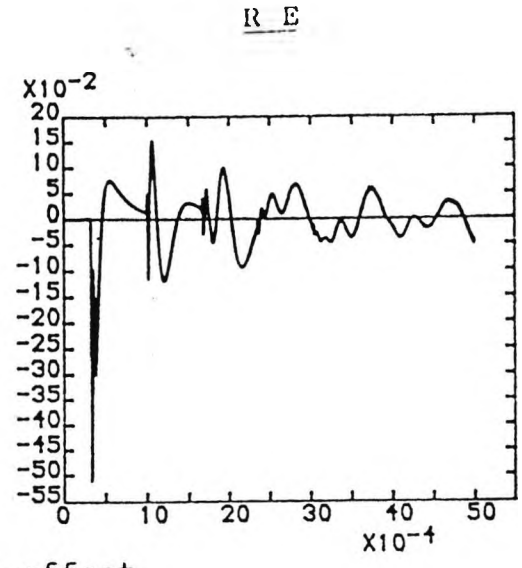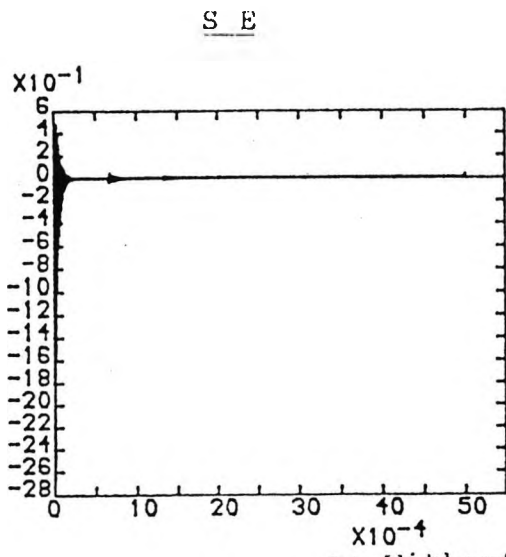
a: Without arc effect
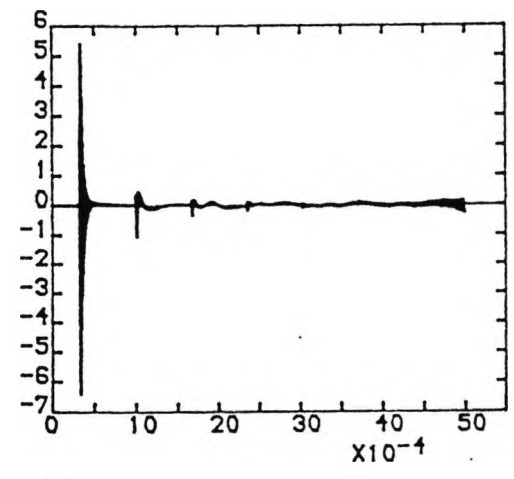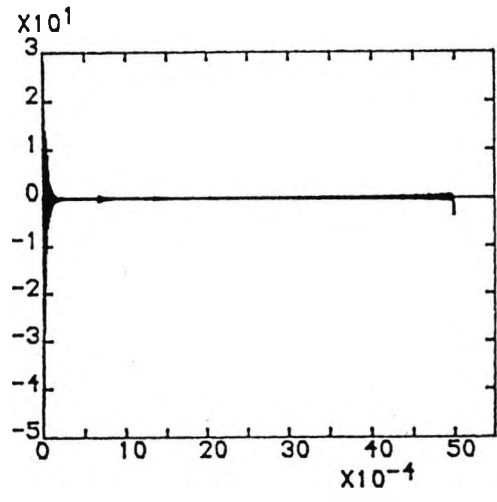
b: With arc effect

X axis: <u>TIME</u> - Seconds
Y axis: <u>VOLTAGES</u> - Volts

(TUNER OUTPUT)

Figure 8.3   COMPARISON OF RESPONSES FOR ARC EFFECT
AT ZERO FAULT INCEPTION ANGLE

S E

R E
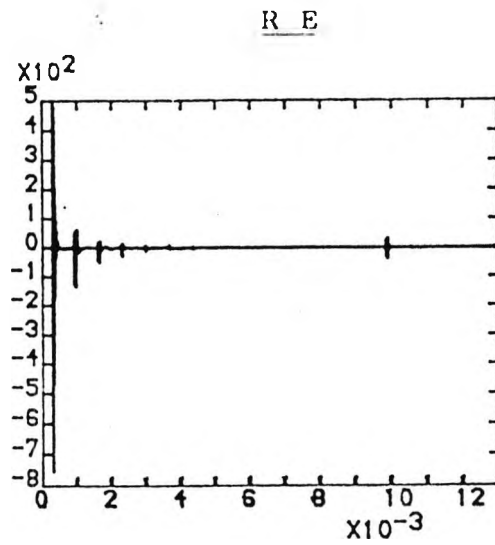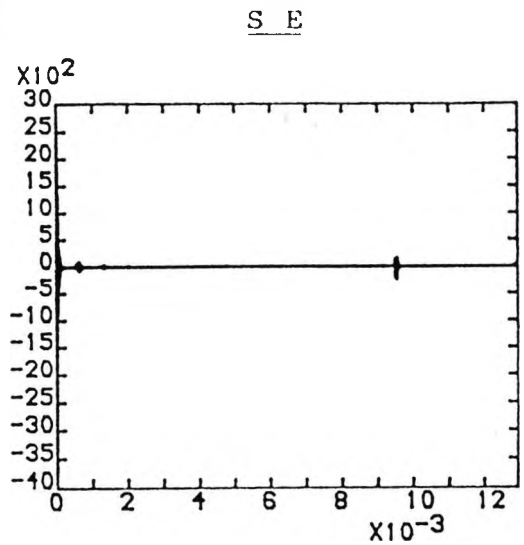
X axis: TIME - Seconds
Y axis: VOLTAGES - Volts

(TUNER OUTPUT)

Figure 8.4   ARC EFFECT REPEATING EVERY HALF CYCLE
AT ZERO FAULT INCEPTION ANGLE

S E   R E
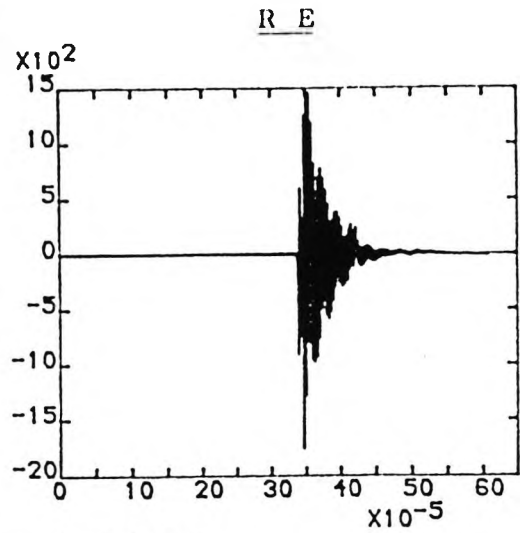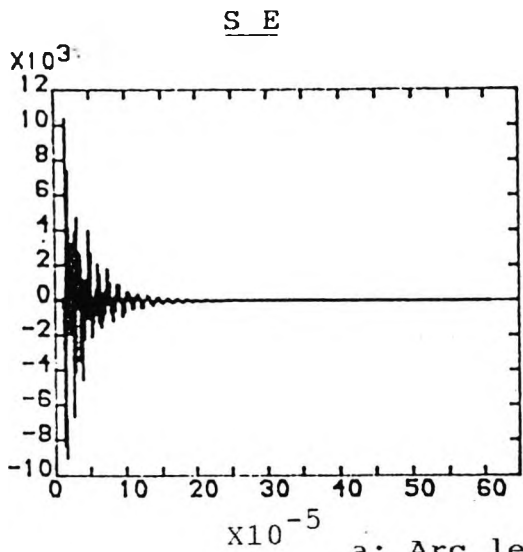
a: Arc length - 2 meters
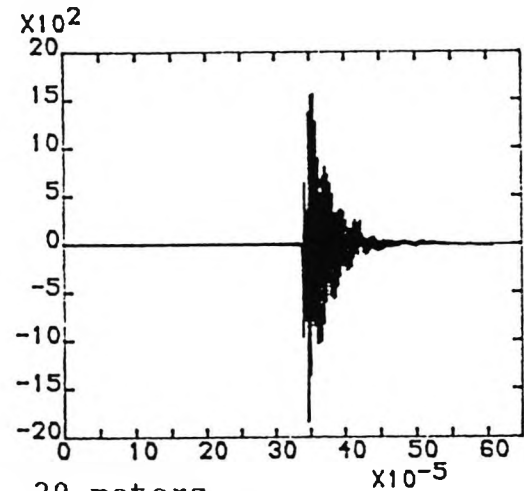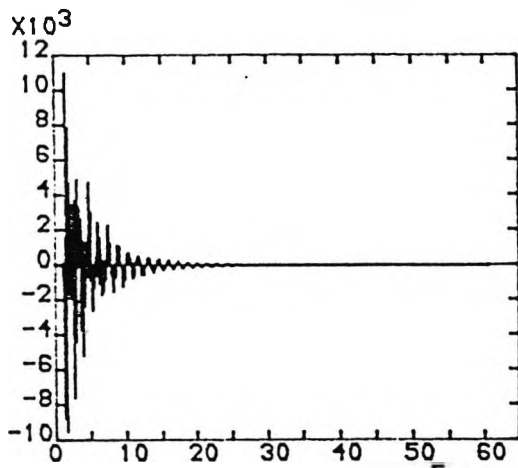
b: Arc length - 20 meters
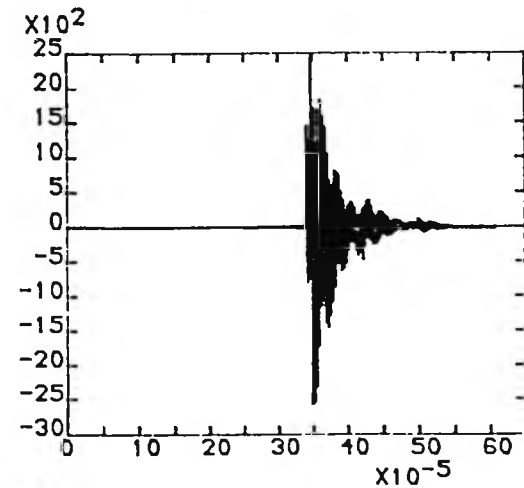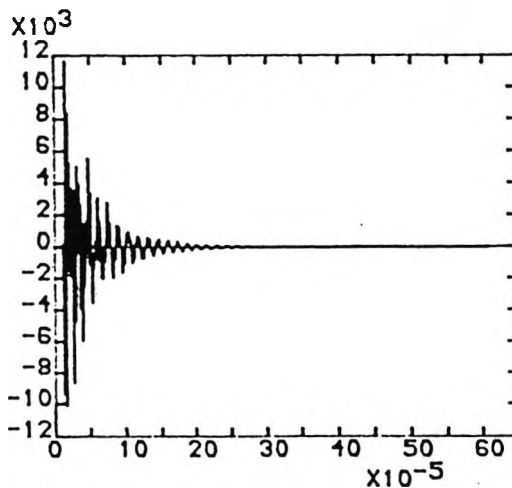
c: Arc length - 40 meters

X axis: TIME - Seconds
Y axis: VOLTAGES - Volts

Figure   8.5   EFFECT OF DIFFERENT ARC LENGTHS
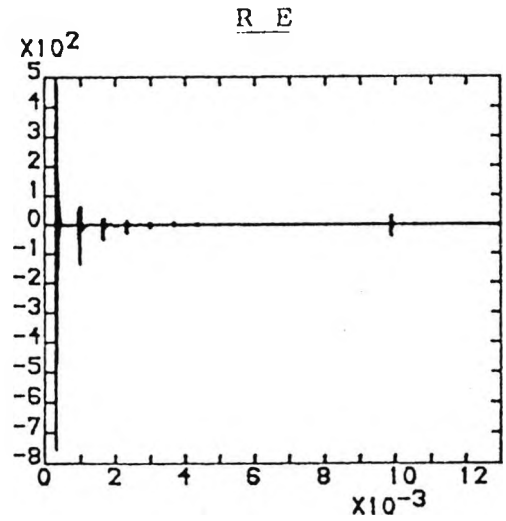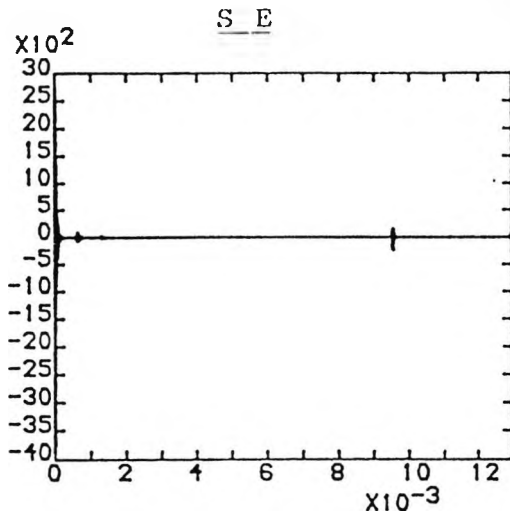
a: 300±2.5 kHz
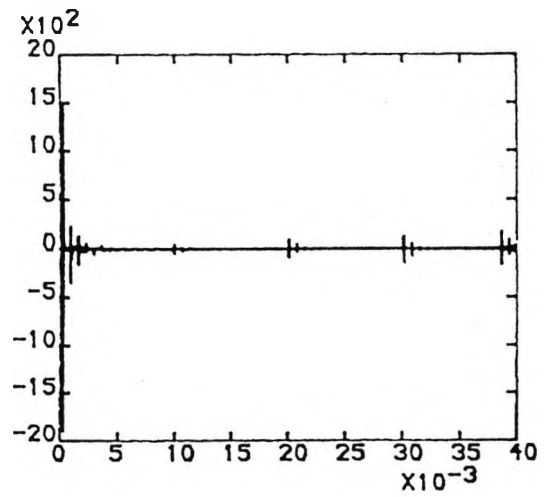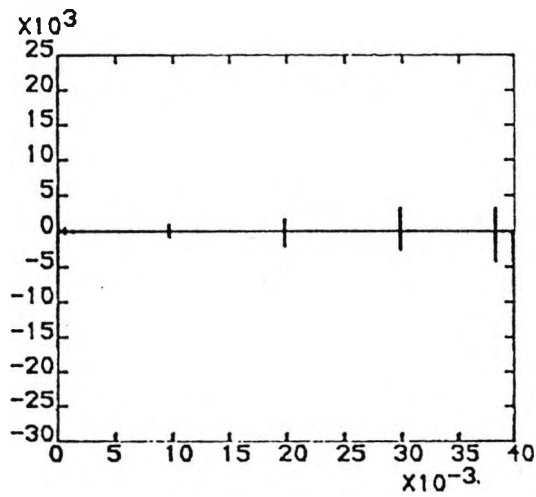
b: 100±2.5 kHz

X axis: TIME - Seconds
Y axis: VOLTAGES - Volts

(TUNER OUTPUT)

Figure 8.6   ARC EFFECT REPEATING EVERY HALF CYCLE   AT
90 DEGREES FAULT INCEPTION ANGLE
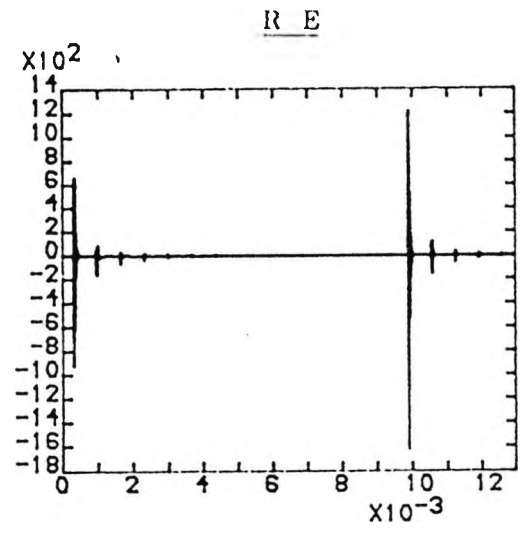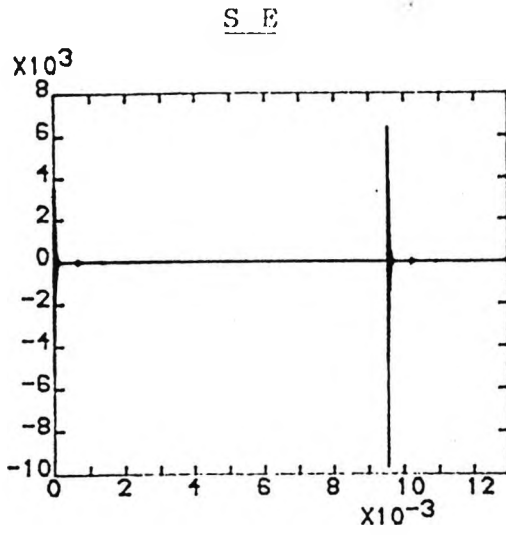
Figure 8.7 ARCING FAULT RESPONSE AT HALF CYCLE FOR VOLTAGE
MAXIMUM FAULT WITH 80 METER LONG ARC

S E   R E
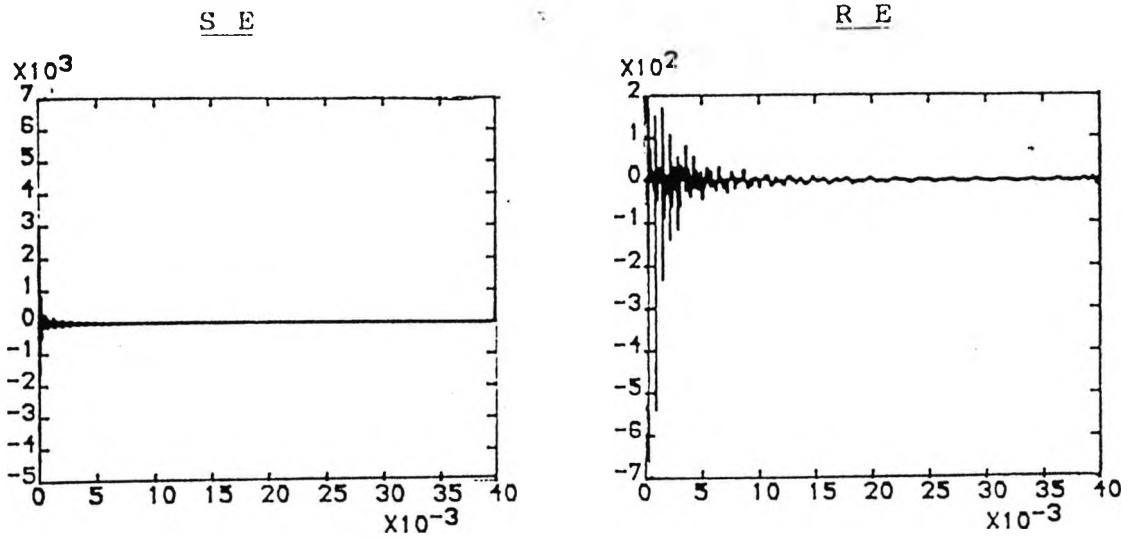
a: Without arc effect
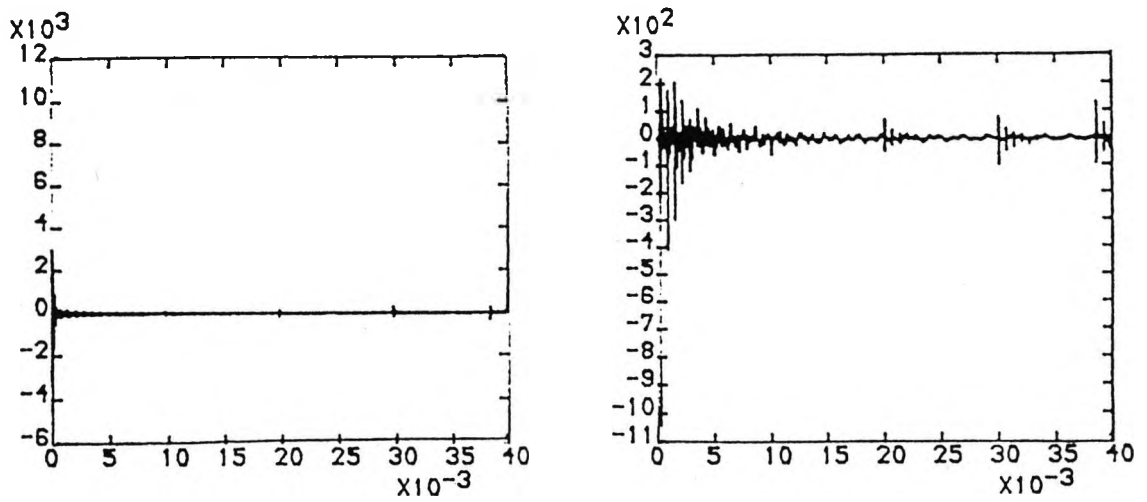
b: With arc effect

X axis: TIME - Seconds
Y axis: VOLTAGES - Volts

Figure 8.8 COMPARISON OF ARCING FAULT RESPONSES AT TUNER
MID-FREQUENCY 50±40 kHz

CHAPTER 9

CONCLUSION

This thesis concludes with a successful approach to a new technique of UHS protection of EHV transmission lines based on detection of high frequency signals of the fault generated noise. The scheme is of non unit type having features of unit type of protection i.e. independent of the communication link. For detecting the reverse faults, a high speed directional detector (dd) has been used which inhibits the operation of the breaker. At the same time, this dd makes a change in the stack tuner such that the response at other end is always below a threshold value which inhibits the operation of the breaker at the other end also. For internal faults, response is always higher than the threshold value and goes to a logic circuit linked with a forward direction of a dd which gives a tripping signal for operation of the breakers at both the ends. Theoretical, operational and design aspects have been established successfully for different applications: (1) transmission lines with negligible bus bar capacitance, (2) transmission line with considerable bus bar capacitance, typically 0.1 microfarads. Since most faults involve electric arc or some other discharge, effect of the

electric arc in both the cases have been considered and the proposed scheme has been established for both the applications based on faulted phase voltage responses. The threshold value has been recommended on the basis of correlation output function as it gives better discrimination for internal and reverse faults.

With a view of cancelling out the affect of other noises, three phase outputs have been combined in the modal form 2 (1, -2, 1) and the principle has been established successfully. Responses have been found of considerable amount for various other faults: (1) at different points on the 100 km long transmission line i.e. 1 km, 25 km and 50 km, (2) faults in different phases, (3) three phase faults, (4) two phase fault.

Effect of different source capacities has been also studied and it has been established that the scheme is practically independent of source capacities.

The effect of different fault inception angles has been also studied and satisfactory responses have been noticed for fault inception angles of 15 degrees or more. As it is known that most faults take place near 90 degrees of fault inception angle, the response for faults below 15 degrees of fault inception angles is not relevent practically.

Response at different stack tuner frequencies tuned in narrow band at 300 kHz, 200 kHz, 100 kHz, and wide band in 100 - 300 kHz, 10 - 90 kHz shows the responses at 200 kHz about twice of that of 300 kHz, 100 kHz about twice of that of 200 kHz and considerable responses for 300 - 100 kHz and 10 - 90 kHz. This explains that the stack tuner can be

tuned to any frequency which may not interfere with other carrier frequencies, if used. For the present work, 300 kHz has been used as stack tuner frequency due to consideration of size of components.

The system has been digitally simulated to establish various aspects of the scheme. In order to study the effect of electric arc, a linearised arc cyclogram with reignition effect has been considered. Reignition voltage has been calculated approximately to check its effect.

As the UHS protection schemes based on travelling wave phenomena are considered faliures at zero degree fault inception angle, responses due to electric arc have been studied and two important observations have been found: (1) response is about ten times more than the case of without electric arc, (2) considerable amount of response has been noticed repeating every half a cycle. With this observation, a new concept has been revolutionized for the success of travelling wave based UHS protection schemes at zero degree fault inception angle.

Tests have been also carried out for different arc lengths and higher responses have been noticed for longer arc lengths.

With a view to study the effect of electric arc repeating every half a cycle at 90 degree fault inception angle, various tests have been carried out and significant responses repeating every half a cycle have been noticed. This observation has given birth to a new concept of UHS protection of EHV transmission lines based on arcing faults.

CHAPTER 10

SUGGESSIONS FOR FUTURE WORK

Based on the experience gained in the present thesis, the following works are suggested which may be carried out in the future.

[1]   a stack tuner may be designed and fabricated for a transmission line system with a view of field trial for different applications: (1) with negligible bus bar capacitance, (2) with considerable bus bar capacitance.

[2]   In the present work, the reignition voltage for considering the electric arc effect has been evaluated using a very simplified expression to enable to study its effect. Future work may be carried out using a more accurate expression for the evaluation of the reignition voltage.

[3]   The effect of the frequency shift constant in the Modified Fourier Transform (reference Chapter 3) for evaluating the time domain components from the time varying components has been noticed considerably for the case of the bus bar capacitance. This makes

153

difficult to evaluate the discrimination factor (reference Chapter 4) for the purpose of the discrimination of the forward and the reverse fault. Probably some more work can be done to identify the appropriate value of the frequency shift constant to get more realistic values of the responses for the purpose of the establishment of the scheme.

[4] A field trial of the fabricated model (suggested for future work) is suggested to confirm an improvement in the operation at lower fault inceptional angles of the voltage waveform due to the concept of the travelling waves due to the arcing faults.

[5] A relaying scheme based on the arcing faults is suggested to be designed and fabricated. A field trial of the scheme is also suggested to confirm the operational principle based on the arcing faults.

CHAPTER 11

REFERENCES

[1] "Review of recent practices and trends in protective relaying", a report by IEEE Committee, IEEE Trans. on power Apparatus ans Systems, Vol.PAS-100, No. 8, August 1981, pp.4054-4064.

[2] "EHV protection problems", a report by IEEE Power System Relaying Committee, IEEE Trans. on Power Apparatus and Systems, Vol.PAS-100, No. 5, May 1981, pp.2399-2415.

[3] Beehler, J E: "One -cycle breakers - are they required?", Paper No. C74-175-6, IEEE PES Winter Meeting, New York, NY, January 1974.

[4] Hicks, K L and Butt, W H: "Feasibility and economics of ultra-high-speed fault clearing", IEEE Trans. on Power Apparatus and Systems, Vol.PAS-99, No.6, Nov./Dec. 1980.

[5] Berglund, R O and co-authohs: "One-cycle fault interruption at 500 kV: system benefits and breaker design", IEEE Trans. on Power Apparatus and Systems, Vol.PAS-93. N0.5, Sept./Oct. 1974, pp.1240-1253.

[6] Johns,A.T.,"Computer simulation studies of new

methods of distance protection for EHV lines",a report on Science Research Council,Nov.1975, University of Bath.

[7] Johns, A T: "New ultra-high-speed directional comparision technique for the protection of EHV transmission lines", IEE Proc., Vol.127, July 1980, pp.228-239.

[8] Johns, A T and Martin, M A: "New ultra-high-speed distance protection using finite-transform techniques", IEE Proc., Vol.130, Pt.C, No.3, May 1983, pp.127-138.

[9] Gilbert, J.G.,Udren, E.A., Sackin, M. "Evaluation of algorithms for computer relaying", 1977 IEEE Summer PES Meeting, Mexico City, Maxico.

[10] Girgis, A.A., Grover Brown, R. "Application of Kalman Filtering in computer relaying", IEEE Trans. on Power Apparatus and Systems, Vol.PAS-100, No.7, pp.3387-3397, July 1981.

[11] Chamia, M and Liberman, S: "Ultra-High-speed relay for EHV/UHV transmission lines - development, design and application", IEEE trans. on Power Apparatus and Systems, Vol.PAS-97, No.6, Nov/Dec.,1978.

[12] Takagi, T and co-authors: "Fault protection based on travelling wave theory - Part I Theory", IEEE PES Summer Meeting, July 17-22, 1977, Paper No. A77-759-3.

[13] Takagi, T and co-authors: "Fault Protection based on travelling wave theory- Part 2:Sensitivity analysis and laboratory test", 1978 Winter PES Meeting, New

York, NY, January 29 - Feburary 3, Paper No. A78 220-6.

[14] Takagi, T and co-authors: "Feasibility study for current differential carrier relay system based on travelling wave theory", IEEE PES Winter Meeting, Jan.29-Feb.3, 1978, Paper No. A78-132-3.

[15] Takagi, T and co-authors: "Digital differential relaying system for transmission line primary protection using travelling wave theory - its theory and field experience", IEEE PES Winter Meeting, Feb. 4-9, 1979, Paper No. A79-096-9.

[16] Dommel, H W and Michels, J m: "High Speed Relaying using Travelling Wave Transient Analysis", IEEE PES Winter Meeting, New York, NY, Jan.29- Feb.3, 1978, Paper No. A78214-9.

[17] Johns, A T: "New ultra-high-speed directional compariso technique for the protection of e.h.v. transmission lines", IEE Proc., Vol.127, Pt.C, No.4, July 1980, pp.228-239; Discussion in IEE Proc., Vol.128, Pt.C, No.3, May 1981, pp.169-172.

[18] Vitins, M. "A correlation method for transmission line protection", IEEE Trans. on Power Apparatus and Systems, Vol. PAS-97, No. 5, pp.1607-1617, Sep./Oct. 1978.

[19] Swift, G W: "The spectra of fault induced transients", IEEE Trans. on Power Apparatus and Systems, Vol. PAS-98, No.3, pp.940-947, May/June 1979.

[20] Crossley, P A and McLaren, P G: "Distance Protection

Based on Travelling Waves", IEEE Trans. on Power
Apparatus and Systems, Vol. PAS-102, No.9, September
1983

[21] Mehdi, A.M: "A new approach to EHV transmission lines
protection", A thesis submitted to the University of
Bath,for the degree of Doctor of Philosphy, Oct.1984.

[22] Johns, A.T.: "Proposal for New Power Circuit
Protection Apparatus based upon detection fault
generated noise". British Technology Group Research
Report, BTG/RP/1, pp12, 1985.

[23] Shields, F.J: "The Problem of Arcing Faults in Low-
Voltage Power Distribution System", IEEE
Trannsactions on Industry and General Applications,
Vol. IGA-3, No.1, pp. 15 - 25, Jan/Feb 1967.

[24] Dunki-Jacobs, J. R: "The Effects of Arcing Ground
Faults on Low-Voltage System Design", IEEE
Transactions on Industry Applications, Vol. 1a-8,
No.3, pp.223-230, May/June 1972.

[25] Fisher, L. E: "Arcing-Fault Relays for Low-Voltage
Systems", IEEE Summer General Meeting and Nuclear
Radiation Effects Conference, Toronto, Ont., Canada,
Paper 63 - 947, June 16 - 21, 1963.

[26] Kaufmann, R. H. and Page, J. C: "Arcing Fault
Protection for Low- Voltage Power Distribution
Systems - Nature of the Problem", Paper 60 - 83, AIEE
Winter General Meeting, New York, N.Y., pp. 160 -
166, Jan.31 - Feb.5, 1960.

[27] "Protective Relays Application Guide", a book by GEC
Measurements, 2nd Edition, March 1975, The General

Electric Company Ltd (UK).

[28] "Applied Protective Relaying", a book by Westinghouse Electric Corporotation , Relay- Instrument Division, Coral Springs, Florida 33060, USA.

[29] Van C Warrington, A R:"Protective Relays - their theory and practice", Vol.1 - 1976, Vol.2 - 1977, published by Champan Hall Ltd.

[30] Mason, C R: "The Art and Science of Protective Relaying", a book published by John Wiley Inc., 1956.

[31] Edels, H.: "Properties and theory of the electric arc", Proc.IEE, 1961, 108A, pp. 55 - 69.

[32] Compton, K. T.: "The electric arc", Trans. AIEE, June 1927, 46, pp. 868 - 878.

[33] Aryton, H. "The Electric Arc", The Electrician, London,1902.

[34] King, L. A.: "The voltage gradient of the free burning arc in air or nitrogen", ERA Report, Ref. G/XT 172, 1961.

[35] Strom, A. P.: "Long 60-Cycle Arcs in Air", Trans. Aiee, March 1946, 65, pp. 113-117.

[36] Maikopar, A. S.: "The quenching of an open arc", Electichestvo (USSR), 1960, No.4, pp. 64-69.

[37] Eaton, J.R., Peck, J.K. and Dunham, J.M.: "Experimental study of arcing faults on a 75 kV transmission system", Trans. AIEE, 1931, 50, pp. 1469 - 1479.

[38] Browne, T.E., Jr.: "The electric arc as a circuit element", Jour. Electrochemical Society,1955, 102, (1), pp.27 - 37.

[39] Eaton, J. R.: "Factor affecting arc extinction on a Peterson Coil system", Trans. AIEE, Nov. 1939, 58, pp. 576- 581.

[40] Slepian, J.: "Extinction of a long a-c arc", Trans. AIEE, 1930, 49, (2), pp. 421 - 430.

[41] Fukunishi, M., and co-authors: "Laboratory study on dead time on high speed reclosing of 500 - kV system", CIGRE, Paris, Paper No. 31-03, 1970.

[42] Johns, A.T. and Al-Rawi, A.M.: "Digital simulation of EHV systems under secondary arcing conditions associated with single pole autoreclosure", IEE Proc. Vol. 129, Pt. C, No.2, March 1982.

[43] Johns, A.T. and Al-Rawi, A. M.: "Developments in the simulation of long-distance single-pole-switched EHV systems", IEE Proc., Vol. 131, Pt. C, No. 2, March 1984.

[44] Cornick, K.J., Ko, Y. M., Pek, B.: "Power system transients caused by arcing faults", IEE Proc., Vol. 128, Pt. C, No.1, Jan. 1981.

[45] Udo, T., and Kawai, M., "Fault generated impulse noise voltage in a transmission line", T-PAS 67Jun., pp. 678-684.

[46] IEEE Guide for Power-Line Carrier Applications, IEEE STD 643, 1980, sponsored by Power System Communications Committee of the IEEE Power Engineering Society.

[47] "Power System Protection", Volume 2, A book edited by the Electricity Council, (UK), 1969.

[48] Johns, A. T. and Agarwal, R. K., "Digital Simulation

of faulted ehv transmission lines with particular reference to very high speed protection", Proc.IEE, 1976, 123, (4), pp 353-359.

[49] Galloway, R.H., Shorrocks, W.B., Wedepohl, L.M., "Calculation of electrical parameters for short and long polyphase Transmission lines", pp.2051-2059, Proc IEE, VOL.116, No.12, Dec. 1964.

[50] Banerjee, A.R.: "Fault transient analysis of multiconductor EHV transmission lines with particular reference to line protection", Thesis for the degree of Ph D, University of Bath, 1976.

[51] Carson, J.R: "Wave propagation in overhead wires with ground return", Bell System Tech. Journal, 1926, 5, pp. 539-554.

[52] Bickford, J.P.: "Analysis of multi conductor lines", M.Sc. Course Notes, UMIST, Manchester, 1977

[53] Anjo, K., Terase, H. and Kawaguchi, Y.: "Self-extinction of arcs created in long air gaps", Elec. Engg. in Japan, 1968, 88, (4), pp.83-93.

CHAPTER 12

APPENDIX A

POWER LINE CARRIER

In Chapter 3, a principle of Power Line Carrier Communication and the design criteria have been explained. In this appendix, Power Line Carrier components and Power Line Characteristics have been described.

POWER LINE CARRIER COMPONENTS

The major carrier components are :

1. Line Trap
2. Coupling Capacitor
3. Drain Coil
4. Line Tuner
5. Coaxial Cable

These components are shown in Figure A-1

Line Trap

The line trap consists of a parallel tuned resonent circuit which presents a high impedance to the operating carrier frequency but a negligible impedance at system frequency. The line trap serves two functions:

1. Prevents carrier energy from flowing into the station bus.

2. Prevents an external ground fault (F1) behind the protective relays from short circuiting the carrier signal on the unfaulted line.

Three types of line traps are available: single frequency, double frequency, and broad band. Typical carrier frequency impedance characteristics of the three types of traps are shown in Figure A-2.

1. Single-frequency traps

The MS single-frequency line trap (Figure A-2a) covers the 30-to-300 kHz range in four divisions: 30-90, 50-150, 70-200, and 90-300 kHz. This trap has a minimum impedance of 400 ohms over a bandwidth of ±5% of the centre frequency (±2% for the 30-to-90 kHz range). Both low- and high-Q tuning are available; the high-Q trap is used for a single-frequency relaying channel. The low-Q trap, which has a lower but relatively constant impedance over a moderate frequency band, is used for a group of closely spaced frequencies.

2. Double-frequency Traps

The MD double-frequency line trap (Figure A-2b) covers the 30-to-300 kHz range in the same four ranges as the single-frequency trap. It may be tuned to any two frequencies between 30 and 300 kHz, but both the upper and lower frequencies must be in the same tuning range. The impedance will be greater than 400 ohms over a bandwidth of ±5% of the centre frequency (±2% for the 30-to-90 kHz range), provided the upper and lower frequencies are separated by 25 kHz or 25 percent of the upper frequency, whichever is greater. Both low- and high-Q tuning are available and are applied as for single-frequency traps.

3. Broad-band Traps

The broad-band trap presents a moderate but fairly constant impedance over a wide frequency range and is used to isolate a group of widely spaced carrier frequencies from a station bus. There are three varities of broad-band traps: fixed, field adjustable, and factory adjusted. These cover a wide range of applications:

1. **Fixed 90-200 kHz Type MW Trap** for applications in the 50-205 and 100-300 kHz range where a 400-ohm trap impedance (0.265 mH) is adequate. The characteristics are shown in Figure A-2c. This trap is not adjustable.

2.   **Field-adjustable Type MWA Traps-** for applications in the 50-205 and 100-300 kHz frequency bands with impedance levels of 600,750 or 1000 ohms at moderate bandwidths. Typical characteristics are shown in Figure A-2d and A-2e. This trap has a 0.265 mH main coil.

3.   **Factory adjusted Type MWA Traps-** for applications involving wider frequency bands and higher trap impedance levels than are available with the field adjustable traps. typical characteristics of two of these traps are shown in Figures A-2f through A-2i. These curve show that , for a given geometrical mean frequency (GMF), the bandwidth at a desired impedance level increases with the increase in main coil inductance. The inductance range is from 0.265 to 1.590 mH.

A typical example of the tuning of a Type MWA trap is shown in Figure A-2f, where a GMF of 154 kHz is chosen for a 0.265 mH line trap. A minimum impedance (R_O) of 600 ohms gives an upper frequency (F_U) of 198 kHz and a lower frequency (F_L) of 118 kHz. The corresponding curve of impedance versus frequency (Figure A-2g) shows both the impedance and resistive components, Z and R, respectively. The bandwidth, F_U-F_L or 198-118 kHz is 80 kHz.

Coupling Capacitor

The carrier signals are coupled to the power line by the coupling capacitor, C_c. This unit, a series of stacked capacitors mounted inside procelain insulators, has a

capacitance of the order of 0.002 to 0.02 uF, depending on system ac voltage and potential burden requirements. Standard coupling capacitor ratings are listed in Table A-1.

Drain Coil

The drain coil, mounted in the base of the coupling capacitor, provides a low-impedance path for the flow of power-frequency current through the capacitor to ground, thus minimizing the system-frequency voltage developed from point X to ground (Figure A-1). At carrier frequencies, on the other hand, the drain coil has a high impedance, minimizing r-f losses to ground at this point. The carrier loss introduced by the drain coil does not exceed 0.5 dB.

Line Tuner

Applied in conjunction with the coupling capacitors, the line tuners (Figure A-1) provide an impedance match with low losses between the coaxial cable and the transmission line. Both resonent and broad-band line tuners are used. Two types of resonant tuners are available: single frequency and double frequency (Figure A-3). In the single-frequency tuner (Figure A-3a), the inductive reactance of L1 cancels the capacitive reactance of the coupling capacitor C_c and isolating capacitor C_s at one frequency, thus providing a low-loss coupling circuit for the carrier-frequency energy. The transformer (T1) matches

the impedance of the coaxial cable to the surge impedance (Z_O) of the power line.

The two-frequency resonant tuner (Figure A-3b) provides low-loss coupling at two separate frequencies from a single coaxial cable to the power line. The two-frequency tuner shown in Figure A-3c is used for isolating two different sets of carrier equipment. The path from each coaxial cable includes a matching transformer, (T1 or T2) tuning inductance, and a trap circuit tuned to the other carrier frequency. In both cases, the isolating capacitor, C_s, prevents the system-frequency current (50 or 60 Hz) from the coupling capacitor from flowing through the tuning coil and matching transformer. Such a current flow might mask the relatively small carrier-frequency current.

For the two-frequency tuners, the minimum frequency separation is 25 percent of the lower frequency. Frequency response curves of the single- and double-frequency line tuners are shown in Figure A-4.

Where more than two frequencies are coupled to a power line, a wide band coupling device known as a Hi-Coupler is used in place of a resonant tuner. The Hi-Coupler is a high-pass filter (Figure A-5) in which the coupling capacitor (C_c) servers as part of the filter. The filter is terminated by the line impedance Z_O. Radio-frequency hybrids or series L-C circuit, which are part of the associated transmitter output filters (Figure A-5a), are used to isolate channel equipment connected to the coaxial cable. The frequency range of the Hi-Coupler is 40 to 300 kHz. The capacitance of the coupling capacitor should be

0.002uF or higher. Figure A-5c shows the Hi-Coupler insertion loss characteristics.

Coaxial Cable

Low-loss concentric cable is used to connect the line tuner and the carrier transmitter-receiver assemblies. Type RG8/U coaxial, recommended for this purpose, has a characteristic impedance of 52 ohms and an attenuation of about 0.4 to 0.9 dB/1000 ft, increasing gradually over the 30-to-300 kHz frequency range (Figure A-6). The coaxial cable is generally grounded at the terminal equipment end only to prevent system-frequency 50 or 60 Hz current from flowing over the coaxial cable shield during a ground fault. If both ends of the coaxial cable shield must be grounded to improve the shielding effect, a 4/0 copper cable should be run in the same duct to interconnect the ground points at the two ends of the coaxial cable. This arrangement will eliminate the possibility of current burning the coaxial cable shield open in the event of a ground fault.

POWER-LINE CHARACTERISTICS

Carrier frequencies exceed power frequencies by a factor of 1000 or more. as a result, a transmission line's response to carrier frequencies will be appreciably different from its response to power frequencies. At 50 or 60 Hz, all power lines are electrically short. At carrier

frequencies, however, most lines are several wavelengths long because of the much shorter wavelength of the higher frequencies.

The relative efficiency of power- and carrier-frequency transmission also differs significantly. Although the conductor size is relatively large on transmission lines, the carrier-frequency energy flows mainly on the surface of the conductors. This skin effect increases with higher frequencies. Other factors influencing the carrier losses include shunt leakage losses, conductor spacing, radiation, and ground resistance.

In carrier application work, the transmission characteristic of a system (or channel) can be conveniently considered in terms of attenuation-the decrease in power level along a transmission line. The ratio between the voltages, currents, or power at any two points is a measure of the attenuation between these two points. Losses expressed in these ratios, however, cannot be added to give the total loss but must be multiplied. It is more convenient to express losses in decibels (dB), which can be added directly. Decibels are defined as follows:

$$dB = 10 \, Log_{10} \frac{P_1}{P_2} \qquad \text{(A1)}$$

$$dB = 20 \text{ Log}_{10} \frac{V_1}{V_2} \qquad \text{(A2)}$$

$$dB = 20 \text{ Log}_{10} \frac{I_1}{I_2} \qquad \text{(A3)}$$

Equations (A2) and (A3) are valid only if the impedance levels of the circuits are identical where the two voltages or currents are measured.

Various power and voltage or current ratios, with the corresponding dB values, are listed in Table A-2.

Another term widely used in the field of communications is dBm, a level of dB relative to 1 milliwatt. Thus, a power level of one milliwatt is zero dBm. Other power levels in watts and dBm are:

Watts	dBm
10.0	+40
1.0	+30
0.1	+20
0.01	+10
0.001	0
0.0001	-10
0.00001	-20

170

Most electronic voltmeters are calibrated in dB relative to a zero-voltage reference level that would produce one milliwatt of power with a 600 ohm load. Most carrier signal levels, however, are measured across a coaxial cable of 50-to-70 ohm impedance level. Assuming a 60-ohm coaxial cable impedance, 10 dB must be added to the scale dB value to give a true dBm reading. Assuming a 50-ohm coaxial cable impedance, 10.8 dB (11 dB is usually close enough) would have to be added. Similarly, for a 70-ohm impedance, 9.34 dB would have to be added.

For example 10-W (+40-dBm) transmitter will develop 24.5 V rms across 60 ohms. A voltmeter calibrated in dB for a 600-ohm impedance will read +30 dB. To obtain a true dBm, 10 dB must be added to the scale reading giving +40 dBm. To avoid confusion, actual scale readings should be recorded, and the values converted to true dBm later.

Line Attenuation

As indicated above, line attenuation depends on a number of factors. Higher voltage lines usually have a lower loss, since the longer insulator strings reduce carrier leakage and dielectric losses in the insulation. The use of bundled conductors on EHV and UHV lines also reduces the series resistance loss.

Typical fair-weather losses for transmission lines from 34.5 kV to 765 kV are shown in Figure A-7. As indicated in Table A-3a, foul-weather losses are estimated by adding 25 percent to the values shown for lines 230 kV or higher, and

50 percent for lines less than 230 kV. The corrections for transpositions are shown in Figure A-3b. The coupling corrections are shown in Table A-4.

Characteristic Impedance

Another important line characteristic for carrier is characteristic impedance, or input impedance of an infinitely long line for a given design. If a line of finite length is terminated in its characteristic impedance, there will be no energy reflected from the termination when an ac signal is applied to the line. That is, the characteristic impedance, designated Z_O is the ratio of the applied voltage to the resulting current flowing into the line. Carrier terminals and line coupling equipment must be matched to Z_O for best power transfer. Table A-5 indicates the range of characteristic impedance values for a variety of lines.

Power-line Noise

The main factor limiting the allowable attenuation on a power-line carrier channel is the noise level of the line itself. Receiver filters will accept a fraction of the total noise voltage, yielding a certain signal-to-noise ratio (rms-signal-to-average noise). The channel becomes unsatisfactory when this ratio drops below a designated value, about 20 dB for on-off carrier relaying and as low as 10 dB for frequency-shift carrier.

Most power-line consists of a mixture of impulse and random noise, in which noise predominates and random noise occupies the space between the pulses. (Impulse noise consists of sharp, well separated pulses caused by specific electrical discharges, random noise has a continuous spectrum.) The average value of line noise is the measure of its interfering properties with a function such as protective relaying.

Figure A-8 shows typical fair and foul-weather average noise levels at 230 kV in a 3-kHz bandwidth. The dBm figures are based on a reference level (zero dBm) of one milliwatt. For convenience, a millivolt scale is also included. These curves, based on field data and calculated values from several sources, show that noise decreases with increasing frequency. This phenomena partially compensates for the increase in line attenuation at the higher frequencies.

To determine line-noise levels at other system voltages, the appropriate correction factor (Table A-6) must be added to the value read from the curve in Figure A-8. In this way, the line noise in a 3-kHz band at any carrier frequency and line voltage can be estimated.

The average noise-power accepted by a carrier receiver is proportional to its bandwidth. for a receiver in the standard type TC carrier set, for example, the noise response will be 3 dB less than the values given in Figure A-8, since the TC receiver has a 1500-Hz bandwidth. The correction factor for receivers of different bandwidths are given in Table A-7

173

For example, the expected foul-weather noise level at 100 kHz on a 500-kV line is calculated as follows for a type TCF wide-band receiver.

From Figure A-8:

Average noise level at 100 kHz   = -17dBm

From Table A-6

Correction factor for 500-kV line voltage = +5 dB

From Table A-7

Correction factor for receiver bandwidth = -8 dB

Therefore,

Total noise level accepted by receiver   = -20 dBm

The attenuation and noise level values given here, although typical of field values, are intended only as a guide. Specific line values may show some deviation for any number of reasons: the age of the line, type of line construction, conductor size, transpositions, insulator leagage, ground wire, ground conductivity, weather conditions, and the test setup. The accuracy of the attenuation and noise level figures is sufficient to determine the type and rating of carrier terminal equipment required for a given application.
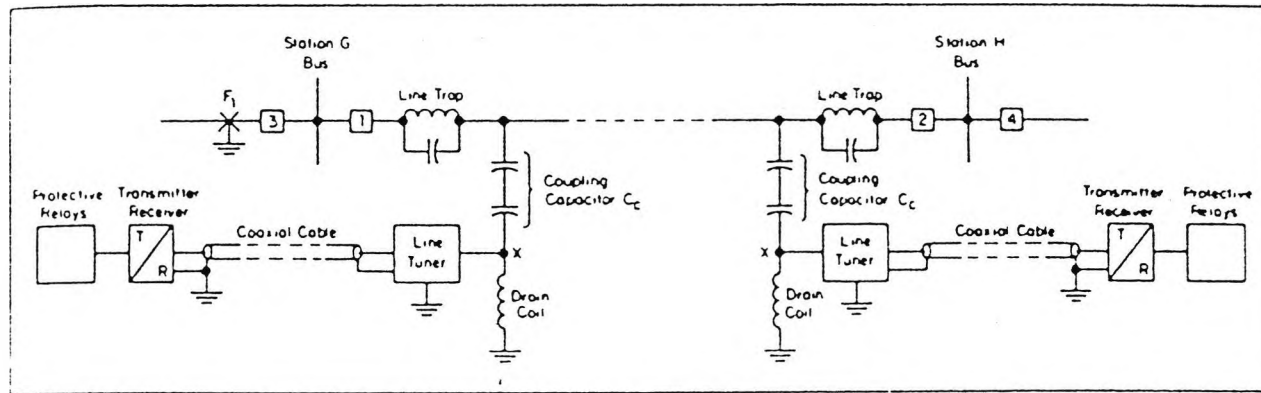
Figure   A-1   BASIC DIAGRAM OF ONE LINE SECTION   SHOWING   MAIN
CARRIER COMPONENTS FOR PROTECTIVE RELAYING CHANNEL
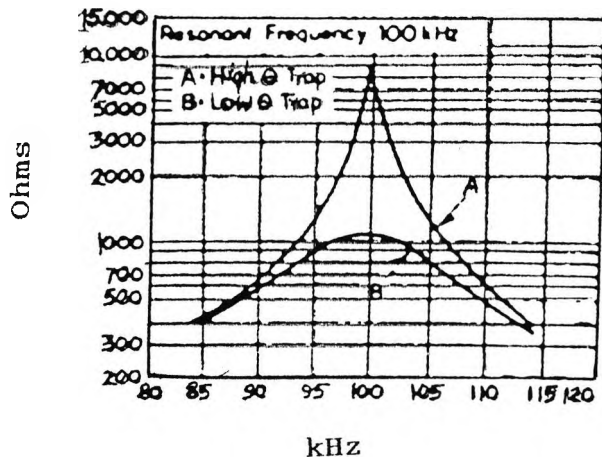
'a'   Typical impedance values 100 kHz
          Single Frequency   Type MS Traps
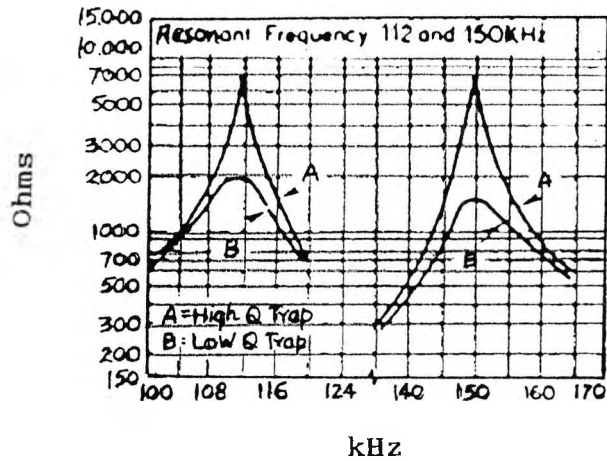
'b' Typical impedance values 112 and 150 kHz
        Double Frequency Type MD Traps
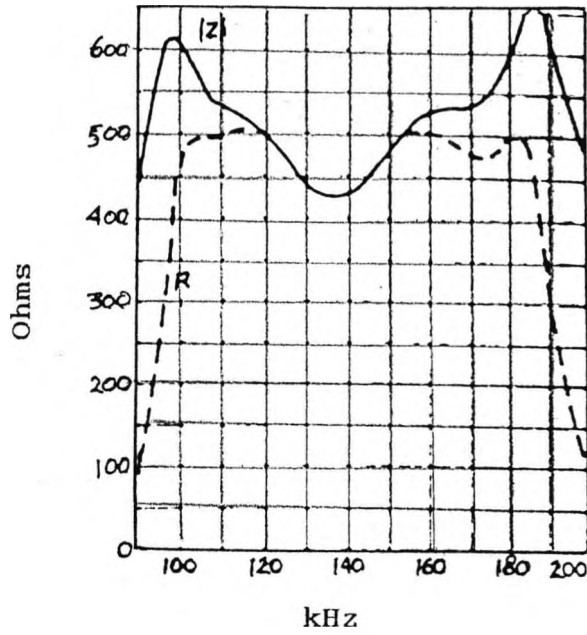
'c' Typical impedance values |z| and resistive
    component R for Fixed Type MW Trap (0.265mH)
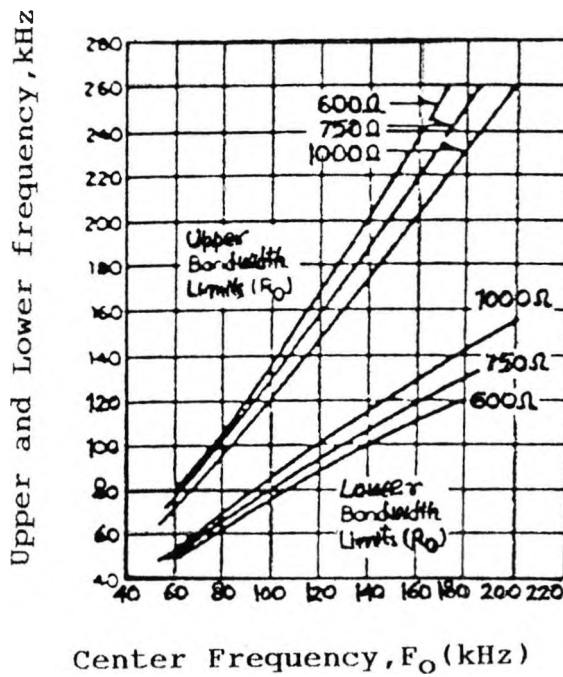
'd' Bandwidth characteristics of the 0.265 mH
    field Adjustable Wide Band Line
    Trap 50-205 kHz
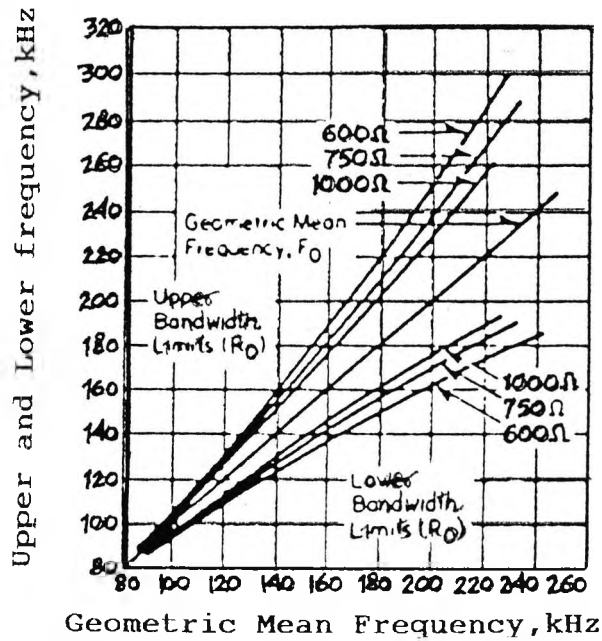
'e' Bandwidth characteristics of the 0.265 mH
    field Adjustable Wide Band Line
    Trap 100-300 kHz
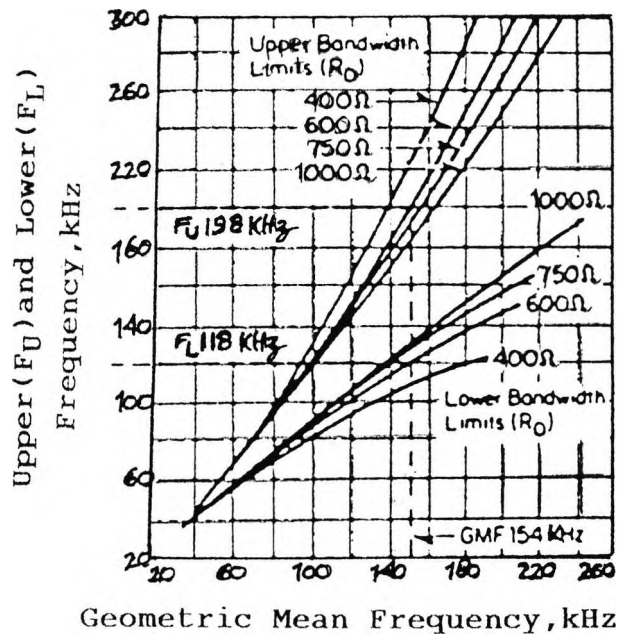
'f' Upper and Lower Frequencies vs Geometeric
    Mean Frequency (0.265mH Factory Adjusted
    Type MWA Trap)
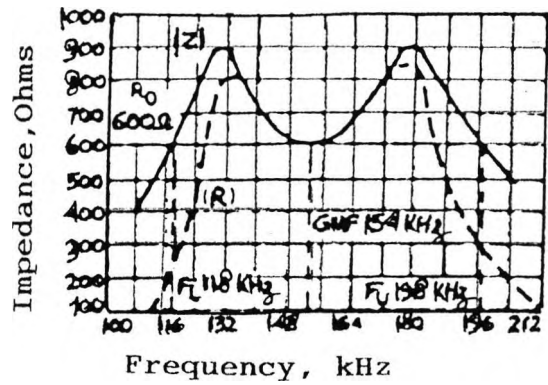
'g' Typical impedance vs frequency (0.265mH)
   Factory Adjusted Type MWA Trap)
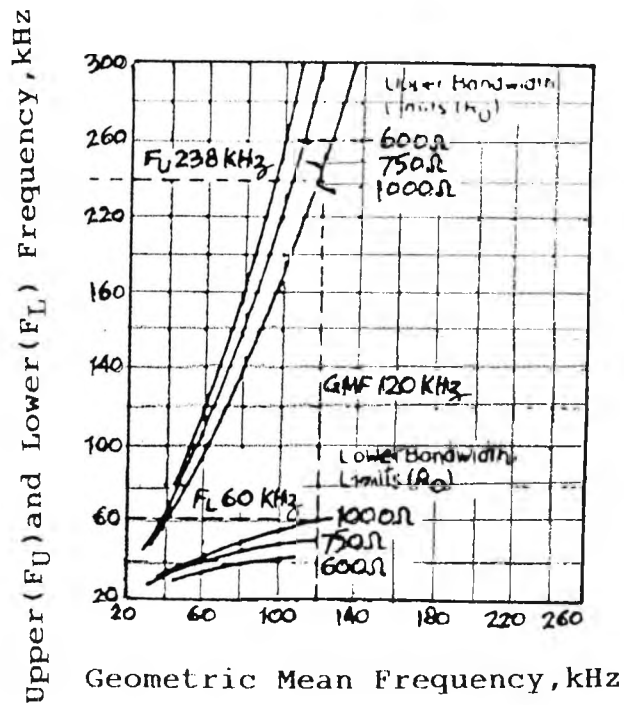
'h' Upper and Lower Frequencies vs Geometeric
     Mean Frequency (1.590mH Factory Adjusted
     Type MWA Trap)
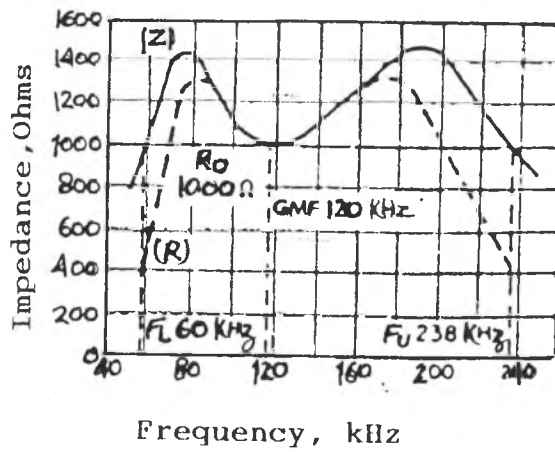
Frequency, kHz

'i' Typical impedance vs frequency (1.590mH)
   Factory Adjusted Type MWA Trap)

Figure A-2 TYPICAL LINE TRAP CHARACTERISTICS
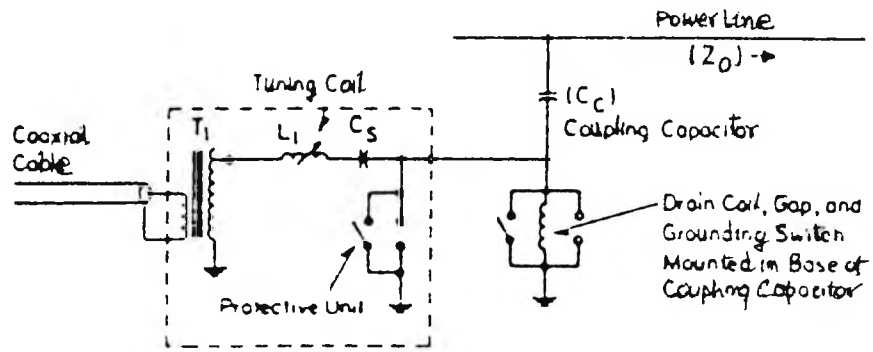
'a' Single frequency tuner
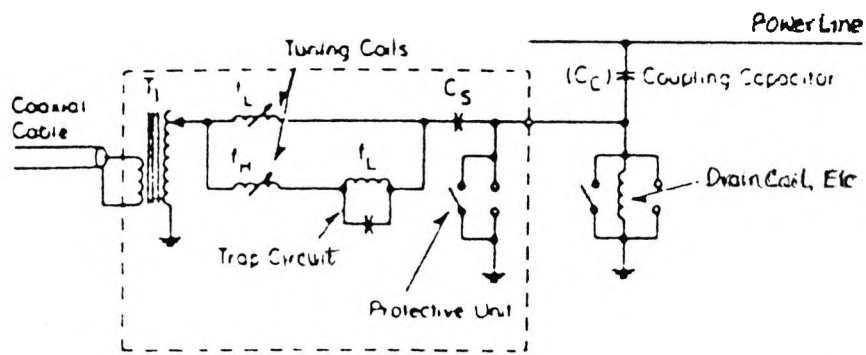
'b' Double frequency tuner for one coaxial cable
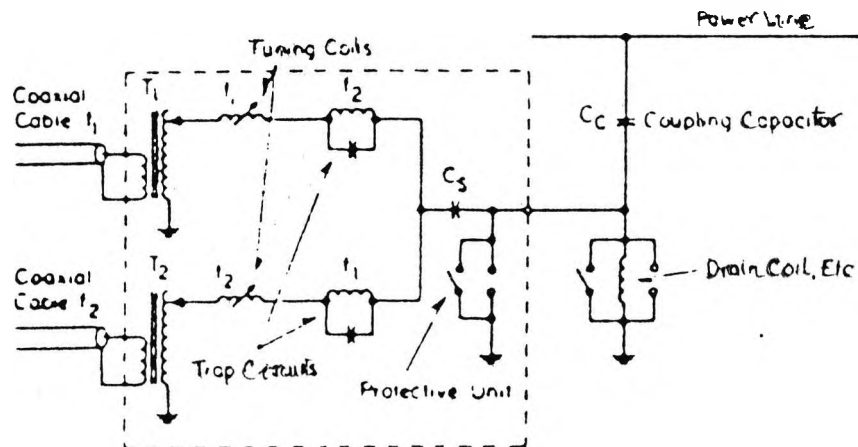
'c' Double frequency tuner for two coaxial cables

Figure A-3 SCHEMATIC DIAGRAM OF SINGLE AND DOUBLE
FREQUENCY RESONANT LINE TUNERS

Frequency in kHz
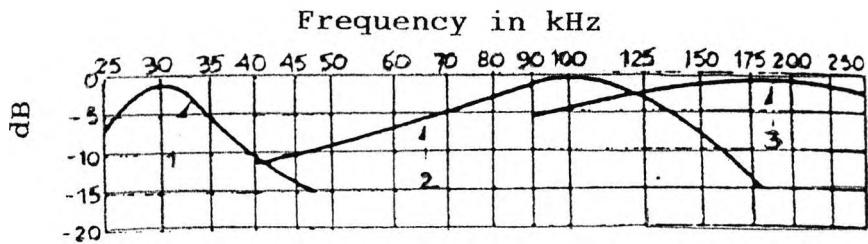
Frequency response Type jz 716 Tuner
curve 1 tuned to 30 kHz
curve 2 tuned to 100 kHz
curve 3 tuned to 300 kHz
 coupling capacitor 1870 MMF, Load resistance 300 Ohms
'a' Response curves of jz 716 Single Frequency Tuner

Frequency in kHz

| Tuned to 30 | Tuned to 80 | Tuned to 160 |
| and 37.5 kHz | and 100 kHz | and 200 kHz |
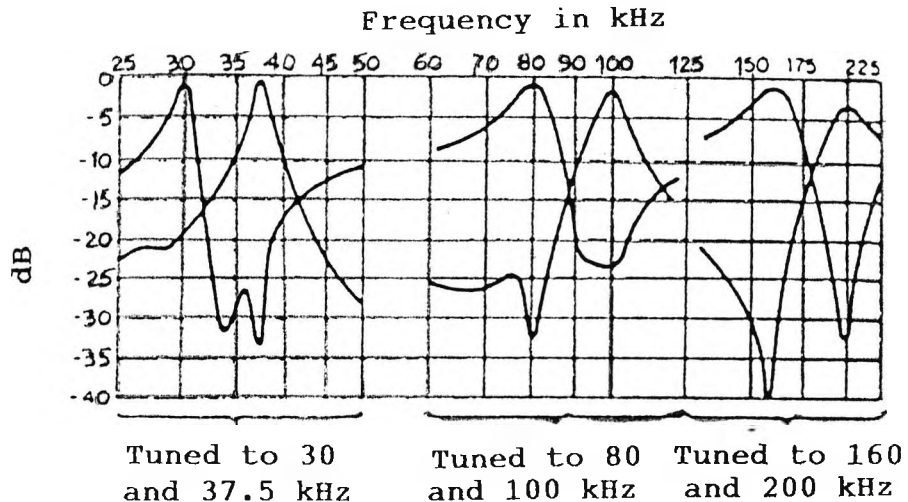
Frequency response Type jz 726 Line Tuner
Coupling Capacitor 1870 MMF, Load resistance 300 OHMS
'b' Response curves of jz 726 Two frequency tuner

Figure   A-4 TYPICAL FREQUENCY RESPONSE CURVES
              OF SINGLE   AND DOUBLE FREQUENCY
              RESONANT LINE TUNERS
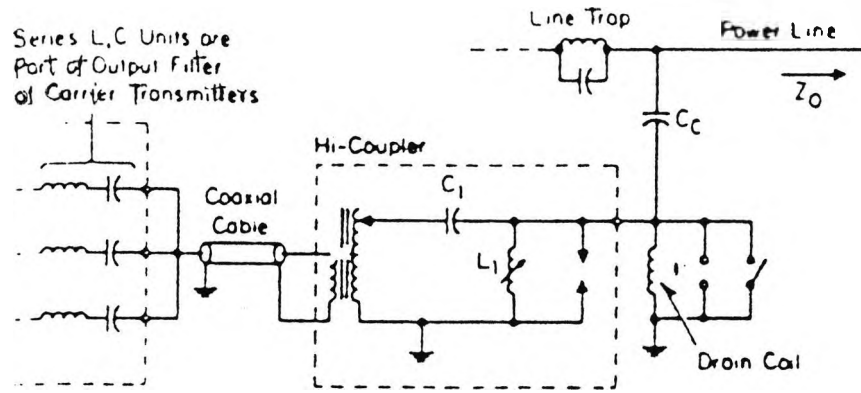
'a' Wide Band High Pass Filter (Hi-Coupler)
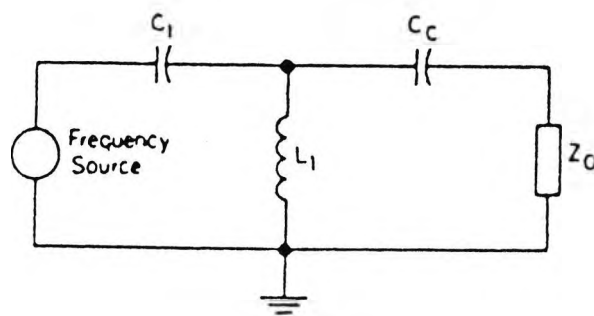
'b' Equivalent circuit of Hi-Coupler
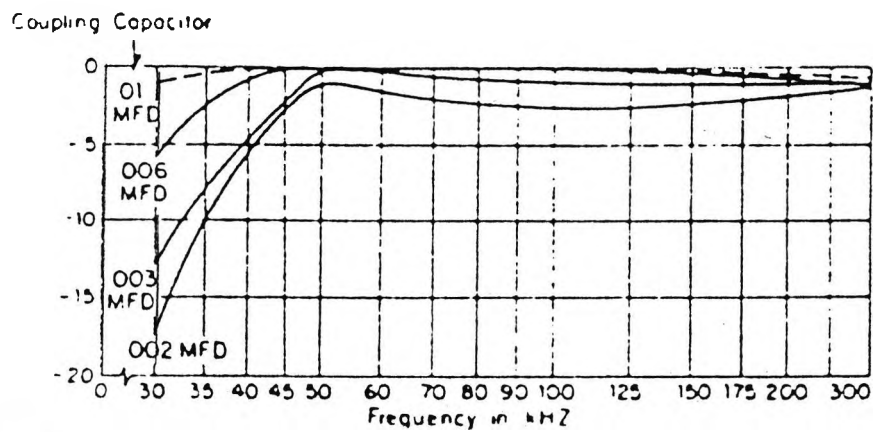
'c' Hi-Coupler Insertion Loss for a 500 Ohm Load

Figure A-5 SCHEMATIC DIAGRAM, EQUIVALENT CIRCUIT,
TYPICAL RESPONSE CURVES FOR A
HI-COUPLER UNIT
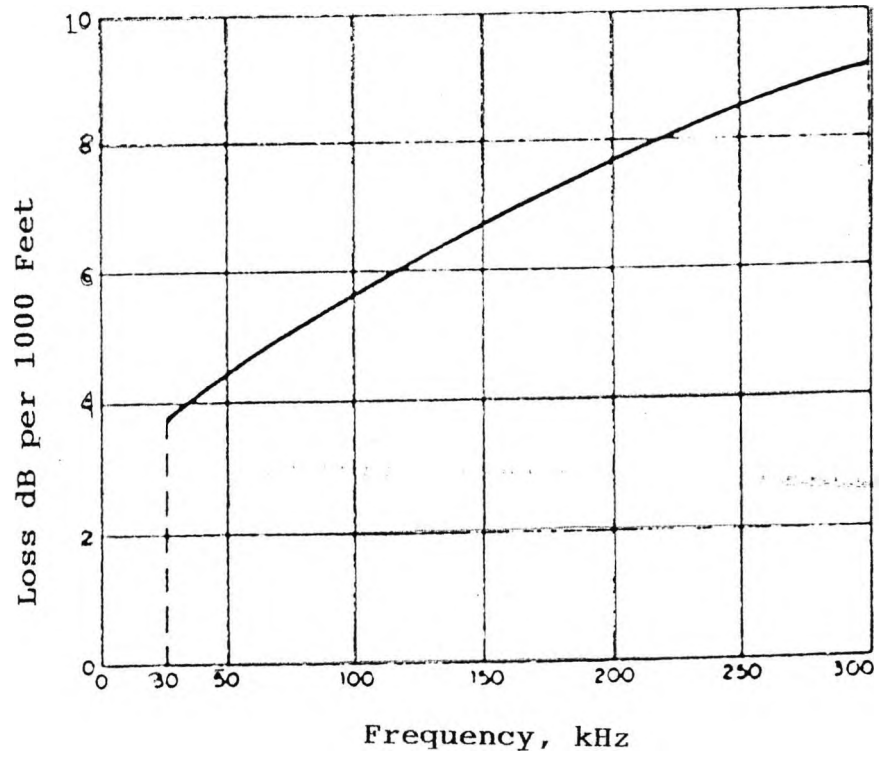
Figure A-6 ATTENUATION OF RG 8/U COAXIAL CABLE
AT CARRIER FREQUENCIES
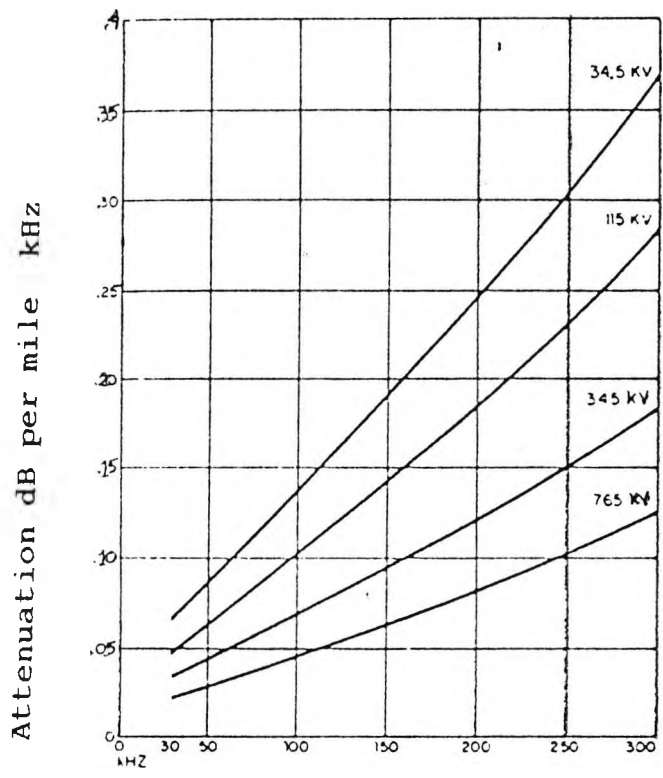
'a' Typical Attenuation curves for Power Lines
    at 34.5, 115, 345, and 765 kV
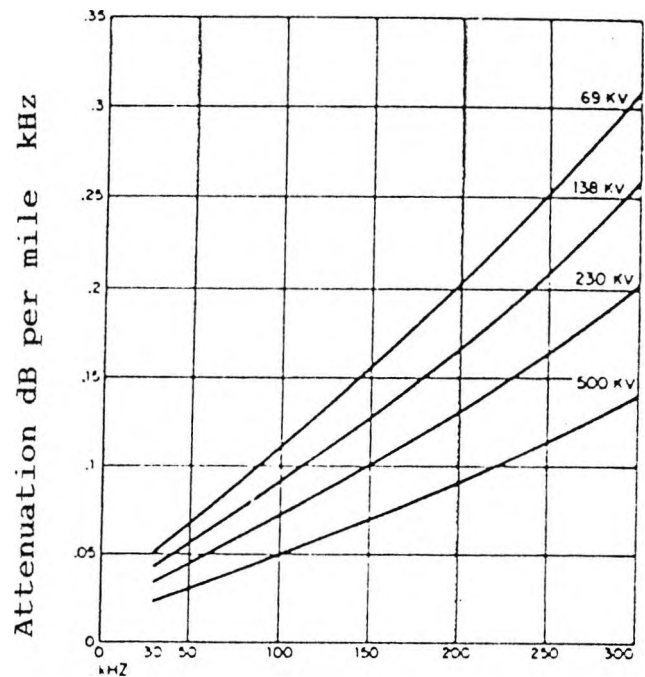
'b' Typical Attenuation curves for Power Lines
    at 69, 138, 230, and 500 kV

Figure A-7 LINE ATTENUATION VS CARRIER FREQUENCY
          FOR DIFFERENT SYSTEM VOLTAGES
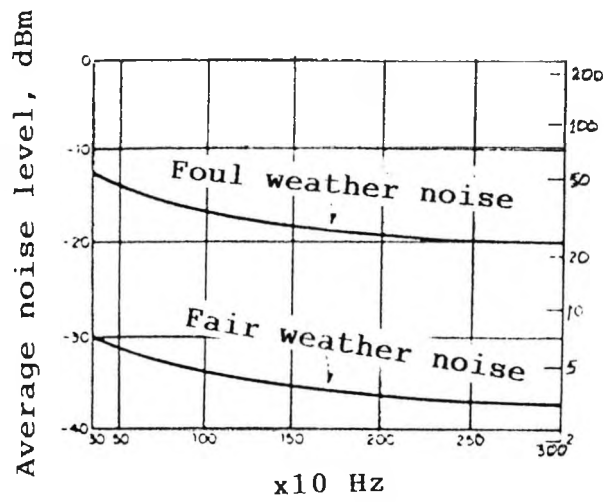
Figure A-8 <u>TYPICAL AVERAGE NOISE LEVELS ON A 230 kV</u>
<u>LINE IN A 3 kHz BANDWIDTH</u>

Table A-1

Coupling capacitor rating

System Voltage (kV)	Capacitance (uF) PCA-5	PCA-7
69	0.01	-
115	0.006	0.025
138	0.005	0.021
161	0.0043	0.018
230	0.003	0.012
345	0.002	0.008
500	0.0015	0.006
765	-	0.00376

Table A-2

Power, Voltage or Current Ratios, and Decibels equivalents

Power Ratio	Voltage or Current Ratio	Decibels (dB)
1.26	1.12	1.0
1.58	1.26	2.0
2.00	1.41	3.0
4.00	2.00	6.0
10.00	3.16	10.0
100.00	10.00	20.00
1000.00	31.60	30.00
10^4	100.00	40.00
10^5	316.2	50.00
10^6	1000.00	60.00
10^8	10^4	80.00

Table A-3a

Attenuation Correction for Foul Weather

34.138 kV	Add 50 percent
230.765 kV	Add 25 percent

Table A-3b

Transposition Correction in dB for 345 kV & higher

Number	< 10 mi	>100 mi
1	0	6
2.4	0	8
5 or more	0	10

Table A-4

Coupling Corrections for Two Terminals- in dB

Type of Coupling	>50-mi line
Mode 1	-2
Center-to-outer Phase	0
Center-to-ground Al or Cu gnd Wire	+1
Steel gnd wire	+4
Outer-to-outer Phase (Push-Push Op.)	+3

Table A-5

Range Of Characteristic Impedance of Power-line Carrier Circuits

Transmission-line Conductor, Each Phase	Characteristic Impedance (Ohms)	
	Phase-to -Ground	Phase-to -Phase
Single	350-500	650-800
Bundled(two wires)	250-400	500-600
Bundled(four wires)	200-350	420-500

Table A-6

Noise Level Correction Factor for other Line Voltages

Voltages (kV)	Correction Factor (dB)
66-115	-8
138-161	-4
230	0
345*	+2
500*	+5
765*	+12

* bundled conductors

Table A-7

Correction Factor for other Receiver Bandwidths

Receiver	Bandwidths (Hz)	Correction Factor (dB)
Standard TC	1500	-3
Narrow-Band TC	500	-8
Wide-band TCF	500	-8
Narrow-band TCF	220	-11

APPENDIX B

STACK-TUNER FREQUENCY RESPONSE DATA

In Chapter 3.1, the design aspects of the stack tuner have been explained. The output gain versus frequency characteristics have been plotted in the open mode and the close mode of the stack tuner when tuned in for the different frequencies 300 ±2.5 kHz, 200 ±2.5 kHz, 100 ±2.5 kHz, 200 ±100 kHz, and 50 ±40 kHz. Similarly, the impedance versus frequency characteristics have been plotted. Since most of the simulated test results are based on the stack tuner mid-band frequency of 300 ±2.5 kHz, the actual data of the stack tuner when tuned in for the mid-band frequency of 300 ± 2.5 kHz are presented in Table B-1. The column 1 shows the frequencies. The column 2 shows the short/close mode impedance. The column 3 shows the open mode impedance. The column 4 shows the open mode gain. The column 5 shows the short/close mode gain. The gain has been defined in Chapter 3.1.

Table B-1
Stack tuner frequency response data

Frequency	Close mode impedance	Open mode impedance	Open mode gain	Close mode gain
2000.00	39807.16	42842.91	0.00	0.00
3000.00	26536.64	30904.66	0.00	0.00
4000.00	19900.94	25435.26	0.00	0.00
5000.00	15919.17	22457.18	0.00	0.00
6000.00	13264.36	20660.31	0.00	0.00
7000.00	11367.82	19496.99	0.00	0.00
8000.00	9945.20	18703.26	0.00	0.00
9000.00	8838.51	18139.03	0.00	0.00
10000.00	7952.99	17724.43	0.00	0.00
11000.00	7228.31	17411.31	0.00	0.00
12000.00	6624.27	17169.34	0.00	0.00
13000.00	6113.02	16978.65	0.00	0.00
14000.00	5674.68	16825.80	0.00	0.00
15000.00	5294.67	16701.47	0.00	0.00
16000.00	4962.05	16599.02	0.00	0.00
17000.00	4668.46	16513.64	0.00	0.00
18000.00	4407.39	16441.74	0.00	0.00
19000.00	4173.71	16380.65	0.00	0.00
20000.00	3963.31	16328.31	0.00	0.00
21000.00	3772.86	16283.14	0.00	0.00
22000.00	3599.65	16243.88	0.00	0.00
23000.00	3441.43	16209.55	0.00	0.00
24000.00	3296.31	16179.37	0.00	0.00
25000.00	3162.74	16152.69	0.00	0.00
26000.00	3039.37	16128.99	0.00	0.00
27000.00	2925.07	16107.85	0.00	0.00
28000.00	2818.88	16088.91	0.00	0.00
29000.00	2719.95	16071.87	0.00	0.00
30000.00	2627.56	16056.50	0.00	0.00
31000.00	2541.07	16042.58	0.00	0.00
32000.00	2459.93	16029.93	0.00	0.00
33000.00	2383.65	16018.41	0.00	0.00
34000.00	2311.81	16007.88	0.00	0.00
35000.00	2244.03	15998.24	0.00	0.00
36000.00	2179.96	15989.38	0.00	0.00
37000.00	2119.31	15981.23	0.00	0.00
38000.00	2061.80	15973.71	0.00	0.00
39000.00	2007.20	15966.76	0.00	0.00
40000.00	1955.28	15960.32	0.00	0.00
41000.00	1905.86	15954.35	0.00	0.00
42000.00	1858.74	15948.80	0.00	0.00
43000.00	1813.78	15943.63	0.00	0.00
44000.00	1770.82	15938.80	0.00	0.00
45000.00	1729.73	15934.30	0.00	0.00
46000.00	1690.38	15930.08	0.00	0.00
47000.00	1652.68	15926.13	0.00	0.00
48000.00	1616.51	15922.43	0.00	0.00
49000.00	1581.78	15918.95	0.00	0.00
50000.00	1548.40	15915.67	0.00	0.00
51000.00	1516.30	15912.59	0.00	0.00
52000.00	1485.40	15909.68	0.00	0.00
53000.00	1455.63	15906.94	0.00	0.00
54000.00	1426.93	15904.35	0.00	0.00
55000.00	1399.25	15901.90	0.00	0.00
56000.00	1372.52	15899.58	0.00	0.00
57000.00	1346.70	15897.38	0.00	0.00
58000.00	1321.73	15895.29	0.00	0.00
59000.00	1297.59	15893.32	0.00	0.00
60000.00	1274.22	15891.43	0.00	0.00

Stack tuner frequency response data 10 Sheets

Frequency	Close mode impedance	Open mode impedance	Open mode gain	Close mode gain
2000.00	39807.16	42842.91	0.00	0.00
3000.00	26536.64	30904.66	0.00	0.00
4000.00	19900.94	25435.26	0.00	0.00
5000.00	15919.17	22457.18	0.00	0.00
6000.00	13264.36	20660.31	0.00	0.00
7000.00	11367.82	19496.99	0.00	0.00
8000.00	9945.20	18703.26	0.00	0.00
9000.00	8838.51	18139.03	0.00	0.00
10000.00	7952.99	17724.43	0.00	0.00
11000.00	7228.31	17411.31	0.00	0.00
12000.00	6624.27	17169.34	0.00	0.00
13000.00	6113.02	16978.65	0.00	0.00
14000.00	5674.68	16825.80	0.00	0.00
15000.00	5294.67	16701.47	0.00	0.00
16000.00	4962.05	16599.02	0.00	0.00
17000.00	4668.46	16513.64	0.00	0.00
18000.00	4407.39	16441.74	0.00	0.00
19000.00	4173.71	16380.65	0.00	0.00
20000.00	3963.31	16328.31	0.00	0.00
21000.00	3772.86	16283.14	0.00	0.00
22000.00	3599.65	16243.88	0.00	0.00
23000.00	3441.43	16209.55	0.00	0.00
24000.00	3296.31	16179.37	0.00	0.00
25000.00	3162.74	16152.69	0.00	0.00
26000.00	3039.37	16128.99	0.00	0.00
27000.00	2925.07	16107.85	0.00	0.00
28000.00	2818.88	16088.91	0.00	0.00
29000.00	2719.95	16071.87	0.00	0.00
30000.00	2627.56	16056.50	0.00	0.00
31000.00	2541.07	16042.58	0.00	0.00
32000.00	2459.93	16029.93	0.00	0.00
33000.00	2383.65	16018.41	0.00	0.00
34000.00	2311.81	16007.88	0.00	0.00
35000.00	2244.03	15998.24	0.00	0.00
36000.00	2179.96	15989.38	0.00	0.00
37000.00	2119.31	15981.23	0.00	0.00
38000.00	2061.80	15973.71	0.00	0.00
39000.00	2007.20	15966.76	0.00	0.00
40000.00	1955.28	15960.32	0.00	0.00
41000.00	1905.86	15954.35	0.00	0.00
42000.00	1858.74	15948.80	0.00	0.00
43000.00	1813.78	15943.63	0.00	0.00
44000.00	1770.82	15938.80	0.00	0.00
45000.00	1729.73	15934.30	0.00	0.00
46000.00	1690.38	15930.08	0.00	0.00
47000.00	1652.68	15926.13	0.00	0.00
48000.00	1616.51	15922.43	0.00	0.00
49000.00	1581.78	15918.95	0.00	0.00
50000.00	1548.40	15915.67	0.00	0.00
51000.00	1516.30	15912.59	0.00	0.00
52000.00	1485.40	15909.68	0.00	0.00
53000.00	1455.63	15906.94	0.00	0.00
54000.00	1426.93	15904.35	0.00	0.00
55000.00	1399.25	15901.90	0.00	0.00
56000.00	1372.52	15899.58	0.00	0.00
57000.00	1346.70	15897.38	0.00	0.00
58000.00	1321.73	15895.29	0.00	0.00
59000.00	1297.59	15893.32	0.00	0.00
60000.00	1274.22	15891.43	0.00	0.00

62000.00	1229.66	15887.94	0.00	0.00
63000.00	1208.39	15886.32	0.00	0.00
64000.00	1187.77	15884.78	0.00	0.00
65000.00	1167.75	15883.31	0.00	0.00
66000.00	1148.31	15881.90	0.00	0.00
67000.00	1129.43	15880.56	0.00	0.00
68000.00	1111.07	15879.28	0.00	0.00
69000.00	1093.23	15878.05	0.00	0.00
70000.00	1075.86	15876.88	0.00	0.00
71000.00	1058.96	15875.75	0.00	0.00
72000.00	1042.51	15874.68	0.00	0.00
73000.00	1026.48	15873.65	0.00	0.00
74000.00	1010.87	15872.66	0.00	0.00
75000.00	995.64	15871.71	0.00	0.00
76000.00	980.79	15870.80	0.00	0.00
77000.00	966.31	15869.92	0.00	0.00
78000.00	952.17	15869.08	0.00	0.00
79000.00	938.37	15868.28	0.00	0.00
80000.00	924.90	15867.50	0.00	0.00
81000.00	911.73	15866.76	0.00	0.00
82000.00	898.87	15866.04	0.00	0.00
83000.00	886.29	15865.35	0.00	0.00
84000.00	873.99	15864.68	0.01	0.00
85000.00	861.96	15864.04	0.01	0.00
86000.00	850.19	15863.42	0.01	0.00
87000.00	838.67	15862.83	0.01	0.00
88000.00	827.39	15862.25	0.01	0.00
89000.00	816.35	15861.70	0.01	0.00
90000.00	805.53	15861.16	0.01	0.00
91000.00	794.93	15860.65	0.01	0.01
92000.00	784.54	15860.15	0.01	0.01
93000.00	774.35	15859.67	0.01	0.01
94000.00	764.37	15859.21	0.01	0.01
95000.00	754.57	15858.76	0.01	0.01
96000.00	744.96	15858.32	0.01	0.01
97000.00	735.53	15857.91	0.01	0.01
98000.00	726.28	15857.50	0.01	0.01
99000.00	717.19	15857.11	0.01	0.01
100000.00	708.27	15856.73	0.01	0.01
101000.00	699.51	15856.37	0.01	0.01
102000.00	690.90	15856.01	0.01	0.01
103000.00	682.45	15855.67	0.01	0.01
104000.00	674.13	15855.34	0.01	0.01
105000.00	665.96	15855.02	0.01	0.01
106000.00	657.93	15854.71	0.01	0.01
107000.00	650.03	15854.41	0.01	0.01
108000.00	642.26	15854.12	0.01	0.01
109000.00	634.62	15853.84	0.01	0.01
110000.00	627.10	15853.57	0.01	0.01
111000.00	619.70	15853.31	0.01	0.01
112000.00	612.42	15853.05	0.01	0.01
113000.00	605.25	15852.81	0.01	0.01
114000.00	598.19	15852.57	0.01	0.01
115000.00	591.24	15852.34	0.01	0.01
116000.00	584.39	15852.12	0.01	0.01
117000.00	577.64	15851.90	0.01	0.01
118000.00	571.00	15851.69	0.01	0.01
119000.00	564.45	15851.49	0.01	0.01
120000.00	558.00	15851.30	0.01	0.01

122000.00	545.36	15850.93	0.01	0.01
123000.00	539.18	15850.75	0.01	0.01
124000.00	533.08	15850.58	0.01	0.01
125000.00	527.06	15850.42	0.01	0.01
126000.00	521.13	15850.26	0.01	0.01
127000.00	515.27	15850.11	0.01	0.01
128000.00	509.50	15849.96	0.01	0.01
129000.00	503.79	15849.82	0.01	0.01
130000.00	498.17	15849.68	0.01	0.01
131000.00	492.61	15849.55	0.01	0.01
132000.00	487.13	15849.42	0.01	0.01
133000.00	481.72	15849.30	0.01	0.01
134000.00	476.37	15849.19	0.01	0.01
135000.00	471.09	15849.08	0.01	0.01
136000.00	465.87	15848.97	0.01	0.01
137000.00	460.72	15848.87	0.01	0.01
138000.00	455.63	15848.77	0.01	0.01
139000.00	450.60	15848.67	0.01	0.01
140000.00	445.63	15848.58	0.01	0.01
141000.00	440.72	15848.50	0.01	0.01
142000.00	435.86	15848.42	0.01	0.01
143000.00	431.06	15848.34	0.01	0.01
144000.00	426.32	15848.27	0.01	0.01
145000.00	421.63	15848.20	0.01	0.01
146000.00	416.99	15848.14	0.01	0.01
147000.00	412.40	15848.08	0.01	0.01
148000.00	407.86	15848.02	0.01	0.01
149000.00	403.37	15847.97	0.01	0.01
150000.00	398.93	15847.92	0.01	0.01
151000.00	394.54	15847.87	0.01	0.01
152000.00	390.19	15847.83	0.01	0.01
153000.00	385.89	15847.80	0.01	0.01
154000.00	381.63	15847.76	0.01	0.01
155000.00	377.41	15847.73	0.01	0.01
156000.00	373.24	15847.71	0.01	0.01
157000.00	369.11	15847.69	0.01	0.01
158000.00	365.02	15847.67	0.01	0.01
159000.00	360.98	15847.65	0.01	0.01
160000.00	356.97	15847.64	0.01	0.01
161000.00	353.00	15847.64	0.01	0.01
162000.00	349.07	15847.63	0.01	0.01
163000.00	345.17	15847.64	0.01	0.01
164000.00	341.31	15847.64	0.01	0.01
165000.00	337.49	15847.65	0.01	0.01
166000.00	333.71	15847.66	0.01	0.01
167000.00	329.96	15847.68	0.01	0.01
168000.00	326.24	15847.70	0.01	0.01
169000.00	322.56	15847.72	0.01	0.01
170000.00	318.91	15847.75	0.01	0.01
171000.00	315.29	15847.79	0.01	0.01
172000.00	311.70	15847.82	0.01	0.01
173000.00	308.15	15847.86	0.01	0.01
174000.00	304.62	15847.91	0.01	0.01
175000.00	301.13	15847.96	0.01	0.01
176000.00	297.67	15848.01	0.01	0.01
177000.00	294.23	15848.07	0.02	0.01
178000.00	290.83	15848.14	0.02	0.01
179000.00	287.45	15848.20	0.02	0.01
180000.00	284.10	15848.28	0.02	0.01

Sheet 3

182000.00	277.48	15848.44	0.02	0.01
183000.00	274.21	15848.53	0.02	0.01
184000.00	270.97	15848.62	0.02	0.01
185000.00	267.75	15848.72	0.02	0.01
186000.00	264.56	15848.82	0.02	0.02
187000.00	261.39	15848.93	0.02	0.02
188000.00	258.25	15849.04	0.02	0.02
189000.00	255.13	15849.16	0.02	0.02
190000.00	252.03	15849.29	0.02	0.02
191000.00	248.96	15849.42	0.02	0.02
192000.00	245.91	15849.56	0.02	0.02
193000.00	242.88	15849.71	0.02	0.02
194000.00	239.88	15849.86	0.02	0.02
195000.00	236.89	15850.02	0.02	0.02
196000.00	233.93	15850.19	0.02	0.02
197000.00	230.99	15850.36	0.02	0.02
198000.00	228.07	15850.54	0.02	0.02
199000.00	225.17	15850.73	0.02	0.02
200000.00	222.29	15850.93	0.02	0.02
201000.00	219.43	15851.14	0.02	0.02
202000.00	216.59	15851.35	0.02	0.02
203000.00	213.77	15851.58	0.02	0.02
204000.00	210.97	15851.81	0.02	0.02
205000.00	208.19	15852.05	0.02	0.02
206000.00	205.43	15852.31	0.02	0.02
207000.00	202.68	15852.57	0.02	0.02
208000.00	199.95	15852.85	0.02	0.02
209000.00	197.24	15853.13	0.02	0.02
210000.00	194.55	15853.43	0.02	0.02
211000.00	191.87	15853.75	0.02	0.02
212000.00	189.22	15854.07	0.02	0.02
213000.00	186.57	15854.41	0.02	0.02
214000.00	183.95	15854.76	0.02	0.02
215000.00	181.34	15855.13	0.02	0.02
216000.00	178.75	15855.51	0.02	0.02
217000.00	176.17	15855.91	0.03	0.02
218000.00	173.61	15856.32	0.03	0.02
219000.00	171.06	15856.76	0.03	0.02
220000.00	168.53	15857.21	0.03	0.02
221000.00	166.02	15857.68	0.03	0.02
222000.00	163.52	15858.18	0.03	0.02
223000.00	161.03	15858.69	0.03	0.02
224000.00	158.56	15859.23	0.03	0.03
225000.00	156.10	15859.79	0.03	0.03
226000.00	153.66	15860.37	0.03	0.03
227000.00	151.22	15860.99	0.03	0.03
228000.00	148.81	15861.63	0.03	0.03
229000.00	146.41	15862.30	0.03	0.03
230000.00	144.02	15863.00	0.03	0.03
231000.00	141.64	15863.73	0.03	0.03
232000.00	139.28	15864.50	0.03	0.03
233000.00	136.92	15865.31	0.03	0.03
234000.00	134.59	15866.16	0.03	0.03
235000.00	132.26	15867.05	0.03	0.03
236000.00	129.95	15867.98	0.03	0.03
237000.00	127.65	15868.96	0.03	0.03
238000.00	125.36	15869.99	0.04	0.03
239000.00	123.08	15871.07	0.04	0.03
240000.00	120.81	15872.21	0.04	0.03

242000.00	116.32	15874.68	0.04	0.03
243000.00	114.08	15876.01	0.04	0.04
244000.00	111.86	15877.43	0.04	0.04
245000.00	109.66	15878.92	0.04	0.04
246000.00	107.46	15880.49	0.04	0.04
247000.00	105.27	15882.16	0.04	0.04
248000.00	103.09	15883.93	0.04	0.04
249000.00	100.93	15885.81	0.04	0.04
250000.00	98.77	15887.80	0.04	0.04
251000.00	96.62	15889.92	0.05	0.04
252000.00	94.49	15892.17	0.05	0.04
253000.00	92.36	15894.57	0.05	0.04
254000.00	90.25	15897.13	0.05	0.04
255000.00	88.14	15899.86	0.05	0.05
256000.00	86.04	15902.79	0.05	0.05
257000.00	83.96	15905.92	0.05	0.05
258000.00	81.88	15909.27	0.05	0.05
259000.00	79.81	15912.88	0.06	0.05
260000.00	77.76	15916.76	0.06	0.05
261000.00	75.71	15920.94	0.06	0.05
262000.00	73.67	15925.46	0.06	0.05
263000.00	71.64	15930.34	0.06	0.06
264000.00	69.61	15935.63	0.06	0.06
265000.00	67.60	15941.38	0.06	0.06
266000.00	65.60	15947.63	0.07	0.06
267000.00	63.60	15954.45	0.07	0.06
268000.00	61.61	15961.90	0.07	0.06
269000.00	59.63	15970.08	0.07	0.07
270000.00	57.66	15979.06	0.08	0.07
271000.00	55.70	15988.97	0.08	0.07
272000.00	53.75	15999.92	0.08	0.07
273000.00	51.81	16012.08	0.08	0.08
274000.00	49.87	16025.61	0.09	0.08
275000.00	47.94	16040.73	0.09	0.08
276000.00	46.02	16057.69	0.09	0.09
277000.00	44.11	16076.82	0.10	0.09
278000.00	42.21	16098.47	0.10	0.09
279000.00	40.31	16123.11	0.11	0.10
280000.00	38.43	16151.30	0.11	0.10
281000.00	36.55	16183.76	0.12	0.11
282000.00	34.68	16221.36	0.12	0.12
283000.00	32.82	16265.24	0.13	0.12
284000.00	30.97	16316.84	0.14	0.13
285000.00	29.12	16378.05	0.15	0.14
286000.00	27.29	16451.36	0.16	0.15
287000.00	25.47	16540.08	0.17	0.16
288000.00	23.65	16648.73	0.18	0.17
289000.00	21.85	16783.56	0.19	0.18
290000.00	20.06	16953.38	0.21	0.20
291000.00	18.29	17170.88	0.22	0.22
292000.00	16.53	17454.71	0.24	0.24
293000.00	14.80	17833.03	0.27	0.27
294000.00	13.09	18349.23	0.29	0.31
295000.00	11.41	19071.55	0.32	0.35
296000.00	9.78	20108.03	0.36	0.41
297000.00	8.23	21625.20	0.39	0.49
298000.00	6.79	23846.17	0.43	0.59
299000.00	5.56	26906.46	0.47	0.72
300000.00	4.69	30223.45	0.49	0.85

302000.00	4.79	29602.26	0.49	0.84
303000.00	5.71	26462.81	0.46	0.70
304000.00	6.95	23548.70	0.43	0.58
305000.00	8.36	21460.93	0.39	0.48
306000.00	9.88	20032.25	0.35	0.40
307000.00	11.45	19049.68	0.32	0.35
308000.00	13.06	18359.34	0.29	0.31
309000.00	14.68	17861.88	0.27	0.27
310000.00	16.32	17494.36	0.25	0.25
311000.00	17.97	17216.53	0.23	0.22
312000.00	19.62	17002.12	0.21	0.20
313000.00	21.28	16833.57	0.20	0.19
314000.00	22.93	16698.90	0.18	0.17
315000.00	24.59	16589.72	0.17	0.16
316000.00	26.24	16500.07	0.16	0.15
317000.00	27.90	16425.58	0.15	0.14
318000.00	29.54	16363.06	0.14	0.14
319000.00	31.19	16310.08	0.14	0.13
320000.00	32.83	16264.81	0.13	0.12
321000.00	34.47	16225.83	0.13	0.12
322000.00	36.11	16192.03	0.12	0.11
323000.00	37.74	16162.54	0.11	0.11
324000.00	39.37	16136.64	0.11	0.10
325000.00	41.00	16113.79	0.11	0.10
326000.00	42.62	16093.52	0.10	0.09
327000.00	44.24	16075.46	0.10	0.09
328000.00	45.85	16059.30	0.10	0.09
329000.00	47.46	16044.78	0.09	0.08
330000.00	49.07	16031.68	0.09	0.08
331000.00	50.67	16019.83	0.09	0.08
332000.00	52.27	16009.07	0.08	0.08
333000.00	53.86	15999.27	0.08	0.07
334000.00	55.45	15990.32	0.08	0.07
335000.00	57.04	15982.12	0.08	0.07
336000.00	58.62	15974.60	0.07	0.07
337000.00	60.20	15967.67	0.07	0.07
338000.00	61.77	15961.29	0.07	0.06
339000.00	63.34	15955.38	0.07	0.06
340000.00	64.91	15949.91	0.07	0.06
341000.00	66.47	15944.83	0.07	0.06
342000.00	68.03	15940.11	0.06	0.06
343000.00	69.58	15935.71	0.06	0.06
344000.00	71.13	15931.61	0.06	0.06
345000.00	72.68	15927.77	0.06	0.06
346000.00	74.22	15924.18	0.06	0.05
347000.00	75.76	15920.82	0.06	0.05
348000.00	77.30	15917.66	0.06	0.05
349000.00	78.83	15914.69	0.06	0.05
350000.00	80.36	15911.90	0.05	0.05
351000.00	81.89	15909.27	0.05	0.05
352000.00	83.41	15906.78	0.05	0.05
353000.00	84.93	15904.44	0.05	0.05
354000.00	86.44	15902.22	0.05	0.05
355000.00	87.95	15900.12	0.05	0.05
356000.00	89.46	15898.13	0.05	0.04
357000.00	90.96	15896.24	0.05	0.04
358000.00	92.46	15894.45	0.05	0.04
359000.00	93.96	15892.75	0.05	0.04
360000.00	95.45	15891.13	0.05	0.04

362000.00	98.45	15888.12	0.04	0.04
363000.00	99.91	15886.73	0.04	0.04
364000.00	101.39	15885.39	0.04	0.04
365000.00	102.87	15884.12	0.04	0.04
366000.00	104.34	15882.90	0.04	0.04
367000.00	105.82	15881.74	0.04	0.04
368000.00	107.28	15880.62	0.04	0.04
369000.00	108.75	15879.56	0.04	0.04
370000.00	110.21	15878.53	0.04	0.04
371000.00	111.67	15877.56	0.04	0.04
372000.00	113.12	15876.62	0.04	0.04
373000.00	114.57	15875.72	0.04	0.03
374000.00	116.02	15874.85	0.04	0.03
375000.00	117.47	15874.02	0.04	0.03
376000.00	118.91	15873.22	0.04	0.03
377000.00	120.35	15872.45	0.04	0.03
378000.00	121.79	15871.71	0.04	0.03
379000.00	123.22	15871.00	0.04	0.03
380000.00	124.65	15870.32	0.04	0.03
381000.00	126.08	15869.66	0.03	0.03
382000.00	127.51	15869.02	0.03	0.03
383000.00	128.93	15868.40	0.03	0.03
384000.00	130.35	15867.81	0.03	0.03
385000.00	131.77	15867.24	0.03	0.03
386000.00	133.18	15866.69	0.03	0.03
387000.00	134.59	15866.16	0.03	0.03
388000.00	136.00	15865.64	0.03	0.03
389000.00	137.41	15865.14	0.03	0.03
390000.00	138.81	15864.66	0.03	0.03
391000.00	140.21	15864.19	0.03	0.03
392000.00	141.61	15863.74	0.03	0.03
393000.00	143.00	15863.31	0.03	0.03
394000.00	144.40	15862.89	0.03	0.03
395000.00	145.79	15862.48	0.03	0.03
396000.00	147.17	15862.08	0.03	0.03
397000.00	148.56	15861.70	0.03	0.03
398000.00	149.94	15861.32	0.03	0.03
399000.00	151.32	15860.96	0.03	0.03
400000.00	152.70	15860.61	0.03	0.03
401000.00	154.07	15860.27	0.03	0.03
402000.00	155.45	15859.94	0.03	0.03
403000.00	156.82	15859.62	0.03	0.03
404000.00	158.18	15859.31	0.03	0.03
405000.00	159.55	15859.01	0.03	0.03
406000.00	160.91	15858.71	0.03	0.02
407000.00	162.27	15858.43	0.03	0.02
408000.00	163.63	15858.15	0.03	0.02
409000.00	164.99	15857.88	0.03	0.02
410000.00	166.34	15857.62	0.03	0.02
411000.00	167.69	15857.37	0.03	0.02
412000.00	169.04	15857.12	0.03	0.02
413000.00	170.39	15856.88	0.03	0.02
414000.00	171.73	15856.64	0.03	0.02
415000.00	173.07	15856.41	0.03	0.02
416000.00	174.41	15856.19	0.03	0.02
417000.00	175.75	15855.98	0.03	0.02
418000.00	177.09	15855.76	0.02	0.02
419000.00	178.42	15855.56	0.02	0.02
420000.00	179.75	15855.36	0.02	0.02

Sheet 7

422000.00	182.41	15854.77	0.02	0.02
423000.00	183.73	15854.79	0.02	0.02
424000.00	185.06	15854.61	0.02	0.02
425000.00	186.38	15854.43	0.02	0.02
426000.00	187.69	15854.26	0.02	0.02
427000.00	189.01	15854.10	0.02	0.02
428000.00	190.33	15853.93	0.02	0.02
429000.00	191.64	15853.77	0.02	0.02
430000.00	192.95	15853.62	0.02	0.02
431000.00	194.26	15853.47	0.02	0.02
432000.00	195.56	15853.32	0.02	0.02
433000.00	196.87	15853.18	0.02	0.02
434000.00	198.17	15853.03	0.02	0.02
435000.00	199.47	15852.90	0.02	0.02
436000.00	200.77	15852.76	0.02	0.02
437000.00	202.07	15852.63	0.02	0.02
438000.00	203.36	15852.51	0.02	0.02
439000.00	204.65	15852.38	0.02	0.02
440000.00	205.95	15852.26	0.02	0.02
441000.00	207.23	15852.14	0.02	0.02
442000.00	208.52	15852.02	0.02	0.02
443000.00	209.81	15851.91	0.02	0.02
444000.00	211.09	15851.80	0.02	0.02
445000.00	212.37	15851.69	0.02	0.02
446000.00	213.65	15851.59	0.02	0.02
447000.00	214.93	15851.48	0.02	0.02
448000.00	216.21	15851.38	0.02	0.02
449000.00	217.48	15851.28	0.02	0.02
450000.00	218.76	15851.19	0.02	0.02
451000.00	220.03	15851.09	0.02	0.02
452000.00	221.30	15851.00	0.02	0.02
453000.00	222.56	15850.91	0.02	0.02
454000.00	223.83	15850.82	0.02	0.02
455000.00	225.09	15850.74	0.02	0.02
456000.00	226.36	15850.65	0.02	0.02
457000.00	227.62	15850.57	0.02	0.02
458000.00	228.88	15850.49	0.02	0.02
459000.00	230.14	15850.41	0.02	0.02
460000.00	231.39	15850.34	0.02	0.02
461000.00	232.65	15850.26	0.02	0.02
462000.00	233.90	15850.19	0.02	0.02
463000.00	235.15	15850.12	0.02	0.02
464000.00	236.40	15850.05	0.02	0.02
465000.00	237.65	15849.98	0.02	0.02
466000.00	238.89	15849.91	0.02	0.02
467000.00	240.14	15849.85	0.02	0.02
468000.00	241.38	15849.78	0.02	0.02
469000.00	242.62	15849.72	0.02	0.02
470000.00	243.86	15849.66	0.02	0.02
471000.00	245.10	15849.60	0.02	0.02
472000.00	246.34	15849.54	0.02	0.02
473000.00	247.58	15849.49	0.02	0.02
474000.00	248.81	15849.43	0.02	0.02
475000.00	250.04	15849.38	0.02	0.02
476000.00	251.27	15849.32	0.02	0.02
477000.00	252.50	15849.27	0.02	0.02
478000.00	253.73	15849.22	0.02	0.02
479000.00	254.96	15849.17	0.02	0.02
480000.00	256.18	15849.12	0.02	0.02

Sheet 8

482000.00	258.63	15847.00	0.02	0.02
483000.00	259.85	15848.98	0.02	0.02
484000.00	261.07	15848.94	0.02	0.02
485000.00	262.29	15848.90	0.02	0.02
486000.00	263.51	15848.86	0.02	0.02
487000.00	264.72	15848.81	0.02	0.02
488000.00	265.93	15848.77	0.02	0.02
489000.00	267.15	15848.74	0.02	0.01
490000.00	268.36	15848.70	0.02	0.01
491000.00	269.57	15848.66	0.02	0.01
492000.00	270.78	15848.62	0.02	0.01
493000.00	271.98	15848.59	0.02	0.01
494000.00	273.19	15848.55	0.02	0.01
495000.00	274.40	15848.52	0.02	0.01
496000.00	275.60	15848.49	0.02	0.01
497000.00	276.80	15848.46	0.02	0.01
498000.00	278.00	15848.42	0.02	0.01
499000.00	279.20	15848.39	0.02	0.01
500000.00	280.40	15848.36	0.02	0.01
501000.00	281.60	15848.34	0.02	0.01
502000.00	282.79	15848.31	0.02	0.01
503000.00	283.99	15848.28	0.02	0.01
504000.00	285.18	15848.25	0.02	0.01
505000.00	286.37	15848.23	0.02	0.01
506000.00	287.56	15848.20	0.02	0.01
507000.00	288.75	15848.18	0.02	0.01
508000.00	289.94	15848.15	0.02	0.01
509000.00	291.13	15848.13	0.02	0.01
510000.00	292.31	15848.11	0.02	0.01
511000.00	293.50	15848.09	0.02	0.01
512000.00	294.68	15848.07	0.01	0.01
513000.00	295.86	15848.04	0.01	0.01
514000.00	297.04	15848.02	0.01	0.01
515000.00	298.22	15848.01	0.01	0.01
516000.00	299.40	15847.99	0.01	0.01
517000.00	300.58	15847.97	0.01	0.01
518000.00	301.76	15847.95	0.01	0.01
519000.00	302.93	15847.93	0.01	0.01
520000.00	304.10	15847.92	0.01	0.01
521000.00	305.28	15847.90	0.01	0.01
522000.00	306.45	15847.89	0.01	0.01
523000.00	307.62	15847.87	0.01	0.01
524000.00	308.79	15847.86	0.01	0.01
525000.00	309.96	15847.84	0.01	0.01
526000.00	311.13	15847.83	0.01	0.01
527000.00	312.29	15847.82	0.01	0.01
528000.00	313.46	15847.80	0.01	0.01
529000.00	314.62	15847.79	0.01	0.01
530000.00	315.78	15847.78	0.01	0.01
531000.00	316.95	15847.77	0.01	0.01
532000.00	318.11	15847.76	0.01	0.01
533000.00	319.27	15847.75	0.01	0.01
534000.00	320.43	15847.74	0.01	0.01
535000.00	321.58	15847.73	0.01	0.01
536000.00	322.74	15847.72	0.01	0.01
537000.00	323.90	15847.72	0.01	0.01
538000.00	325.05	15847.71	0.01	0.01
539000.00	326.20	15847.70	0.01	0.01
540000.00	327.36	15847.69	0.01	0.01

542000.00	329.66	15847.68	0.01	0.01
543000.00	330.81	15847.68	0.01	0.01
544000.00	331.96	15847.67	0.01	0.01
545000.00	333.11	15847.66	0.01	0.01
546000.00	334.25	15847.66	0.01	0.01
547000.00	335.40	15847.66	0.01	0.01
548000.00	336.54	15847.65	0.01	0.01
549000.00	337.69	15847.65	0.01	0.01
550000.00	338.83	15847.65	0.01	0.01
551000.00	339.97	15847.64	0.01	0.01
552000.00	341.11	15847.64	0.01	0.01
553000.00	342.25	15847.64	0.01	0.01
554000.00	343.39	15847.64	0.01	0.01
555000.00	344.53	15847.64	0.01	0.01
556000.00	345.67	15847.64	0.01	0.01
557000.00	346.80	15847.63	0.01	0.01
558000.00	347.94	15847.63	0.01	0.01
559000.00	349.07	15847.63	0.01	0.01
560000.00	350.20	15847.64	0.01	0.01
561000.00	351.34	15847.64	0.01	0.01
562000.00	352.47	15847.64	0.01	0.01
563000.00	353.60	15847.64	0.01	0.01
564000.00	354.73	15847.64	0.01	0.01
565000.00	355.86	15847.64	0.01	0.01
566000.00	356.99	15847.64	0.01	0.01
567000.00	358.11	15847.65	0.01	0.01
568000.00	359.24	15847.65	0.01	0.01
569000.00	360.37	15847.65	0.01	0.01
570000.00	361.49	15847.66	0.01	0.01
571000.00	362.61	15847.66	0.01	0.01
572000.00	363.74	15847.66	0.01	0.01
573000.00	364.86	15847.67	0.01	0.01
574000.00	365.98	15847.67	0.01	0.01
575000.00	367.10	15847.68	0.01	0.01
576000.00	368.22	15847.68	0.01	0.01
577000.00	369.34	15847.69	0.01	0.01
578000.00	370.46	15847.69	0.01	0.01
579000.00	371.57	15847.70	0.01	0.01
580000.00	372.69	15847.71	0.01	0.01
581000.00	373.81	15847.71	0.01	0.01
582000.00	374.92	15847.72	0.01	0.01
583000.00	376.03	15847.73	0.01	0.01
584000.00	377.15	15847.73	0.01	0.01
585000.00	378.26	15847.74	0.01	0.01
586000.00	379.37	15847.75	0.01	0.01
587000.00	380.48	15847.76	0.01	0.01
588000.00	381.59	15847.76	0.01	0.01
589000.00	382.70	15847.77	0.01	0.01
590000.00	383.81	15847.78	0.01	0.01
591000.00	384.92	15847.79	0.01	0.01
592000.00	386.02	15847.80	0.01	0.01
593000.00	387.13	15847.81	0.01	0.01
594000.00	388.23	15847.82	0.01	0.01
595000.00	389.34	15847.83	0.01	0.01
596000.00	390.44	15847.84	0.01	0.01
597000.00	391.54	15847.85	0.01	0.01
598000.00	392.65	15847.86	0.01	0.01
599000.00	393.75	15847.87	0.01	0.01
600000.00	394.85	15847.88	0.01	0.01

APPENDIX C

CALCULATION OF TRANSMISSION LINE BASIC PARAMETERS

The basic line parameters are the series impedance [Z] and the shunt admittance [Y]. These are usually considered as being uniformally disrtibuted along the whole length of the line. For a multiconductor line, the basic line parameter matrices have been formulated [49] for realistic transient studies and are presented in this appendix.

SERIES IMPEDANCE MATRIX

The series impedance matrix [Z] consists of 3 main components:

1. the impedance due to physical geometry of the conductor $[Z_g]$ which is due to electromagnetic coupling between them,

2. the internal or self impedance $[Z_{SF}]$,

3. the impedance which accounts for the earth return path $[Z_e]$.

Thus, the series impedance matrix of a multiconductor line is of the form;

$$[Z] = [Z_g + Z_{SF} + Z_e] \tag{C1}$$

The series impedance matrix [Z] and each of its component matrix are of the order 3p + q, where p = number of circuits and q = number of earth wires.

Impedance due to physical geometry:

The impedance matrix due to the physical geometry of the line conductors as shown in Figure C-1:

$$[Z_g] = jX_g = j\ wu/2\pi\ \ [B] \tag{C2}$$

[B] is known as the charge-coefficient matrix and its elements are defined as:

$$B_{ij} = Log_e\ (D_{ij}/d_{ij}) \tag{C3}$$

where

D_{ij} = distance between the i th conductor and image of the j th conductor,

$d_{ij} \neq$ distance between the i th conductor and j th conductor (for i = j)

= radius of the i th conductor for (i=j)

The self impedance of the conductor:

Consider a single circuit EHV line with two earth wires, the self impedance matrix of the line conductor is one where the diagonal elements represent the self impedance of the phase conductors and earth wires, and whose off-diagonal elements are zero as given by Equation (C4)

$$[Z_{SF}] = \text{Diag } [Z_{sf} + Z^{sf} + Z^{sf} + Z^{se} + Z_{se}] \qquad (C4)$$

Since it is a common practice to bundle the conductors of EHV lines, the self impedance of the bundle conductors is:

$$Z_{sf} = Z_{ssf}/N_b$$

where,

Z_{ssf} = self-impedance of a sub-conductor of the bundle

N_b = number of sub-conductors consistig the bundle.

The calculation is difficult due to various factors: non-uniform current density, steel core, stranding of conductors etc.

Different methods have been suggested for low frequency (below 500 Hz) and high frequency (above 500 Hz) applications.

For low frequency .applications, uniform current

disrtibution is assumed and influence of steel core or
stranding of conductors is neglected. In such case elements
of matrix are given by:

$$[Z_{SF}] = R_{dc} + j \ w \ u/2\pi \ \log_e \ (r/r_{gm}) \tag{C5}$$

where, R_{dc} = dc resistance

r = phase conductor or earth-wire radius

r_{gm} = phase conductor or earth wire geometric mean
radius given by the manufacturer.

$$R_{dc} = \frac{R_C}{n \ \pi \ r_s{}^2} \tag{C6}$$

where, R_C = conductor resistivity

n = number of conductor strands

r_s = radius of earth strand

For high frequency applications, the skin effect plays an
important role and is responsible for non-uniform current
distribution. In such a case, resistance increases and
inductance decreases with the increase of frequency.
Figure C-2 shows a typical variation of resistance and self
inductance with the increase of frequency. This
information is normally stored in a piece-wise linearised
form for computational purposes [6].

For very high frequency applications(above 2.5 kHz), Galloway [49] has suggested a method:

$$Z_{sf} = R_{sf} + j \, X_{sf}$$

where,

$$R_{sf} = X_{sf} = k_1 \, R_c \, m/[2 \, r_o \, (n_o + 2)\pi \,]^{1/2} \qquad \qquad (C7)$$

and, $m = [\, w \, u/R_c \,]^{1/2}$

r_o = radius of each outer strand

n_o = number of strands in the outer layer

k_1 = a factor accountig for conductor stranding (=2.5)

In the present work, the standard conductor is substituted by a solid aluminium conductor of the same overall radius, and the self impedance is evaluated on the basis of non-uniform current density due to skin effect. This method is commonly used for the evaluation of the self impedances of ACSR conductors [50].

Impedance due to earth return path:

Carson [51] has suggested a method to find out the impedance due to earth return path by using an infinite

180

series. Galloway [49] has expressed his method for
computatioal purpose as:

$$[Z_e] = 2 \; w \; \mu/2\pi \; [P + j \; Q] \tag{C8}$$

where μ = permeability

P and Q are calculated in terms of r_{ij} and Θ_{ij} as
indicated in the Figure C-1 where,

$$r_{ij} = [(w \; u/R_c) \; D_{ij}]^{1/2},$$

and have different formulas [49] according to the value of
r_{ij} greater than 5, $(r_{ij}>5)$, or smaller or equal to 5
$(r_{ij}\leq 5)$.

SHUNT ADMITTANCE MATRIX

Neglecting the air conductance of free-space, the shunt-
admittance   matrix   contains   only   imaginary   terms
corrosponding to the capacitance coupling between the
conductors, and conductors and earth. It is a matrix of
the order of 3p + q, where p is number of circuits and q is
number of earth-wires conductors. It is expressed as:

$$[Y] = j \; 2\pi \; w\epsilon \;\;\; [B]^{-1} \tag{C9}$$

where, $[B]^{-1}$ is the inverse of the matrix [B] given earlier

Let $[C] = 2\pi\varepsilon \quad [B]^{-1}$

Then, the elements of the matrix $[C]$ define the various capacitances as below:

$$C_{ij} = -C_{ij}, \text{ for } (i \neq j)$$

$$C_{ij} = \sum_{j=1}^{j=3p+q} C_{ij}, \text{ for } (i = j)$$

where C_{ij} = capacitance between conductors i and j, for $i \neq j$

C_{ij} = capacitance between the conductor i and the earth, for $i = j$

ELIMINATION OF EARTH WIRE

In the present study, voltage and current in the earth wire have not been considered , and therefore, it is suggested to eliminate the rows and columns corrosponding to the earth wire both in the series impedance matrix and shunt admittance matrix to make the analysis simplified. Moreover the performance of the conductors does not change [6,50]. For elimination, the following method has been used:

since earth-wires are earthed at regular intervals,

standing voltage between towers can be neglected and zero potential can be assumed in the earth wire. In such a case, the elements of the shunt admittance matrix corrosponding to the earth wire in the rows and columns can be discarded directly. In the series impedance matrix, the matrix is first inverted and then the elements in columns and rows corrosponding to the earth-wire are eliminated. Finally, the matrix is again re-inverted back.
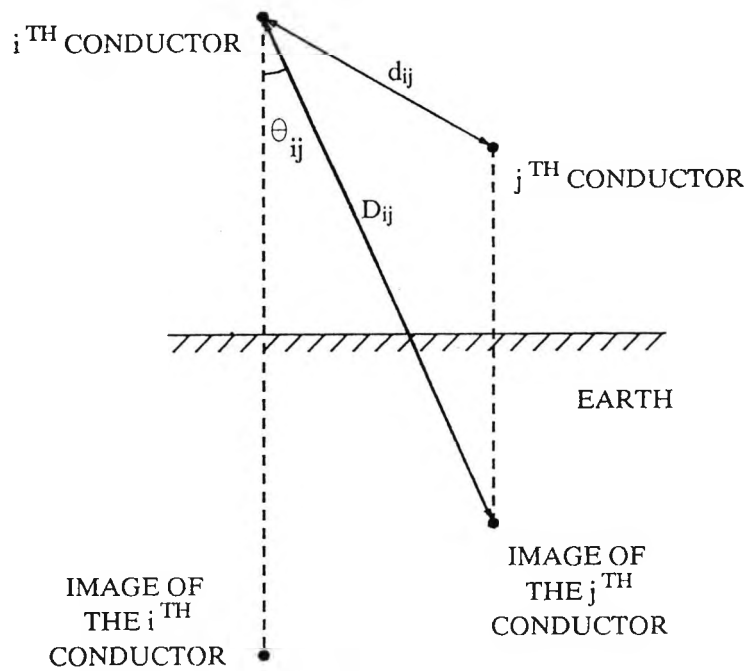
FIGURE C-1 SCEMATIC DIAGRAM OF CONDUCTOR POSITIONS
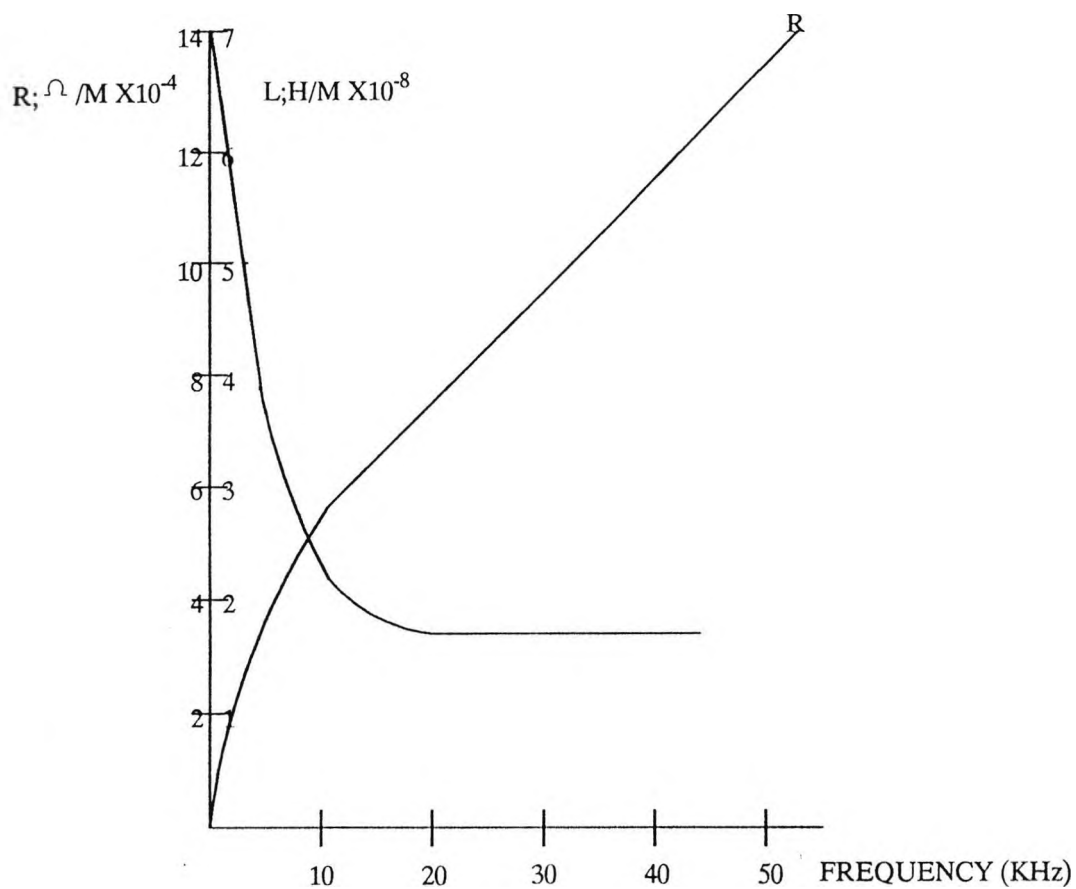
FIGURE C-2 VARIATION OF LINE
INDUCTANCE (L) AND
RESISTANCE (R) WITH FREQUENCY

APPENDIX D

PROGRAM FOR BAND-PASS FILTER

In Chapter 5.3.2, the application of the band-pass filter has been explained. The band-pass filter has been used to filter most out of the frequency band 300 ± 2.5 kHz components. For this purpose the band-pass filter has been designed with nine sections. For the purpose of the simulation of the band-pass filter, the computer program has been shown in Figure D-1. The design details are given in Figure D-2.

```
$ TY BPFILTER.FOR
C    Program to calculate the element values for
C    Butterworth band-pass filters
C    for operation between equal source and load resistances.
         DIMENSION AR(10),AL(10),AC(10),B(10),F(10)
10       CONTINUE
         WRITE (6,*) 'How many sections in the filter?'
         READ(5,*) N
         IF (N.GT.20) GOTO 500
         IF (N.LT.11) GOTO 20
         WRITE(6,*) 'ERROR! No. of sections exceeds 10'
         GOTO 10
20       CONTINUE
         WRITE(6,*) 'Enter the Centre Freq. of the band-pass filter'
         READ(5,*) F0
         WRITE(6,*) 'Enter the band-width of the band-pass filter'
         READ(5,*) BW
         WRITE(6,*) 'Enter the surge impedance of the line'
         READ(5,*) RL
         RS=RL
         PI=3.1415926
         WC = 2.0*PI*BW
         WO = 2.0*PI*F0
         FC2 = 0.5*(SQRT((BW*BW)+4*F0*F0)+BW)
         FC1 = FC2 - BW
C    Where FC2 and FC1 are the upper and lower 3dB cut-off freqs.
         CALL BUT11(B,N)
         I = 1
100      CONTINUE
C   The element values of the low-pass prototype are now being calculated
C   The prototype network is of the form of Fig. 10.4 and Fig. 10.7
C
         AL(I) = B(I)
         AL(I) = (RL*AL(I))/WC
         AR(I) = 0.1
         AC(I) = 1.0/(WO*WO*AL(I))
         I = I + 1
         IF (I.GT.N) GOTO 105
         AC(I) = B(I)
         AC(I) = (AC(I))/(WC*RL)
         AR(I) = 1.0E+9
         AL(I) = 1.0/(WO*WO*AC(I))
         I = I + 1
         IF (I.GT.N) GOTO 105
         GOTO 100
105      CONTINUE
         WRITE(6,*) 'The element values for a '
         WRITE(6,*) N, 'Section band-pass Butterworth Filter'
         WRITE(6,*) '        '
         WRITE(6,*) 'RL = ',RL,' ohms'
         WRITE(6,*) 'RS = ',RS,' ohms'
         WRITE(6,*) '        '
         WRITE(6,*) 'Centre-freq. = ',F0,' Hz'
```

Figure D-1 <u>PROGRAM FOR BAND PASS FILTER</u>   4 Sheets

sheet 1

```fortran
      WRITE(6,*) 'Upper cut-off freq. = ',FC2,' Hz'
      WRITE(6,*) 'Lower cut-off freq. = ',FC1,' Hz'
      WRITE(6,*) 'Band-width = ',BW,' Hz'
      WRITE(6,*) '            '
      WRITE(6,*) '            '
      WRITE(6,*) 'The elements L(1) and C(1) are'
      WRITE(6,*) 'in series with each other'
      WRITE(6,*) ' and the series combination of L(1) and C(1)'
      WRITE(6,*) 'is in series with RL'
      WRITE(6,*) '            '
      WRITE(6,*) 'The elements with odd subscripts are '
      WRITE(6,*) 'in series with each other'
      WRITE(6,*) 'and the elements with even subscripts are '
      WRITE(6,*) 'in parallel with each other'
      WRITE(6,*) '            '
      WRITE(6,*) 'The element values are: '
      WRITE(6,*) '            '
C
      WRITE(24,*) 'The element values for a '
      WRITE(24,*) N, 'Section band-pass Butterworth Filter'
      WRITE(24,*) '            '
      WRITE(24,*) 'RL = ',RL,' ohms'
      WRITE(24,*) 'RS = ',RS,' ohms'
      WRITE(24,*) '            '
      WRITE(24,*) 'Centre-freq. = ',F0,' Hz'
      WRITE(24,*) 'Upper cut-off freq. = ',FC2,' Hz'
      WRITE(24,*) 'Lower cut-off freq. = ',FC1,' Hz'
      WRITE(24,*) 'Band-width = ',BW,' Hz'
      WRITE(24,*) '            '
      WRITE(26,*) ' *   The element values for a '
      WRITE(26,*) ' * ', N, ' Section band-pass Butterworth Filter'
      WRITE(26,*) ' *       '
      WRITE(26,*) ' * RL = ',RL,' ohms'
      WRITE(26,*) ' *  RS = ',RS,' ohms'
      WRITE(26,*) ' *       '
      WRITE(26,*) ' * Centre-freq. = ',F0,' Hz'
      WRITE(26,*) ' * Upper cut-off freq. = ',FC2,' Hz'
      WRITE(26,*) ' * Lower cut-off freq. = ',FC1,' Hz'
      WRITE(26,*) ' * Band-width = ',BW,' Hz'
      WRITE(26,*) ' *       '
      WRITE(24,*) 'The elements L(1) and C(1) are'
      WRITE(24,*) 'in series with each other'
      WRITE(24,*) ' and the series combination of L(1) and C(1)'
      WRITE(24,*) 'is in series with RL'
      WRITE(24,*) '            '
      WRITE(24,*) 'The elements with odd subscripts are '
      WRITE(24,*) 'in series with each other'
      WRITE(24,*) 'and the elements with even subscripts are '
      WRITE(24,*) 'in parallel with each other'
      WRITE(24,*) '            '
      WRITE(24,*) '            '
```

```
          WRITE(24,*) 'The element values are: '
          DO 200 I=1,N
          WRITE(6,*) 'L(',I,') = ', AL(I), ' henrys'
          WRITE(6,*) 'C(',I,') = ', AC(I), ' farads'
          WRITE(6,*) '          '
          WRITE(6,*) '          '
C
          WRITE(24,*) 'L(',I,') = ', AL(I), ' henrys'
          WRITE(24,*) 'C(',I,') = ', AC(I), ' farads'
          WRITE(24,*) '          '
          WRITE(24,*) '          '
C
200       CONTINUE
          WRITE(6,*) '          '
          WRITE(6,*) '          '
          WRITE(24,*) '          '
          WRITE(24,*) '          '
          IN=1
          IN1=3
          IN2=4
950       CONTINUE
          WRITE(6,901)IN,IN1,IN2,AC(IN)
          WRITE(26,901)IN,IN1,IN2,AC(IN)
          WRITE(24,901)IN,IN1,IN2,AC(IN)
901       FORMAT(' C',I1,1X,I3,1X,I3,1X,E10.4)
          IN3=IN2+1
          WRITE(6,902)IN,IN2,IN3,AL(IN)
          WRITE(26,902)IN,IN2,IN3,AL(IN)
          WRITE(24,902)IN,IN2,IN3,AL(IN)
902       FORMAT(' L',I1,1X,I3,1X,I3,1X,E10.4)
          IN4=IN3+1
          WRITE(6,903)IN,IN3,IN4,AR(IN)
          WRITE(24,903)IN,IN3,IN4,AR(IN)
          WRITE(26,903)IN,IN3,IN4,AR(IN)
903       FORMAT(' R',I1,1X,I3,1X,I3,1X,E10.4)
          IF(IN.EQ.N) GOTO 960
          IN=IN+1
          AR(IN) = 1.0E+9
          WRITE(6,904)IN,IN4,AC(IN)
          WRITE(26,904)IN,IN4,AC(IN)
          WRITE(24,904)IN,IN4,AC(IN)
904       FORMAT(' C',I1,1X,I3,1X,'0',1X,E10.4)
          WRITE(6,905)IN,IN4,AL(IN)
          WRITE(26,905)IN,IN4,AL(IN)
          WRITE(24,905)IN,IN4,AL(IN)
905       FORMAT(' L',I1,1X,I3,1X,'0',1X,E10.4)
          WRITE(6,906)IN,IN4,AR(IN)
          WRITE(26,906)IN,IN4,AR(IN)
          WRITE(24,906)IN,IN4,AR(IN)
906       FORMAT(' R',I1,1X,I3,1X,'0',1X,E10.4)
          IN1=IN4
          IN2=IN4+1
```

```fortran
        IN=IN+1
        IF(IN.GT.N) GOTO 955
        GOTO 950
955     CONTINUE
        WRITE(6,*) 'Error  n  is  even'
        WRITE(26,*) 'Error  n  is  even'
960     CONTINUE
        WRITE(6,907)IN4,RS
        WRITE(26,907)IN4,RS
        WRITE(24,907)IN4,RS
907     FORMAT(' RS',1X,I3,2X,'1 ', E10.4)
        WRITE(6,908)RL
        WRITE(26,908)RL
        WRITE(24,908)RL
908     FORMAT(' RL',1X,'3',2X,'0 ', E10.4)
        GOTO 10
500     CONTINUE
        END
        SUBROUTINE BUT11(A,N)
C  This subroutine is to be used when r = 1 in Table 10.1
        DIMENSION A(N), B(10,10)
        DATA B/2.0,1.4142,1.0,0.7654,0.618,0.5176,0.445,0.3902,0.3473,
     1  0.3129,0.0,1.4142,2.0,1.8478,1.6180,1.4142,1.247,1.1111,1.0,
     2  0.908,2*0.0,1.0,1.8478,2.0,1.9319,1.8019,1.6629,1.5321,1.4142,
     3  3*0.0,0.7654,1.618,1.9319,2.00,1.9616,1.8794,1.7820,
     4  4*0.0,0.6180,1.4142,1.8019,1.9616,2.00,1.9754,5*0.0,0.5176,
     5  1.2470,1.6629,1.8794,1.9754,6*0.0,0.4450,
     6  1.1111,1.5321,1.7820,7*0.0,0.3902,1.00,1.4142,8*0.0,0.3743,
     7  0.9080,9*0.0,0.3129/
        DO 10 I=1,N
        A(I) = B(N,I)
10      CONTINUE
        RETURN
        END
```

```
$ TY 10BPOUT.DAT
  *  The element values for a
  *              9 Section band-pass Butterworth Filter
  *
  *  RL =     450.0000      ohms
  *   RS =     450.0000      ohms
  *
  *  Centre-freq. =    300000.0      Hz
  *  Upper cut-off freq. =      305041.7      Hz
  *  Lower cut-off freq. =      295041.7      Hz
  *  Band-width =     10000.00      Hz
  *
C1    3    4 0.1132E-09
L1    4    5 0.2487E-02
R1    5    6 0.1000E+00
C2    6    0 0.3537E-07
L2    6    0 0.7958E-05
R2    6    0 0.1000E+10
C3    6    7 0.2565E-10
L3    7    8 0.1097E-01
R3    8    9 0.1000E+00
C4    9    0 0.6647E-07
L4    9    0 0.4234E-05
R4    9    0 0.1000E+10
C5    9   10 0.1965E-10
L5   10   11 0.1432E-01
R5   11   12 0.1000E+00
C6   12    0 0.6647E-07
L6   12    0 0.4234E-05
R6   12    0 0.1000E+10
C7   12   13 0.2565E-10
L7   13   14 0.1097E-01
R7   14   15 0.1000E+00
C8   15    0 0.3537E-07
L8   15    0 0.7958E-05
R8   15    0 0.1000E+10
C9   15   16 0.1050E-09
L9   16   17 0.2681E-02
R9   17   18 0.1000E+00
RS   18    1 0.4500E+03
RL   3    0 0.4500E+03
```

Figure D-2 DESIGN DETAILS OF THE BAND PASS FILTER

APPENDIX E

SIMULATED TEST RESULTS OF THE ARC CYCLOGRAM

LINEARISED ARC CYCLOGRAM

The simulation technique for the arc cyclogram has been explained in Chapter 7. For the purpose of the simulated test of the arc cyclogram, the arc current of the sinusoidal waveform has been selected. Mathematically, this can be represented as:

$$i_{arc} = 100 \sin(100 * Pi * T) \qquad\qquad (E1)$$

The waveform for a period of one cycle has been shown in Figure E-1. Figure E-2 shows the arc cyclogram as explained in Chapter 7. For a positive half cycle, curve 1-2-3 is followed. For the negative half cycle, the the curve 1'-2'3' is followed. V_p is the peak voltage which is 10.3 Volts. The arc voltage waveform v_{arc} has been shown in Figure E-1. The peak voltage 10.3 Volts and different gradients at the point of the voltage reversal are clearly shown.

ARC-CYCLOGRAM WITH REIGNITION EFFECT

For the purpose of the simulated test of the arc cyclogram with reignition effect, the arc current

$$i_{arc} = 100\sin(1000*Pi*T) \qquad\qquad (E2)$$

with holding the current zero near the cycle reversal has been considered.

Figure E-3 shows the current and voltage waveforms of the arc with re-ignition effect for a period of 10 cycles. At each point of the current reversal, 1, 1', 2, 2', 3, 3', 4, 4', 5, 5', 6, 6', 7, 7', 8, 8', 9, 9', 10, the effect of zero current holding has been clearly shown. The reignition voltage corresponding to the each point is evaluated as explained in Chapter 7. As such a current waveform with holding current zero near the voltage reversal has been found to be difficult. Some criterion is required for the time of the current to remain zero. For the purpose of simulated testing, a simplified criterion has been selected. This criterion is that the moment the arc voltage drops to a value equal to the reignition voltage, the current is zero and it remains zero upto the time of the reversal of the current. Figure E-4 shows the reignition voltage V_r at each current reversal by the points 1 to 10 and 1' to 9'. V_p is the maximum voltage which is 10.3 Volts. For the positive half cycle, the curve a-b-c is followed and for the negative half cycle the curve a'-b'-c' is followed.

X10¹ Figure E-1 ARC CURRENT AND VOLTAGE WAVEFORMS

CURRENT, Amps/VOLTAGE, Volts

i_{arc}

v_{arc}

TIME, Seconds   X10⁻³

Figure E-2 ARC CYCLOGRAM

VOLTAGE, Volts

CURRENT, Amperes   X10¹
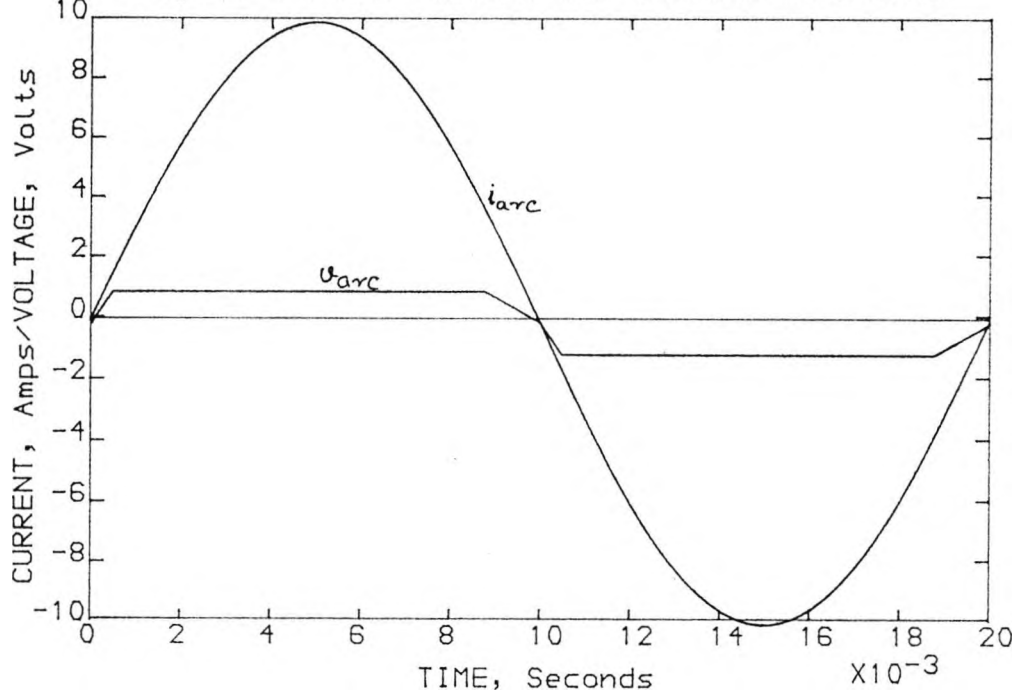
X10¹ Figure E-3 ARC CURRENT AND VOLTAGE WAVEFORMS
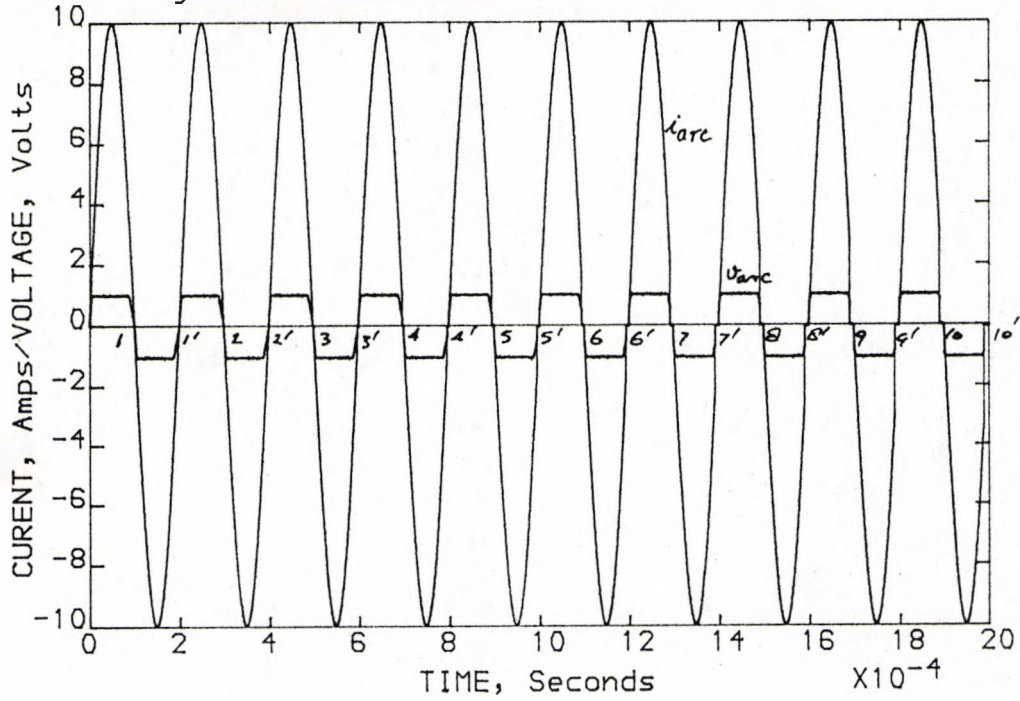
Figure E-4 ARC-CYCLOGRAM WITH REIGNITION EFFECT